A RADIO STUDY OF IONIZATION IN METEOR TRAILS

by

Brian J. Stone

B.Sc.(Hons.)

A Thesis

presented for the degree of

Doctor of Philosophy

in the Physics Department

of the University of Adelaide,

November 1965 and March 1967.

THE UNIVERSITY OF ADELAIDE

DEPARTMENT OF PHYSICS

CABLE AND TELEGRAPHIC ADDRESS:

"UNIPHYSICS"
'PHONE: 23 4333

24th October, 1967

I, hereby, consent to the loan and/or photocopying of my thesis "A radio study of ionization in meteor trails".

Brian J. Stone

TO MY WIFE JOYLEEN

CONTENTS

SUMMARY

A radio study has been made of the ionized trails of meteors, to examine statistically both the variation along the trails of the density of ionization, and the height and time dependence of its rate of diffusion. The observations, carried out over 13 months in 1960-61 with a multi-station continuous-wave equipment, provided very detailed descriptions of almost 2200 meteors.

The present state of knowledge in each of the two fields of interest is critically reviewed. In regard to ionization profiles, existing theory is shown to be capable of simple extension to calculate the profile resulting from fragmentation of a meteoroid. By making allowance for systematic error in two previous studies of trail profile shapes, reasonable agreement is secured between these results and those of other photographic and radio experiments covering magnitudes +3 to +9. In regard to diffusion coefficient measurements, attention is given to all mechanisms which have been suggested to account for the large scatter among observed values. A first-order correction is proposed for the effect of one such mechanism, viz. movement of the specular reflection point along the trail due to the latter's rotation in the presence of wind shear. Previous difficulties in finding a suitable statistical technique to describe the height dependence of the diffusion coefficient are described, and the existence of a more appropriate method is pointed out.

Results are presented from two techniques for analyzing the trail profile data. One employs a set of model profiles, and the other introduces the concept of an "equivalent Gaussian profile". Both indicate that typical trails extend for 5 to 7 Km. between heights of half maximum ionization, in agreement with the previous results (corrected where necessary). A tendency for trails to begin abruptly is demonstrated. Results from a preliminary attempt to estimate the total electron content of the trail appear promising.

From several techniques used in analyzing the diffusion coefficient data the following major points emerge.

(a) The scatter in diffusion coefficient D at any height and time (and in electron line density at neighbouring pairs of points on a trail) is

reduced by the correction for reflection point motion only if the reflection points concerned are very close (~200m.) to each other. This is tentatively ascribed to small-scale irregularity of the typical ionization profile.

(b) A diurnal variation in D, with a maximum in the morning, is evident at all heights, and increases in amplitude with height.

(c) Profiles of D vs. height taken each 4 hours and integrated over individual months show a tendency to oscillation (wavelength ~10 Km.) about a smooth curve. The uppermost cycle, at 105±5 Km., is especially noticeable in profiles obtained by the alternative method of integrating the height gradient of D measured on individual trails.

(d) Plasma resonance with transverse incident polarization makes a small but detectable difference in the value measured for D.

(e) The diffusion coefficient scale height values from the two kinds of profiles in (c) disagree, apparently due to the irregular ionization mentioned in (a), and considerably exceed the pressure scale height.

(f) Diffusion coefficient scale heights for the Geminid shower are exceptional in being close to the pressure scale height; this shower is known to produce unusually long and smooth trails.

PREFACE

This thesis contains no material which has been submitted or accepted for the award of any other degree or diploma in any University.

To the best of my knowledge and belief, the thesis contains no material previously published or written by another person, except where due reference is made in the text.

University of Adelaide (Brian J. Stone)

March , 1967

ACKNOWLEDGEMENTS

The multi-station meteor survey in 1961 was planned and initiated jointly by Dr. W. G. Elford and the late Dr. A. A. Weiss. Dr. Elford has directed the work of the meteor research group since the mid-1950's. After several fruitful years spent attached to the group, Dr. Weiss was transferred interstate by C.S.I.R.O. late in 1960, but retained a keen interest in the meteor work. The author is deeply grateful for the friendly guidance and encouragement given to him by these two gentlemen at all times.

In the survey, the author was fortunate in having as colleagues Messrs. (now Drs.) C. S. Nilsson and R. G. Roper. In addition to designing and constructing much of the equipment for the near outstations, and operating and maintaining them and the St. Kilda main station during 1961, they provided, in reducing their results, basic data needed in the ionization profile and diffusion work. The author is indebted to them for much practical help and for many informative and rewarding discussions. Mr. (now Dr.) E. L. Murray also gave helpful advice, both scientific and technical, on numerous occasions. Thanks for advice are due, too, to Mr. J. W. Smith, who also provided the camera and VHF transmitter used by the author for the distant outstation. In matters of electronic construction, the experienced craftsmanship of Mr. E. J. Welsby, who built most of the main station equipment, was an asset to the group.

But for the interest of Mr. B. Rofe (P.O./Flight Projects Group, W.R.E. Salisbury), it would have been impossible to gain sufficiently frequent access to the 7090 computer, with which most of the analysis was done, for developing the programmes or for running them repetitively to obtain detailed results. For this assistance he has the author's warm thanks.

Each of the following young ladies has spent many long hours in film-reading, calculation, or drawing connected with the author's work, and has earned his gratitude for cheerful and willing work: Misses J.Allister, M.Bartlett, M.Chapman, A.von Einem, L.Glastonbury, J.Gordon, F.Maddocks, Mrs.J.Laing, Mrs.M.McInnes.

Finally, the author takes the opportunity to express his thanks

to his wife, for a great deal of time spent helping in film-reading and typing, and for her unfailing patience and encouragement.

Finance for the ionization profile and diffusion studies came from the Radio Research Board and a University Research Grant.

CHAPTER 1

INTRODUCTION

For thousands of years man has watched meteors in the night sky with interest, often combined with fear and superstition. Only in the last hundred years, however, have his observations been precise enough to yield scientifically useful information about the phenomenon. Thus, by about 1925, it was known that at least a majority of these bodies moved in closed orbits about the sun, and attempts had been made to deduce some properties of the atmosphere at the heights (70 to 110 Km.) where the meteors were observed. After the Second World War these visual and photographic studies were complemented by the advent of radar, with its advantages of independence of time of day and visibility conditions, and virtually unattended operation. At present meteor work has three main aspects, to each of which both radio and optical methods contribute. These aspects are the astronomy of meteors and of their relationship with the rest of the solar system, the physics of meteor flight, heating and ablation in the atmosphere, and the study of atmospheric parameters and movements using meteors and their luminous and ionized trails as tracers.

This thesis describes two closely connected investigations, forming part of a radio survey for which the observations were taken in Adelaide in late 1960 and throughout 1961. The first project described is an analysis of the amplitudes of radio echoes from the meteor trails in terms of the ionization-height profiles of the trails. In the second, the time and height dependence of the ambipolar diffusion coefficient, which is the most important factor determining the rate of decay of many echoes, is studied by measuring the decay characteristics of (in general) the same echoes used in the first project. Both experiments are also similar in making good use of the very complete descriptions of each meteor's atmospheric trajectory, and of the wind field acting on each trail, provided by the multi-station continuous-wave equipment. Thus,

although ionization profiles belong to the field of meteor physics and the diffusion coefficient work is essentially an atmospheric study, so much of the data-reduction process is common to both that they are combined in this report.

The fact that up to four values per trail (one per receiving station) of the density of ionization are available forms the basis of the methods of deducing the shape of a typical profile. Both of the main methods are thought to be original. In each of them the values of ionization density for each meteor trail are analyzed in pairs. Information about the other observed points on the trail is not discarded when dealing with each pair of values. Instead, the analysis also requires the position of the height of maximum ionization to be estimated, and for this all data for the trail are employed. In the first method the height gradients of the electron line density found from all pairs of usable observed points are compared with the gradients predicted for each of four "model profiles" which have appeared in the literature. The model profile which best fits the present observations is thus found, and the changes in it which are desirable for a still better fit are pointed out. Secondly, limits are found for the length of an "equivalent Gaussian profile" in analyzing the results in pairs. A simple qualitative attempt to classify the measured profiles by shape is also made, and in this section of the work all data points on each trail are used jointly.

In the diffusion coefficient experiment there are again up to four measurements per trail of the variable of interest, viz. the decay time-constant of the echo. These values are processed in two ways. Firstly they are combined into scatter diagrams of log D versus height, where D is the diffusion coefficient, without any attempt being made to connect or otherwise signify the points from each individual trail. Secondly each possible pair of measurements on a trail is used to derive an estimate of the local height gradient of log D. The coefficients themselves and these gradients are displayed similarly in scattergram form. Also, statistical measures of the distribution of log D and $\frac{d}{dh}$ (log D) with height are found, together with profiles showing the mean values of these quant-

-ities in each 1 Km. height interval. The data are analyzed and displayed in this fashion for each month's recording period, in 4-hour and 24-hour intervals. Thus information on the diurnal and seasonal variation of the diffusion coefficient is made available in more detail than previously. Particular emphasis is given to the diffusion scale height (a measure of the rate of change of ln D with height) in the diurnal and seasonal analysis, because of earlier controversy about this quantity. Care is taken to use a valid statistical technique for estimating the diffusion scale height.

A simple method is proposed for correcting the measured diffusion coefficients for errors due to the motion of the specular reflection points along a non-uniformly ionized trail which becomes distorted in the presence of wind shear. By applying this correction to the experimental data, the importance of the mechanism is evaluated and found to be small. Indirect evidence suggests that much of the scatter arises from small-scale irregularity of the ionization profiles. The suggestion is confirmed by examination of data for Geminid meteors, whose trails are known to be largely free of such irregularity.

CHAPTER 2

METEOR PHYSICS

2.1 The meteoroid.

The term "meteor" may mean either a particle entering the earth's atmosphere at high velocity, or the set of phenomena caused by its entry. To distinguish the particle itself we can use the word "meteoroid", while reserving "meteorite" for those particles which are not completely evaporated before reaching the earth's surface.

It is literally accurate, rather than picturesque, to refer to the vast majority of meteors as interplanetary dust, for dust and sand particles as we normally encounter them have similar sizes and masses to those of small visible meteors. Thus, for example, a meteor which is just visible with the naked eye from a distance of 100 Km. under favourable conditions is a light source of maximum stellar magnitude +4 or +5. If its velocity is about 40 Km/sec relative to the earth, recent estimates by McKinley (1961) and Whipple (1963) suggest that the mass of the meteoroid is of order .01 - .4 gm., and propose densities from 0.1 to 0.4 gm/cc. These low values of density are commonly accounted for by assuming a fragile, porous structure for the meteoroid. Although even lower densities such as .01 gm/cc. have been accepted until recently, most of these measurements are now thought to represent, partly, the space density of the cloud of fragments shed by the meteor in its flight (Hawkins and Southworth 1963). The physical picture, then is of a low-density, fragile accretion of stony and iron particles, the composition being known roughly from the emission spectra of photographed meteors. Solid ices (CO_2, CH_4, H_2O) probably hold the constituent grains together.

There are several sources of information to support the idea of a "dustball" or "stoneflake" structure (the names have appeared in the literature). Some of the meteors with visual magnitude M_v +3, photographed and discussed by Jacchia (1955), and a large percentage of those detected by the radar system of Hawkins and Southworth at $M_v \sim +9$, decelerated in such a way that they must have disintegrated early in their ablation

into several thousands of fragments, all closely following the original trajectory. The dynamic pressures causing break-up were only about 10 gm-wt./cm^2, and a crushing strength of this order is comparable with that of cigar ash, rather than a solid body.

Some direct evidence of the physical structure of these particles is available from an experiment (Hemenway, Soberman et al. 1961) in which micro-meteorites were collected by a rocket above 90 Km. Micro-meteorites are particles so small that a few collisions with atmospheric molecules decelerate them to terminal velocity before appreciable heating or fragmentation occur. Those collected often had an open, irregular, "fluffy" structure, composed of smaller particles of mass $\sim 10^{-15}$ gm. Others were more compact, and could have originally been part of similar agglomerates on a larger scale.

Finally, support for the dustball hypothesis comes from the accepted identity between most meteors and the debris of comets. This association is known from the correlation of meteor shower orbits with those of comets observed to pass close to the earth. It is generally agreed that the dust particles are ejected from cometary nuclei into slightly modified orbits when some of the ices of the nuclei sublime during perihelion passage. Perturbations of the meteor orbits by approaches to the major planets account for orbits no longer associated in shower streams. A fragile structure for the meteors is a natural consequence of Whipple's (1950) icy-conglomerate model of the comet's nucleus, which is still stated to give the best explanation currently available of the observed behaviour of comets (Whipple 1963).

Only a very few of the brightest fireballs are considered to be solid bodies with the density of stone or iron. This type of meteoroid, which may be both large enough and strong enough to survive as a meteorite, is thought to be asteroidal material. Although, as has been mentioned, individual solid particles appear to form part of the micrometeorite population also, the cometary origin seems more probable for this end of the mass scale.

It is only the very high velocity with which a meteoroid enters the atmosphere that makes their mutual interaction detectable at all.

Geocentric velocity of the meteor can range from 8 Km/sec., the velocity attained by a body which falls through the earth's gravitational field from rest at infinity, to 73 Km/sec., corresponding to the head-on approach of a meteor moving in a parabolic orbit. The momentum and kinetic energy available to each meteor atom greatly exceed those of the air molecules encountered, since few of the latter have thermal speeds larger than 1 Km/sec.

2.2 The atmosphere at meteor heights

Most meteors producing detectable light and/or ionization do so between altitudes of 70 and 120 Km. Meteors were virtually the only source of information about these levels of the atmosphere from the early 1920's, when they were first so used, until high-altitude rockets became available, and the lack of alternative data made the evaluation of theories in meteor physics difficult. Nowadays it is possible both to improve our knowledge of meteor phenomena by using atmospheric data of improved accuracy, and to use meteors as sensors with which to refine our models of the atmosphere. This complementary situation is illustrated by the project described in this thesis, in which observations of both ionization profiles, i.e. the meteoroid, and ambipolar diffusion coefficients, i.e. the atmosphere, are affected by the local wind gradient, another atmospheric parameter.

Table 2.1 summarizes the important parameters of the atmosphere as it concerns this project. Since there is no need to consider composition in detail, the atmosphere is treated as a single gas of mean molecular weight $\bar{m}$.

The mean values quoted apply near the equinoxes, and are abstracted from the U.S. Standard Atmosphere 1962. In some cases an indication of the ranges of variation expected due to seasonal and/or diurnal changes is given. These ranges have been estimated by reference to the COESA Interim Supplemental Atmospheres (1964) and Stroud and Nordberg (1961) respectively.

Table 2.1. Approximate atmospheric parameters at meteor heights, with ranges of seasonal variation where available, for latitude 37^{o}.

Height (Km.)	60	70	80	90	100	110	120
Temperature (^{o}K)	255±10	230±10	180±15	180±15	210±15	255±20	350±40
Pressure (mm. Hg)	0.17	.041	.0077	.0013	2.3×10^{-4}	5.5×10^{-5}	1.9×10^{-5}
Density (10^{-6} Kg/m^3)	310±50	88±10	20±2	3.2	0.5	.098	.024
N^{o}. density (10^{18} m^{-3})	6400	1800	420	66	10	2.1	0.52
Scale height (Km.)	7.6	6.6	5.4	5.4	6.4	7.9	11.0
Neutral mean free path (m.)	.00027	.00092	.0041	.026	.16	.82	3.2
Molecular weight	28.96	28.96	28.96	28.96	28.88	28.56	28.07

N.B.: Summer colder than winter above 60 Km.

Let us, finally, discuss air movements. Meteor techniques (e.g. Greenhow(1955), Roper and Elford(1965)) have been prominent in showing that the motion at a given point, averaged over a half-hour or so, is determined by a combination of a seasonally varying prevailing wind with tidal motions of periods 24, 12 and 8 hours. These prevailing and tidal components all vary in amplitude and direction with height. The resultant "mean" winds have amplitudes up to 80 metres/sec., and have superimposed on them turbulent motions with a range of scales from 50m. to 200Km. (Elford and Roper, 1966). Because large-scale vertical motion is strongly inhibited by buoyancy forces, the total wind vector is observed to lie always within some 10^{o} of the horizontal. Three-dimensional isotropy probably holds only for turbulent

motion with scales of a few hundred metres or less. In contrast, the largest eddies (horizontal scale ~ 200Km.) involve vertical displacements of no more than approximately 1Km., while the sums of mean and tidal wind vectors, at points separated in height by 5 - 10Km. at any time, are at most weakly correlated.

Apparent stratification has been observed by sodium trail methods in certain wind profiles (e.g. Blamont and de Jager, 1961). There is also some evidence (Gregory, 1961) that the fluctuations of electron density in the lower ionosphere may exhibit maxima of amplitude at height intervals of order 10Km. The reality of both these apparent effects is still the subject of discussion.

By observing rocket-laid sodium trails it has been shown (Kochanski, 1964) that wind shear suddenly decreases above 105Km., where small-scale turbulence is no longer evident from the trail's appearance.

2.3 Evaporation theory of meteor trails

The physical processes involved in the formation of a meteor trail are quite complicated. Remarkably accurate hypotheses were advanced by Öpik as early as 1937, and also since then (e.g. his book in 1958). Much valuable work was done around 1950 by Herlofson (1948) and by Whipple and co-workers at Harvard (Whipple et al., 1951-1955). The "classical" theory set up by these authors describes the heating and ablation of a spherical, solid particle which is smaller than the local mean free path of an air molecule. This particular case, applicable in reality only to a meteorite-type particle, at very great heights, is currently the starting-point for treatment of the more common cometary meteors. No detailed theory is available which initially postulates a fragile, granular meteoroid.

Relative to the meteoroid, diatomic air molecules possess kinetic energies from 60 to 800eV, depending on the meteor's velocity, and collide as individuals with its surface. Most of the collisions are inelastic, i.e. the impinging air

molecules are trapped in the surface, giving up kinetic energy $\frac{1}{2}mv^2$. Most of the energy appears as heat in the meteoroid surface, causing evaporation of meteor (and trapped air) atoms. Such evaporated atoms have thermal energies of a few eV relative to the meteoroid, but since its speed and theirs are essentially the same relative to previously undisturbed air molecules, evaporated atoms have kinetic energy in the range 50 - 1000 eV in collisions with air molecules. These energies are well above the ionization threshold. Following Herlofson (1948), we can equate heat supplied to the meteor in inelastic collisions with latent heat carried away by the evaporated atoms while a height interval dh is traversed, obtaining

$$4\Pi r^2 d\, \ell\, dr = \tfrac{1}{2} r^2\, \rho\, v^2 \sec x\, dh \qquad \ldots 2.3.1$$

Here r, d, ℓ and v are respectively radius, density, latent heat of ablation (corrected for the efficiency of heat transfer), and velocity for the meteoroid. ρ is air density, and the meteor trajectory makes an angle x with the vertical. Conservation of momentum is expressed by

$$\tfrac{4}{3}\Pi r^3\, d\, dv = \Pi r^2 \rho \sec x\, dh \qquad \ldots 2.3.2$$

These two equations can be integrated to give

$$r/r_\infty = \exp -(v_\infty^2 - v^2)/12\ell \qquad \ldots 2.3.3$$

and

$$\frac{\rho H \sec x}{r_\infty} = \frac{2N_0\, d}{3} \exp\left(\frac{-v_\infty^2}{12\ell}\right)\left[\mathrm{Ei}\left(\frac{v_\infty^2}{12\ell}\right) - \mathrm{Ei}\left(\frac{v^2}{12\ell}\right)\right] \qquad \ldots 2.3.4$$

where the subscript ∞ refers to the meteor before it entered the atmosphere, and Ei(x) is the integral logarithm. N_0 is Avogadro's number, and H is the pressure scale height in an assumed isothermal atmosphere. The number of atoms (mass m) evaporated per unit length of trail is

$$n = -4\Pi r^2\, d\, \frac{dr}{dt}\, \frac{N_0}{mv} . \qquad \ldots 2.3.5$$

Now from 2.3.1 and 2.3.5, putting for the mass of the meteor

outside the atmosphere $M_\infty = \frac{4}{3}\pi r_\infty^3 d$, we have

$$n = \frac{9M_\infty \cos x}{2mH}\left(\frac{\rho H \sec x}{r_\infty d}\right)\left(\frac{r}{r_\infty}\right)^2\left(\frac{v^2}{12\,\ell}\right) \qquad \ldots\ 2.3.6$$

Equations 2.3.3 to 2.3.6 may now be used as follows to predict the behaviour of a meteoroid of known size (r_∞), initial trajectory (v_∞, x) and physical properties in a chosen model atmosphere. From 2.3.4 is found the velocity v at any height. This value for v is used in 2.3.3 to obtain r/r_∞, which in turn is substituted in 2.3.6, yielding n at the given height.

Improvements in the above theory await more detailed experimental information on the processes involved. While much has been learnt by combining various workers' results into a more or less coherent picture (c.f. Ch.4), this present knowledge exists largely as empirical correlations among parameters. A major stumbling-block is the present absence of artificial-meteor techniques capable of achieving speeds above 15 Km/sec.

2.4 The ionization and light profiles

It was pointed out in Section 2.3 that evaporated meteor atoms have kinetic energy well above the threshold for ionization in collisions with air particles. However, the probability of excitation to higher energy states is much lower for two-heavy-particle interactions than for electron-heavy-particle ones. This applies also to the probability of ionization. The reason is that, to transform a given amount of energy into excitation, a larger transfer of momentum is needed for the case of heavy particles than for electrons. In the case of interest to us, the collision of two heavy particles, energies $\simeq$10 KeV may be needed to attain ionizing probabilities approaching unity.

Thus it is to be expected that the kinetic energy of the evaporated atoms will appear mainly as heat, with a small

fraction as light and rather less as ionization. A further fact tending to reduce the production of light and ionization is that most atmospheric molecules below 100 Km. are diatomic, and hence present large cross-sections for rotational excitation. There are considerable difficulties in finding either relative or absolute probabilities for heating, light emission and ionization. The difficulties are both theoretical (Öpik 1937; Lazarus and Hawkins 1961) and experimental (Whipple 1955; Verniani and Hawkins 1964). Results depend strongly on meteoroid velocity and size. It is more or less agreed, though, that the ratio $\frac{\text{ionizing efficiency}}{\text{luminous efficiency}} \propto v^2$.

In proceeding with the evaporation theory of Section 2.3 to discuss ionization, it is convenient to define an ionizing probability factor β as the probability that a single ablated atom will produce one free electron before being slowed to thermal velocity in the atmosphere by multiple collisions. If a total of α electrons are produced per metre of trajectory, we write $\alpha = \beta n$ ... 2.4.1
where it is usually assumed that β depends on the meteoroid velocity v according to $\beta = \beta_0 v^{\eta}$ 2.4.2
Estimates of the exponent η range from 0 to 6; a recent review of all the data concerning β_0 and η by Verniani and Hawkins (1964) has led to $\beta = 1{\cdot}0 \times 10^{-20} v^4$,
where v is in metres/sec. However, it is not very clear how wide a range of meteoroid sizes is covered by this expression.

An approximation to the ionization profile defined by 2.3.6 and 2.4.1 is often used. It is

$$\alpha = (\beta/mH)\, M_\infty \cos x\, (\rho/\rho_{max})(1 - \tfrac{1}{3}(\rho/\rho_{max}))^2$$

$$\rho_{max} = (8\mathcal{A}/3v_\infty^2)(r_\infty d/H)\cos x$$

$$\alpha_{max} = 4/9\ (\beta/mH) M_\infty \cos x \qquad \text{... 2.4.3}$$

Equations 2.4.3 are obtained by neglecting deceleration and assuming $v^2 >> 12\mathcal{C}$ and also $v^2 >> 3\mathcal{C}(2+\eta)$. Since $\mathcal{C} \simeq 3\times10^7$ joule/Kg. and $\eta \simeq 4$, these assumptions may not hold for slow meteors ($v^2 \simeq 10^8$ m^2/sec^2, say). This failure has been discussed at length by Weiss (1958).

Figure 2.1 illustrates the exact solutions for $\eta = 0,5$, and for $\nu = v_\infty^2/12\mathcal{C} = 4$, 12 and 36, together with the approximate solution 2.4.3. The reduced height used in the figure to remove dependence of plotted functions on d and r_∞ is defined as $h' = H \ln(\rho H \sec x/r_\infty d)$; the factor in brackets arose in Eq. 2.3.6, and the form of the definition is analogous with $h-h_0 = -H \ln(\rho/\rho_0)$. Points worth noting are:-

(1) As implied by Eq. 2.3.6, the ionization curve first rises with the increasing air density, and subsequently falls away as the effect of diminishing meteoroid radius becomes dominant;

(2) Deceleration is small until the particle is near the end of its path;

(3) Other factors being equal, fast meteors burn out higher in the atmosphere and produce greater electron line density α than slow meteors;

(4) The approximate formulae 2.4.3 always over-estimate α_{max} and ρ_{max}, most seriously for large η and small ν ; and

(5) Formulae 2.4.3 predict a more sudden termination of the profile than the exact solutions, but generally fit well above the height of maximum ionization.

The normalizing constants $K_1(\eta)$ and K_2 in the electron density graphs are such as to accentuate, respectively, the failure of approximations 2.4.3 for small ν , and the velocity dependence of α . They are defined by

$$K_1(\eta) = 4\cdot5\beta_0 M_\infty v_\infty^\eta \cos x/mH \qquad \ldots\ 2.4.4a$$

$$K_2 = (v_c/v_\infty)^\eta\ K_1(\eta)\ ,\ v_c = 40\ \text{Km/sec.} \qquad \ldots\ 2.4.4b$$

In finding v_∞ for use in K_2 it is necessary to assume a value of $\mathcal{C}$, since the un-normalized graphs are computed as functions of ν. The value $\mathcal{C} = 3\times10^7$ joule/Kg. has been used.

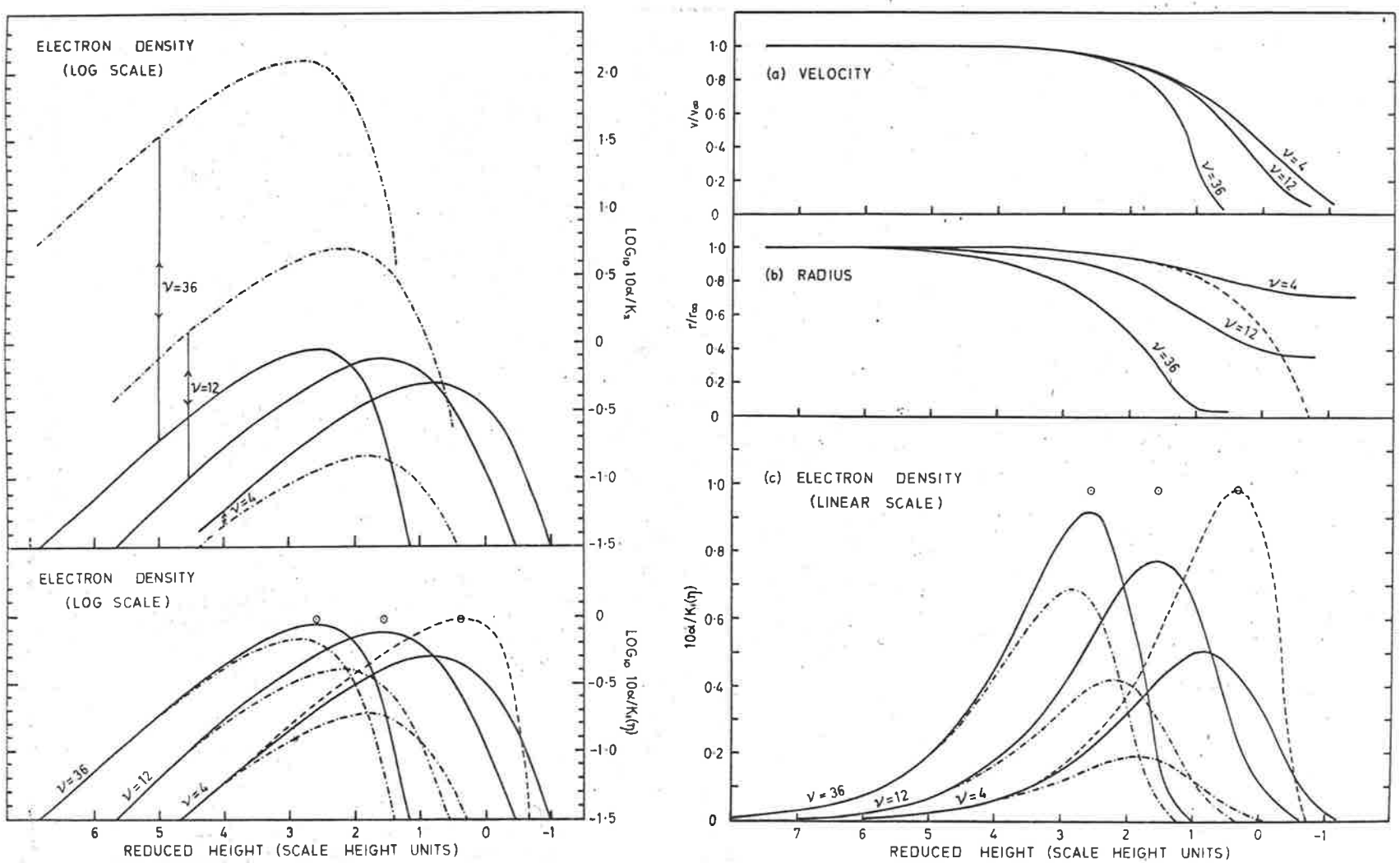

Fig. 2.1. Meteoroid velocity and radius, and electron line density, according to the evaporation theory. (After Weiss, with additions). Exact solutions ——— ($\eta=0$), -·-·- ($\eta=5$). Approximate solution - - - ($\nu=4$, all η), ⊙ (peaks, $\nu=12,36$, all η). The normalizing constants $K_1(\eta)$, K_2 are defined in the text.

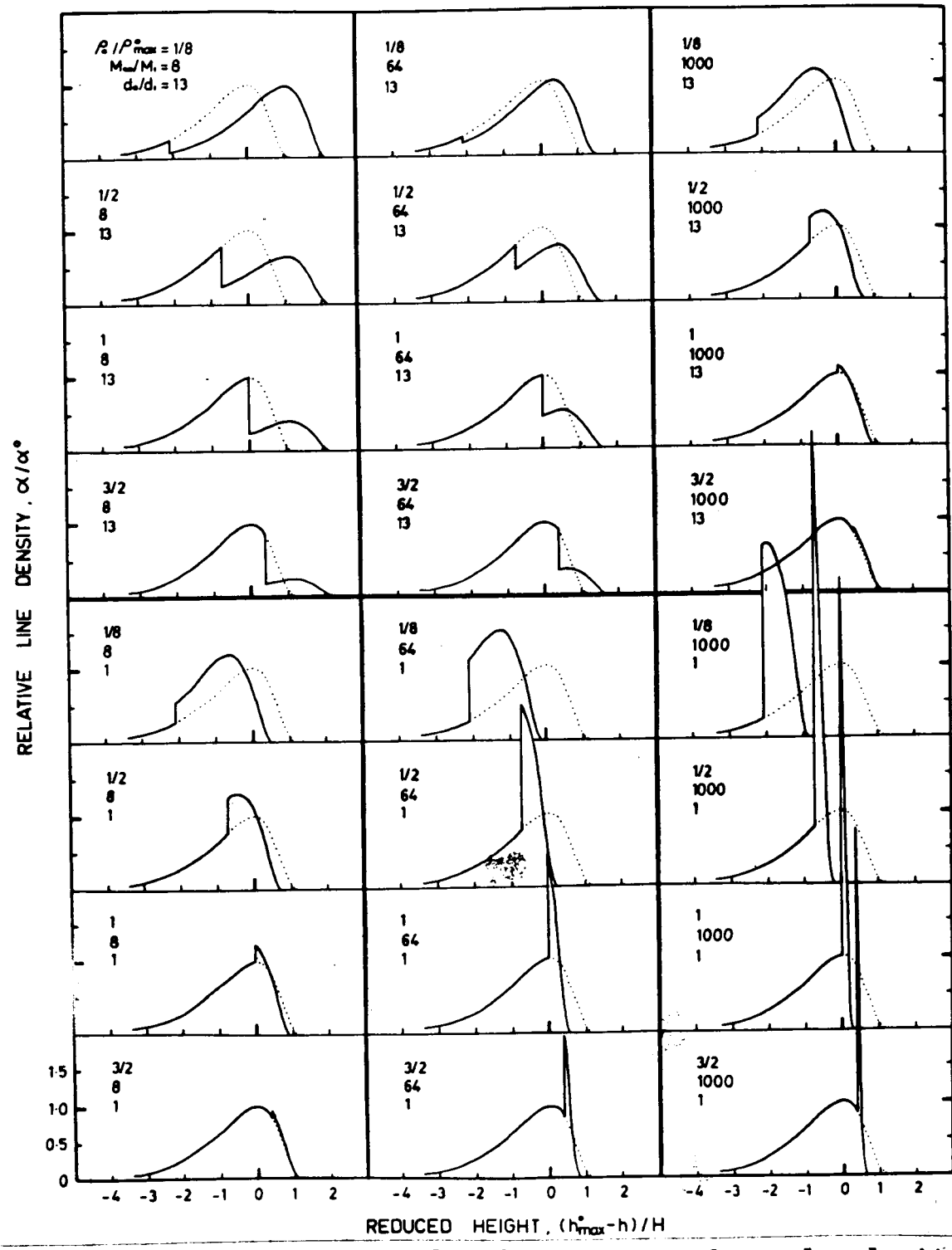

Fig. 2.2. Line density profiles for meteors of equal velocity, mass, and radiant zenith angle, fragmenting at the height where $\rho=\rho_0$. α° and h°_{max} are maximum line density and height expected in absence of fragmentation. (For $d_0/d_1=13$ read $d_0/d_1=1/13$).

Finally, note that variation from $\eta=0$ to $\eta=5$ and from $v=4$ to $v=36$ produces ionization profiles which are generally similar in shape, but differ in amplitude α and have their peak amplitudes at different values of the reduced height h'. Table 2.2 illustrates the similarity in shape by comparing the pairs of values of $(h-h_{max})$ at which $\alpha=0{\cdot}5\alpha_{max}$ and $\alpha=0{\cdot}2\alpha_{max}$ for the various profiles. (Here h replaces h' for the reduced height,, and h_{max} is the height where $\alpha=\alpha_{max}$). The table also illustrates the poor accuracy of the approximate profile below h_{max} and for small v.

Table 2.2. Shape of evaporation profiles.

Profile		Above h_{max}		Below h_{max}	
η	v	$\frac{h_{.2}-h_{max}}{H}$	$\frac{h_{.5}-h_{max}}{H}$	$\frac{h_{max}-h_{.5}}{H}$	$\frac{h_{max}-h_{.2}}{H}$
	4	2.62	1.48	1.10	1.50
0	12	2.63	1.50	0.98	1.42
	36	2.46	1.40	0.82	1.05
	4	2.53	1.43	0.96	1.47
5	12	2.57	1.44	0.94	1.36
	36	2.50	1.42	0.84	1.13
Approx. (all η,v)		2.80	1.30	0.68	0.90

There is no need for equally detailed discussion of the light curve. It is sufficient to say that, in the case of a solid particle, since deceleration is small along most of the path, differences in the dependence of ionization and of light emission on velocity will not make the ionization and light profiles greatly dissimilar in shape. However, as mentioned in Section 2.3, the distribution of power between these two processes at all times should depend strongly on v_∞.

Weiss (1959) has examined the changes needed when formulae 2.4.2 are applied to a linear atmosphere, i.e. one in which H varies linearly with height. Reference to Table 2.1

will show that the height gradient of H is negative below the mesopause (80-90 Km.), and increasingly positive above it. Below 110 Km., i.e. for most radio meteors, the predicted changes in profile shape are small in comparison with the effects of meteoroid break-up, or fragmentation.

2.5 Fragmentation and the ionization curve

We have seen how most meteors between visual magnitudes +1 and +10 appear to break up fairly early in flight into many (possibly less fragile) smaller particles. We now use the evaporation theory to describe the resulting ionization curve.

Extension of a result due to Weiss (1960) shows that N particles of mass M_1, inserted together at speed into an isothermal atmosphere, at a level where the density is ρ_0, produce by independent evaporation a trail described by

$$\alpha = (\beta/mH) M_0 \cos x \frac{\rho}{\rho'_{max}} \left(1 - \tfrac{1}{3}\frac{\rho - \rho_0}{\rho'_{max}}\right) \quad \ldots 2.5.1a$$

where $\rho_0 < \rho < \rho_0 + 3\rho'_{max}$, and we have put $M_0 = NM_1$. The density is ρ'_{max} at the height where each particle, if entering the atmosphere from outside, would produce maximum ionization. Its value can be found from Eq. 2.4.3b. In arriving at 2.5.1a the usual approximations discussed in Section 2.4, chiefly the neglect of deceleration, are used. Weiss also states that, at the point of maximum ionization,

$$\alpha_{max} = 4/9 \, (\beta/mH) \, M_0 \cos x \, (1 + \rho_0/\rho'_{max})^3 \quad \ldots 2.5.1b$$

and

$$\rho_{max} = \rho'_{max} + \rho_0/3 \quad \ldots 2.5.1c$$

Consider the parent meteor, which fragments at the level where $\rho = \rho_0$ when its mass has decreased to M_0 from an initial value M_∞. Let the parent body's density be d_0, and that of each daughter particle d_1. Using 2.4.3, we can easily show

$$\rho'_{max} = \rho^0_{max}/r \quad \ldots 2.5.2$$

where

$$r = (M_\infty/M_1)^{\frac{1}{3}} (d_0^2/d_1^2)^{\frac{1}{3}}$$

and $\rho^{\bullet}_{max}$ is the height where maximum ionization would have occurred if the meteoroid's crushing strength had been great enough to inhibit fragmentation. It is assumed that both parent and daughter bodies have the same latent heat of ablation $\mathcal{L}$ (corrected for efficiency of heat transfer). Otherwise, the expression for r must be multiplied by the ratio of values of $\mathcal{L}$ before and after fragmentation.

Thus the complete profile, combining 2.4.3 and 2.5.1, is

$$\alpha = (\beta/mH)\, M_{\infty} \cos x\, F(\rho) \;;$$

$$F(\rho) = \frac{\rho}{\rho^{\bullet}_{max}} \left(1 - \tfrac{1}{3} \frac{\rho}{\rho^{\bullet}_{max}}\right)^{2} \;, \quad \rho < \rho_o \;;$$

$$F(\rho) = \frac{M_o}{M_{\infty}} \frac{\rho r}{\rho^{\bullet}_{max}} \left(1 - \tfrac{1}{3} \frac{(\rho - \rho_o) r}{\rho^{\bullet}_{max}}\right)^{2} \;, \quad \rho_o < \rho \leq \rho_o + \frac{3\rho^{\bullet}_{max}}{r} \;;$$

$$\rho_{max} = \rho^{\bullet}_{max} + \rho_o/3 \qquad \ldots\ 2.5.3$$

From the evaporation theory it can be shown that, in an isothermal atmosphere, and assuming constant meteoroid velocity,

$$M_{\bullet}^{\frac{1}{3}} = M_{\infty}^{\frac{1}{3}} \left\{ 1 - \tfrac{1}{3} \left(1 - \frac{h^{\bullet}_{max} - h}{h^{\bullet}_{max}} \right) \frac{\rho_o}{\rho^{\bullet}_{max}} \right\} \qquad \ldots\ 2.5.4$$

Hence with quite good accuracy

$$M_o^{\frac{1}{3}} = M_{\infty}^{\frac{1}{3}} \left(1 - \frac{\rho_o}{3\rho^{\bullet}_{max}} \right) \qquad \ldots\ 2.5.5$$

Following the cometary-origin theory we may take as a representative value for the density of cometary material the figure 0·2 gm/cc. If a meteoroid of such material gives rise to stony fragments of density ≃ 2·5 gm/cc., we have $d_o/d_1 \simeq 1/13$.

Figure 2.2 shows ionization curves according to 2.5.3 and 2.5.5 for M_{∞}/M_1 = 8, 64 and 1000, for several different heights of fragmentation as defined by $\rho_{\bullet}/\rho^{\bullet}_{max}$, and for d_o/d_1 = 1/13 and 1 . The curves are for meteors of identical mass M_{∞}, velocity, and radiant zenith angle x . Note how

the severity of the step in the profile is controlled jointly by M_∞/M_1 and d_0/d_1, while the length of trail below the height of fragmentation depends on all three parameters. Note also how more trails, if not far above the detection threshold of a given equipment, will appear to begin suddenly than to end suddenly.

For comparison, Fig. 2.3 shows some light curves obtained by Jacchia and published by McKinley (1961) for very bright meteors, showing the same smooth initial rise in brightness, followed by "flare" behaviour which shortens the remainder of the trail. From Fig. 2.2, it is apparent that a light curve like Fig. 2.3(c) probably implies $d_0 \sim d_1$ and $M_\infty/M_1 \sim 100$.

Note that, whereas the above approximate treatment neglects deceleration, the increased surface-area/mass ratio of the fragments relative to their parent body implies a more rapid deceleration after fragmentation. Thus, although it gives results consistent with observation, this simple theory stands in need of considerable refinement.

2.6 The formative stages of the trail

The term "coma" is applied by Öpik to the evaporated meteor atoms which, close to the meteoroid at the head of the trail, have not yet been slowed down by collisions to thermal velocities. While only large telescopes come near to resolving the coma optically, its dimensions are often similar to the wavelength of radio equipment used for meteor study. So the conditions at the head of the trail have considerable bearing on the results given by many radio experiments.

Factors influencing the trail's initial radius have been discussed by Öpik (1958), Manning (1958), and Kashcheyev and Lebedinets (1963) on a theoretical basis. Manning shows that in a single early collision a meteor atom can be expected to retain a fraction $2/3 \leq K \leq 1$ of its original speed,

and to retain its original direction of motion as the most probable direction of rebound ("persistence of velocity"). Thus its path will not be a three-dimensional random walk. If it were, and the mean path between collisions were L, then after J collisions the trail would have a radial Gaussian cross-section whose characteristic radius depends on J (or time) and L.

Let the atmospheric particles and neutral evaporated meteor atoms have mean free path L_o at thermal energies. Meteor ions move, under the same conditions, with a mean free path $L_i \sim L_o/5$. For generality in what follows, let L' represent either L_o or L_i as required.

Manning shows how to allow for velocity persistence by applying random walk theory to the resultant translations of meteor particles after several (n) collisions. Integration over J collisions (overall time t) still gives a radial Gaussian density distribution

$$n(r) \propto \exp(-r^2/r_v^2) \qquad \ldots 2.6.1$$

whose characteristic radius r_v now depends on J (or time), L', K, and the ratio of mean-square translations over a set of collisions with, and without. velocity persistence. (This ratio is of order 5).

If all the ions are meteoric in origin, or are formed in collisions occurring very close to the meteor, then the "atom-trail", described by 2.6.1 with $L' = L_o$, contains a concentric inner "ion-trail" ($L' = L_i$) of radius $r_{vi} \simeq r_v/5$. The characteristic radii r_v and r_{vi} increase sharply with time for a few milliseconds after t = 0 (meteoroid passage), and then turn over to give a very slow continued growth. That is, the rapid expansion makes a lasting contribution r_v or r_{vi} to the total atom-trail or ion-trail radius. After the initial expansion it is no longer valid to neglect the movement of the air molecules, and the solution 2.6.1 is joined to the result for ordinary thermal diffusion or ambipolar diffusion. For ions, r_{vi} is bridged to the radius arising from ambipolar diffusion, viz. $r^2 = 4D(t + t_D - t_T)$, by making the two curves tangent at time t_T (see Fig. 2.4).

Here $(t_D - t_T)$ is the effective head-start given to the diffusion by the high initial energy of the diffusing particles. We shall henceforth write r_o for the radius of the ion-trail at time t_T (or at t=0 if precise time resolution is unnecessary).

The explicit radii and times in Figure 2.4 are found by substituting quantities appropriate to heights near 93 Km. Further substitution over a range of heights indicates that, for most purposes, it is adequate to think of the ionized trail as forming instantaneously with radius $r_o \sim 3L_o \sim 13L_i$, surrounded by a concentric cylinder of neutral atoms from the meteor with radius $\sim 13L_o$. These figures should vary only slightly with meteor velocity. If neutral atoms are still effective in producing ionization of air molecules after the first few collisions, the estimate for r_o should be larger.

The predictions published by Öpik are roughly equivalent to those of Manning. Those of Kashcheyev and Lebedinets, involving more approximations, indicate a much stronger dependence of r_o on v, and this is supported by their radio measurements upon 39 meteor trails. They claim that their method of experimentation eliminates certain errors which are large if trails measured are not truly underdense (see Sec. 3.1), and they criticize results of Greenhow and Hall (1960a, 1960b) on this account. (The latter data - somewhat more numerous - show no variation of r_o with v). The criterion of underdense trails proposed by the Russians is further discussed in Sec. 3.4 .

2.7 Ambipolar diffusion: dissipation of trail ionization

In this section are described various processes causing dissipation of the ionization in a meteor trail. They are ambipolar diffusion, thermal diffusion due to the heat released in the meteoroid's passage, recombination, attachment, and eddy diffusion due to atmospheric turbulence.

Firstly, following Kaiser (1953), we discuss the behaviour of electron density in a cross-section of the trail,

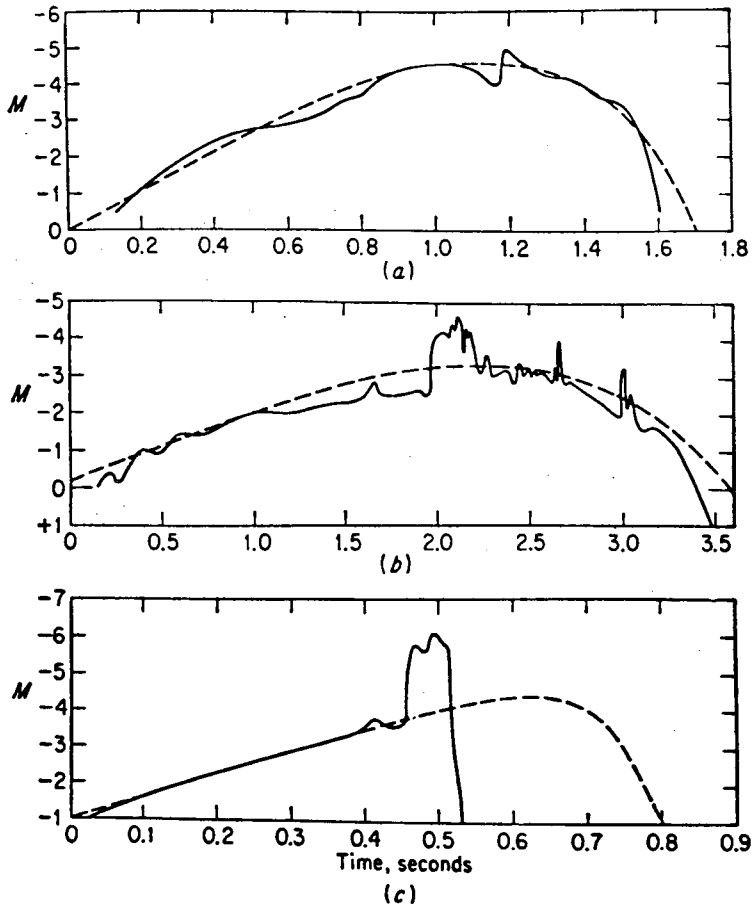

Fig. 2.3. ———, observed light curves of three bright meteors; – – –, theoretical light curves. Velocities: (a)36, (b) 25, (c)69 Km/sec. (After Jacchia).

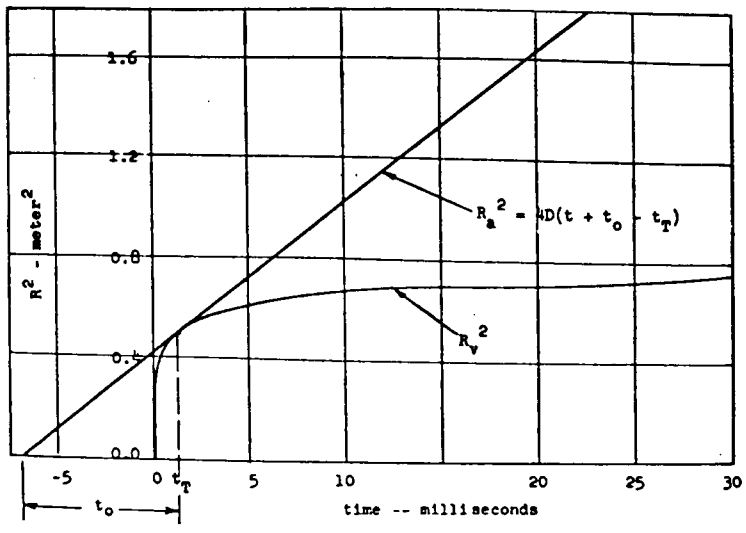

Fig. 2.4. Joining of Manning's initial radius estimate to expansion curve for ambipolar diffusion at time t_T.

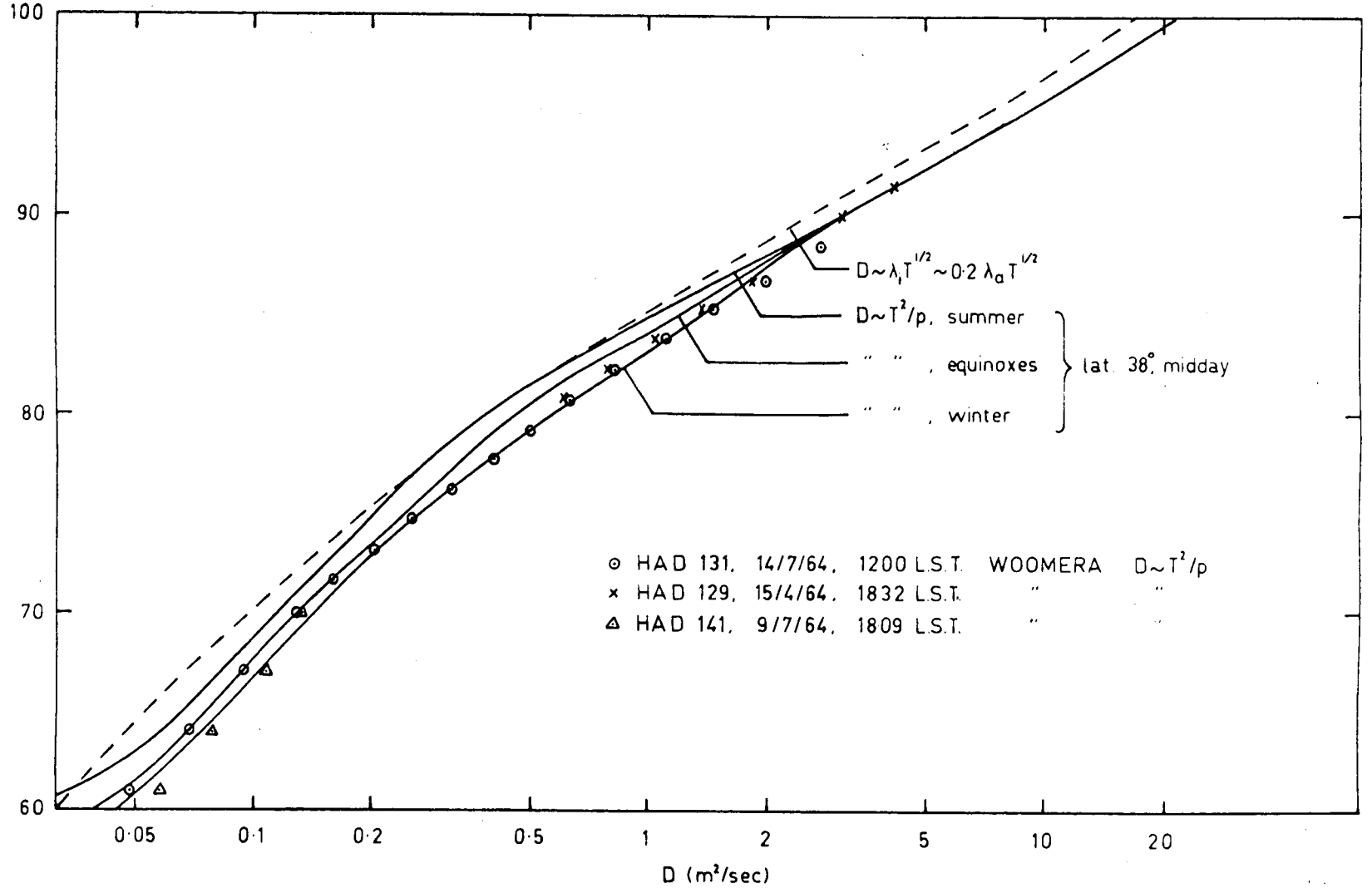

Fig. 2.5. Ambipolar diffusion coefficient D vs. height in Km. ——— , predictions for latitude of Adelaide from Eq.2·7·8 using U.S.Std. and COESA Int. Suppl. Atmospheres; × , ⊙ , △ , similar predictions using rocket data from Woomera (lat. 35°); – – – , Eq,2·7·5 using U.S.Std. Atmosphere.

considering ambipolar diffusion alone. In the absence of a magnetic field, and assuming cylindrical symmetry, coaxial (superimposed) distributions of electrons and positive ions diffuse according to

$$\frac{\partial n_e}{\partial t} = \frac{D_e}{r}\frac{\partial}{\partial r}\left(r\,\frac{\partial n_e}{\partial r}\right) + \underset{\sim}{\nabla}\cdot\frac{e\underset{\sim}{E}n_e}{m_e\nu_e} \qquad \ldots\ 2.7.1a$$

and

$$\frac{\partial n_i}{\partial t} = \frac{D_i}{r}\frac{\partial}{\partial r}\left(r\,\frac{\partial n_i}{\partial r}\right) - \underset{\sim}{\nabla}\cdot\frac{e\underset{\sim}{E}n_i}{m_i\nu_i} \qquad \ldots\ 2.7.1b$$

respectively. Here r is radius, t time, and the n are number densities, the D diffusion coefficients, and the ν collision frequencies for electrons (subscript e) and ions (subscript i). Also e is the electronic charge, $\underset{\sim}{E}$ is the space charge electric field, and the quantities of form $e\underset{\sim}{E}/m\nu$ are the drift velocities of the particles in this field.

In all but the outermost, least dense parts of the cylindrical column, n_e and n_i are nearly equal, due to the space-charge forces, and so will their spatial derivatives. Francey (1963a) has recently published the results of a computer solution of 2.7.1, confirming these statements for very dilute trails. Hence $\underset{\sim}{E}$ can be eliminated between 2.7.1a and 2.7.1b, giving

$$\frac{\partial n}{\partial t}e = \frac{D}{r}\frac{\partial}{\partial r}\left(r\,\frac{\partial n}{\partial r}e\right) \qquad \ldots\ 2.7.2$$

where the ambipolar diffusion coefficient D is defined by

$$D \simeq \left[D_i + (m_e\nu_e/m_i\nu_i)D_e\right] / (1 + m_e\nu_e/m_i\nu_i) \qquad \ldots\ 2.7.3$$

From the kinetic theory of gases,

$$m_e\nu_e/m_i\nu_i = (L_i/L_e)\,(T_e/T_i)^{\frac{1}{2}}(m_e/m_i)^{\frac{1}{2}} << 1\ ,$$

and

$$D_e/D_i = (L_e/L_i)\,(T_e/T_i)^{\frac{1}{2}}(m_i/m_e)^{\frac{1}{2}}\ ,$$

where the L are mean free paths and the T temperatures.

Huxley (1952) states that it is valid to put $T_e \simeq T_i \simeq T$, whence

$$D \simeq D_i(1 + T_e/T_i) = 2D_i \qquad \ldots 2.7.4$$

On substituting for D_i the expression given by the kinetic theory, and taking the ions and neutral molecules to be of approximately equal mass $\bar{m}$, we have

$$D = 3{\cdot}5L_i\,(2kT/\pi\bar{m})^{\frac{1}{2}} \qquad \ldots 2.7.5$$

and

$$L_i = (\sqrt{2}\pi\, n_a\, A)^{-1} \qquad \ldots 2.7.6$$

where n_a is the atmospheric particle density and A is the mean collision diameter for ions and neutral molecules. In most upper-atmosphere diffusion studies it is hard to evaluate collision diameters, and we can more readily find L_i for use in 2.7.5 by substituting $L_i \simeq L_o/5$ (vide Sec. 2.6) and taking values of L_o from a model atmosphere.

Weiss (1955) describes an alternative method for prediction of D, due to Huxley and Robertson, who expressed D in terms of temperature and pressure. They used the relation

$$D_i = a_i\, kT/e \qquad \ldots 2.7.7$$

connecting D and ionic mobility a_i for a group of singly charged ions. Experimental results for a_i , measured for various metallic ions at room temperature and pressure, were invoked, on the assumption that the a_i for meteor ions vary only slightly with temperature. This had previously been shown to hold for N_2^+ and Cs^+ in N_2 . Since $a_i \propto 1/n_a$, there resulted

$$D = 2D_i = 1{\cdot}13\times10^{-7}\ T^2/p\ \ m^2/sec. \qquad \ldots 2.7.8$$

where pressure p is expressed in mm. of Hg.

Figure 2.5 shows values of D predicted by Equations 2.7.5 and 2.7.8, using atmospheric data as in Table 2.1.
Pearson (1965) has kindly made available temperature and pressure profiles from falling-sphere experiments conducted at Woomera, and formula 2.7.8 has been used to convert these to D values which also appear in Fig. 2.5 . The agreement of

all the predictions is striking. Note that over the height range 80-100 Km., D increases very nearly exponentially, with a scale height $H_D \simeq 5{\cdot}5$ Km. The agreement of these predictions with measurements from meteor echoes (described later) is not good.

Given D, it is possible to integrate 2.7.2 for suitably chosen initial conditions. If the trail cross-section is initially a radial Gaussian of characteristic radius r_0, the result obtained for time t is the expanded Gaussian

$$n_e(r,t) = \frac{\alpha}{\pi(4Dt+r_0^2)} \exp\left(\frac{-r^2}{4Dt+r_0^2}\right) \quad \ldots 2.7.9$$

The simplification for zero initial radius, i.e.a line distribution at t=0, is obvious.

In Section 3.7 it is pointed out that under suitable conditions an incident radio signal may excite in the trail ionization a resonance whose magnitude depends on the diffuseness of the boundary of the electron cloud. Now if heating of the trail were significantly to alter the diffusion process, the trail would have sharper boundaries, because temperature would decrease with both radius and time. Experiments designed to test the strength of the resonance (Billam and Browne 1956) have not indicated any discrepancy with the behaviour expected from Gaussian trails, and so heating may be presumed unimportant, as calculations indicate it should be.

Trails in which $\alpha \gg 10^{14}$ electrons/m. produce long-enduring radio echoes, whose durations are, however, much shorter than would be expected if ambipolar diffusion alone were responsible for the dissipation of ionization. It has been demonstrated (Manning and Eshleman 1959) that the well-known process of radiative recombination

$$A^+ + e \rightarrow A + h\nu$$

has too low a rate to account for these short durations. A recent suggestion (Robinson, 1965) is that the alternative reaction

$$A^+ + e + e \rightarrow A + e$$

may be responsible. The predicted limiting of duration according to this latter theory is, if anything, too strong for agreement with observation; thus recombination may yet account for the brevity of the echoes from very heavily ionized trails. Attachment of the electrons to neutral particles also acts to reduce the durations of these echoes, especially below about 90 Km. The attachment process is still the subject of considerable discussion (e.g. Manning, 1964). Again, as with recombination, the law of time variation of electron density is such that only the longest-enduring echoes should be significantly reduced in duration. For the very slightly overdense trails ($\alpha > 10^{14}$ electrons/m.) producing echoes of duration 1 second or less (the longest used in the present survey) recombination and attachment are at present thought to be unimportant.

Finally eddy diffusion should be mentioned. According to the Kolmogoroff turbulence theory discussed in Section 2.2, instability of the mean wind field results in the production of eddies. Energy is transferred from the mean flow to large-scale eddies and thence through a range of eddies of decreasing sizes until a scale η is reached at which energy is instead dissipated in overcoming viscous forces. This minimum characteristic scale is given by

$$\eta = (\nu^3/\epsilon)^{1/4} \qquad \ldots\ 2.7.10$$

where ν is the kinematic viscosity ($\sim 10 m^2/sec.$ at 95 Km.) and ϵ is the turbulent dissipation rate ($\sim$ .03 watt/Kg. at 95 Km., according to Roper (1962)). With the typical values quoted, $\eta \sim 15$ m. Since the trail does not reach a diameter of this order for some seconds, and rocket work has found no eddies with scales less than even 50 m. at 95 Km., it is clear that trails observed for only a second or less should not give evidence of turbulence effects if observed at 95 Km. approximately. It is possible that near the lower boundary of the meteor region, at heights of 70 to 80 Km., the time scale of the smallest eddies may be as small as 1 second. At these heights the rate of detection of meteors by a typical radio equipment is very much less than at 95 Km.; thus at most a small minority of echoes with durations of a second or less may be influenced by eddy diffusion.

2.8 The meteor population

In this Chapter the characteristics of meteor trails have been related to the parameters of the atmosphere and of the meteoroids themselves. The following remarks outline two of the statistical relationships among the meteoroid parameters.

The first relationship is that between meteoroid mass (inferred from maximum optical magnitude or ionization in the trail) and frequency of occurrence. Normally the differential form

$$dN = M^{-s}\, dM \qquad \ldots 2.8.1$$

is used to denote the relative number of meteors dN in the mass interval (M, M+dM). To find the exponent s for a range of values of M, one establishes a distribution of either maximum brightness or maximum electron density, or of the height at which one of these occurs. In addition, the response of the observing system as a function of mass, velocity, and the position of the trail relative to the observer, must be carefully taken into account. In this way it has been shown by various workers that $s \simeq 2$ for the range of meteor sizes observable with the Adelaide equipment.

The last statement needs the qualification that for some meteor showers $s \neq 2$, i.e., the passage of the earth through the meteor stream causes not only the observing rate to change, but also the proportion of (say) bright meteors within the total sample detected in a given period.

Also note that ionization and light profiles differ considerably from meteor to meteor, and from shower to shower. Thus, for example, Draconid meteors, associated with the "new" Giacobini-Zinner comet, are very fragile, and collapse uncommonly readily into dust grains, producing high, short, intense trails for a given mass. The Geminids, on the other hand, produce long, fairly smooth trails, showing small deceleration, and hence are deduced to be of unusually robust structure. Their parent comet was probably an "old" one, so that only the densely packed core of its nucleus remained when the meteor stream was ejected (Jacchia 1963).

Corresponding variability is therefore to be expected among "sporadic" (non-shower) meteors, manifesting itself in the profiles and heights of occurrence of the trails, if the idea of universal cometary origin is accepted.

CHAPTER 3

RADIO SCATTERING FROM TRAIL IONIZATION

In this chapter the processes of radio scattering from a meteor trail are summarized and the interpretation of pulse and continuous-wave echo waveforms is discussed. The effects of finite initial trail radius, plasma resonance, and the geomagnetic field are also examined. Estimates are given for the heights at which the latter two effects may be influenced by Faraday rotation of the transmitted wave's polarization. Finally existing theory which predicts the effect of wind shear on some echo parameters is summarized. An extension to it is proposed by which observed values of echo amplitude and decay time may be more accurately converted to electron density and diffusion coefficient.

3.1 Basic theory for an underdense trail

The radio scattering behaviour of a section of an ionized meteor trail falls into one of two classes, according as the local value of linear electron density α is "underdense" or "overdense". In the former case electrons scatter independently of each other and in phase with the incident wave, and the received signal amplitude isdirectly proportional to α . In overdense trails the volume density of electrons is sufficiently high that the wave does not completely penetrate the trail, and it is convenient to formulate the theory in terms of reflection from a metallic cylinder of suitable equivalent radius. Radar signals returned from overdense trails vary in maximum amplitude roughly as $\alpha^{1/4}$. In practice a broad transition range of α exists for which echoes share both under- and overdense characteristics.

Underdense echoes arise as follows. The power flux at a point on the trail, distant R from a transmitter radiating power P_T with aerial gain G_T (over an isotropic radiator), is $P_T G_T / 4\pi R^2$ watts/m^2. If the receiving antenna, of gain G_R ,

is matched to the receiver, its effective absorbing area is $G_R\lambda^2/4\pi$ (where λ is the radio wavelength). If the transmitter and receiver are close together, the power delivered to the receiver by the radiation scattered from a single trail electron is

$$\Delta P_R = (P_T G_T/4\pi R^2)(\sigma_e/4\pi R^2)(G_R\lambda^2/4\pi) \quad \ldots 3.1.1$$

where σ_e is the back-scattering cross-section for a free electron.

To find the total signal from the trail, the electric fields due to all the electrons must be added vectorially. If ρ is the receiver input impedance, the peak voltage at the receiver input due to a single electron is $(2\rho\ \Delta P_R)^{\frac{1}{2}}$. Integrating along the trail between $s=-\infty$ and $s=s_1$, where s is a general position coordinate measured downwards along the trail and s_1 is the instantaneous position of the meteoroid we obtain for the total amplitude

$$A_R = (2\rho\ \Delta P_R)^{\frac{1}{2}} \propto \int_{-\infty}^{s_1} \sin(2\pi ft - 4\pi R/\lambda)\ ds \quad \ldots 3.1.2$$

In the integration it is assumed that α is constant along the trail and that all electrons in an element ds scatter coherently. These oversimplifications will be examined below.

Near the point on the trajectory where the range is a minimum (see Figure 3.1), the integration can be carried out using an approximate expression for the range, and yields

$$A_R = (\rho\ \Delta P_R\ R_o\lambda/2)^{\frac{1}{2}} \propto [C(x)\sin\phi - S(x)\cos\phi] \quad \ldots 3.1.3$$

where $C(x) = \int_{-\infty}^{x} \cos\ (\pi x^2/2)\ dx$

and $S(x) = \int_{-\infty}^{x} \sin\ (\pi x^2/2)\ dx$

are the Fresnel integrals. The meteoroid's position has been expressed in terms of the quantity $\ell_F = (2R_o\lambda)^{\frac{1}{2}}$ by the transformation $x = 2s/\ell_F$. Averaging over several RF cycles

(still a short time relative to the fluctuations of C and S), we find that the received power during the averaging period is

$$P_R = A_R^2/2\rho$$

$$= \alpha^2\left[\frac{C^2+S^2}{2}\right]\Delta P_R\, R_o\lambda/2 \qquad \ldots\ 3.1.4a$$

$$= \alpha^2\left[\frac{C^2+S^2}{2}\right](P_T G_T G_R \sigma_e)/(128\pi^3 R_o^3 \lambda^3) \ldots\ 3.1.4b$$

The length ℓ_F, above, is the total length measured along the trail of the principal Fresnel zone centred about the point of minimum range. The completed trail extends, in general, for some distance on either side of the point of minimum range. With increasing distance from this point, the fluctuations of C and S diminish rapidly in depth and period, and it can be shown that $\left[\frac{C^2+S^2}{2}\right] \to 1$ if the trail covers several Fresnel zones on each side of the central zone. If so, then from 3.1.4 the power received from the trail is equal to that from $\alpha(R_o\lambda/2)^{\frac{1}{2}}$ electrons scattering coherently; this number is one-half the number of electrons in the central Fresnel zone.

Thus we have established that the strength of the radar echo from a fully-formed trail depends strongly on the electron line density in the central Fresnel zone, and much less on the character of the remainder of the trail. Now the point of minimum range also has the property that a normal to the trail, drawn at that point and in the plane of the incident and reflected signal paths, bisects the angle between those two paths. Hence it is appropriate to refer to this point on the trail as the "specular reflection point", and to think of the echo as representing this point. The instant when the meteoroid passes the specular reflection point can be identified with moderate accuracy from the echo waveform and is commonly called "t_o"; by association, the specular reflection point is often spoken of as the "t_o point".

The form of Eq. 3.1.5b, with the factor $\left[\frac{C^2+S^2}{2}\right]$ equal to unity, was derived for meteor trails by Lovell[2] and Clegg (1948).

The Fresnel integrals are often represented by the Cornu spiral, which is an orthogonal plot of S versus C with the position (or time) variable x as parameter. In Fig. 3.2 is shown an appropriate Cornu spiral, which has been inverted about the horizontal axis, relative to its usual orientation, because of the negative sign in Eq. 3.1.4 . In this figure the line F_r joins the points on the spiral which represent the beginning and the instantaneous lower terminal of the trail, and represents the instantaneous echo signal in amplitude and phase. For a non-coherent system the "radar" waveform sketched in Fig. 3.1 is obtained with the trail taken to begin at $-\infty$; the length of phasor F_r then increases monotonically before t_o and oscillates thereafter about $\sqrt{2}$, corresponding to the condition $\left[\frac{C^2+S^2}{2}\right] = 1$. A continuous-wave (CW) equipment, as used at Adelaide, adds a constant, phase-invariant reference s ignal F_d to the echo signal F_r. In the Adelaide case F_d arrives at the aerial by ground-wave propagation, and F_r is often called the skywave. It is evident from Fig. 3.2 how the length of the resultant phasor F_{r+d} , i.e. the amplitude of the total signal, oscillates about generally non-zero values both before and after t_o , producing an echo waveform like the one marked "CW" in Fig. 3.1 .

The above treatment is a condensation of McKinley's (1961), from which Figures 3.1 and 3.2 are adapted. It provides a convenient framework to which we shall later add corrections for the initial simplifying assumptions that the trail has zero radius and constant electron line density everywhere.

3.2 Overdense trails

The treatment of scattering in the last section assumed that all electrons in a short element of trail length scatter in phase coherence with the incident wave and each other. For this assumption to be valid for electrons in the trail interior we require first that the trail radius be

negligible compared with the radio wavelength. Given this, the phase with which interior electrons scatter depends on the dielectric constant in the outer layers.

The dielectric constant of an ionized gas is given by

$$\kappa = 1 - n_e \lambda^2 r_e / \pi \qquad \ldots 3.2.1$$

for an incident wave with wavelength λ. Here n_e is the electron volume density, and r_e is the classical electron radius. By definition, the critical density n_c, which suffices to cause total reflection for normal incidence upon a plane sheet of ionization, is that for which $\kappa = 0$. An overdense trail is one in which $n_e \geq n_c$ in a region of sufficient diameter to make the assumption of coherent scattering untenable. Now in a newly-formed, narrow underdense column also, κ may be highly negative near the axis, as we shall see when discussing resonant scattering in Section 3.6. In the absence of such resonance, however, the coherent scattering from the outer layers can greatly exceed the contribution from the over-critically dense core if the diameter of the latter is small, which is the case in underdense trails.

One criterion to distinguish overdense from underdense reflection requires that the region of negative κ be large enough and dense enough to attenuate the wave by 1/e at the axis of the overdense trail. Putting $\kappa = 0$ in Eq. 3.2.1 and using Eq. 2.7.9, we obtain

$$n_c = \pi / \lambda^2 r_e$$

$$= \frac{\alpha}{\pi(4Dt + r_0^2)} \exp\left(\frac{r_c^2}{4Dt + r_0^2}\right) \qquad \ldots 3.2.2a$$

in which the instantaneous trail radius, from Eq. 2.7.9, is given by

$$a^2(t) = 4Dt + r_0^2 \qquad \ldots 3.2.2b$$

We define the critical density radius r_c by $n_e(r_c) = n_c$.

A wave incident normally upon a slab of plasma for which $n_e = n_c$ would penetrate a distance $\lambda/2\pi$ before its

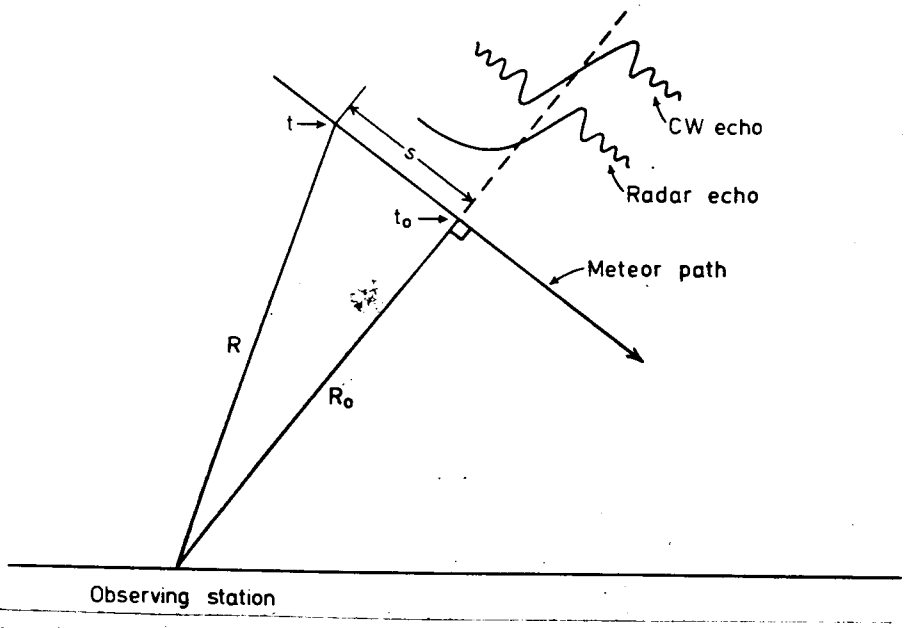

Fig. 3.1. Geometry of specular reflection, with idealized echo waveforms.

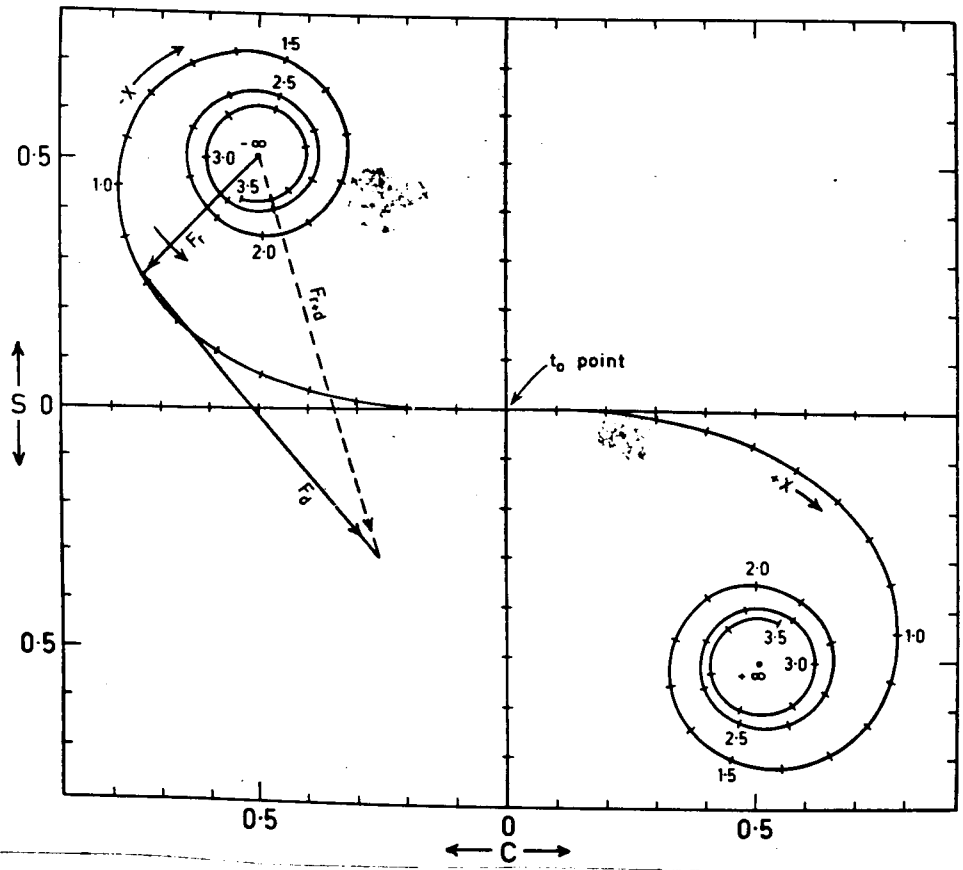

Fig. 3.2. The Cornu spiral applied to radio reflection from a meteor trail.

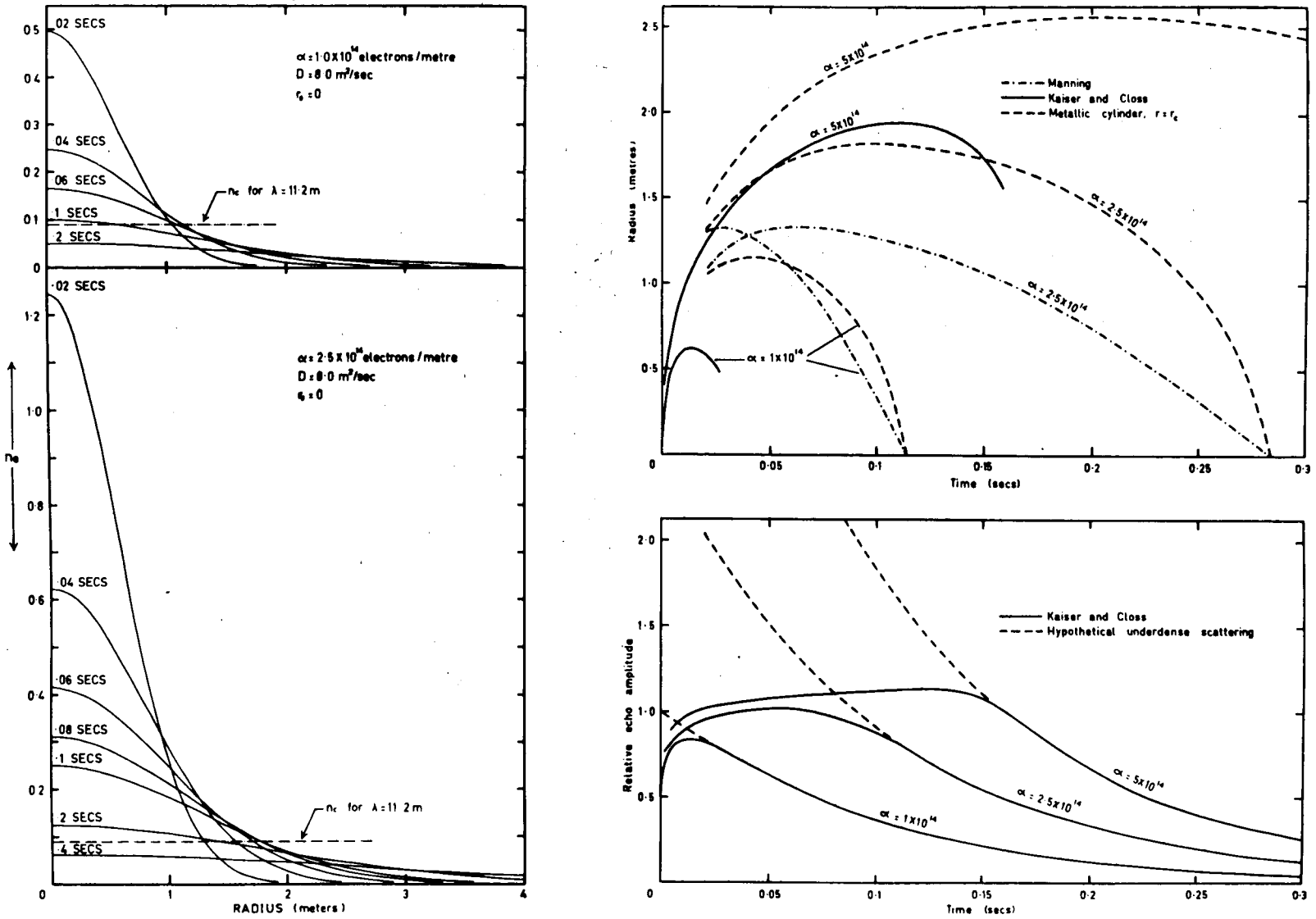

Fig.3.3. Left, electron volume density (units of 10^{14} m^{-3}) in two decaying trails with Gaussian cross-sections, showing critical density n_c. Upper right, time variation of three expressions for radius of an equivalent metallic cylinder. Lower right, time variation of echo amplitude. All curves for wavelength 11·2 m.

amplitude decreased by the factor $1/e$. Hence we may arbitrarily fix a transitional value of α by requiring that when $a^2(t) = (\lambda/2\pi)^2$, then also $r_c^2 = a^2(t)$. Hence

$$\alpha_{tr} = e/4r_e \sim 2{\cdot}4\times10^{14} \text{ electrons/m.} \quad \ldots 3.2.3$$

This value is the same as that used by Kaiser and Closs (1952) in the first unified treatment of both under- and overdense trails of Gaussian cross-section. Their analysis contained approximations which are valid, for underdense trails, if throughout the trail

$$|\kappa(r)(2\pi r/\lambda)^2| \ll 1 \quad \ldots 3.2.4$$

where r is the radial distance of a general point from the axis. The physical assumption leading to 3.2.4 is a restriction on the phase perturbation imparted to the radio wave in reaching the trail axis. For overdense behaviour, the converse of inequality 3.2.4 must hold, and also $\kappa < 0$, over some region within the column. If equality of the left side of 3.2.4 to unity be taken as the transition from one sort of scattering to the other, α_{tr} is again given by Eq. 3.2.3.

Two alternative definitions of the transition point are also in use (Hines and Forsyth 1957 ; Manning and Eshleman 1959). Neither is as satisfactory as that of Kaiser and Closs except in special circumstances. Both lose their justification if r_o is non-zero. Hence we adopt Equation 3.2.3 as the definition of α_{tr} in this thesis.

The basic difficulty in formulating a more precise theory of reflection from trails with $\alpha \sim 10^{14}$ m^{-1} is to avoid imposing a sharp transition line, such as the critical density contour in the metallic-reflection model, within a smooth cross-section. Both Manning (1952, 1963) and Kaiser and Closs have attempted to take into account the influence of the electrons at radii above and below r_c. The former used a ray-tracing treatment to describe the distortion of the incident wavefront outside the critical

region in very large trails. The latter authors, to obtain bridging formulae for the reflection coefficient of slightly overdense trails, assumed that the trail reflects like a metallic cylinder whose radius is the larger of the two values satisfying $\kappa(r)(2\pi r/\lambda)^2 = -1$. That is, they tried to allow for penetration by the wave of narrow regions of over-critical density. Each of these corrections indicates a smaller reflection coefficient, in the range of α to which it applies, than that obtained by replacing the trail with a metallic cylinder of radius r_c. However, the latter over-simplification is still the model in most general use.

We can now find expressions describing the form of the echo received from an overdense trail. From Equations 3.2.1 and 3.2.2,

$$r_c^2 = a^2 \ln(\alpha/\pi n_e a^2)$$
$$= (4Dt+r_o^2) \ln\left(\frac{\alpha\lambda^2 r_e}{\pi^2 (4Dt+r_o^2)}\right) \qquad \ldots 3.2.5$$

The maximum value of this expression is

$$r_{c(max)}^2 = \frac{\alpha\lambda^2 r_e}{\pi^2 \exp(1)} \quad . \qquad \ldots 3.2.6$$

From Kaiser and Closs (1952) it may be deduced that the scattering cross-section of an infinite smooth metallic cylinder of radius r is given by

$$\left.\begin{aligned} \sigma_\perp &= 8\pi^5 R_o r^4/\lambda^5 \ , \ r < \lambda/2\pi \\ \sigma_{//} &= R\lambda/(\pi/2 + 2/\pi.(\ln 1.781\pi r/\lambda)^2) \ , \\ &\qquad r < \lambda/2\pi \end{aligned}\right\} \ldots 3.2.7$$

and $$\left.\sigma_\perp = \sigma_{//} = \pi R_o r \ , \ r \gg \lambda/2\pi\right\}$$

when it is illuminated from a distance R_o by a spherical wavefront. The subscripts $\perp$ and // indicate that the electric vector in the incident wave is respectively perpendicular and parallel to the trail axis. (The scattering cross-section of an object is defined as the projected area of a sphere which re-radiates isotropically all the energy intercepted by it, giving rise to the same back-scattered flux as

that produced by the actual object.) It follows from Eq's. 3.2.6 and 3.2.7 that for $r_c \gg \lambda/2\pi$, the maximum echo power is

$$P_{R(max)} = \frac{P_T G_T G_R}{64\pi^3 \sqrt{e}} (\lambda/R_o)^3 r_e^{\frac{1}{2}} \alpha^{\frac{1}{2}} \quad . \quad \ldots 3.2.8$$

Thus the maximum echo amplitude now varies as $\alpha^{1/4}$, in contrast with its direct proportionality to α for underdense trails.

Many authors have contributed to the literature on reflection from meteor trails without deviating far from the outline given above. Most of the modifications have been concerned either with the forward-scatter mode of reflection, in which receiver and transmitter are widely separated, or with initial radius effects (v. Sect. 3.5).

3.3 Echo decay

This section describes the changes in the echo signal (or its skywave component in a CW system) which result from the radial expansion of the trail. For convenience it is initially assumed that ambipolar diffusion is the only process causing the expansion, and that the trail's initial radius r_o is small compared with the wavelength. Since discussion of resonance phenomena is postponed to Section 3.7, the treatment of underdense trails given here applies to the case of parallel polarization only.

Neglecting attachment and recombination processes is equivalent to assuming that α does not vary with time, at a given point on the trail, although the characteristic radius a of the Gaussian cross-section expands according to 3.2.2, viz. $a^2 = r_o^2 + 4Dt$. Figure 3.3a shows the electron volume density n_e in cross-sections of an underdense ($\alpha = 10^{14}$ m^{-1}) and an overdense trail ($\alpha = 5\times10^{14}$ m^{-1}), to the same scales, at several equal increments of time after the formation of the trails. The value 8 m^2/sec., common in Adelaide echoes,

is used for the ambipolar diffusion coefficient D, and for simplicity r_o is set equal to zero. It is evident from the figure how the critical density radius in the overdense trail first expands rapidly, then varies slowly for most of the echo duration, and finally contracts rapidly and vanishes. Figure 3.3 also illustrates the variation of echo amplitude, critical radius, and Manning's equivalent radius with time, for each trail. For the lifetime of the region of over-critical density in the overdense trail, the echo amplitude formulae of Kaiser and Closs (Eq's. 3.2.7a, 3.2.7c, and 3.2.8) have been used. The final exponential decay of each type of echo arises as follows.

For the underdense trail, and the final "underdense" decay of the larger trail, Herlofson (1948) and later workers (e.g. Eshleman, 1955; Brysk, 1958) have shown that the wavelets scattered from the elements of volume in any short section interfere, causing at time t a reduction in echo amplitude

$$A_R(t)/A_R(0) = \exp(-4\pi^2 a^2/\lambda^2) \qquad \ldots 3.3.1$$

Since a is a function of D, t, and r_o only, D can in principle be calculated for any trail showing this exponential decay. If the trail is initially overdense, it is also theoretically possible to find r_o. Eq. 3.3.1 is exact only for back-scatter, and in the central Fresnel zone. The correction factor to the exponent, if the transmitter-receiver base line subtends an angle γ at the trail, is $\cos^2\gamma$. For the Adelaide equipment the value of γ never exceeds 20°, i.e. $\cos^2\gamma \gtrsim 0{\cdot}9$, and hence the correction has not been applied in this project. Unless α varies fairly violently in or close to the central Fresnel zone, contributions which come from more distant parts of the trail and do not quite follow the relation 3.3.1 will largely cancel (but see Section 4.7).

The diffraction oscillations are short-lived, relative to the expansion-controlled signals from the complete trail, unless diffusion is very rapid. If we neglect these oscillations, the skywave amplitude for an underdense trail has its maximum very close to the time of closest approach of the meteoroid, and is given by

$$\left.\begin{aligned} A_R(t) &= A_R(0)\ \exp(-t/\tau) \\ \tau &= \lambda^2/16\pi^2 D \end{aligned}\right\} \qquad \ldots\ 3.3.2$$

where $A_R(0)$ is found from Eq.3.1.4 .

For an overdense trail the time dependence of A_R is found from the appropriate branch of Eq.3.2.7 in general, or from 3.2.8 in the most usual case, viz. radius exceeding $\lambda/2\pi$. Equation 3.2.5 indicates that the critical density radius vanishes at the time

$$t_{ov} = \alpha\lambda^2 r_e/4\pi^2 D \qquad \ldots\ 3.3.3$$

Thus the overdense echo duration for a given equipment varies directly as α .

The assumptions underlying Manning's equivalent radius estimate make it better applicable to highly overdense trails than to the slightly overdense column in Fig. 3.3 . However, its form is included in the figure for comparison. It should be emphasized that, in a trail to which this correction is appropriate, the exponential decay ordinarily takes such a small fraction of the total duration as to be obscured by other factors.

Many underdense trails exhibit exponential echo decay just as predicted by Eq.3.3.2 . In some cases the exponential form is distorted by resonance, by the effects of non-uniformity of ionization along the trail, or by reflection point movement along the trail due to changes in trail orientation. However, only a few of the shortest-lived overdense echoes (durations $\lesssim$ 10 sec.) have the time dependence suggested by

Eq's. 3.2.5 and 3.3.4 . After a second or two, atmospheric turbulence frequently distorts the trail so that several regions reflect specularly at the same time. The random phase relationships among these skywave components produce beats, often highly irregular, in the amplitude envelope of the resultant signal. Although loss of electrons by attachment (v. Section 2.7) is probably not of great importance for echoes with durations of the order of a minute or less, it is held responsible for the severe reduction of duration observed in very highly ionized trails, relative to the expectation based on ambipolar diffusion alone. McKinley (1961) states, for example, that the echo duration near maximum ionization, for a meteor of magnitude -5 and velocity 40Km/sec., should theoretically exceed three hours with a radar of 10 m. wavelength. In practice such an echo has a typical duration of about 5 minutes, at a height considerably above that of maximum ionization, and persists for a shorter time at the height of maximum ionization.

3.4 The continuous-wave "Doppler beat" from a moving trail

The presence at the receiver of a reference phase signal from the transmitter, in a system of the continuous-wave type, makes it possible to measure variations in the phase of the skywave signal from a meteor trail.This information is valuable in determining the line-of-sight component of the wind acting on the principal Fresnel zone of the trail, and in velocity and turbulence measurements. In this section the form of the received signal in an equipment like that at Adelaide is briefly described, with emphasis on the effect of a steady drift of the whole trail in a uniform wind.

If no meteor echo is present a small signal of essentially constant amplitude and phase reaches the receiving antenna by ground wave propagation. Therefore the receiver output, using a normal diode detector, is a constant non-zero DC voltage. This voltage is closely proportional to

the amplitude of the radio-frequency groundwave input, provided the diode is operated in the linear region of its characteristic. As a meteor trail is formed, we can use the geometry of the Cornu spiral (Fig. 3.2) to visualize the resultant RF signal. During the passage of the meteoroid, the skywave phasor F_r first rotates at a decreasing rate and slowly grows in length, and then increases comparatively rapidly in length as the rotation rate passes through zero. The increased length represents the non-cancelling reflection from the central Fresnel zone, which is of course at a random phase relative to the groundwave F_d. Finally the amplitude and phase of F_r exhibit oscillations of decreasing amplitude and period about the line joining the points $\pm\infty$ on the spiral. If the echo is underdense the length of this line will now contract due to the exponential decay at each height, controlled by the local diffusion coefficient according to Eq.3.3.2 . Hence the resultant signal F_{r+d} eventually decays back to the quiescent groundwave F_d.

Now let a uniform wind whose line-of-sight component is u move the trail bodily away from the observing system. The phase path of the echo signal now increases at the rate of $4\pi u/\lambda$ radians/sec., and F_r rotates relative to F_d at this angular rate. F_{r+d} , the third side of the phasor triangle determined by F_r and F_d, may be found at any instant by solving the triangle. The conventional diode detector takes account only of the amplitude of the signal, i.e. of the length of F_{r+d} , and not its varying phase.

Figure 3.4 is an idealized representation of the form of the diode output for an underdense echo in which the skywave amplitude initially exceeds the groundwave amplitude. The diffraction oscillations are ignored, i.e. the factor $\left[\frac{C^2+S^2}{2}\right]$ in Eq.3.1.5 is set equal to unity at the time of minimum meteoroid range. Because the above explanation can be replaced by an equivalent one in terms of the Doppler shift given to the skywave frequency upon reflection from the moving trail, the characteristic regular beat waveform in Fig. 3.4 is called the "Doppler beat" or "body Doppler". In it, successive minima (or maxima) occur at time intervals of $\lambda/2u$ sec., and the cusped minima facilitate accurate measurement of this interval. Since the turning-points correspond to in-phase

and anti-phase conditions between the groundwave and skywave, RF phase information is conveniently preserved in the Doppler record. The latter, in the Adelaide equipment, is at sub-audio frequencies. Hence the necessary phase comparisons are much simpler than they would be at the actual radio frequency (27 Mc/s).

The locus of the maxima of the Doppler beat, viz. the upper branch of the envelope of the signal, has the same decay time-constant as the decaying skywave signal, given by $\tau = \lambda^2 / 16\pi^2 D$. Note how the locus of the minima, or lower branch of the envelope, if reflected in the horizontal axis when $F_r \geq F_d$, would give the figure symmetry about the quiescent groundwave level GW. In processing the records for amplitude measurement, this reflection is automatically performed in order to use all the early minima of the beat.

Obviously it is not necessary for wind determination that the echo should decay exponentially. However, it is always best to measure the Doppler frequency early in the record because (a) wind shear may progressively increase the frequency, as shown in a later section, and (b) persistent (overdense) echoes frequently contain two or more distinct but fairly similar skywave components, from physically separated reflecting points, whose interference modulates the resultant Doppler frequency and echo envelope.

3.5 Initial trail radius

Two mechanisms, each associated with the radius of the part of the trail immediately behind the meteoroid, combine to reduce the amplitudes of underdense echoes, and the durations of the overdense variety. The extent of the reduction depends strongly on the height of the reflection point. In recent years there has been much controversy as to how severe this attenuation is, and the question is still not completely resolved. We shall now summarize the theory of the attenuation processes, and indicate the approximate trail radii involved. The question of experimental selection possibly arising in the Adelaide data from these causes is discussed later.

We have seen that the total echo amplitude from a fully formed,

smooth, cylindrical trail is roughly half of the contribution from the central Fresnel zone, whose length is $(2R_o\lambda)^{\frac{1}{2}}$. However, this zone is least cylindrical in form at the instant when its formation is just complete and the meteoroid is at its lower end, because its radius at the meteoroid is just the initial radius r_o, whereas the radius at the upper end of the zone is $(r_o^2 + 4Dt_F)^{\frac{1}{2}}$, where $t_F = (2R_o\lambda)^{\frac{1}{2}}/v$ is the time taken to form the zone. At metre wavelengths r_o is essentially constant over the height interval containing the central zone*. The diffusive expansion expressed by the term $4Dt_F$ leads to a conical form for the trail, which would be a truncated paraboloid of revolution* in the limit of vanishing r_o. (At metre wavelengths D also does not vary significantly over the central Fresnel zone). To calculate the total echo amplitude expected from a quasi-paraboloidal trail as a function of time, an involved numerical integration across and along the trail is required. This has been done in various ways (Eshleman 1956; Leowenthal 1956; Hawkins 1956). The results indicate that, to the accuracy warranted by the actual non-uniform ionization profiles, it is adequate to calculate the echo returned from a cylindrical central Fresnel zone with radius equal to the instantaneous radius at the t_o point. The approximation breaks down if the effective reflecting region is shorter than the principal Fresnel zone, as occurs at short wavelengths.

Using Eq. 3.3.1, the attenuation of the signal relative to that from a line distribution of electrons can now be evaluated. The result derived by McKinley (1961) is

$$\text{Loss in dB} \simeq 970R_o^{\frac{1}{2}}D/v\lambda^{3/2} + 343(r_o/\lambda)^2 \quad \ldots 3.5.1$$

For example, a radius $(r_o^2+4Dt_F) = \lambda/2\pi$ at the t_o point produces a loss of about 9 dB, but a radius three times as large produces about 80 dB. It is customary to associate the labels "finite-velocity" or "diffusion" with the first term of the attenuation formula 3.5.1, and "initial radius" with the second.

---

* Figure 8-6 of McKinley (1961) is misleading on these points.

For a given equipment one can estimate the signal loss in dB, and hence the trail radius at the reflection point, which will lead to failure to detect all underdense trails. The increase of D and r_o with height thus imposes a "ceiling" above which underdense trails should not be detectable. It is very hard to predict an exact ceiling level for a given radar, because of the considerable experimental difficulty of measuring D and r_o. For the Adelaide equipment, reference to McKinley (1961) sets the 40 dB attenuation altitude at about 112 ± 5 Km. This is not inconsistent with experiment, but because other effects discussed later also lead to a cutoff at these heights, the ceiling expressed by Equation 3.5.1 may be appreciably higher.

A slightly different approach is to calculate the minimum electron line density necessary to produce an echo of overdense form at a given height. This line density will always exceed the theoretical limit α_{tr} (v. Section 3.2), because the echo from a trail with non-zero r_o is the same as that from a trail of initially zero radius which has expanded for an additional equivalent time t_{eq} prior to t_o. If the overdense core of the latter hypothetical trail would vanish in a time $t_{ov} \leq t_{eq}$, (where t_{ov} is given by Eq.3.3.3), then the actual trail will return only an exponentially decaying signal. The largest values of r_o suggested in the recent controversy lead to the conclusion that all overdense trails below approximately 100 Km. should give detectably overdense-type records with the Adelaide recording system, despite a delay in starting the record which is discussed in Ch. 7. Smaller current r_o values give about 105 Km. for this level.

Vigorous discussion of initial radii to be expected for a given height and meteor velocity followed publication of articles by Greenhow and Hall (1960a,b). These workers measured r_o by means of simultaneous observations of individual trails at 17m. and 8.3m. wavelengths. Unfortunately they could only estimate heights from measurements of D, a most unsatisfactory method. (See Ch. 5 for discussion of the D measurements themselves). However, their results, whose centroid was at about (r_o=1.75 m., D=16 m^2/sec.) for all velocities, agreed roughly with the

prediction of Opik (1958), and have also been supported by results obtained by Kashcheyev and Lebedinets (1963) centred at (r_o=0.8 m., D=6.4 m^2/sec.). The Russian workers differed from the others in claiming that r_o was proportional to the first power of the meteor velocity. They explained the failure of Greenhow and Hall to find such a dependence as being due to insufficient discrimination against echoes with $\alpha \simeq \alpha_{tr}$.

The other school of thought on initial radius values supported Manning's estimate (Eq. 2.6.1), which gives a radius about half as large as Greenhow and Hall's near 105 Km. and a much smaller fraction of their values at lower altitudes. Most of the argument dealt with the consistency or otherwise of each set of radius estimates with various previously reported distributions of reflection point height and meteor velocity. Because of experimental uncertainties in all this supporting evidence, it was difficult to see just what adjustments should have been made in order to reconcile the directly measured values of r_o with theory.

Unfortunately this situation persists to the present day. Subsequent experiments (Greenhow and Watkins 1964; Evans and Brockelman 1963) have used very high power and extremely directive aerials at V.H.F. in efforts to observe only the short region just behind the meteoroid in which the supposed rapid transient expansion occurs. However, the groups mentioned do not even agree whether the meteors observed by Greenhow and Watkins were overdense or not, a point vital to their estimation of r_o in this experiment. Hence the conclusion of their paper, viz. that no rapid expansion process is observable and the initial radius results from early fragmentation alone, is open to question. Thus, too, little weight can be given to the agreement of their initial radius value with the earlier estimate by Greenhow and Hall, since Evans and Brockelman claim that a more correct interpretation of the results of Greenhow and Watkins would yield the value $r_o \sim$ 15 cm. instead of 1.5 m.

3.6 Resonant and geomagnetic effects

We now examine circumstances under which underdense trails do not obey the earlier assumptions that the electrons scatter independently of each other, and as Hertzian dipoles.

The treatment in Section 3.1 of reflection from the underdense trail dealt only with the case of parallel polarization, for which the electric vector of the incident wave is parallel with the trail axis. Herlofson (1951) demonstrated the possibility of plasma resonance for transverse polarization, and examined the details for a trail model in which electron volume density was constant out to some radius and then decreased linearly to zero. If the constant electron density in the interior exceeded the critical value for the radio wavelength, resonance occurred due to the production, by the electric field in the wave, of a net space charge at the trail boundary. The amplitude was controlled by the slope (diffuseness) of the electron density profile at the outer surface, i.e. by the rate of change of dielectric constant with radius in the annulus in which the dielectric constant passed through zero.

The equations set up by Herlofson were solved by Kaiser and Closs (1952) for trail cross-sections of the form $n_e \propto (a/a_o)^s$, where a is radius, with emphasis on the Gaussian case, $s = 2.0$. Whereas Herlofson's model exhibited resonance for a dielectric constant $\kappa = -1$ in the interior, the axial dielectric constant in the Gaussian trail for maximum excitation of the resonance must be -1.4 . Again the resonant enhancement of transversely polarized reflection relative to the parallel case depends on the diffuseness of the boundary, i.e. on the exponent s in this treatment. The maximum value of the ratio $\frac{\text{resonant echo amplitude}}{\text{non-}\quad''\quad\quad''\quad\quad''}$ is 2.0 for the Gaussian cross-section. We shall refer to this ratio as the "polarization ratio". Figure 3.5, which summarizes the relevant results of Kaiser and Closs, shows that the resonance is strongest for trails of small radius and low electron density, in which it must occur very early while a core of highly negative dielectric constant persists (c.f. Fig. 3.3, left). In practice, the rapid expansion to the finite initial radius greatly accelerates the passage of a trail of small line density through this phase, and for all practical purposes resonance is not resolved in echoes from trails with $\alpha \lesssim 10^{12} m^{-1}$.

The theory giving the maximum polarization ratio as 2 has been satisfactorily confirmed by experiment (Billam and Browne, 1956).

Figure 3.5 suggests that resonance can seriously reduce the accur-

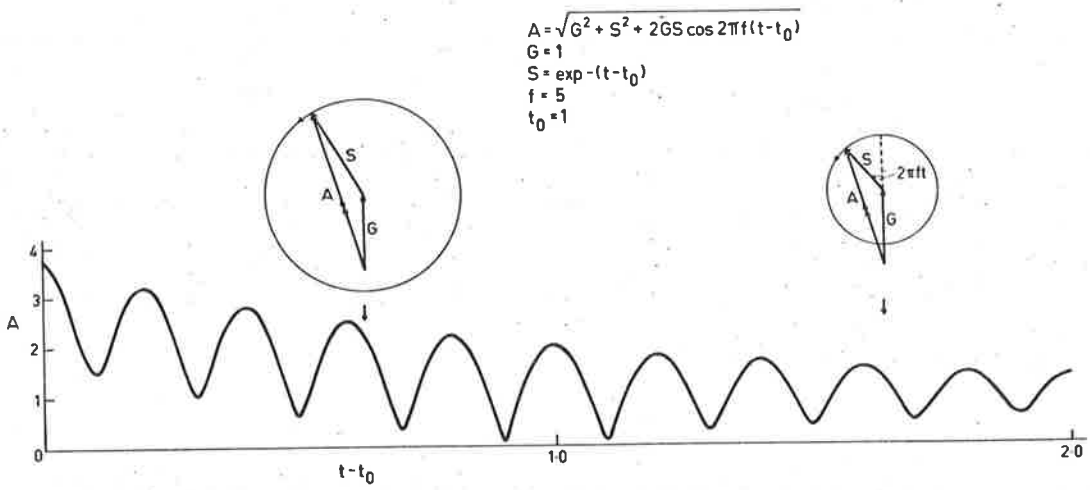

Fig. 3.4. Model of echo received from underdense trail by CW system, showing time variation of echo amplitude A. Doppler frequency f=5c/s; decay time constant = 1 sec; skywave S at first exceeds groundwave G.

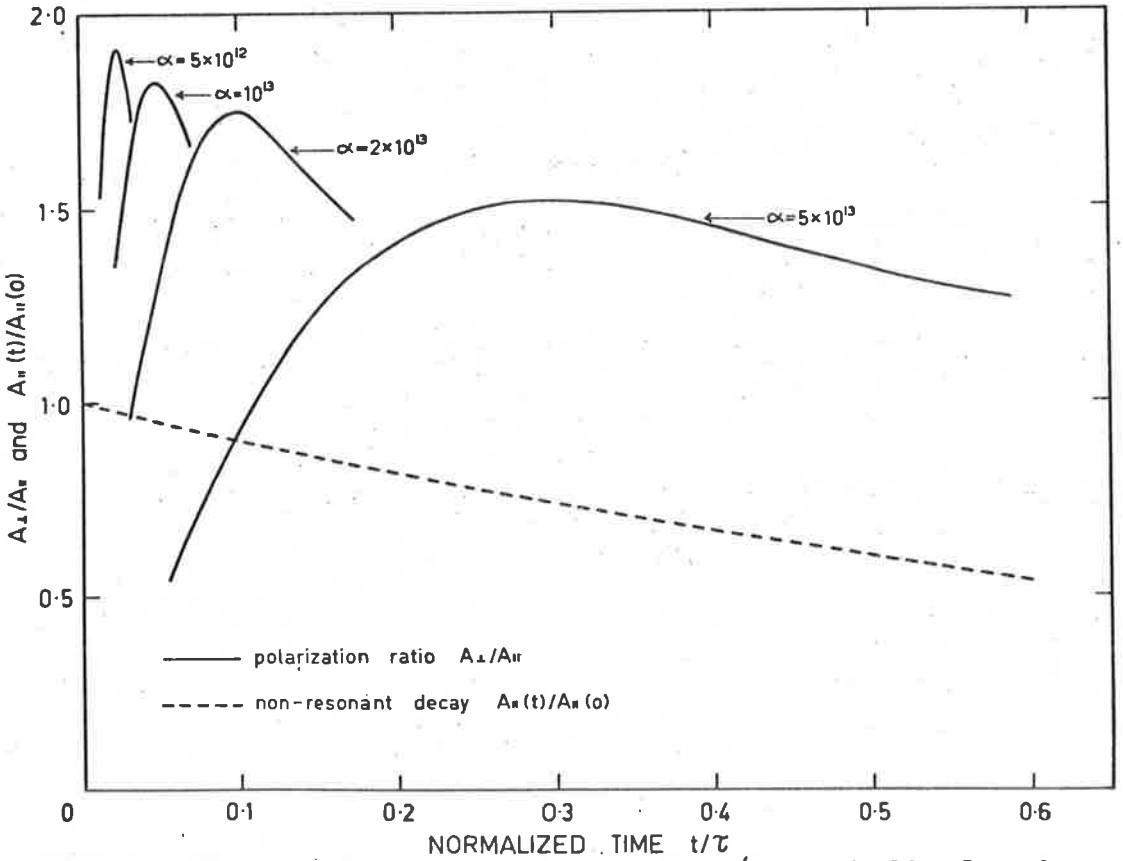

Fig. 3.5. Variation of ratio transverse/longitudinal echo ampl. with time and line density, showing resonance (transverse case) and decay of non-resonant echo (longitudinal case).

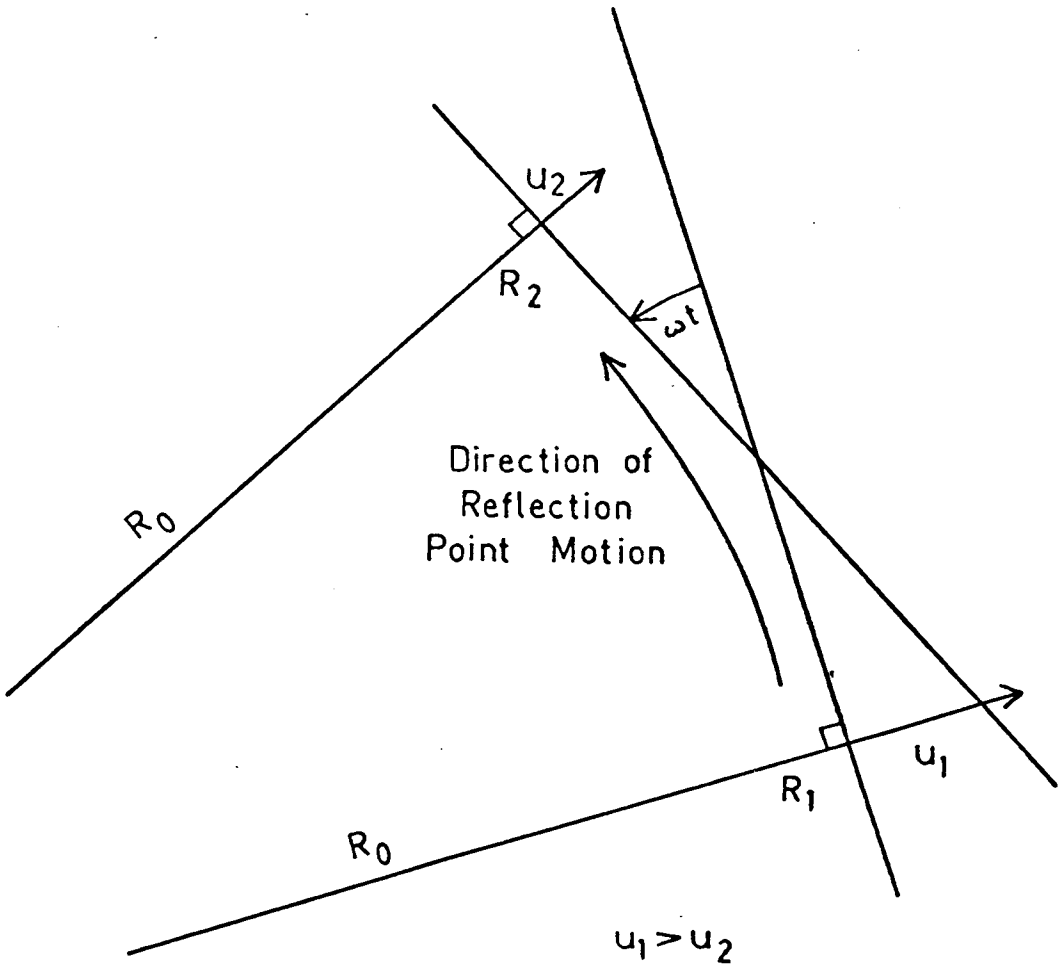

Fig. 3.6. Rotation of trail and consequent motion of specular reflection point in the presence of wind shear (after Roper).

acy of decay time-constant measurements, if not taken into account. It is undesirable in making such measurements to wait until resonance should have subsided, because the likelihood of other errors, due for example to distortion of the trail by winds, increases with time. In very few cases is it possible to determine with certainty the presence or absence of resonance in a given echo waveform by inspection. However, if the necessary geometrical information is available, it is possible to calculate the angle between the electric vector in the transmitted wavefront and the trail axis. This calculation is complicated by the possibility of Faraday rotation of the polarization of the upgoing wave as it traverses the lower E region of the ionosphere. From Burgess (1963) we find that the number of rotations Ω imparted on a one-way trip is given by

$$K\Omega = n_v F \cos\delta \sec Z \quad . \qquad \ldots 3.6.1$$

Here n_v is the total electron content of a 1 cm^2 vertical column, F is the strength of the geomagnetic field (~ 0.6 oersted over Adelaide), δ is the angle between the field and the ray path, Z is the zenith angle of the ray path, and K is a factor which varies as the square of the radio frequency. For 54 Mc/s, K is given as 7.757 c.g.s. units. Using electron content figures from Belrose (1963) and putting

$$\cos\delta \sec Z \sim 1{\cdot}0 \ ,$$

we find values of Ω near 60° for a 27 Mc/s. system at 100 Km. altitude on a quiet day, but less than 10° below 90 Km., or at night for any height.

We must also examine the effect of the earth's magnetic field upon reflection processes at the trail itself. In the last chapter it was stated that the diffusion of the electrons is controlled by the space-charge forces constraining them to occupy very nearly the same volume as the positive ions, so that $D \sim 2D_i$. The coefficient of diffusion of the electrons transversely to a uniform magnetic field is reduced in the ratio $\nu_e^2/(\nu_e^2+\omega_e^2)$, where ω_e is the angular velocity of the gyrating electrons and ν_e is their collision frequency. At about 100 Km. this reduction is such that the electrons alone would naturally diffuse at the same rate as the ions, whence $D \sim D_i$, i.e. a decrease in D by a factor of 2. At greater heights the more slowly diffusing electrons in fact retard the ions, the space charge field being reversed. In general, then, the trail

has an elliptical cross-section, unless it is formed parallel to the magnetic field. In the latter case the trail has radial symmetry, but expands more slowly than if the field were absent.

To the author's knowledge there exists no full rigorous treatment of radio scattering from a trail in a magnetic field. Francey (1964) has examined the special cases in which, if the direction of wave propagation and the magnetic field vector respectively define orthogonal x and z axes, the trail lies along the y axis or the z axis. His argument indicates* that in each of these cases the amplitude decay time-constant is

$$\tau' = \lambda^2 (\nu_e^2 + \omega_e^2)/16\pi^2 D\nu_e^2 \qquad \ldots\ 3.6.1$$

where D is the diffusion coefficient expected in the absence of the field. Further, in the first case where the field and the trail are at right angles, the presence of the magnetic field reduces the back-scattered echo amplitude to the fraction $\nu_e/(\nu_e^2+\omega_e^2)^{\frac{1}{2}}$ of its expected value. There is no such reduction in the second case, where trail and field are parallel, and the theory does not extend to the case of specular reflection from a trail which lies normal to the field when the signal path is parallel to the field. Below 100 Km. neither the time-constant nor the amplitude of the echo will be altered by a factor of more than 2; the largest possible factor is smaller at lower altitudes. The collision frequency ν_e does not change sufficiently rapidly with height to alter significantly the apparent shape of the section of any single trail profile which is observed with the Adelaide equipment, and the scatter in the diffusion coefficient at any height is considerably more than a factor of two. Hence it is not thought that geomagnetic effects can invalidate the results of the present investigation,

3.7 Wind shear and reflection point motion

In this Section, a brief summary is first given of existing theory relating to the motion of the specular reflection point along the trail under conditions of wind shear (Kaiser 1955; Elford 1954). As will be described later, the author has investigated whether the same reflection

---

* The time constants actually given by him are in error by a factor 2.0 .

point motion might account for much of the scatter reported in diffusion coefficient measurements. (The hypothesis seemed particularly attractive because this process, unlike resonance or magnetic effects, could produce dissimilar effects upon the signals from two or more reflection points on a single trail). The extensions of the theory, which are required in order to predict how measurements of the diffusion coefficient will be perturbed by reflection point motion, are developed in the remainder of the Section.

With reference to Section 3.1 and Fig. 3.1, we can visualize the motion of the trail if the wind component in the plane of the figure and normal to the meteor path is u(s), at a general point on the trail situated a distance s from the specular reflection point. It is safe to neglect the perturbation of the meteor trajectory itself due to the wind, but as soon as the meteor has passed the point s the ionization at s is blown away from the meteor's path. In the case of a uniform wind the trail retains its linear form, but lies at an angle ~ u/v to the trajectory, where v is the meteor's velocity.

Kaiser (1955) has integrated an equation corresponding to our Eq. 3.1.2, to find the instantaneous echo amplitude received from the partly formed trail if the line density α is constant along the trail, diffusion is negligible, and $u(s) = u_o + u's$. This is the case of a mean wind plus a constant shear of gradient u'. (We shall always take the wind speed difference in the gradient of a wind shear to be measured at right angles to the trail, and the separation of the points at which the speeds are measured to lie along the trail. Both of these conditions apply to radio meteor work). Kaiser's solution can be written as

$$A_R = (\rho R_e \lambda \Delta P_R / 4(1-\delta))^{\frac{1}{2}} \alpha [C(\nabla)\sin(\phi-\theta) - S(\nabla)\cos(\phi-\theta)] \quad ..3.7.2$$

where $\delta = 2u'R_o/v < 1$,

$$\nabla = \frac{2-\delta}{[R_e\lambda(1-\delta)]^{\frac{1}{2}}} v \left[t - \frac{2u_e R_e}{v^2(2-\delta)} \right] = \frac{2}{(R_o\lambda)^{\frac{1}{2}}} v_a (t-t_a) ,$$

and

$$\theta = \frac{2\pi}{\lambda} \left[u_e t \left(\frac{2-\delta}{1-\delta} \right) - \frac{\delta^2 v^2 t^2}{4(1-\delta)R_e} - \frac{R_e u_o^2}{(1-\delta)v^2} \right]$$

$$= \frac{4\pi}{\lambda} \left(\int u_a(t)dt - R_e \right) - \frac{\pi}{2}\nabla^2$$

As measured from the resulting waveform, t_a, v_a, and u_a are the apparent time of minimum range ("t_o"), meteor velocity, and line-of-sight wind component respectively. The other symbols are the same as in Section 3.1 and in particular C and S are the Fresnel integrals with argument ∇ .

Typically we might have $u' = \pm 10$ m/sec/Km., $v = 40$ Km/sec., $R_o = 150$ Km., giving $\delta \sim \pm 0.1$, and leading to errors of 1% in meteor velocity, and 5% in the time displacement of echoes received at spaced stations. Apparent wind velocity is $u_a \simeq (1 \pm 0.05)u_o - 0.1t$ m/sec. Shear gradients as large as 50 m/sec/Km. are observed, and with the other parameters unaltered would yield $\delta \sim 0.4$, $v_a \sim v(1 \pm 0.05)$, $u_a = 1.4u_o - 4.0t$ m/sec., and $\Delta t = 1.3\Delta t_o$. (In this survey, the wind velocities are uncorrected, and are simply read as early as possible in the echo in order to minimize the time-dependent error term in u_a . However, the time intervals Δt and the meteor velocities are corrected, assuming the shear between any two successive reflection points to be linear).

It is useful now to consider the physical picture of reflection. Neglecting the bodily translation of the trail due to the mean line-of-sight wind u , the effect of a uniform shear u' is to rotate the trail with angular velocity $\omega = u'$. This is illustrated in Fig. 3.6 (after Roper, 1962). To maintain specular reflection, the reflection point will, in time Δt , run along the trail from R_1 to R_2 , a distance of $R_o \Delta t$. The reflection point's speed along the trail is therefore

$$V = R_o u' \qquad \ldots 3.7.3$$

Note that we retain the convention of measuring u positively outwards along the line of sight, and distance s positively along the trail in the direction of meteoroid motion. Thus, in the diagram, $u' = \frac{du}{ds} < 0$ since $u_1 > u_2$, and a positive shear gradient u' will always cause reflection point motion V down the trail. For the typical case above ($u' = 10$m/sec/Km., $R_o = 150$ Km), we obtain $V = 1.5$ Km/sec. from Eq. 3.7.3, while the extreme case $u' = 50$ m/sec/Km. gives $V \sim 7.5$ Km/sec.

Kaiser's theory applies to a uniformly ionized trail whose expansion due to ambipolar diffusion can be neglected. Using the ideas of the last paragraph, we can form a qualitative idea of the echo to be expected

from a non-uniform trail under conditions of wind shear. If the trail is everywhere underdense, the initial amplitude A_o of the echo from a certain point s_o is proportional to the linear electron density α at s_o . The exponential decay $A(s_o,t) = A_o \exp(-t/\tau)$ of this echo is now multiplied by a function P(Vt), where

$$\alpha(s) = \alpha(s_o)P(s-s_o) \quad ,$$

i.e. P describes the form of the ionization profile which is traversed by the moving reflection point. For some trails the profile P is sufficiently smooth that the observed decay is indistinguishable from an exponential, although the decay constant measured is not the value τ due to ambipolar diffusion at s_o . On the other hand, a rapid variation in α over a short region of trail near s_o will render the echo envelope no longer recognizable as an exponential decay. For an overdense trail, the duration of an echo lasting a second or more is obviously determined as much by the profile P and hence reflection point speed V as by the value of α at the t_o point, in view of the large distance which the reflection point can traverse in a second. We can also see how an initially decay-type echo may conceivably change into one of persistent form under the influence of reflection point movement if there is an overdense region somewhere on the trail.

To exemplify the perturbations to be expected in measurements of D due to reflection point motion, consider an underdense trail, with an ionization profile described by $\alpha = \alpha(h)$, which is formed instantaneously at time $t = 0$. This avoids the complication introduced by non-zero values of the angle u/v which exists between trail and trajectory due to the mean wind u , and of the time delay t_a between the instants of minimum range and specular reflection. Let the specular reflection point for given transmitter and receiver locations be at height h when $t = 0$. Then we shall write the skywave amplitude at time t in the form

$$A(h,t) = a_o\, \alpha(h-Vt\cos\chi)\, \exp(-t/\tau(h-Vt\cos\chi)) \quad \ldots\ 3.7.4$$

The factor a_o , describing propagation and scattering, is available from Eq's. 3.7.2 or 3.1.4, and is taken not to vary significantly over the part of the trail considered. As usual, $\tau(h) = \lambda^2/16\pi^2 D(h)$. The plain

brackets above and in the remainder of this section imply functional dependence, not multiplication.

The reduction of experimental data is done by fitting, to a sequence of samples of A taken in the time interval (t_1, t_2), a curve describing an exponential decay with time. In general, not every sample of A will lie on the fitted curve, and indeed none need do so if there are more than three samples. However, any valid fitting process will lead to two or more (possibly coincident) intersections of the fitted line and the true envelope function A(h,t). These points of equality, of course, do not necessarily coincide with the samples. Let such intersections occur at times t_3 and t_4 within the interval (t_1, t_2), and write the fitted exponential, similarly to 3.7.4, as

$$B(h,t) = B(h,0)\ \exp(-t/T) \qquad \ldots\ 3.7.5$$

Then we have

$$B(h,t_3) = B(h,0)\ \exp(-t_3/T) = A(h,t_3)$$

and similar equations at time t_4, so that B(h,0) and T are defined by $B(h,0) = A(h,t_3)\ \exp(t_3/T) = A(h,t_4)\ \exp(t_4/T)$ ... 3.7.6

Then from Eq. 3.7.4,

$$\frac{A(h,t_4)}{A(h,t_3)} = \frac{\alpha(h-Vt_4\cos x)}{(h-Vt_3\cos x)}\ \exp\left(\frac{t_3}{\tau(h-Vt_3\cos x)} - \frac{t_4}{\tau(h-Vt_4\cos x)}\right) \cdot$$

$$\approx \left[1 - \frac{V[t_4-t_3]\cos x\,\frac{d}{dh}\alpha(h-Vt_5\cos x)}{\alpha(h-Vt_5\cos x)}\right] \cdot$$

$$\cdot \exp\left(\frac{t_3-t_4}{\tau(h-Vt_5\cos x)}\right) \qquad \ldots\ 3.7.7$$

where $t_5 = (t_3+t_4)/2$. This sort of approximation, less precise for D than α , is appropriate because past measurements of D indicate that its height dependence, if smooth, is probably associated with a scale height greater than the

pressure scale height. By contrast, even the evaporation profile varies everywhere more rapidly than the local pressure. Equation 3.7.7 can be thought of as a statement that the measurements made on the echo waveform apply best to the instant t_5 and the height $(h-Vt_5\cos x)$, which correspond to the centre of the observing period.

Combining Eq's. 3.7.6 and 3.7.7, and writing X for the factor enclosed in square brackets in 3.7.7, we obtain

$$\exp\left(\frac{t_3-t_4}{T}\right) = X \exp\left(\frac{t_3-t_4}{\tau(h-Vt_5\cos x)}\right) .$$

Hence $$\tau(h-Vt_5\cos x) = \frac{t_4-t_3}{\ln X + [t_4-t_3]/T} \qquad \ldots 3.7.8$$

Thus we have found a corrected value for the time-constant, at a certain height within the range traversed by the moving reflection point. To find this value, X must be evaluated, which in turn requires $\frac{1}{\alpha}\frac{d\alpha}{dh}$ to be known at the same height. Given this information, the definitions 3.7.4 and 3.7.6 lead to

$$A(h,t_5) = B(h,0)\, e^{-t_5/T}$$
$$= A(h-Vt_5\cos x\ ,0)\ \exp\left(\frac{-t_5}{\tau(h-Vt_5\cos x)}\right)$$

whence $$A(h-Vt_5\cos x\ ,0) = B(h,0)\ \exp\left(-\frac{t_5}{T} + \frac{t_5}{\tau(h-Vt_5\cos x)}\right) \qquad \ldots 3.7.9$$

The value of line density α at the height $(h-Vt_5\cos x)$ can now be found from the echo amplitude given by 3.7.9, using the propagation constant a_0 from Eq. 3.7.4. In practice, the corrections should be made as the exponential 3.7.5 is being fitted, so that t_3 and t_4 are readily estimated. (Unfortunately the corrections were not developed by the author until after the fitting process was complete for all the data, and hence the times of the first and last data points in the decay phase of the echo were used for t_3 and t_4 respectively. Details of the estimation of $\frac{1}{\alpha}\frac{d\alpha}{dh}$ are given in Chapter 7).

In summary, the turbulent motions at meteor heights produce significant differences in the winds measured at spaced reflection points on a single trail. If this wind shear is assumed to be constant along the trail, its effects on t_o point spacing, Doppler beat frequencies, and apparent meteor velocity can be allowed for by the use of established theory. A constant shear causes the trail to rotate as a whole, and, to maintain specular geometry, the reflection points move along the trail. They traverse a generally non-constant profile of electron density. Echo amplitudes therefore vary with time according to the profile shape, in addition to their decay as imposed by the local ambipolar diffusion coefficient. We have shown that approximate corrections to the measured diffusion coefficients and initial echo amplitudes are possible.

A distinction should now be made between this mechanism of reflection point movement and the mechanism suggested by Rao and Armstrong (1958). The latter theory was meant to account for the anomalous durations of echoes from certain overdense trails. It postulated a trail which, by the combined action of turbulence and initial small-scale irregularities in ionization, was able to behave as an efficient non-specular reflector soon after its formation. For such a trail it was shown that although reflection might be at first largely specular, after some few seconds the strongest remaining scattering region would be at a height h_1 determined by the electron density profile and the increase of ambipolar diffusion coefficient with height. Therefore if the original (and, at first, specular) reflection point was not at the level h_1, it would appear to move towards h_1. Hence the durations of echoes from points originally located anywhere on the trail would be essentially the duration appro-priate for height h_1. Evidently neither the mechanism, nor the class of echoes to which the theory applies, nor the time scale involved are the same as in the theory put forward in this Section.

With the "glint" theory (Ellyett 1950; Manning 1959) there is no such difference in principle. The "glint" theory of the amplitude fading seen in long-duration echoes is that the presence of wind shear can cause the ionized trail to become curved and hence to undulate about the

trajectory of the meteoroid. Therefore there will usually be just such a movement of the specular reflection point as the author has considered, to a nearby region which, after the passage of a short time, has become properly oriented to reflect specularly at the expense of the original reflecting region. The term "glints" refers to the fact that after an initial delay, more distant parts of the trail may also be rotated into normality with the line of sight from the radar, giving rise to multiple reflections. Thus this approach differs from the author's only in concentrating on times of order half a second or more after trail formation.

CHAPTER 4

REVIEW OF TRAIL PROFILE MEASUREMENTS AND ANALYSIS

In this chapter a critical review is made of those experiments, using both photographic and radio methods, which have yielded significant information about the height profiles of brightness and electron density in meteor trails. The aim is to establish a basis for later comparison with the results presented in this thesis.

4.1 Photographic observations and their analysis

There are strong contrasts between radio and photographic observations of meteor trail structure. In the first place, optical methods record light from the immediate vicinity of the meteoroid only, whereas the ionization causing a radio reflection remains detectable for some time after the passage of the meteoroid. Persistent luminous trails are rare. Secondly, the precision of light intensity measurements from a photographic plate is considerably better than that of echo power determinations. The latter are complicated by aerial gain uncertainies, and their interpretation in terms of electron density in the trail rests on the rather naïve theory given in Chapter 3. Perhaps the most important practical distinction is that the field of view and exposure time in a photographic experiment are arranged to record the whole luminous history of the meteor, but radio experiments in general are essentially sampling techniques, because of the specular reflection requirement. For a given trail, transmitter, and receiver, this condition weights very heavily the information returned from a unique short region of the trail, namely the central Fresnel zone.

Because of these contrasts, the data from the two categories of experiments are complementary. For comparison with the present results, both sources have been used impartially, relying on the fairly close proportionality between brightness and electron density, along most of a trail, to which attention has already been drawn.

The concept of the fragile dust-ball meteoroid was originally developed to explain the extremely short light-curves of the Giacobinid

(Draconid) meteors, photographed in 1946 (Jacchia, Kopal and Millman 1950). The light-curves of Figure 2.3 exemplify the typical "flare" fragmentation of bright meteors, and the smooth rise of brightness, adhering closely to the theoretical curve, which generally precedes any flares. In Figure 4.1 are illustrated the results of an examination of 360 fainter meteors recorded on Super-Schmidt photographs (Hawkins and Southworth 1958). Many of these were as faint as second or third magnitude. For each meteor two points are plotted in Figure 4.1, at the heights of the beginning and end of the detectable part of the trail (relative to the height of maximum light). The other co-ordinate of each point is the difference in magnitude between that terminal of the trail and the brightest point. Almost every observation falls inside the theoretical evaporation-theory curve, which is also plotted. A notable difference between these meteors and brighter ones such as in Figure 2.3 lies in the strong tendency towards irregularities in the early part of the light curves of the Super-Schmidt meteors. Here, then, is strong evidence for fragmentation, and for a trend to more complete break-up early in flight in the case of the smaller meteoroids.

It is customary to operate meteor cameras with a rapidly-rotating shutter disc in front of the lens. Further evidence for fragmentation into numerous small particles lies in the fairly general blurring of the ends of the low-altitude segments of the resulting images, due to slight velocity differences among individual fragments.

The data for the sporadics observed by Hawkins and Southworth were further analyzed by Weiss (1960). He was able to show that the relation between brightness and velocity was incompatible with the evaporation theory, either in the simple form of Equation 2.4.3 or in a form modified by him to allow for a linear gradient of scale height with height. He went on to predict, on the basis of the photographic data, what height distribution should have been followed by some smaller (sixth magnitude) sporadic meteors observed by Evans (1954), using radio equipment. The experimental radio height distribution was significantly narrower than predicted. It also fitted the evaporation theory better than the photographic meteors had

Hence, once again, the scatter attributable to fragmentation was seen to differ in degree between groups of meteors of differing mean mass. The difference could have been interpreted as one of physical structure. If so, the closer approach of the smaller meteoroids to the predictions of the evaporation theory would have implied that they behaved essentially as solid particles. However, the explanation preferred by Weiss postulated identical physical structures, differing only in the number of their constituent particles. On this basis the fragmentation of a small meteoroid, with relatively few particles, would be completed at an earlier point on the flight path through the atmosphere than the crumbling of a large meteoroid. The extension of radar studies of fragmentation to still fainter meteors has lent support to this view (v. section 4.5).

Greenhow and Hall (1960a) made a similar comparison to that given by Weiss, between the same photographic data and a radio height distribution, which was again for sporadic meteors of $\sim+6$ average magnitude. Extrapolating the photographic results in magnitude, Greenhow and Hall noted that the radio meteors were detected at levels which fell increasingly lower than the extrapolated heights with increasing velocity. Their interpretation was that all radio-derived height distributions are distorted from the "true" form (which holds for photographic observations) by the attenuation occurring at the higher altitudes due to non-zero initial trail radius. While this effect undoubtedly exists, it is generally considered that Greenhow and Hall overstated their claim that it invalidated most previous deductions from distributions of reflection point heights.

Some attention should be given here to two other commentators on the light curve data, Ananthakrishnan (1961, 1962) and Levin (1962, 1963). Both of these workers made ad hoc modifications to the evaporation theory which shortened the theoretical light curve and gave a rather better fit to the data points of Figure 4.1 <u>below</u> h_{max}. (Recall that an exact calculation of the evaporation profile gives a still <u>longer</u> region below h_{max} than does the approximate profile, taken as a starting point by both workers). The remaining irregularities above

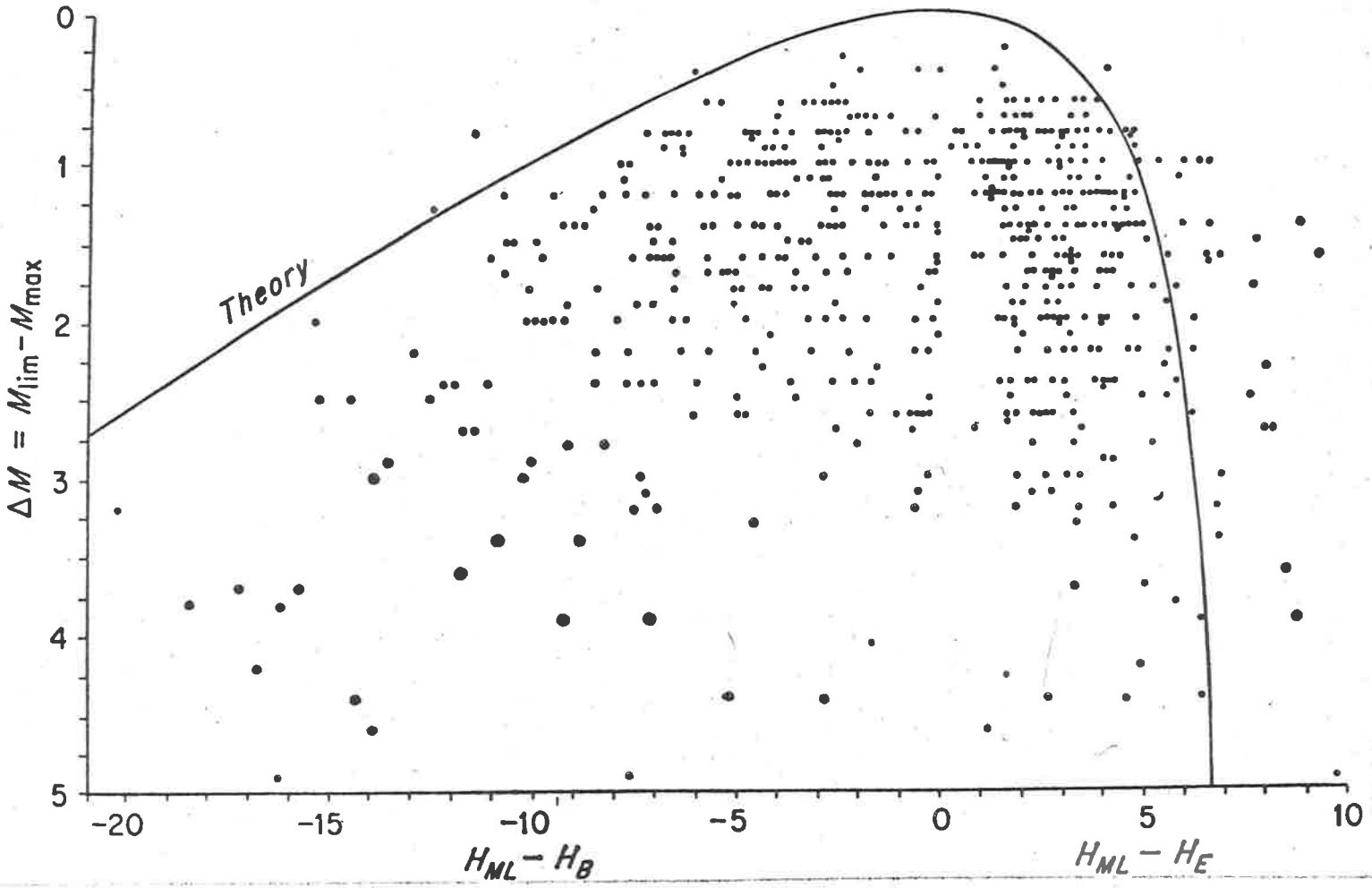

Figure 4.1. Beginning and ending heights of light curves for 360 Super-Schmidt meteors (Hawkins and Southworth 1958).

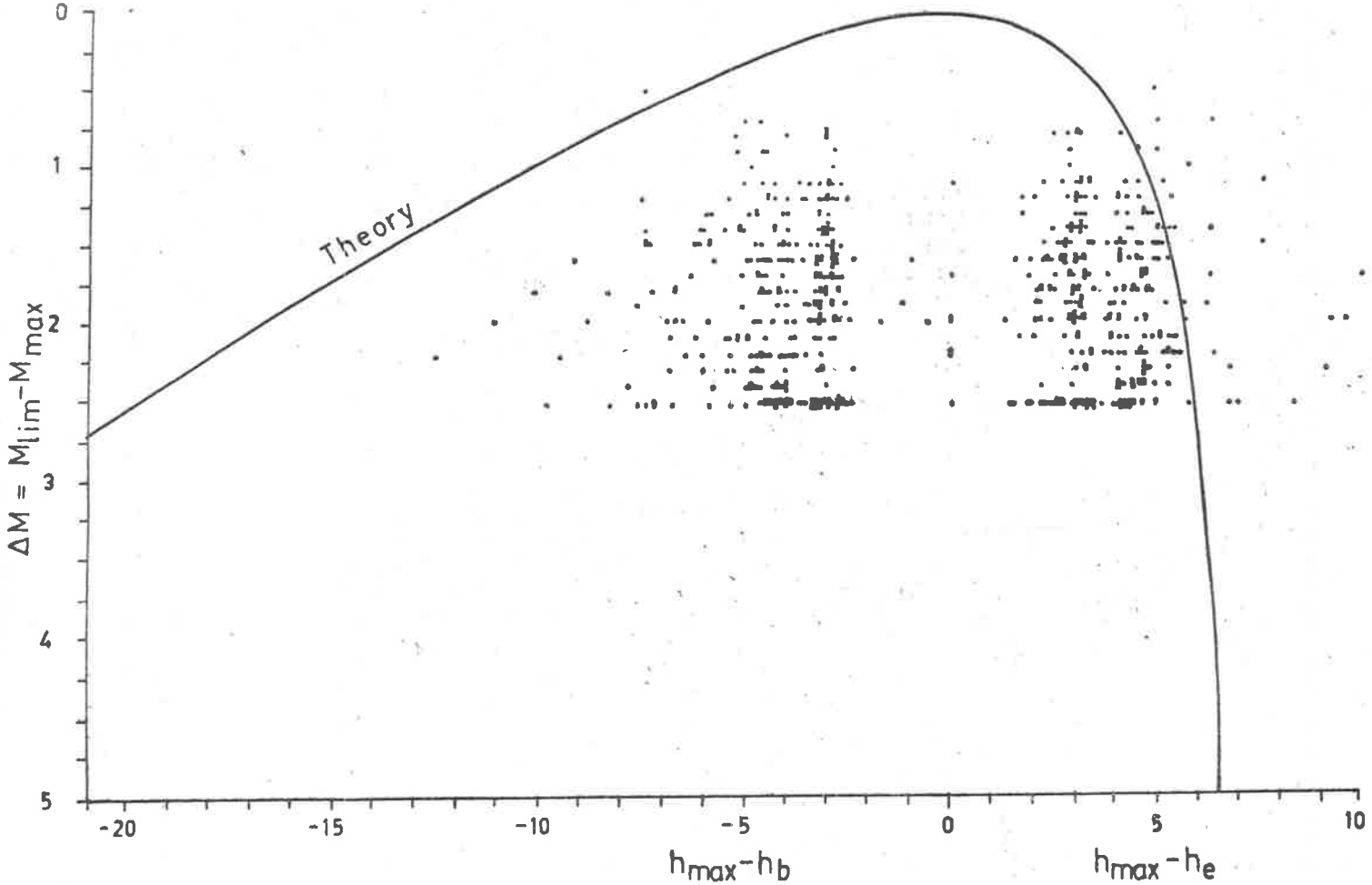

Figure 4.2 Beginning and ending heights of parabolic ionization profiles fitted to data for 320 radio meteors (Hawkins and Southworth 1963); for comparison with Figure 4.1.

h_{max} were taken to result from fragmentation. One is inclined to question whether the upper part of the evaporation profile could not be arbitrarily shortened in like manner, and on equally slender physical grounds, to bring the profile closer to the beginnings of the trails.

Using the unmodified theory, and mass estimates supplied by Hawkins and Southworth, Levin claimed also to have found a remarkably good correlation among mass, magnitude, and a simple index of the shape of the light curve. The correlation is indeed good, provided the original mass estimates were not in fact made on the basis of magnitude and a similar trail shape index.

4.2 Medium frequency radar methods

To the author's knowledge only three radio experiments, other than the present investigation, have been conducted at medium frequencies to gather direct information about ionization profiles. By "direct" is meant information which at least partly describes the profiles of individual trails. These three experiments, and an earlier, less direct, but nevertheless pertinent investigation, are described below.

The "indirect" method was that of Manning, Villard and Peterson (1953). These workers operated two continuous-wave Doppler equipments separated by 100 Km., and studied the simultaneous detection of meteors by both stations. A "coincidence" was defined to occur when specular echoes were recorded at both stations in a short time interval of suitably chosen length. The numbers of experimental coincidences, expressed as a function of the difference in the times of appearance for each echo pair, were compared with the numbers of coincidences expected to arise by

chance alone. Only time intervals of 0.4 sec. or less gave a significant excess of coincidences over the expectation for chance events. The excess varied from 25% to 45% for various time interval values below 0.4 sec., and the total number of significant excess coincidences was approximately 4% of the total number of usable echoes at either station. That is, approximately one in every 24 meteors producing an acceptable echo at one station also produced such an echo at the other.

Because individual meteor velocities and trail directions were not measured, it was necessary to make statistical assumptions about these quantities in deriving the distribution of reflection point spacings. The assumptions were that the radiants of the meteors were uniformly distributed across the sky, and that the mean velocity was 50 Km/sec. The latter figure is at least 10, and probably 15Km/sec., too high. Numerous workers (e.g. Weiss, 1959) have since shown that the first assumption of a uniform radiant distribution is also far from correct, but its effect on this analysis is uncertain. The conclusions were expressed in the form of a curve indicating the relative probabilities of occurrence of trails of various lengths. Because of the spread of velocities about the mean, the breadth of the curve as presented (approximately $\pm$18Km. to points of half peak probability) is not very significant. The most probable trail length was found to be 28Km. If the above comment on mean velocity is correct, this length becomes instead approximately 20Km.

Eshleman (1957) presented a theoretical discussion of the probable distribution of meteor trail lengths, showing that the most likely (modal) trail length is 12 sec x Km. for sporadic meteors whose radiant is at zenith angle x. This theory, which was based on the evaporation model of the ablation processes, gave a predicted curve of trail length versus frequency of occurrence whose agreement with the experimental curve of Manning et al. was quite good. Eshleman commented that the agreement was evidence against the application of the then recently proposed theory of fragmentation to the faint meteors ($M \approx +5$) involved in the experiment, since fragmentation would make the most probable trail length considerably less than 12 sec x Km. Conversely, when correction is made to the mean velocity estimate used by Manning et al.,

the results indicate that the observed trails were significantly shorter than if evaporation had been the sole ablative process.

Greenhow and Neufeld (1957) used an entirely different experimental arrangement from that of Manning, Villard and Peterson, with a single pulsed transmitter on 36 Mc/s, one receiver at the transmitting site, and second receiver 20 Km. away. The transmitting array was directed at 45° to the horizontal over the distant station, and had a bandwidth of $\pm 25^{\circ}$ to the first zero of the main beam. No information on minor lobes was given, other than that timing (range) measurements were used to reject echoes from outside the main beam. In earlier use of the same equipment Greenhow (1954) inferred the angle of elevation E of the reflection point from the recorded range, assuming the reflection point to lie at the mean altitude found by other methods, viz. 92.5 Km. Apparently the same method was applied in the experiment under review. Velocity v was inferred from the rate of increase in echo amplitude as the meteor crossed the central Fresnel zone, or, in the case of very slow meteors, from the post-t_o diffraction fluctuations.

The height difference of each pair of reflection points was used in the analysis in preference to their spacing vt measured along the trail. t is the time interval between the appearances of the echo at the two stations. For a meteor whose path is in the vertical plane containing both stations, it can be shown that the height difference Δh is given approximately by $\Delta h \simeq (v^2 t^2 \cot E)/l$ . ... 4.2.1 where l is one-half the distance separating the stations. It is by no means obvious how accurately this expression represents the general case of a meteor whose path makes a non-zero angle with the vertical plane through the stations. In comparing the results of this work and the author's (Chapter 8), we shall return to the topic of these height difference measurements and their accuracy.

The largest and smallest observable values of the ratio

$$r = \frac{\text{echo amplitude at upper reflection point}}{\text{echo amplitude at lower reflection point}}$$

were limited by the signal-to-noise amplitude ratio S/N at which the weaker echo could be reliably detected, and consequently by the decrease, with increasing r, in the frequency of occurrence of meteors

whose stronger echo was of amplitude r.S/N or greater. Meteors were analyzed in two main classes which differed in the signal-to-noise ratios required of the echoes, and hence in the bounds imposed upon r. Echo pairs for which 4.2.1 gave height differences Δh smaller than a certain (unstated) value were not used. The minimum spacing required appears to have been approximately $\Delta h = 3$ Km., and an upper limit of 5 Km. was set by the geometry of detection. Of the remaining echo pairs, 75% fell in the range $3.92 \text{ Km.} \leq \Delta h \leq 4.07 \text{ Km.}$ and hence comparison with the evaporation theory was made using $\Delta h = 0.6H \simeq 4$ Km. We shall require these details later.

Where a meteor trail returned a detectable echo to only one station, only an upper or a lower bound to the true value of r could be found. This was still useful. In the few cases where very large or very small ratios were actually measurable, Δh was again approximately 4 Km., and this allowed single-station echoes to be included in the results.

Using a graphical method, Greenhow and Neufeld estimated the distribution of values of r to be expected if all meteors obeyed the evaporation theory. There was considerable discrepancy with their experimental distribution of r. Therefore a model profile was synthesized, which reproduced the experimental distribution very well. This profile, together with the evaporation profile and two which represent the photographic results discussed previously, is shown in Figure 8.10.

As one might expect from the photographic evidence discussed earlier in this chapter, the most notable failure of the evaporation theory was in the region above the height of maximum ionization, i.e. where $r \ll 1$. With a reflection point spacing of 0.6H, no values of r smaller than 0.56 can possibly be obtained from trails obeying this theory, whereas ratios as low as 0.1 were both observed and also predicted using the empirical profile. The physical meaning of these low ratios is, of course, that many trails exhibited a much greater rate of increase of ionization before α_{max} than expected, with experimental rates of increase up to five times the theoretical rate being observed. Even more rapid rates of increase could be inferred in cases where a trail was underdense ($\alpha \simeq 10^{14}$/m) at the upper reflection point and definitely overdense ($\alpha > 10^{15}$/m) only a few kilometres below at the

other reflection point, or in cases where the diffraction patterns indicated an absence of ionization in the central Fresnel zone of the higher reflecting region. In one instance of the latter kind a rise in α from zero to maximum in a trail length $vt < 800m$. was noted.

The aim of Greenhow and Neufeld was to show that actual trail profiles are generally shorter, with more abrupt commencements, than the evaporation theory predicts. In this they succeeded. Later it is suggested that, in fact, they erred on the side of caution, and over-estimated the height extent of their "mean profile".

A second equipment which has given data on individual trail profiles, the system operated in collaboration by Harvard College Observatory and Smithsonian Astrophysical Observatory, is noteworthy for generating power of order 2 MW. at the relatively low frequency of 41 Mc/sec. Because the cutoff due to finite trail radius is much less severe at this frequency than in the V.H.F. range (120 Mc/sec. or more) in which other high-power transmitters have operated, the Harvard system can detect meteors as faint as magnitude +9.7 on the photographic scale. A total of 6 spaced receiving stations, one of which is at the transmitter site, pick up echoes from up to 6 distinct points spaced along a meteor trail. From this set of data the velocity, orbit, deceleration, and at least a segment of the ionization profile can be determined for a suitable meteor. A general description of the equipment, and some early results, have been given by Hawkins (1963), and detailed information on various aspects of the continuing research has appeared largely in reports intended for restricted circulation, e.g. Hawkins and Southworth(1963).

The latter report and that of Verniani and Hawkins (1965) are those which deal most directly with the topic of the ionization profiles of the trails formed by these small meteors. In them use is made of the results from some 320 radio meteors for which heights could be found and for which the observational data have been fully reduced. In Figure 4.2 the author has plotted profile data for these meteors in the same format as Figure 4.1, which illustrates the behaviour of a random sample of Super-Schmidt meteors with average magnitude +1.5 (Hawkins and Southworth, 1958). The equivalent peak photographic magnitude for the radio

meteors ranged from +6.8 to +9.7 (Verniani and Hawkins, 1965), with the mean value +8.05. Slight differences in trail length between the two figures can be discerned, together with some asymmetry about h_{max} in the radio meteors; these differences receive attention in a later chapter.

Whereas the beginning, maximum and ending heights are all readily determined in the photographic case, the set of reflection points on a given trail in the radar case does not necessarily enclose all (or any) of these three heights. For each meteor an inverted parabolic profile is fitted to the individual electron line-density values, and where necessary the fitted profile is extrapolated to give estimated values for any of the three height parameters which may be missing. This procedure is concluded by the removal of parts of the parabola which specify large numbers of electrons outside the range of the observations. The last step is the only one capable of causing any asymmetry in the fitted profile. Such asymmetry may achieve an improved fit to the actual profile, or it may arise purely as a consequence of the reflection geometry and thereby fail to represent adequately the true profile shape. Clearly, useful information could be derived from a more detailed study of the individual profiles observed with the Harvard equipment.

The third medium-frequency method for directly obtaining information about individual trail profiles was different in several ways from those already described. It was described by Rice and Forsyth (1964). A minor point of difference lay in the use of forward, rather than backscatter geometry. The chief novelty, however, was as follows.

Although data taken from a meteor echo waveform are often assumed to represent the central Fresnel zone only, the "diffraction" fluctuations in fact arise from the sequential addition of Fresnel zones to the head of the ionized trail, and therefore convey information about parts of the trail which may be quite remote from the point of specular reflection. Rice and Forsyth demonstrated that, with care, the incremental echo amplitude due to the segment of trail just behind the meteoroid can be recovered as a function of time from the diffraction waveform, in addition to the meteoroid's position coordinate. That is, local elect-

ron density can be found as well as instantaneous meteoroid velocity. As shown in Section 3.1, the Cornu spiral can be used to represent the manner in which the total echo amplitude, at any instant during trail formation, is built up as the integral of amplitude-and phase-varying reflected signals from all the trail elements formed prior to that instant. By recording both phase and amplitude information, these workers were able to reconstruct the "Cornu" spiral for three echoes, which were chosen for good signal-to-noise ratio and for exponential decay of total amplitude. The lengths of the sections of these spirals which corresponded to equal successive increments of time were plotted against time, yielding curves which could be immediately interpreted as depicting the ionization profiles.

The electron density profiles thus derived were of uncertain extent in height or in distance along the trail, since the range and geometry of detection were not known. It was possible, however, to locate the Fresnel zones relative to the profiles by further measurements on the Cornu spirals. Consideration of possible Fresnel zone lengths and meteor velocities indicated that the measured sections of the trails were in the range from 5 to 25 Km. in length. The complete trails were approximately twice as long.

A most striking feature of all three profiles was their extreme irregularity. Each one showed, superimposed on a reasonably convex overall profile, quasi-periodic fluctuations with depths of order 50% of the background electron line density, and with typical spacing along the trail such that several fluctuations occurred in the half-length of the principal Fresnel zone. Despite the indifferent signal-to-noise ratio in the published records, only the smallest of the fluctuations appear capable of having resulted from noise.

4.3 VHF radar methods

There are two experiments to be described in completing this review of earlier work. They are those of Evans and Brockelman (1963) and Greenhow and Watkins (1964), to whom we shall refer as E&B and G&W for brevity. Both were conducted at frequencies in the VHF range.

G&W simultaneously operated a medium-frequency radar to find the line density in trails giving VHF echoes. Their VHF detection rate was much smaller than that obtained by E&B, due partly to lower peak transmitter power, and partly to non-optimum VHF beam elevation, chosen to reduce the effects of ground reflections on their medium-frequency polar diagram.

At VHF the aspect sensitivity of the reflection process is lessened because the effects of rapid initial expansion and finite meteoroid velocity, summed up in Eq. 3.5.1, greatly shorten the length of trail which is able at any moment to reflect these short-wavelength signals at a detectable level. From their results G&W estimated this scattering region to be about 50 meters long, and E&B found the same figure for meteors of velocity 10 to 20 Km/sec., with a reduction to 8 m. scattering length for the 40-80 Km/sec. velocity group. Thus, even at the lowest velocities, successive pulses at intervals of 16 or 20 msec. would have been reflected from non-overlapping sections of the trail. Hence it is interesting to compare the discussion by E&B of pulse-amplitude - time envelopes with the evidence of Rice and Forsyth indicating irregular ionization over small height intervals. Of 681 VHF records examined by E&B, 58% had envelopes (i.e. ionization profiles) approximately Gaussian in character; 27% showed "broken" profiles made up of several or many resolvable peaks; and in 15%, termed "scintillating", there was little correlation in amplitude from pulse to pulse. This scintillating behaviour, similar to that seen at longer wavelengths, was as usual put down to the interference of reflections from two distinct scattering centres, which, it is important to note, must in this context have been separate meteoroid fragments. The broken profiles can presumably be linked with those noted by Rice and Forsyth, thus providing useful confirmation of the existence of rapid fluctuations in the rate of production of ionization. This concept is further discussed from the point of view of its effect on measurements of diffusion coefficient in the next chapter. At this stage we may accept these rough trails as evidence of the nature of fragmentation in some meteors.

In regard to overall profile lengths, both pairs of workers were

In reasonable agreement. G&W gave a mean distance of 3 Km. between half-maximum-ionization points, and E&B estimated a mean length of 6 to7 Km. depending on velocity. On considering the Harvard radio results for trails of peak magnitude ≃ +9 in Figure 4.2 (remembering that an interval of 2.5 magnitudes is equivalent to a factor of 2 in line density) it can be seen that most trails extended over 5 - 10 Km. between half-maximum points. This is slightly less than was found for the Harvard Schmidt meteors (M ≃ +3), shown in Figure 4.1; we note that the VHF experiments suggest that trails at magnitudes +5 to +8 are slightly shorter again. (E&B disagree with G&W in estimating the ranges of magnitude covered by their respective experiments, but the range +5 - +8 probably includes both sets of data). By contrast, the work of Greenhow and Neufeld (1957) gave a typical height differential of 13 Km. between points of half maximum ionization, for meteors of about sixth magnitude. The earliest and least conclusive results (Manning, Villard and Peterson 1953) indicated still longer trails to be the rule.

Certain of these experiments have also provided more or less direct evidence of the sudden commencement of ionization at the upper extremity of at least some trails, and of small-scale irregularities along the whole profile.

CHAPTER 5

REVIEW OF AMBIPOLAR DIFFUSION COEFFICIENT MEASUREMENTS AND ANALYSIS

The few papers which have discussed the height and time variation of the ambipolar diffusion coefficient, based on useful quantities of experimental data, are compared and contrasted in this chapter. The statistical methods applied in most of these papers are examined, and it is pointed out that there exists a more appropriate method than any so far used.

5.1 Observations of the coefficient of diffusion and its height dependence

Enough has been said in previous chapters to indicate that a measurement of the ambipolar diffusion coefficient D, made using the decay of a single meteor echo, is liable to error due to any or all of several pertubing effects.

(a) An apparently underdense-type echo may actually come from a part of a trail where the line density is close to the transitional value 2×10^{14} electrons/metre, in which case the decay may be prolonged, although still approximately of exponential form.

(b) The presence of the earth's magnetic field probably retards diffusion in certain directions.

(c) If a trail is underdense it may, depending on the geometry of the event, exhibit resonance. This increases its reflection coefficient at the start of the echo for a period which is not simply related to the diffusion process, and so again distorts the decay of the echo signal, this time reducing the apparent time-constant.

(d) If a trail is rotated or deformed in a region of non-uniform winds then the echo amplitude as a function of time becomes dependent also on the motion of the reflection point along the trail to maintain specularity, and on the form of the ionization profile traversed by the specular point.

(e) Another perturbation, to be discussed later in this chapter, may affect the decay time-constant if the ionization profile is significantly irregular on a small height scale.

Of the effects just enumerated, only that which involves the geomagnetic field is likely to impart a systematic bias to a large volume of data. Provided, then, that this possibility is kept in mind, the mean of a large number of observations of D at a given height can probably be taken to be largely free from the other effects listed above. However, unless such a set of data can be gathered in a limited period of time, diurnal and seasonal changes in the actual diffusion coefficient appropriate to each height will manifest themselves by an increased scatter among the data points.

Only the workers at Jodrell Bank (Greenhow and Neufeld 1955; Greenhow and Hall 1960, 1961) and at Adelaide (Weiss 1955; Murray 1959) have published and analyzed experimental values of D in any detail. These five papers, representing three different experimental methods altogether, are the only directly relevant observational literature. We shall first describe the experimental procedures and methods of analysis, and then tabulate some of the results.

The apparatus used at Adelaide (Robertson, Liddy and Elford 1953) was generally similar to that used in the 1960-61 survey. The latter equipment is described in Ch. 6. Essentially the earlier system was distinguished by smaller transmitted power (both continuous wave and pulse) and by the absence of outstations. Thus no tests of specularity could be applied and the height accuracy would have been poorer on average. Judging from 1960-61 results we may estimate the earlier standard error in height as perhaps ± 3 Km. There are two reasons why the accuracy of the 1952-53 and 1960-61 measurements of individual D values may conceivably differ. These arise from differences in the quality of the echoes selected for reduction, due to different transmitter power (possibly more transitional, i.e slightly overdense, echoes in the earlier set), and to the fact that in 1960-61 echoes were not chosen in the first instance for the exponential character of their decay. However none of these considerations is of major importance. In each case the shortest usable decay times were those for which approximately one Doppler cycle was visible above noise on the records.

Both Weiss and Murray analyzed results from December 1952 and June and September 1953. Murray also included data for March 1953 and additional data from the December and June recording periods. Each worker fitted to the points a linear regression of log D upon height.

The December and June data included meteors of several showers, recognizable from their times of occurrence and the positions of their reflection points in the sky. These shower meteors were processed separately, as indicated in the following table of results (Table 5.1). It is noteworthy that the slope of the log D vs. h regression for the Geminid meteors in December 1952 was approximately three times the slope found for sporadic meteors in that month. Murray states that the same effect was noted in the December 1953 data.

The first Jodrell Bank studies of the height dependence of D (Greenhow and Neufeld 1955) were made with the "split beam" height-finding system described by Evans (1954). In this method reflection points were located by their radar range and elevation angle, the latter being found from the ratio of echo amplitudes received on two antennas respectively $\lambda/2$ and $\lambda/4$ above ground. The theoretical polar diagrams for the two antennas were used to convert the amplitude ratio to the angle of elevation. Discussing later use of the same or similar equipment, Greenhow and Hall (1960c, 1961) estimated the error in height determinations to be about ± 4 Km. This equipment operated at $\lambda = 8.2$ m. In addition some observations were made in 1955 with a similar split beam system operating on $\lambda = 4.35$ m. In the 1961 paper two-station D measurements were also included. The latter came from the equipment described in Section 4.3 in connection with ionization profile investigations. Pulsed operation was used in all cases, and decay times were measured as the time $t_{\frac{1}{2}}$ taken by the echo amplitude to decay to one-half of its original value. It is not clear whether the remainder of the echo waveform was taken into account (by fitting an exponential curve to it and taking $t_{\frac{1}{2}}$ from the exponential); if not, then clearly the full potential accuracy of the experiments was not realized.

In the paper by Greenhow and Neufeld (1955) the data were divided into eight groups containing equal numbers of points, according to their decay time $t_{\frac{1}{2}}$, and the mean height was found for each group. Figure 5.1 shows, for both the 8.27 m. and 4.35 m. wavelengths used, the selected $t_{\frac{1}{2}}$ values and their mean heights. In each case the points are well fitted by a straight line below the heights marked by the arrows. However, the $t_{\frac{1}{2}}$ values fall progressively below those implied by these lines at greater heights. It was pointed out in the paper that the heights of divergence were those where, for typical meteors, the condition

$$\tau \leq 2(R_o \lambda/2)^{\frac{1}{2}}/v \qquad \ldots 5.1.2$$

was satisfied. The symbols have the same meanings as in preceding chapters. The right hand side of Eq. 5.1.2 is the time taken for the meteor to travel through the principal Fresnel zone, and the left hand side is the "true" decay time-constant, which is given by Eq. 3.3.2 as $\tau = \lambda^2/(16\pi^2 D)$. If the time of travel is in fact comparable with or larger than the decay time, the measured values of τ or $t_{\frac{1}{2}}$ will be greater than the theory predicts. This tendency should increase with increasing D, i.e. with increasing height, as was observed.

From 5.1.2, putting R_o = 150 Km., v = 40 Km/sec. and λ = 11.2 m., we can readily calculate that the Adelaide equipment is likely to underestimate values of D in excess of approximately 18 m^2/sec. The corresponding time-constant τ is .04 sec., approximately half of the triggering delay of the original (and also the present) Adelaide equipment. Recalling the need to record at least one Doppler cycle, we conclude that the probabilityof detection of echoes with τ < .04 sec. is slight. Therefore the predicted bias in observed D values due to the finite velocity effect is not seen. Instead there is an instrumental cutoff of the echoes potentially subject to bias. Confirmation lies in the fact that none of the D values used by Weiss and Murray was in excess of 18 m^2/sec.*

The purpose of Murray's 1959 paper was not so much to present new data as to comment on the methods of analysis required. It was pointed out that Greenhow and Neufeld had essentially found the regression of height h on log D, i.e. the expression giving the most probable height

* In the present survey only 0.4% of D values exceeded 18m^2/sec.

for a particular observed value of log D. In the general case of calculating the regression of a "dependent" variable y on an "independent" variable x, the squared deviations of experimental y values from a straight line, measured parallel to the y axis, are minimized by suitable choice of the line. The assumptions are that the corresponding x values are chosen or measured with negligible error, and that the experimental errors in y are normally distributed. Thus, Murray indicated, the Jodrell Bank results had been analyzed as though they contained negligible errors in the diffusion coefficients, whereas the Adelaide data had been examined taking height as the more precise observable. The slopes of the regression lines obtained can be equal only if the correlation coefficient r of height and log D is unity, i.e. the points lie exactly on a straight line. Otherwise the ratio of the coefficients of log D (say) in the two regressions is fixed for a given r, and is equal to r.

In Section 5.4 the question of statistical treatment for results such as the log D - h distributions, in which there is believed to be an underlying linear relationship and both variables are subject to error, is discussed at some length. Here it is sufficient to say that neither regression is intrinsically right or wrong; their appropriateness depends on the use to which the statistical result is to be put. In some circumstances a line of intermediate slope may be preferable to both regressions.

Greenhow and Hall (1961) replied to Murray's criticism in two ways. Firstly they admitted that it was not appropriate to treat the D values as free from error, and so presented a modified analysis, applied to the January-February 1959 results from the 8.2 m. height-finding equipment. The standard errors in height and ln D were estimated as ± 4 km. (from a calibration of the system) and $\pm \ln(1.3)$ respectively. A method of grouping the data, which depended on the ratio of these errors, was then used to find an estimated slope for the ln D - h profile. It was, of course, difficult to estimate the relative error in D, since not only errors in reading the records but also all the possible effects of wind shear, resonance, finite velocity, and the inclusion of trails with $\alpha \gtrsim 10^{14}$ electrons/metre had to be considered. Unfortunately the

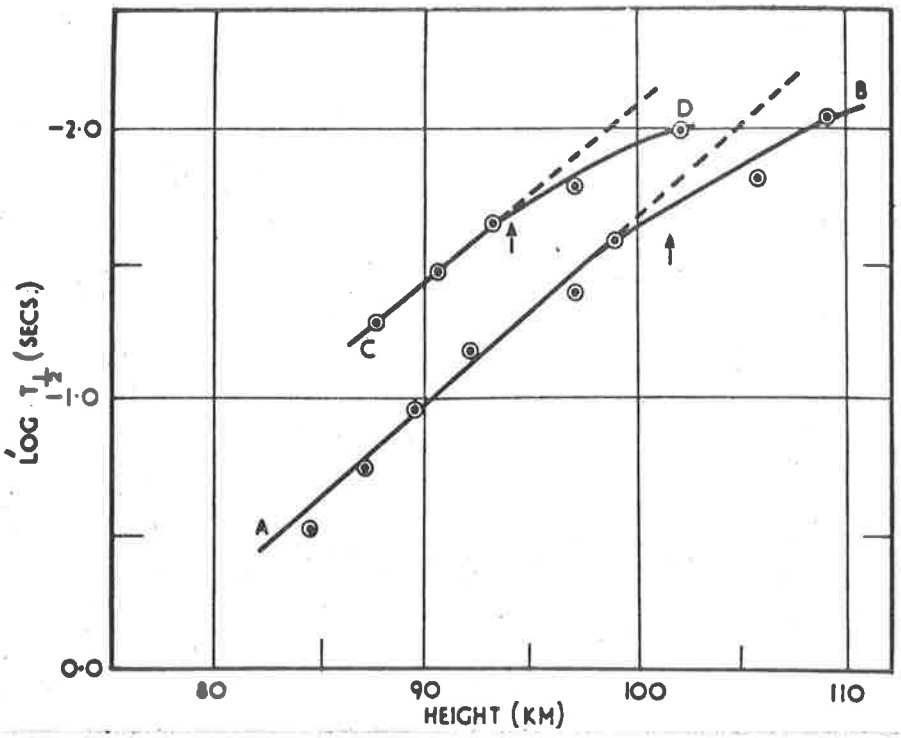

Figure 5.1. Time to half echo amplitude (Greenhow and Neufeld) with wavelengths 8·27m. (AB), 4·35m. (CD).

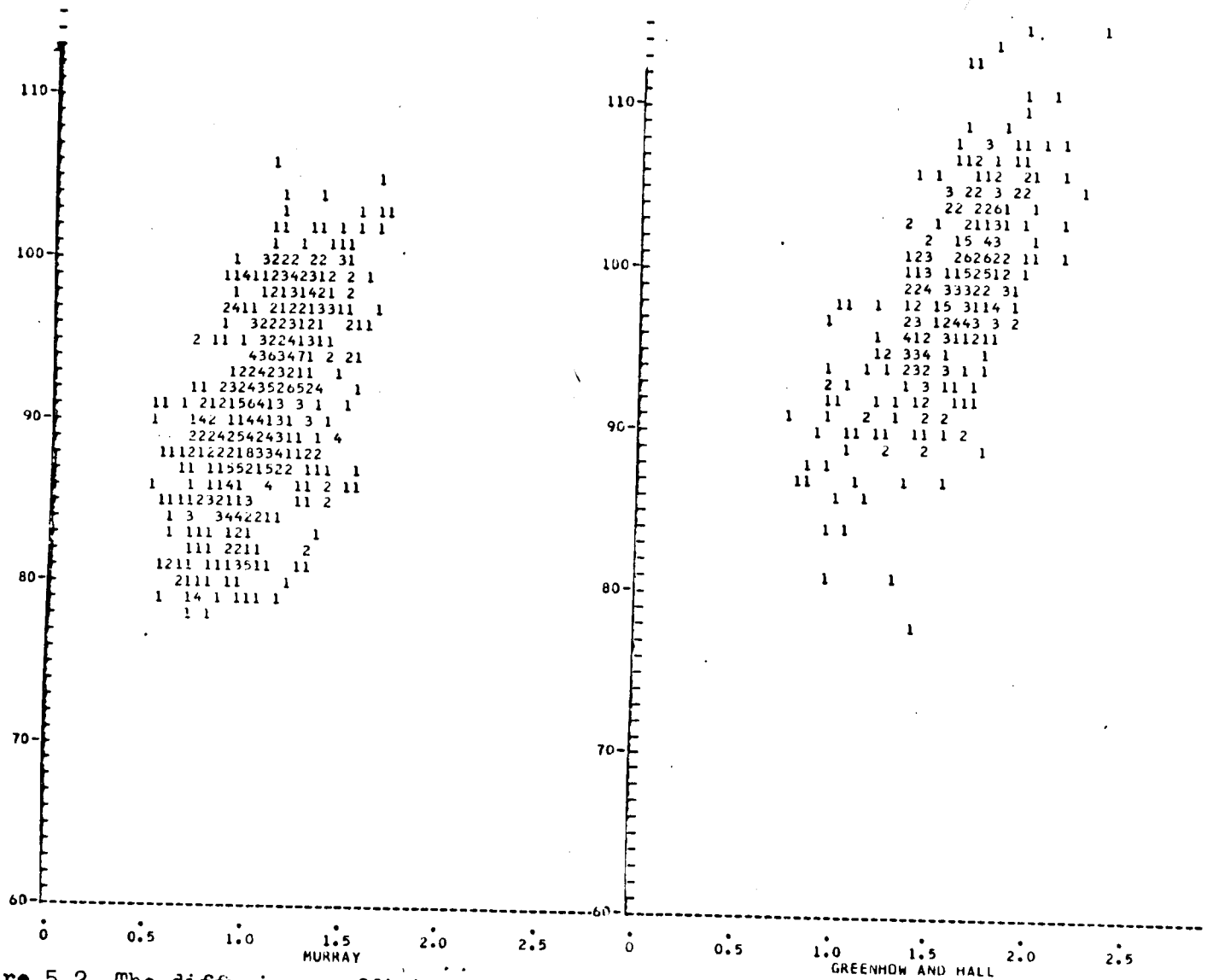

Figure 5.2. The diffusion coefficient results of Murray (1959) and of Greenhow and Hall (1961) on identical scales.

derived slope of the linear function relating h and ln D was strongly dependent on the value adopted for the ratio of the two errors, as can be seen from Table 5.1. In Section 5.4 it is shown that the slope of this relation can be estimated given only the comparatively well known standard error in a height measurement in addition to the set of (D, h) points. The necessity to estimate the standard error of log D is thus avoided.

Table 5.1 also shows that the slopes found by Murray and by the Jodrell Bank workers for the regression of ln D on h, i.e. the one preferred by Murray, differed much more than their values for the slope of the alternative regression. Greenhow and Hall attributed the disagreement in both regressions to the upper limit of 15 - 18 m^2/sec. imposed by the Adelaide CW system on measured values of D, claiming that the calculated regressions reflected distortion of the distribution by this cutoff effect. They made a comparison in histogram form of the frequencies of occurrence of various D values in the echoes from above 100 Km. altitude measured by each system. Since their median value of D at 102 Km. (the mean height of the Adelaide echoes they selected) was approximately 14 m^2/sec., very close to the nominal Adelaide cutoff, it is hardly surprising that the discrepancy between the two histograms was large. It may with justice be observed, too, that the histogram which represented the Jodrell Bank data contained echo heights up to 115 Km., whereas none of Murray's echoes were significantly above 105 Km. Thus the discrepancy between the median D values of the histograms was exaggerated by the difference in the height ranges covered. Also, only 7% of Murray's plotted data lay above 100 Km. This is too small a fraction to have drastically affected the regressions, and we must examine the facts more closely.

To prove the validity of Greenhow and Hall's criticism it is necessary to show (1) that there is no significant difference between the two sets of data over the range of values unaffected by the cutoff and (2) that the cutoff gives the Adelaide distribution an asymmetry about the "true" functional line, or in practice a reasonable estimate thereof, rather than truncating the distribution without bias. In Fig. 5.2 the author has re-plotted the "typical" scatter diagrams given in each paper,

on identical scales. Evidently even the diffusion coefficients in the range 85-95 Km., where the cutoff effect should be little in evidence, are from populations differing in slope, mean value, and scatter. Still more impressive is the almost complete failure of the two distributions to overlap at 100 Km. altitude. Thus it is not the instrumental cutoff which destroys the agreement of these Adelaide and Jodrell Bank results. There must exist some other cause for the discrepancy, and its nature may be geographical or instrumental. Perhaps the only way to determine with certainty whether instrumental effects are involved is to modify the pulsed section of the Adelaide equipment in such a way that pulse-amplitude vs. time records are available, for direct comparison with the continuous-wave echo waveforms.

In the present work, the calculation of the height gradient of ln D from pairs of observations taken on a single trail is unaffected by the errors of individual height determinations, since only height difference measurements are used directly and these are considerably more accurate than the absolute values of total height. As regards the two-station comparisons of D values made by Greenhow and Hall (1961), there is no such gain in accuracy due to the use of a height-difference method. Later it will be shown that the height difference values used by Greenhow and Neufeld (1957) suffered from systematic bias to an extent which depended, inter alia, on the true reflection point height for one station. The same method of calculating the height differences was used by Greenhow and Hall in the two-station diffusion coefficient experiment, and so similar errors must have occurred in the latter work.

The actual analysis of two-station diffusion coefficients used by Greenhow and Hall consisted simply of plotting a scatter diagram of observed differences in ln D versus observed height differences, and fitting a straight line through the origin to these points. The fitting procedure was one involving grouping of the data, similar to the method for estimating the functional dependence of ln D on h employed for single-

* This statement holds, regardless of a difference between the ranges of height difference values accepted in the two experiments.

station data in the same paper. From the above discussion of errors in the height differences it appears that the gradient $\frac{dh}{d(\ln D)}$ of the fitted line, viz. 8.9±0.8 Km., should undergo a correction reducing its value by at least 15%, and probably 50%.

Table 5.1 summarizes the results of the experiments dealt with in this section. For ready comparison the gradients of all regression lines and functional relations have been expressed as the quantity

$$H_D = \frac{dh}{d(\ln D)} = 0.4343 \frac{dh}{d(\log_{10} D)} \qquad \ldots 5.1.3$$

The fitting of a linear regression on height to ln D (or vice versa) is equivalent to fitting an exponential height variation of D itself. Therefore, by analogy with the normal usage for atmospheric pressure, we call H_D the "diffusion scale height". Other statistical quantities are included in Table 5.1 where available.

5.2 Diurnal, seasonal and latitude effects

At the outset it must be said that our knowledge of seasonal and geographical effects upon the ambipolar diffusion coefficient is sketchy in the extreme, and the situation is but little better in regard to diurnal fluctuations. The uncertainty in these effects results directly from the remarkable scatter in values of D measured at any height and time, which tends to mask the temporal and latitudinal variations.

Weiss (1955) looked for diurnal changes in the diffusion coefficient, first dividing the sporadic-meteor data for each recording period into suitable height groups and then forming and plotting D/D_{mean} at hourly intervals for each height group. Here D_{mean} is the mean value of D for all echoes in a height group in the whole recording period. In each of his three recording intervals (Dec. 1952, June and September 1953), he found evening minima and morning maxima in D. These held over the whole height range examined (approximately 80-100 Km.), with a tendency for the strength to increase with height. In Figure 5.3a (after Weiss) the diurnal variations in D/D_{mean} for December and June are compared with the simultaneous wind speed fluctuations. The latter were also expressed, in height groups, as V/V_{mean}, and then averaged for all heights. No correlation is evident, although for a set of selected groups of echoes

Table 5.1

The diffusion scale height H_D and other statistics

Reference	Dates	Wavelength (m.)	Points	$\bar{D}$ (m^2/sec)	$\bar{h}$ (Km.)	Correlation coefficient
Greenhow & Neufeld (1955)	Jan-Jul 1952	4.35	147	3.15≠	94.8	
	Nov 1953	8.27	268	12.0≠	95.5	
Weiss (1955)	Dec 10-15 52	11.2	70	3.21	89.3	
	" 16-20 "	"	112	3.61	89.7	
	Jun 5-12 53	"	43	4.42	90.4	
	" " " "	"	70	4.00	89.5	
	" " " "	"	170	3.27	89.5	
	Sep 7-30 "	"	539	3.06	91.2	
Murray (1959)	Dec 16-20 52	"	370	3.51	91.1	
	Mar 1953	"	322	3.17	91.1	
	Jun 5-12 "	"	372	3.53	89.6	
	Sep 7-30 "	"	539	3.06	90.7	0.55 (0.51≠)
Greenhow & Hall (1961)	Dec 1955	8.27	?	?	?	
	Jan-Feb 1959	"				
	" " "	"	325	9.42	98.6	(0.67≠)
	" " "	"				
	" " "	"				
	" " "	"				
	" " "	"				
	" " "	"				
	" " "	"				
	" " "	"				
	" " "	"				
	" " "	"				

≠ Re-calculated in the present study from published data.

(1) Assuming standard experimental error in heights = 3.0 Km.

(2) " " " " " " = 4.0 Km.

Table 5.1

(continued)

H_D from: Regression ln D on h	H_D from: Regression h on ln D	H_D from: Estimated function	Remarks	
	6.5		D < regression value above 92 Km.	
	6.5		" " " " " 98 Km.	
10.1*			Geminids	
25.9*			Sporadic	
16.8*			χ-Perseids	
24.2*			Arietids	
19.0*			Sporadic	
18.7*			Sporadic	
30.8			Sporadic	
30.7			Sporadic	
29.6			Sporadic	
18.9(18.7≠)	5.6(5.6≠)	(17.8≠(1))	Sporadic, same sample as used by Weiss	
		8.9±0.8	Two-station method	
12.5	6.6	8.2	00-03 hours	$(\delta h/\delta \ln D)^2$=200
12.5(14.3≠)	6.5(6.4≠)	8.0(7.65≠(2))	03-06 hours	" "
12.2	5.5	7.3	06-09 hours	" "
12.4	6.7	8.3	09-12 hours	" "
12.6	5.7	7.6	12-15 hours	" "
14.7	6.0	7.2	15-18 hours	" "
14.4	6.6	7.9	18-21 hours	" "
14.6	6.6	8.2	21-24 hours	" "
13.2	6.3	7.8±0.3	Mean of above gradients	" "
		8.9	Mean gradient using	" 150
		7.3	" " "	" 300

* Murray stated that a correction factor should be applied to Weiss' regression coefficients, equivalent to increasing the original values of H_D by a factor e (=2.718). The correct factor, incorporated above, is 10 ln10 (=23.03).

occurring in short periods during December 1952 there was a better correspondence.

In Weiss's results there is insufficient information to delineate a significant seasonal variation in D.

Greenhow and Hall (1960c) made a study of the diurnal variation in the diffusion coefficients measured with their single-station ("height-finding") equipment. Most of the results were for a 15-day period in Jan.-Feb. 1959, as discussed in Section 5.1; data from a test run of the equipment made on similar dates in 1958 were also included. The diurnal fluctuations were extracted in such a way as to represent the mean (96 Km.) altitude, and are plotted in Figure 5.4. (The scales of log D in Figure 5.4 and log (D/D_{mean}) in Fig. 5.3 are almost equivalent). Evidently the winter diurnal effect found in the Northern Hemisphere is of comparable size with that found for the Southern Hemisphere winter, but much smaller than the summer effect in the latter region. The general pattern of maxima in D near 0900 hours, and minima in the range 1600-2000 hours (local time), is common to all the results.

The 1961 paper of Greenhow and Hall gave information about a method of grouped data points which had been used to calculate H_D in the (1960c) work, and gave values for H_D found in this way from the 1959 data. These values have been included in Table 5.1, and are plotted in Fig. 5.5 . Now the (1960c) article also gave values of H_D, presumably found in the same manner, for these 1959 data combined with those from 1958. Although the admixture of the 1958 data would not be expected greatly to alter the scale height values if these were statistically significant for 1959 alone, the two articles give quite different figures for H_D as a function of time of day. The dots, error bars and dotted line in Fig. 5.5 show H_D as given in the (1960c) paper, and the extent of the disagreement is clear. The use of different estimates of the ratio of the experimental errors in h and log D for the two analyses could have changed all values of H_D by roughly equal amounts and so accounted for a displacement of the two sets of points, but not for the difference in general shape of the diurnal variation. Hence the form of

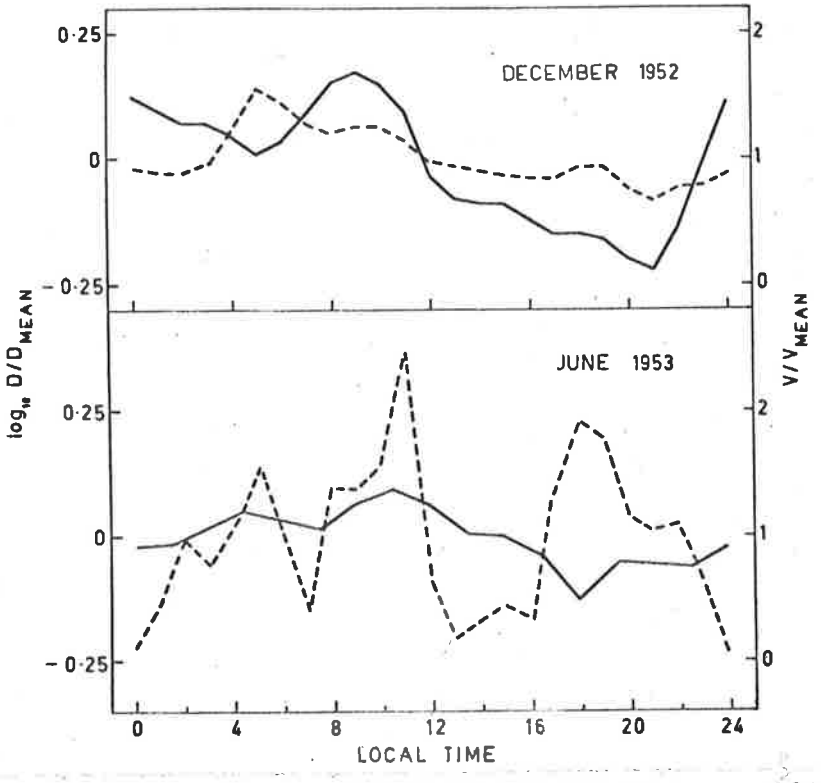

Figure 5.3. Diurnal variation of diffusion coefficient a
wind velocity (after Weiss). ——, diffusion; - - -, wind.

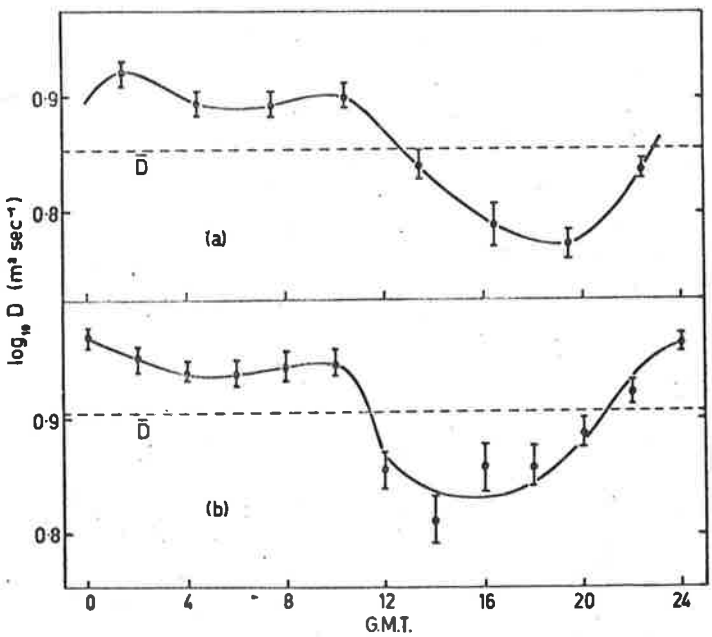

Figure 5.4. Diurnal variation of diffusion coefficient.
(a)Jan.-Feb. 1958, (b)Jan.-Feb. 1959 (Greenhow and Hall

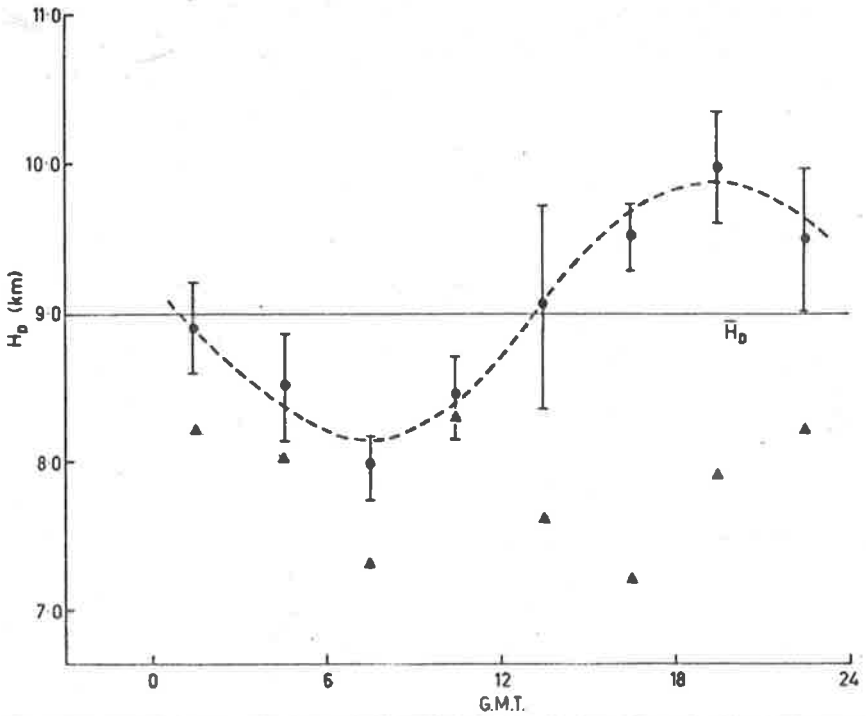

Figure 5.5. Diffusion coefficient scale height from two papers of Greenhow and Hall (see text).

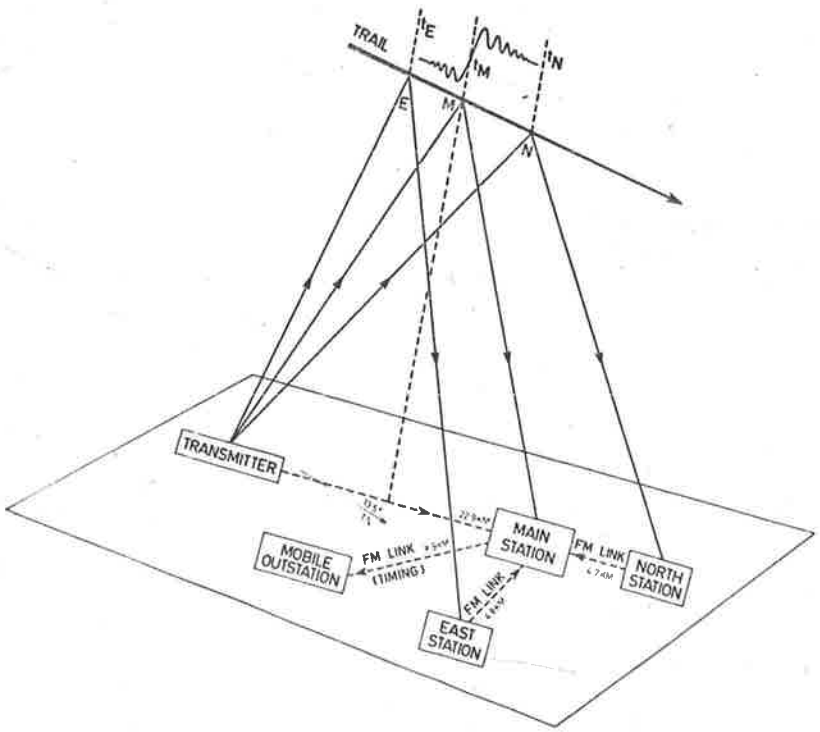

Figure 6.1. Detection of a meteor trail by the Adelaide system.

this fluctuation at Jodrell Bank remains effectively unknown to us. There is a similar discrepancy between the values of H_D calculated in the two papers for all the Jan.-Feb. 1959 echoes. The (1960c) value was 9.2±0.3 Km., but the 1961 article gave 7.8±0.3 Km. as the preferred value and set a probable upper limit at 8.9 Km.

5.3 Irregular ionization and the decay time

Rice and Forsyth (1963) have described an experiment in which they investigated the scatter in observed meteor echo decay time-constants. In addition, they made an important suggestion of a mechanism by which the scatter might be explained.

The experiment, performed in 1955, used three forward-scatter links, identical except in frequency, and with all transmitters and all receivers sited together, to obtain simultaneous reflections at wavelengths of 6, 8 and 9 m. from individual meteor trails. Subject to any frequency-dependent differences in the amount of tropospheric refraction encountered over the long (~1000 Km.), low-angle path, the centres of the principal Fresnel zones at all three frequencies should have been approximately coincident. If so, and assuming uniformly ionized trails, the observed decay time-constants T_λ should have been inversely proportional to the square of the wavelength λ. Alternatively, the three values of

$$T_\lambda' = T_\lambda \cdot 16\pi^2/\lambda^2 \qquad \ldots 5.3.1$$

should have been equal for a given trail. Although the logarithms of the ratios among the values of $T\lambda'$ had a zero mean value, they showed considerable scatter from the mean. Their combined distribution was normal, with an r.m.s. deviation which corresponded to a numerical value of about 1.3 for the ratio itself. This was the magnitude of the scatter found by Greenhow and Hall(1961).

The 30 meteors used in finding the above statistics were all chosen as showing a nearly perfect exponential amplitude decay at all three frequencies, thus eliminating trails that were overdense, or which might have had radial distributions of ionization differing appreciably from Gaussian form. Other requirements of good quality were also imposed. Thus both the statistical correctness of the theoretical relation between

wavelength and decay rate, and the presence of the scatter reported by other workers, were confirmed for echoes of the type selected.

The theory advanced by Rice and Forsyth considered a trail model whose electron density α varied appreciably in a length of trail intermediate between the (nearly equal) lengths of the principal Fresnel zones and their difference in length at two frequencies. The diffusion coefficient D was given exponential dependence on height with the scale height $H_D = H$.

A digital computer was used to integrate (vectorially) the signals from many small segments, into which the trail was divided. Thus the form of the echo as a function of time and at various frequencies could be calculated. The formation of the total echo was described in terms of the Cornu spiral, as in the case of uniform ionization, but now the lengths of successive elementary vectors had an almost random fluctuation. This semi-random character arose because distance along the spiral and along the trail are not proportional but bear a constantly varying ratio to each other. Hence it was shown by the numerical examples that (1) a small movement of the reflection point relative to the sinusoidal "irregularities" in α, or a change in frequency, could considerably change the relative importance of different parts of the trail; (2) because of the variation of D with height, such changes in the position of the dominantly reflecting segment relative to the (stationary) point of specular geometry caused the time-constant T_λ of the total echo to vary; (3)nevertheless, the form of the overall decay remained apparently exponential; and (4) the quasi-random variation in T_λ as λ was varied had sufficient magnitude to account for the inter-wavelength differences in T_λ found in the experiment.

Clearly, actual trails having a non-sinusoidally irregular distribution of line density α over similar lengths of trail to those considered above are equally capable of causing the observed deviations of T_λ from its theoretical value at a given wavelength. Although a causal relationship is not yet established, the case for this theory is greatly strengthened by the demonstration (Rice and Forsyth 1964) that irregular

ionization does, in fact, occur with the right order of scale length in certain trails, whose echo decay is apparently exponential (c.f. Section 4.2). It remains to be seen how common this mechanism is in a large sample of meteors.

5.4 Regression and functionality in the diffusion coefficient-height distribution

The conclusions which were drawn from the experiments reviewed in Section 5.1 and 5.2 were strongly influenced by the statistical techniques used in interpreting the data. In what follows, the statistical problem is first briefly reviewed in general terms. It is then shown how an existing technique, which has not so far been used for the particular case of the diffusion coefficient-height relation, may be profitably applied to this case.

It is assumed that there is an underlying exponential relationship between D and h, i.e. a linear one between log D and h, over some range of heights.* If so, the problem is one of fitting a linear functional relation between two variables, both of which are subject to experimental error.

This general problem is discussed in such texts as that on regression analysis by Williams (1959), who makes the following points.
(1) The assumed functional relationship exists between the "true" values of the variables, but regression relations are based on the variation in both the "true" values and the errors to which they are subject.

---

* The assumption is true for an isothermal atmosphere. Murray's (1959) results in Figure 5.2 show no trend to curvature anywhere in the Adelaide equipment's working height range 80 - 105 Km.; Greenhow and Neufeld (1955) found curvature (finite velocity effect) only at their upper height limit. All results in the literature have been analyzed under this assumption. Hence the assumption is used for the present work, for ease of comparison and pending more refined analysis.

(2) A regression relation will only coincide with a functional relation if the independent variable is free from error, since the former expresses the expected value of one variation in terms of the observed value of the other, while the latter connects expected values of both variables.

(3) If both the "true" values and the errors are normally distributed, i.e. their distributions are completely specified by their respective means and variances, then there is no more information to be found by sampling the data whereby the functional relation can be determined. Some other item of information is needed.

(4) Such extra information may arise either from relationships with external variables or from nonnormality of the observed distributions. The latter possibility leads to methods employing grouping of the data. Clearly artificial grouping of smooth observed distributions is inadmissible (c.f. Greenhow and Hall, 1961). Even if the observed distributions are not smooth, there is still the objection that the group limits will be based on observed values and may not be equivalent to a grouping based on true values.

Lindley (1947) shows how to estimate the functional relation given certain other kinds of extra information. One item of information frequently known in practice is the ratio of experimental-error variances in the two variables. Denote pairs of true values of the independent and dependent variables by (ξ, η) respectively, and their observed values by (x, y). Suppose there are n pairs of observations. Let x and y be distributed normally about ξ and η with variances δ_x^2 and δ_y^2 respectively. Then the ratio of experimental-error variances can be written as $\delta_y^2/\delta_x^2 = \lambda$, and the functional relation which is sought becomes $\eta = \alpha\xi + \beta$ 5.4.1

Lindley shows that the best estimates of α, β, δ_y and δ_x available using the usual experimental sums of deviations, squared deviations, and products of deviations from the experimental means are

$$\left.\begin{aligned} \hat{\alpha} &= \theta + (\theta^2 + \lambda)^{\frac{1}{2}} \\ \text{where} \quad \theta &= (s_{yy} - \lambda s_{xx})/2s_{xy} \end{aligned}\right\} \quad \ldots 5.4.2$$

$$\hat{\beta} = \bar{y} - \hat{\alpha}\bar{x} \qquad \ldots 5.4.3$$

and $$\hat{\delta}_y^2 = \lambda\hat{\delta}_x^2 = (s_{yy} - \hat{\alpha}s_{xy})/(n-2) \qquad \ldots 5.4.4$$

where
$$\left.\begin{aligned} s_{xx} &= \frac{1}{n}\Sigma(x-\bar{x})^2 \\ s_{xy} &= \frac{1}{n}\Sigma(x-\bar{x})(y-\bar{y}) \\ s_{yy} &= \frac{1}{n}\Sigma(y-\bar{y})^2 \end{aligned}\right\} \qquad \ldots 5.4.5$$

Lindley further shows that Eq's. 5.4.2, 5.4.3 and 5.4.4. are consistent estimates. That is, for our specific purpose, the same estimates will be found putting x=ln D, y=h, or vice versa, provided the errors are normally distributed and a functional relation exists. Even if the errors are not normally distributed, the estimates $\hat{\alpha}$ and $\hat{\beta}$ are shown by Lindley to have some justification. The consistency of the estimated functional relation is an important point; compare it with the confusion in the use of observed regression lines, to which Murray (1959) drew attention. Another important point is that if the errors are normally distributed, neither the true values ξ nor the observed values x of the independent variable need follow any particular law in their distribution.

One method of analyzing a distribution of ln D with height is to estimate the ratio λ, which now becomes $\delta^2_{\ln D}/\delta^2_h$, and use the above equations. Greenhow and Hall (1961) estimated just this ratio for the case of their experimental method, although the method of making use of the estimate was not that given above. Consider, though, the steps involved in forming an estimate of the ratio λ. One can judge fairly well the experimental uncertainty δ_h of a height measurement, but the range of echo waveforms leading to the observed D values is so large, and the effects capable of perturbing the decay are

so numerous, that any figure adopted for $\delta_{\ln D}$ can only be a guess based on the observed scatter rather than the experimental technique. Thus λ can be stated less accurately than δ_h, and information would be lost by using it. From another point of view, it is δ_h rather than λ which is intrinsic to the experiment and should be employed.

Fortunately Lindley shows how to apply his analysis to the case where just one error variance is known. If it is δ_y^2 which is known, the estimates for the coefficient in the functional relation and for the other error variance in Eq's. 5.4.2 and 5.4.4 become

$$\hat{\alpha} = (s_{yy} - \delta_y^2)/s_{xy} \qquad \ldots 5.4.6$$

and

$$\hat{\delta}_x^2 = (s_{xx} - s_{xy}/\hat{\alpha})/(n-2) \qquad \ldots 5.4.7$$

As before, $\hat{\beta}$ is given by Eq. 5.4.3 . By the earlier arguments on consistency, x and y may be interchanged to cover the case where δ_x^2 is known, or algebraic manipulation of 5.4.2 and 5.4.6 will lead to the same result. Emphasis on relative freedom from error in one variable, or on dependence and independence of variables, thus become irrelevant.

Let us now apply these ideas to diffusion coefficient data. If in a suitably chosen subset of the data there is a functional relationship

$$D = D_o \exp[(h-h_o)/H_D] \qquad \ldots 5.4.8$$

where H_D is the quantity we have called the diffusion scale height in earlier discussion, we can transform the relation to the linear form

$$\ln D = \frac{1}{H_D} h + (\overline{\ln D} - \bar{h}/H_D) \quad , \qquad \ldots 5.4.9$$

setting the general constants $\ln D_o$ and h_o equal to the observed mean values for convenience. Then with $x \equiv \ln D$ and $y \equiv h$, we have $\hat{\alpha} \equiv 1/H_D$ in Eq. 5.4.6 , while the experimental error in $\ln D$ is estimated by Eq. 5.4.7 .

The practical application of this method to the analysis of results obtained by the author is described in Appendix 3.7.

CHAPTER 6

DESCRIPTION OF EQUIPMENT

6.1 General principles and layout

In the design of the Adelaide multi-station meteor equipment used in 1960-61, the following aims were uppermost:-

(a) Continuation of the existing programme for studying diurnal and seasonal patterns of air motion between 75 and 110 Km. by measurement of meteor trail drift speeds.

(b) Measurement of the relative motion of three or four portions of individual meteor trails, for assessment in terms of atmospheric turbulence.

(c) Delineation of the orbits of individual meteors down to approximately 7th magnitude in a survey with a full year's duration.

The design of the equipment was begun in 1958, and by the beginning of 1960 construction was well advanced. At this date the author joined the group, being assigned the task of:-

(d) A statistical study of the distribution of ionization along meteor trails as deduced from the electron line density measured at three or four points on each trail.*

Of the above aims only the first could have been carried on with the previous equipment (Robertson, Liddy and Elford 1953). This used identical principles for locating the point of specular reflection on an observed trail, but had just one receiving station. Objectives (b) and (c) above depended on the additional fixing, by triangulation, of the flight paths of suitable meteors. To achieve this two outstations were added to the system as originally conceived. Their spacing, on which the distances between the reflection points on each trail depended,

* In 1963, since all the data that would be needed were available in project (d), the author also undertook

(e) Investigation of the temporal, geomagnetic and height influences on the rate of diffusion of the ionization in meteor trails.

was chosen to suit the requirements of both the turbulence (b) and orbit (c) studies.

For the author's project (d) it was felt that proper definition of the ionization profiles demanded an increase in the upper limit of possible distances between the reflection points. A third outstation was therefore constructed by the author, for installation further away from the main station.

The designers of the system (Roper, Nilsson, and others) were careful to provide for reproducibility and accuracy in the timing measurements needed in projects (a), (b), and (c). On the adoption of the trail profile work (d), which required the amplitudes of echoes to be measured in addition to the time data, it was too late to re-design the equipment to give as much stability of overall sensitivity (on a long-term basis, especially) as was desirable. Consequently, certain difficulties were encountered in the reduction of data for projects (d) and (e), and are mentioned later in this chapter and in the next.

In practice, running the complete multi-station system for any useful period required the full-time attention of two or three people. The author's projects depended on having the complete system in operation. Hence the third outstation had to be built somewhat hastily so that it could be operated as part of the system during most of 1961. Also, there could be no question of the author's continuing projects (d) and (e) single-handed after the end of 1961, when experiments (b) and (c) were concluded and their outstations were closed down.

Figure 6.1 shows the general layout of the stations and the way in which specularly-reflected echoes can reach all of the receiving stations from a single, suitably oriented meteor trail. The successive times t_E, t_M, t_N, are those at which the meteoroid passes the specular reflection points for the east, main, and north stations. On every possible trajectory (produced below ground level if necessary) there is exactly one point which satisfies the geometrical conditions for specular reflection of radio waves from the transmitter to a given receiving station. If such a potential reflection point lies on an ionized part of the meteor path an echo is received. The times $t_{\ }$,etc., can then be determined from examination of the diffraction signals at

the commencement of the echoes. Such a diffraction signal is sketched at t in the diagram, with elapsed time increasing in the direction of meteoroid travel. Given the total radio path length, the meteor velocity can be found from the frequency-time relationship in the diffraction oscillations.

If, as at Adelaide, the angle subtended at a reflection point by the base-line joining the transmitter and the appropriate receiver is not large, then the plane containing the reflection point and to which the trail is normal intersects the base-line near its midpoint. That is, the bisector (dashed line) of the angle between the incident and reflected signal paths is normal to the trail and approximately bisects the base-line (exactly, if the reflection point is equidistant from transmitter and receiver). For certain purposes the "mid-point approximation", in which the bisector of the angle is taken to pass through the centre point of the base-line, is a convenient first-order way to describe the geometry of detection.

On finding the velocity as described above, the direction of the trail in space is now determined from the time differences $(t_M - t_E)$ and $(t_N - t_M)$ and the co-ordinates of the stations on the ground. The position of the reflection point for the third ("mobile") outstation can then be calculated, irrespective of whether an echo is received there or not. The calculation is not straightforward, and in practice is done by an iterative method rather than analytically. Similarly the calculation of the direction cosines of the trail is made by an approximate method of sufficient accuracy much more rapidly than is possible if the necessary equations are solved analytically.

A plan showing the location of all the stations is in Figure 6.2. Some added convenience in reducing the data is gained by having the transmitter and three receivers defining rectangular axes with origin at St. Kilda, the main receiving station. However this arrangement is not essential. The two closer outstations to St. Kilda are at Sheedy's Farm, 4.72 Km. northward, and at Direk, a disused railway siding 4.81 Km. eastward. The third outstation is at Salisbury, where the single receiving station of the earlier system was located. Its distance from St.

Kilda is 9.23 Km. Original plans called for it to be later operated at greater distances from the main station, but this was not proceeded with. The relative locations of all the stations except Salisbury are known to an accuracy of order one metre as determined by a tellurometer survey; the Salisbury antenna's position is known to within a few metres from measurements on an aerial photograph.

It can be shown using the mid-point approximation that the largest separation possible between two reflection points on a trail is one-half the distance separating the receiving stations. Thus, considering the Salisbury and Sheedy's Farm stations, the upper limit of observable separations is 5.45 Km.

6.2 Transmitters

Two transmitters are used in the complete system, located together at Adelaide. Their characteristics in 1961 were as follows:-

	CW (continuous-wave)	Radar
Power output	~ 300 W.	~ 10 Kw. peak
Frequency	26.773 Mc/s.	26.773 Mc/s.
Modulation	Phase, 50 c/s sawtooth, deviation 90°.	Pulse, width 10 μs., 100 p.p.s.

Both transmitters (which had, with various modifications, been in use for some years) used disposals components and tubes. The reliability of the CW transmitter was quite good, although the efficiency of its final stage was poor (DC input ~ 750W). The above estimate of 300W is thought to represent fairly well the power actually radiated from June 1961 onwards. At that date a new exciter-and-driver unit was installed; prior to June the radiated power with inadequate drive is estimated to have been approximately 180 W. The pulsed transmitter was less reliable due to the variable characteristics and short life of the VT90 triodes in its output stage. Although the CW power was low, the receiving signal-to-noise ratio was adequate by virtue of the electrically quiet receiver locations, and the low noise figure and narrow bandwidth of the receivers themselves. It was, however, common for an otherwise usable echo to be rejected because of inability to distinguish the radar echo

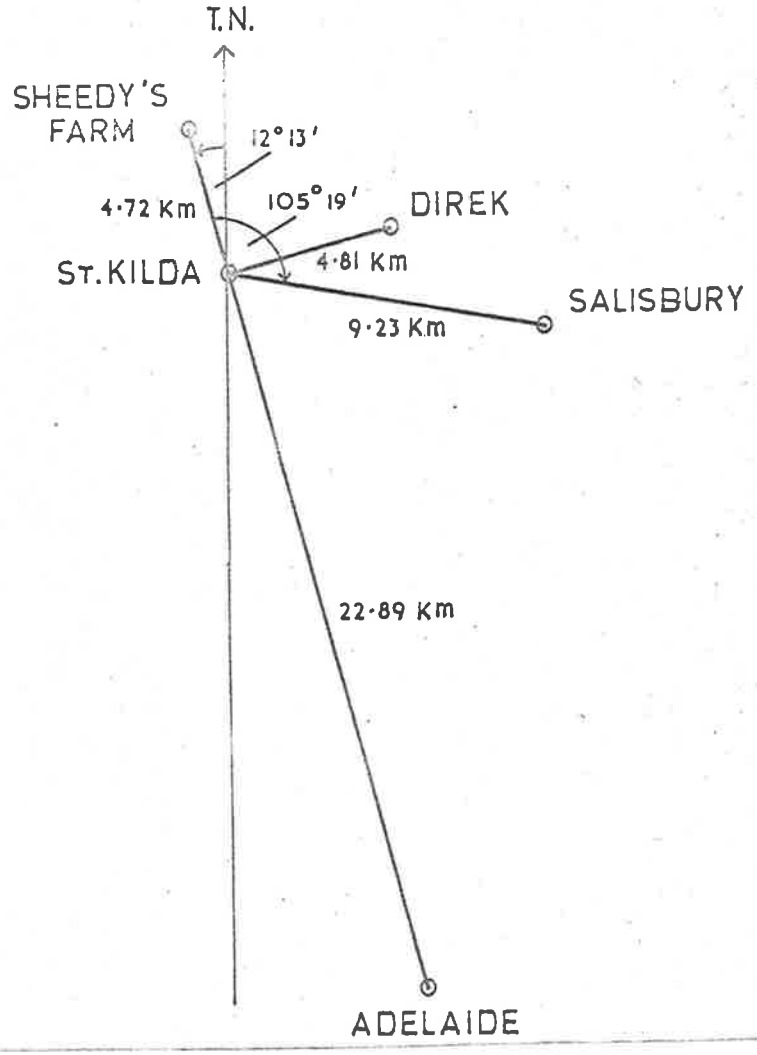

Fig. 6.2. Map of stations.

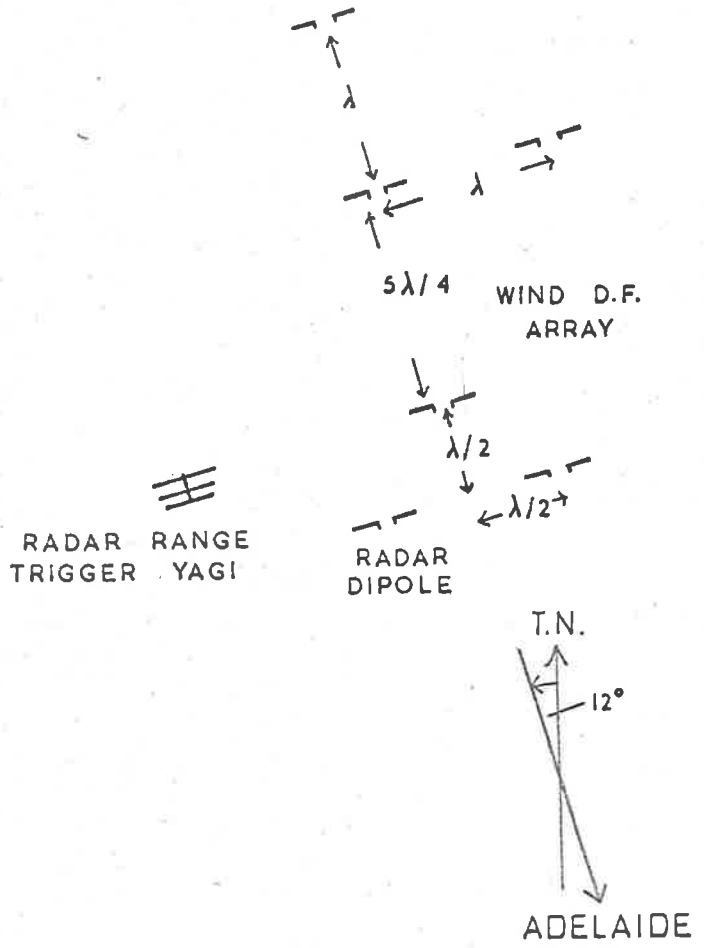

Fig. 6.3. Main station aerials.

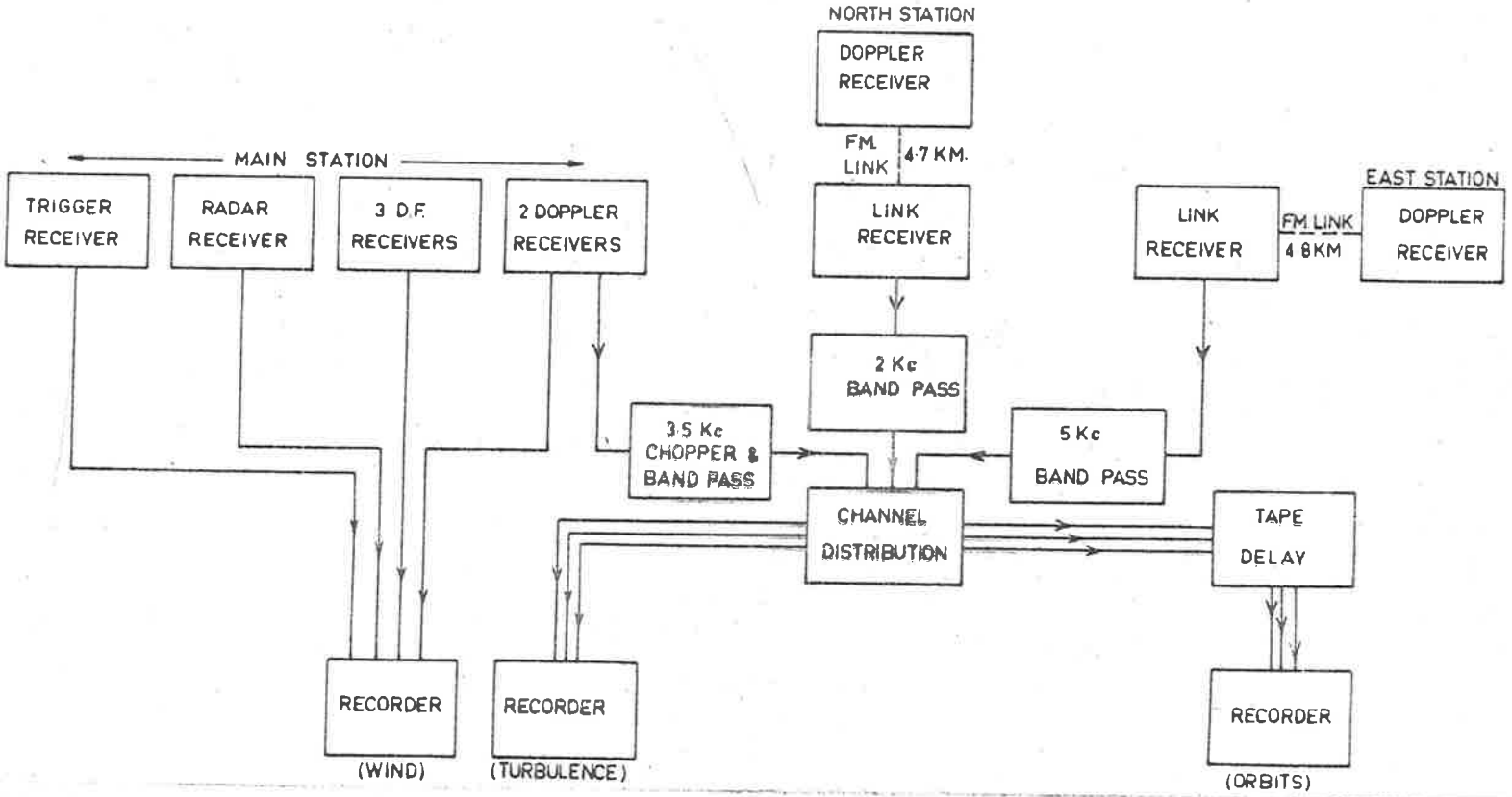

Figure 6.4. Signal flow in the St.Kilda (main), Sheedy's Farm (north) and Direk (east) stations.

from the noise.

The two transmitters were operated from a common crystal oscillator on approximately 700 Kc/s, via separate frequency multiplier chains. In the case of the CW transmitter the phase modulation was introduced at this frequency, with $2\frac{1}{2}^{o}$ deviation. After multiplication (36 times) the deviation at the final frequency was 90^{o}.

Each transmitter fed a separate 3-element Yagi antenna, directed towards the zenith, through balanced transmission line. The antennas were of wire, and were suspended end-to-end between masts at the rear of the Physics Department building containing the transmitters. The distance between the closest points of the two aerials was of order one wavelength, so that some interaction was to be expected. It was established by experiment that the feed-point impedance of the CW antenna was insensitive to changes of the physical structure of the radar antenna and to whether the terminals of the latter were connected to a matching impedance, or an open or short circuit. Hence any interaction was not expected greatly to distort either polar diagram. Results presented in a following chapter indicate that the CW antenna showed an increase in gain in a direction equivalent to the azimuth of the radar antenna, rather than the null usually found end-on to the elements and actually observed at the other end-on azimuth. However the pattern was still a broad beam directed to the zenith, with no evidence of minor lobes. The disturbance was more important at high angles of elevation than in the range of elevation in which most echoes were detected. (Since the total number of electrons produced by a meteor and the extent in height of its ionized trail are both essentially independent of its direction of travel through the atmosphere, the line density of electrons in a horizontal trail is small. Consequently detectable specular reflection from a reflection point at the zenith is unlikely).

Reference to Figure 3.4 will indicate that for a given sky-wave amplitude in a meteor echo, the form and quality of the echo waveform depend on the ground-wave amplitude at the receiving station. Since receiver overload is undesirable, an excessive ground-wave also forces the receiver to be operated with less than the optimum gain for a given

sky-wave-to-noise ratio. Adjustment of the ground-wave level reaching the main receiving station was carried out prior to the start of the 1961 survey by altering the height above ground of the transmitting antennas. The parasitic reflector element of each Yagi antenna minimized the effect of this adjustment on the shape of the main beam.

In 1963 and 1964 both transmitters have been entirely re-designed and rebuilt, with greater power output and different aerials.

6.3 The main receiving station at St. Kilda

The parts of the main station equipment concerned with locating in space the reflection point for that station and measuring its rate of drift are identical in principle with the prototype equipment operated at Salisbury from 1952 to 1959 (Robertson, Liddy and Elford 1953).

The range of the reflection point is found by normal radar techniques, making use of the pulsed transmission. A horizontal Yagi antenna directed towards the transmitters receives the ground-wave pulse, and the output of its receiver, called the trigger receiver, initiates a train of range marker pulses. The sky-wave pulse is received by a half-wave ($\lambda/2$) dipole mounted $\lambda/4$ above ground, connected to a separate receiver which is referred to as the radar receiver. The range markers and the echo pulse are applied as intensity modulation to an oscilloscope tube whose standard A-scan deflection is triggered simultaneously with the range marker pulse train.

All the aerials used to receive the CW transmission are of the same form as the radar antenna, viz. $\lambda/2$ dipoles $\lambda/4$ above ground. There are five CW aerials, all so oriented that the ground-wave presents a plane wavefront to them. Their layout is illustrated in Figure 6.3. By suitable measurements of the relative phases of the sky-wave signals at these antennas the direction cosines of the line of sight to the reflection point can be found.

The radio-frequency phase differences are preserved in the demodulated output of the receivers to which these aerials are connected, in the form of the phase differences among the sub-audio-frequency Doppler beat waveforms. In the data reduction two of the receivers are specifically associated with direction-finding and are hence referred to

as DF 1 and DF 2. Three of the aerials are sequentially connected to DF 1 and DF 2. The other two receivers and aerials, although also involved in the direction-finding process, are called Doppler 1 and 2 because the frequency of the Doppler beat is measured from them for calculation of the drift speed of the trail.

Through the phase modulation of the CW transmission, the sense of the motion of the trail can be determined. The sudden 90° phase jump produced by the flyback of the sawtooth modulating waveform arrives approximately 1 msec. earlier in the ground-wave than by the longer skywave path. As a result each receiver's output contains a series of "phase spikes" whose tips trace out a "phantom beat" Doppler waveform. This either leads or lags the main signal by a phase difference of 90°, according as the trail drifts towards or away from the station.

The receivers for both the pulsed and CW signals are of the single-conversion superheterodyne type, designed to exhibit a very low noise figure combined with stability and high gain. Two stages of radio frequency amplification are used, first a cascode stage and then a conventional pentode amplifier. A pentode mixer is followed by intermediate-frequency stages on 1.9 Mc/s. In the CW receivers there are two IF stages, tuned to give a bandwidth of $\pm$ 4.5 Kc/s between the 3 dB points. The IF amplifiers of the radar and trigger receivers have staggered tuning to achieve the necessary $\pm$ 500 Kc/s bandwidth, and therefore have three stages to make up the loss in voltage gain. In normal operation the narrow-band receivers are set to a voltage gain of approximately 2×10^{6}. The input impedance is 75 Ω, and an input signal of 10 μV from a 75Ω source produces 10V of DC output across the detector diode load. Up to 20V output, departures from receiver linearity are negligible (Roper 1962). Thereafter overload is fairly smooth, but is generally detectable by eye in the records if a Doppler peak exceeds 25V. The option of manual or automatic gain control,(with a 2 second time constant) applied to the IF stages, is provided.

Local oscillator voltage is injected into all receivers via separate buffer amplifiers from a common crystal-controlled oscillator.

High tension for all units at the main station and at Salisbury,

and for all units except the final stage of the link transmitter in the other outstations, is provided by electronically regulated power supplies So also is negative bias for manual gain control in the receivers. In the latter half of 1961 an AC voltage regulator was installed at St. Kilda to supply all tube filaments, because of very poor voltage regulation in the AC mains supply to that station. It is now known that previously the Doppler receivers at this station had been varying in gain at certain times of the day because the gain of the cascode RF stage was dependent on filament voltage. The consequences of this behaviour are discussed later.

As described later in connection with the form of the records obtained, the radar and CW receiver outputs are recorded on a single 35 mm. film when the presence of an echo is detected in the output of Doppler 1 receiver. This record is called the "wind" record, and the equipment so far described is the "wind" equipment.

Figure 6.4 is a block diagram showing the relationship of the wind equipment with the two nearer outstations and with the equipment at St. Kilda which is specifically concerned with them. As can be seen, the Doppler receivers in the outstations have their outputs sent to St. Kilda in the form of amplitude modulation of 2 Kc/s and 5 Kc/s subcarriers, which are in turn impressed as frequency modulation on 167 Mc/s transmissions. In a similar fashion the output of Doppler 1 receiver is chopped and filtered so that it appears as amplitude modulation of a sine wave at the chopping frequency, in this case 3 - 5 Kc/s. A channel distribution unit routes this signal, and the recovered sub-carriers with the outstation information, to the "turbulence" recorder and the tape delay unit.

As its name implies, the turbulence recorder is concerned with recording the differences in line-of-sight wind components observed from the main station and the Sheedy's Farm and Direk outstations. The outputs of the three narrow-band receivers are recovered from their respective sub-carriers and applied after amplification to the deflection plates of oscilloscope tubes. A camera triggered simultaneously with the "winds"

camera records the information. We shall refer to the record produced as the "turbulence" film.

The three-channel tape delay unit performs an essential function in the orbit measurements. To find the velocity of the meteoroid the diffraction oscillations prior to t_o must be recorded. However their amplitude is seldom sufficiently large to cause triggering of the recording sequence. Hence the signals from the channel distribution unit are delayed in a tape unit, where they are mixed electronically and recorded on continuously-moving magnetic tape by a single recording head. They are recovered after the desired delay as the tape passes a single playback head. By means of three bandpass filters, each $\pm$ 600 cycles in bandwidth and centred on one of the sub-carrier frequencies, the separate signals are recovered with negligible cross-modulation. Following demodulation and amplification the delayed signals are recorded by a display and camera similar to the other two. This camera has a higher film speed than the others, to allow full resolution of diffraction whistle frequencies as high as the 600 c/s permitted by the bandpass filters. It commences to run slightly later than the other two cameras when the equipment is triggered, so that the effective delay given the signals is of order 0.6 second. We shall refer to the resulting film record as the "orbit" or "radiant" film, since it is the one chiefly used in finding the meteor's velocity and the direction of its trajectory.

6.4 The outstations at Sheedy's Farm and Direk

These two outstations, which are the ones envisaged in the original design study of the system, operate unattended except for routine maintenance. For protection, the equipment is buried in a steel box at each site, with provision for forced air cooling. The lid of the box is ground level.

The electronic equipment in each outstation rack comprises a narrow-band 27 Mc/s receiver, its crystal-controlled local oscillator, a 167 Mc/s transmitter, a chopper and filter unit which codes the output of the Doppler receiver for transmission, and power supplies. The mains power cable runs underground for approximately 30 yards from the box

before joining the overhead distribution lines. Thus disturbance of the 27 Mc/s aerial polar diagram is avoided. Antenna feeder cables enter the equipment box through vertical two-inch piping which supports the antennas. The 4-element 167 Mc/s Yagi is mounted above the 27 Mc/s dipole. The output power from the frequency-modulated 167 Mc/s transmitters (Philips type 1645/02b) is approximately 10W, ample to cause limiting in the associated receivers (1645/01b) at St. Kilda.

In the chopper and filter unit a multivibrator operating at the chosen sub-carrier frequency drives a diode ring modulator whose signal input is the output of the Doppler receiver. A filter removes harmonics of the multivibrator frequency from the modulator output, leaving a sine wave with amplitude proportional to the signal input. The sine wave is now taken to the link transmitter and frequency-modulates the transmission. By this means the DC output from the receiver, a measure of the amplitude of the 27 Mc/s. ground-wave, is conveyed to the main station in addition to any Doppler beat waveforms.

The 167 Mc/s. link transmitters, and their matching receivers at the main station, are superseded but not obsolete units designed and manufactured by Philips for mobile and/or base-station usage. The overall linearity of each link depends on the linearity of the chopper unit, the transmitter modulator, the discriminator in the receiver and the recording deflection amplifier. Measurements by Roper (1962) show that the signals recorded on the turbulence film follow the inputs to the outstation Doppler receivers with good linearity up to a level determined by the bandwidth of the discriminators. By means of a potentiometer at the input of the chopper unit in each outstation, the level of the subcarrier is adjusted so that excessive deviation is not given to the VHF transmission. Hence the overload characteristics of the outstation plus VHF link are essentially those of the Doppler receiver.

6.5 The distant outstation at Salisbury

For several reasons, the third outstation differs in configuration and operation from those just described. The chief difference is that Doppler echo waveforms are recorded at the outstation rather than

being transmitted to the main station for recording. At Salisbury the recording is of a continuous nature.

If the same arrangement of triggered recording at St. Kilda had been used in this outstation as in the others, then with increasing distance from the main station an increasing fraction of the total number of potential echoes would have been lost. The lost echoes would have been those with short time-constants, occurring at Salisbury prior to St. Kilda; the time of meteoroid travel between the reflection points, added to the delay in triggering the cameras, would in many cases have reduced the echo amplitude to an unreadably small value at the start of the record. If all outstations had been permitted to trigger the recording equipment this objection would not have held. However, construction at St. Kilda of the recording displays and the arrangement for triggering their cameras was too far advanced for the necessary modifications to be practicable.

For recording at Salisbury, then, another VHF link is used to convey to Salisbury the information that the main station equipment has been triggered. Again because of the time of meteoroid travel and the triggering delay time, continuous recording is necessary. A following section describes how this is achieved without excessive film consumption by the camera used. The VHF link in this case carries a tone burst at 2.5 Kc/s to signal that a trigger has occurred, and a burst at 1 Kc/s as a time marker every 15 minutes. Each of these signals produces an indication on the camera record.

The equipment is installed in a disused ammunition-loading building in Penfield Annexe, on the outskirts of the Department of Supply's Weapons Research Establishment.

A block diagram showing the Salisbury outstation equipment, and the equipment associated with it at St. Kilda, appears in Figure 6.5. At the main station the 15-minute and trigger tone bursts are generated, and a frequency-modulation drive signal at 9.019 Mc/s for the link transmitter is produced in a modulating unit. In this the audio tones are produced by valve oscillators of the phase-shift type. The oscillators, each one-half of a 12AX7 twin triode, are turned on in response to the

appropriate voltage changes in the wind equipment by simple transistorized control and delay circuits. The drive to the transmitter is generated in a 12AT7 twin triode of which the first half is a crystal-controlled Pierce oscillator and the second produces phase modulation in an unusual circuit used also in the commercial transmitters of the other outstations.

The Salisbury link transmitter, originally constructed by a colleague, J.W.Smith, was somewhat modified by the author. It uses a 6AU6 buffer and three QQE03/12 twin tetrodes as its tube complement. The first QQE03/12 triples and doubles the frequency in successive halves, the second is a push-pull tripler and the third (the output stage) also operates in push-pull. A meter and switch in the modulator unit allow operating currents in each transmitter stage to be measured for monitoring and tuning. The power output is approximately 8 watts at 162.34 Mc/s, to a Yagi antenna like those in the other outstation links.

Although in 1959 the Salisbury location had been left, in favour of St. Kilda, because it was becoming too noisy for reliable triggering of the wind equipment, the noise level at 27 Mc/s was by no means a barrier to continuous recording. Hence it was hoped that there might be little noise at 162 Mc/s, and the author designed and built a single-conversion receiver at this frequency for use as the Salisbury link receiver. This unit employed EC91 (grounded-grid) and 6AM6 RF amplifiers, a 12AT7 crystal oscillator and multiplier, another 12AT7 as second multiplier and mixer, and two 6AM6 IF amplifiers and a 6AL5 ratio detector at 10.7 Mc/s. Its performance was satisfactory in terms of sensitivity, viz. approximately 10 μV for full output; the incoming signal was of order 100 μV. However, it turned out that although impulse-type noise was little problem, there was a high level of interference near 162 Mc/s from various local voice transmissions. Hence a Philips receiver, as used at St. Kilda, was purchased and installed, as an alternative to reducing RF bandwidth and adding IF limiting stages and audio squelch in the unit just described. Even so there were periods when this interference remained a nuisance during 1961.

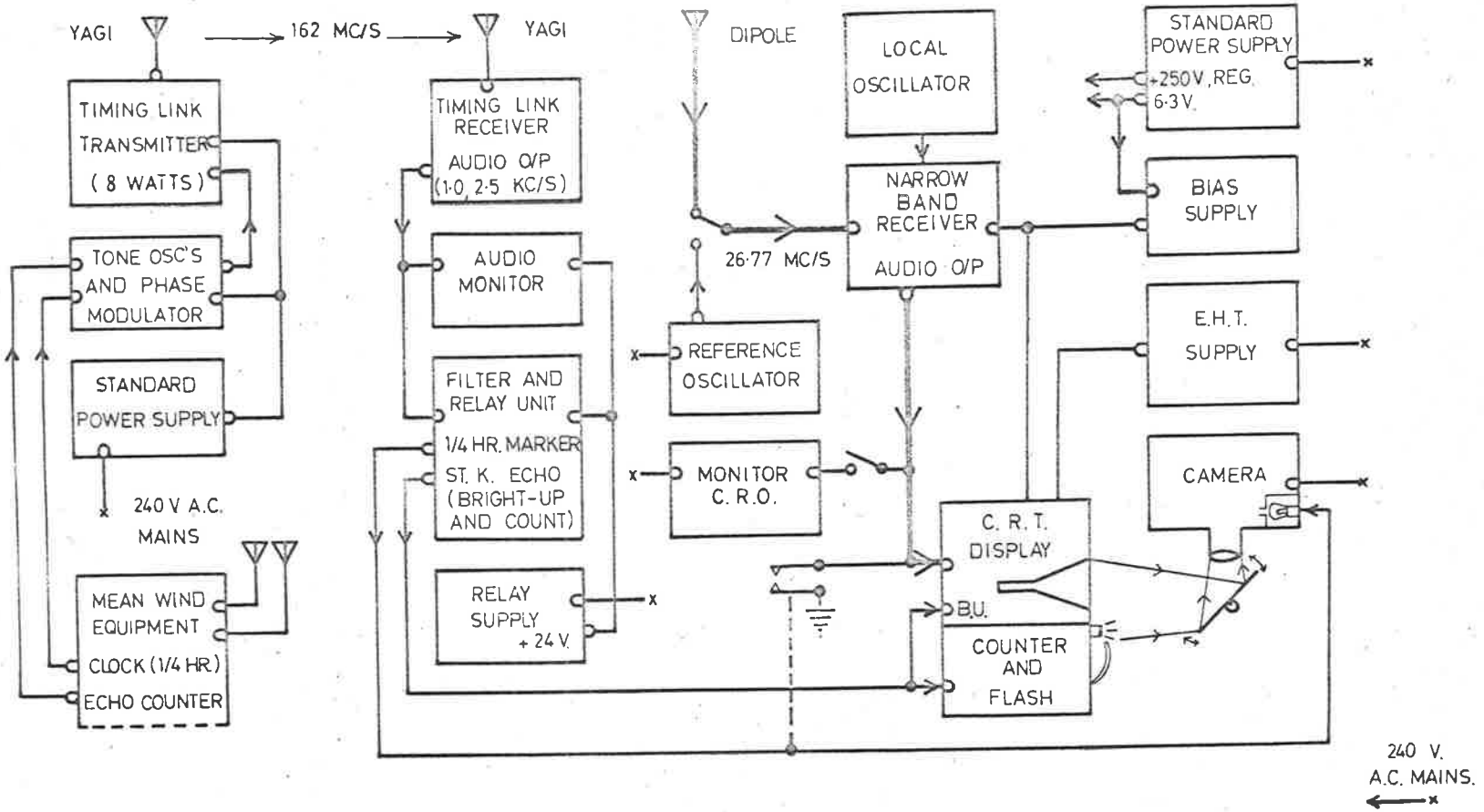

LINK TX.

(ST. KILDA)

RECEIVING STATION

(SALISBURY)

From the link receiver output two cathode followers lower the impedance level of the signal so that it can be applied without mismatch or interaction to two band-pass filters, centred on 1.0 and 2.5 Kc/s and each ± 150 c/s wide. At their output terminals, miniature "Rex" transformers couple the filters to relay-driver circuits, of adjustable sensitivity, each using a 12AT7 tube. The various functions accomplished by the relays on reception of one or other link signal are detailed in the following two sections.

The narrow-band 27 Mc/s receiver in this outstation is identical with those at the other outstations and at the main station. Because the station is visited daily for film changing, the receiver is operated with manual gain control.

At St. Kilda the majority of the oscilloscope display units use cathode-ray tubes of split-beam type with the two traces deflected independently. For such tubes only one deflector plate has to be supplied with each signal, and the central "beam-splitter" electrode between them remains at the fixed potential. Only a single-beam tube is required at Salisbury. Trials indicated that excessive astigmatism was introduced with single-sided deflection of this tube, and a push-pull direct-coupled amplifier with the same circuit as that of the Y amplifier of the Solartron CD568 oscilloscope is used instead.

High voltage for the display tube is obtained from an electronically filtered supply like those in use at the main station. A standard 250V regulated supply, also the same as those at the other stations, provides power for other circuits. Various relays are operated from a non-regulated 24V supply. The remaining units are a crystal-controlled local oscillator and a - 150V gas-tube-regulated supply for receiver gain control and for the display amplifier negative connection.

6.6 Calibration of receiver sensitivity

In order to compare relative electron densities (i.e. underdense echo amplitudes) measured at two or more stations, it is necessary to know the gain of each receiver as a function of time, and the power gain of the transmitting and receiving aerials in the appropriate directions for each meteor trail. If the absolute values of electron line density

are to be meaningful, then at least any obvious long-term changes in transmitter power should be taken into account also.

We have seen that the narrow-band receivers at Salisbury and St. Kilda (Doppler 2) which were used for measuring echo amplitudes in 1961 were operated with manually pre-set gain. Those at Direk and Sheedy's Farm, having to remain unattended for longer periods, normally ran under automatic gain control (AGC). Therefore the DC output (on ground-wave alone) of each one of the first two receivers varied as the product of its voltage gain and the square root of the transmitter power. The output of the latter two receivers was nearly independent of fluctuations in these variables.

At first it was not intended to include in the analysis echo amplitudes from the outstation receivers operating with AGC. Therefore the ground wave level and sensitivity for the Direk and Sheedy's Farm stations were not regularly monitored. At St. Kilda and Salisbury commercial signal generators, which ran continuously in the interests of stability in amplitude, were substituted for the input from the aerials whenever film was changed, or the receiver gains were reset. The standard source e.m.f. was 10 μV, and the signal generators matched the input impedance of each receiver (75 ohms). Comparison of the DC voltages (as recorded on the films) corresponding to the ground wave and the standard signal gives a measurement of the groundwave amplitude at the time of the calibration, to a reading accuracy of 2 - 3%. Any difference in the voltage gain from one such check to the next is evident from the corresponding difference in the output levels with 10 μV input. The time intervals between these gain measurements varied according to circumstances from an hour or so to 48 hours, but were usually about 1 day or less.

The amplitude stability of the two signal generators, a Marconi TF955A/2 at St. Kilda and an Advance 62 at Salisbury, was good. Neither was sensitive to fluctuations in the AC mains voltage, and when on several occasions the generators were compared by substitution in the Salisbury receiver, the discrepancy in their output e.m.f.'s never exceeded 4%.

However, neither had sufficient frequency stability to remain

within the ± 4.5 Kc/s receiver bandwidth for more than a few minutes. Thus automatic standardization of the receiver gains at shorter, regular intervals was not possible using these generators. Special crystal-controlled generators, with good-quality attenuators and amplitude stabilization using a feedback technique, were designed by the author to permit automatic gain calibration, but were not completed in time for use in 1961.

The triggered automatic recording sequence at St. Kilda causes the input terminals of Doppler 2 receiver to be short-circuited for about 0.1 second at the end of each recorded echo. For the echoes of major interest, those of decay type, the receiver output has usually returned to its quiescent value, corresponding to ground wave alone, at this time. Therefore the recorded step in the output level relates distance on the recording film to ground wave amplitude. At Salisbury the same function is accomplished by short-circuiting the receiver output at every 15-minuite marker signal. With normal gain settings as used with the 1961 transmitter, the total output on noise, even with the aerial connected but with the transmitter turned off, was typically 26 dB below the DC output level produced by the ground wave when the transmitter was on. The detectors were linear down to the noise level. Thus any inaccuracy, due to internal receiver noise, in the position of the "zero output" line on the St. Kilda record is negligible.

No such datum level is automatically produced by the other outstations. However, during the film-reading it was found possible to fix the zero-output level on the turbulence film for each ot these stations by reference to the waveform of certain echoes. (Section 7.1 gives details). Suitable echoes for this purpose were recorded at least every 1 - 2 hours, and there was no evidence that DC output of the receivers ever varied so rapidly that this was an excessive interval. It was therefore decided to double the task of reading echo amplitude data from films and process all four echo amplitudes for each meteor whenever possible.

Unfortunately, for several months of 1961, the Doppler 2 receiver at the main station showed gain variations which behaved inversely as the mains supply voltage. These variations were not found until the film-

reading was well advanced, early in 1963. Evidently the mains voltage was lowest while meals were being cooked at the field station (and presumably at other places connected to the same local supply line). At these times gain measurements were naturally infrequent, so that the changes escaped notice. The period affected was from May, when gain standardization as described above became routine, to July. In August an AC mains voltage stabilizer to regulate the filament supply to all tubes was installed, whereupon the receiver gain became stable. The order of the increases in gain was some 30%. To a large extent the analysis has been able to make allowance for these fluctuations.

At the three outstations no trouble of this kind was experienced, the mains regulation being considerably better. However in December 1961, at the end of the survey, an untraced fault in the receiver at Salisbury caused its sensitivity to change at random between two discrete values differing by about 15%. Here the analysis could take account of the changes provided they did not follow each other at intervals of less than an hour or two. The shortest allowable interval depended on the rate at which echoes were being recorded.

6.7 Form of film records

We have seen that three different photographic records were made at the main station. In the echo-amplitude measurements, two of these, the "winds" and "turbulence" films, and the fourth ("profile") record made at the Salisbury outstation, were directly involved. Certain quantities had also to be measured on the remaining ("radiant") film.

Figures 6.6 and 6.7 illustrate all four records for meteor number 123700, which has been selected as an example of a trail with three underdense, and one slightly overdense, reflection points. This same meteor will be used later to illustrate details of the data reduction. The labels in the figures identify each type of record. Time increases from left to right in Figure 6.7, and the time scales indicate the differing film speeds used in the cameras.

In the wind, turbulence and radiant records (Figure 6.6) the films move in a horizontal direction through cameras viewing oscillos-

cope tubes on which the signals appear as vertical deflections.

The wind film contains information of the range and direction of the reflection point, and line of sight velocity, as determined from the main station receivers. The radar display tube (top in Figure 6.6) is intensity-modulated by the echo pulse and by range markers indicating 20 Km. increments of total radar path. The next two lower traces are the signals from receivers Doppler 2 (inverted) and Doppler 1 respectively. The recording sequence is initiated by the sharp change in signal level at t_o, as received by Doppler 1. The Doppler 2 trace, as previously explained, is the one used for measuring the amplitude of the St. Kilda echo. Direction-finding (DF) receivers 1 and 2 each have their input electronically switched between two aerials, one of which is common to both receivers. The rectangular switching waveform is asymmetrical to produce "light" and "dark" traces, as seen at the bottom of the wind record, for identification of the individual aerials. In the traces from receivers Doppler 1 and 2 the 'phase spikes' produced by the phase-modulation of the CW transmitter, and the "phantom beat" waveform traced out by their ends, are clearly visible.

The echo number is added to this film and the others by the firing of an electronic flash tube which illuminates a counter via a Perspex light pipe. While the counters themselves were very reliable, the flash tubes sometimes received an insufficiently large trigger pulse, or had not recovered from a preceding flash, and failed to fire. This accounts for the absence of the echo number from some of the records shown.

The turbulence film (also in Figure 6.6) contains the demodulated Doppler signals from the Direk and Sheedy's Farm outstations, together with the signal from the Doppler 1 receiver. The latter appears twice, once inverted, to facilitate the measuring and comparison of the three wind velocities. Amplitude-time data for the two outstations are obtained from this film. In it and also in the wind record, the film speed in the camera is approximately 0.38 in/sec.

From the point of view of the amplitude measurements, the delay of some 100-200 msec. incurred in the triggering of the equipment after t_o is an unavoidable nuisance. For example, exponential decays must be

extrapolated back to t_o to give the initial echo amplitude for electron line density calculation. Also, the accuracy of determination of the decay time-constant becomes poorer as the time interval, during which it is measured, becomes more remote from t_o. For the orbit work the most valuable part of the diffraction waveform occurs in fact before t_o. In the tape delay unit the outstation and Doppler 1 signals are retained for some 1.3 sec. after real time, so that the diffraction whistles and the t_o points are readily available.

The radiant film (Figure 6.6) contains the delayed information from the tape unit. Because frequency components of the whistles extend up to 600 c/s, this camera operates at higher film speed than the others. To avoid the loss of sections of the post-t_o whistle due to display-amplifier overload on Doppler peaks, the amplifier response is made to roll off below 300 c/s, and at DC the gain is about 10 dB less than at 300 c/s. On this record the phase spikes, at 20 msec. intervals, are very evident, and inspection will show that reference time markers in the form of 1 msec. upward displacements were also added simultaneously to each trace at 140 msec. intervals. Whistle information was read from each trace independently, taking the same time marker as a datum point. Hence, any relative displacement among the three traces along the time axis is immaterial.

Cross-identification of echoes from film to film is made possible by keeping the counters in step. Timing to within 15 minutes is provided by a digital clock photographed every 15 minutes on the wind film. The radiant display contains an accurate 8-day clock which is photographed at the start of each echo, giving time to an accuracy of a few seconds for orbit reduction.

In both the turbulence and the radiant films, the central trace(s) are from the St. Kilda (station 1) receiver, the top echo is from station 2 (Sheedy's Farm) and the bottom one is from station 3 (Direk).

The profile record (Figure 6.7) from station 4 at Salisbury differs considerably from the others, mainly because of its continuous nature. In this case it is unnecessary to achieve any better time resolution than will allow measurement of the Doppler beat. The phase spikes

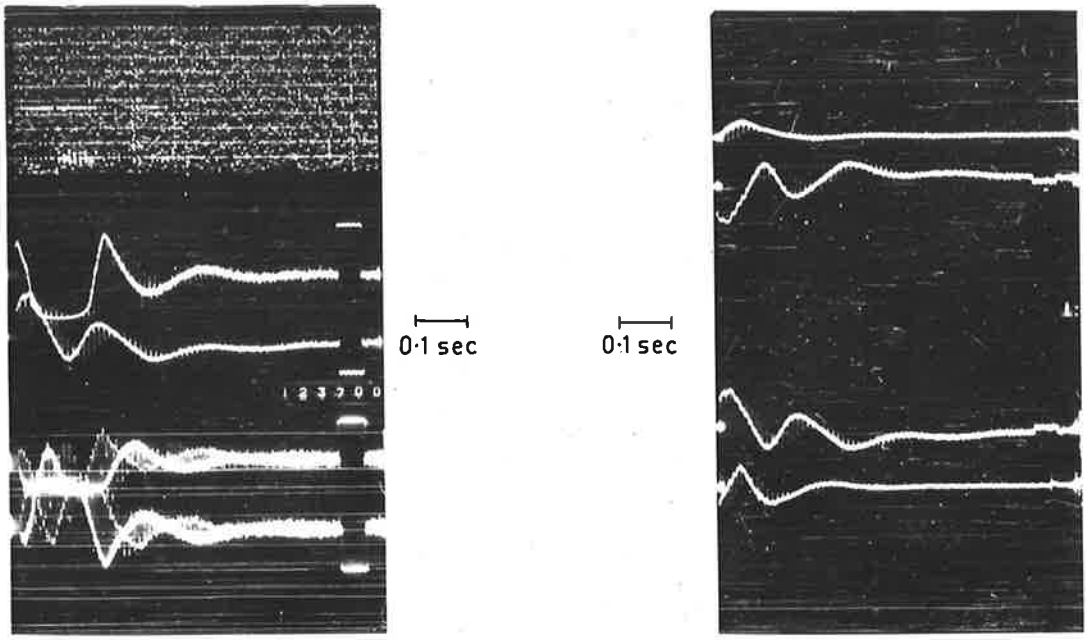

(a) Wind (b) Turbulence

FIG. 6.6 FILM RECORDS FROM ST. KILDA

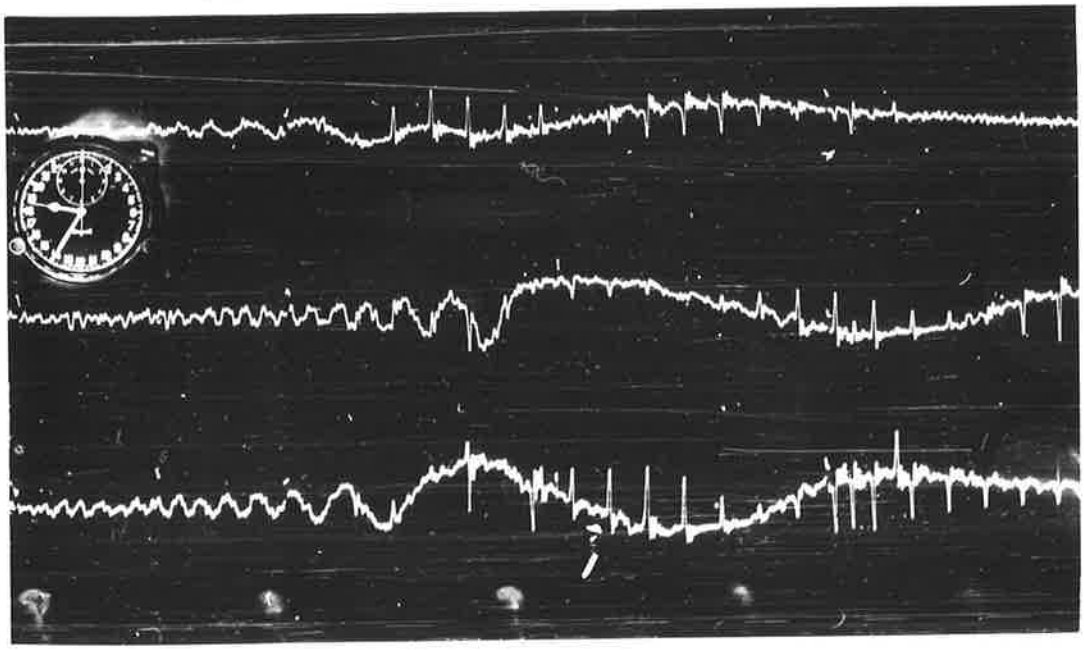

(c) Radiant 0·1 sec

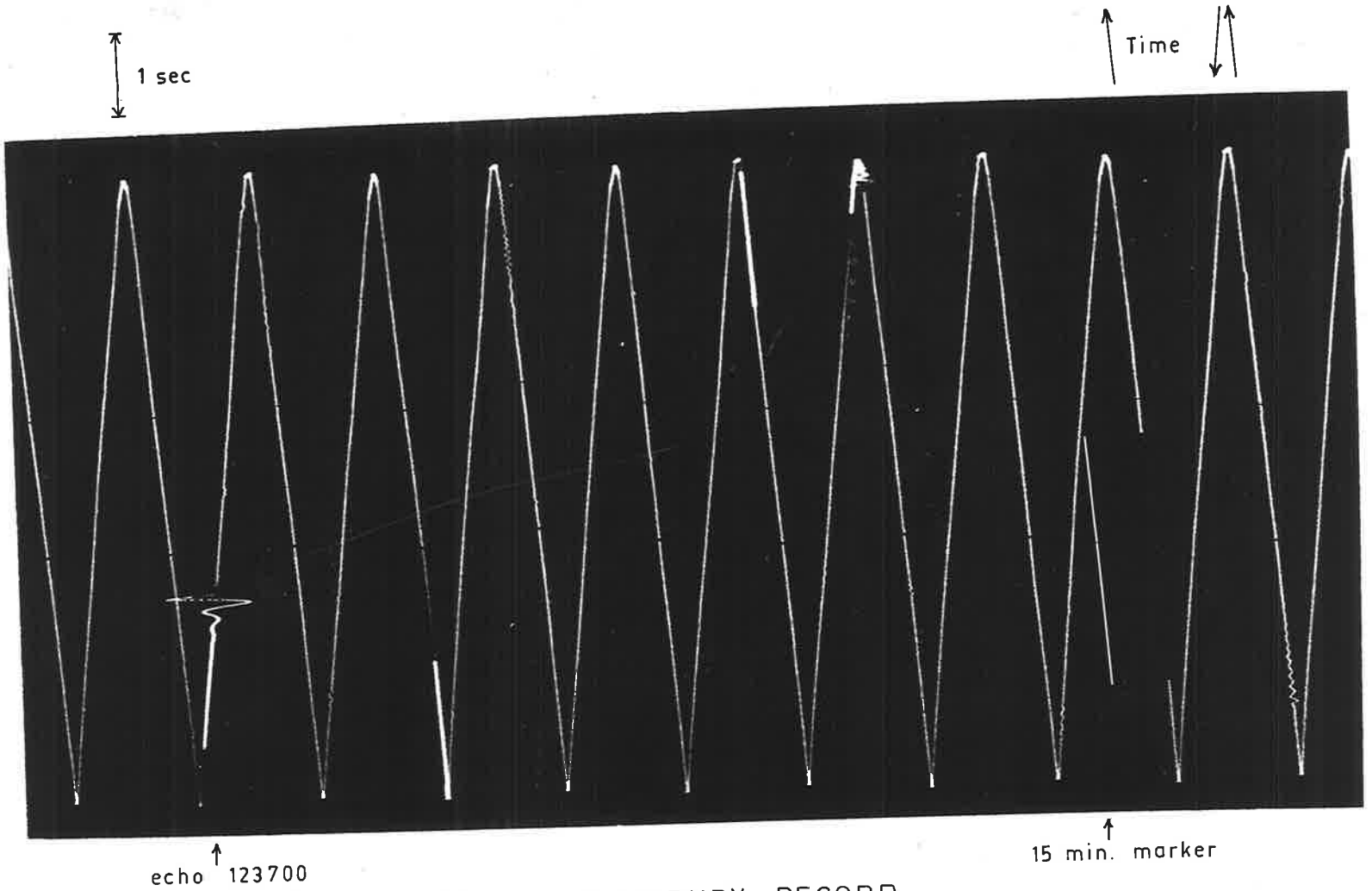

FIG. 6.7 SALISBURY RECORD

need not be resolved because the sense of the line-of-sight wind can reliably be predicted from the speeds at the other three stations. (Among the latter, only one (doubtful) reversal of the sense of trail motion was observed among the 2100 echoes of the 1961 survey). Therefore an existing camera, using 70 mm. unperforated bromide paper, was modified to suit. In it a film speed of 0.8 in./minute (continuous) is combined with a rocking mirror arrangement, driven through a cam by the paper take-up motor, which traverses the image of the oscilloscope tube spot linearly across the film and back every 30 sec. This system gives a total trace length of 1200 ft. per 100-ft. roll of paper (25 hours), or a writing speed along the triangular trace of approximately 0.16 in./sec. The Doppler signal deflects the oscilloscope spot in such a direction that its image moves parallel to the edges of the paper, i.e. nearly at right angles to the triangular trace.

Echo identification on the profile record was achieved in several ways for the 1961 data. On the reception at Salisbury, over the VHF link, of a 2.5 Kc/s tone indicating that the main station equipment has been triggered, the C.R.O. spot is brightened slightly although the intensity control is set to give a visible spot at all times. In addition a flash tube and counter identical with those at St. Kilda are actuated, so that the echo number is recorded on the film. At most times this counter remained fairly well in step with the others, so that the majority of echoes were thus identified without recourse to timing measurements. However, there were some periods of severe interference when echoes had to be related with their counterparts recorded at station 1 by reading the times of occurrence from the radiant film and locating this instant on the profile record. This possibility having been foreseen, the second (1 Kc/s) tone signal is transmitted over the link every time the digital clock in the wind display is photographed, i.e. every 15 minutes. This signal both short-circuits the Doppler receiver output, as seen at the left of Figure 6.7, and lights a lamp to expose a small marker area at the edge of the paper. By interpolating between these quarter-hourly signals, using the triangular trace as a guide, it was usually possible to measure time to an accuracy of about 2 seconds relative to the digital

clock, or about 20 seconds relative to the clock in the radiant equipment. Interference was troublesome for only about 10% of the total recording time. It is estimated that of all the echoes used on the profile records only 1% or less were wrongly identified, since in doubtful cases the Salisbury echo was generally not used.

CHAPTER 7

FILM READING, DATA REDUCTION, AND COMPUTER PROGRAMMES

7.1 Reading of amplitude-time data

Approximately 200,000 meteors were recorded in the 1961 survey. The selection of suitable records for reduction, and the subsequent detailed film-reading for those which were chosen, were long, involved, and tedious tasks. We shall first indicate the overall sequence of operations, and then give the particular details relevant to reading amplitude-time data for the trail profile and diffusion coefficient work.

The following steps, all involving time measurement only, had to be completed before echo amplitude measurements could usefully be commenced.

(1) The films from the radiant display were scanned and a note was taken of all echoes with a promising diffraction waveform on each trace. (Hence overdense trails which drifted into specularly - reflecting orientation after formation were eliminated).

(2) The wind films were read for these echoes, about 20% being suitable for wind analysis. The remainder comprised mainly records lacking the minimal 1 cycle of Doppler beat which was necessary for determining the direction cosines of the reflected signal's path of arrival at the main station. A smaller fraction of the rejected echoes showed confused and unreadable Doppler patterns due to beats among reflections from several reflecting centres on the trails. No statistics were kept of the reasons for rejection, but Weiss (1959), dealing with the earlier Adelaide CW results, gave the analysis in Table 7.1, which should be equally applicable to the 1961 records.

(3) The turbulence films were read for the line-of-sight motion at reflection points 2 and 3. No further losses of echoes were incurred at this stage, since these wind components were available (less conveniently) from the radiant film if the turbulence film had, for example, run out when a given echo occured.

(4) Now the radiant films were read in detail, and winds, wind shears, radiants, and orbits were found from the assembled data, with the aid of

the IBM 1620 and 7090 computers. Following certain quality tests carried out in the course of these calculations, there were left 2204 meteors completely reduced at this stage.

Table 7.1. Echoes rejected as unsuitable for wind measurement (Weiss 1959)

Echo characteristics	Percentage rejected
Low Doppler beat frequency	12
High Doppler beat frequency	0.2
Echo decay too rapid	43
Low echo amplitude	9
High echo amplitude	3
Distorted echo waveform	13
Suitable for measurement	20

The reading of amplitude-time data, which could now proceed, required almost as long a period as the total for stages (1) to (4) above. For compatibility with the magnetic tape of results produced in (4), each of the 2204 meteors represented thereon was processed in some way, even if it was obviously impossible to extract electron line density or diffusion coefficient from some waveforms.

As the first step in amplitude measurements, the author examined all echoes for each meteor and classified the waveforms by assigning to them a value from 0 to 4 for a variable called KIND. A value of 0 indicated that there was no evidence that the echo was other than underdense, i.e., the decay appeared to adhere closely to exponential form throughout. Slightly overdense-type echoes such that the decay appeared to follow a period of nearly constant sky-wave amplitude were given KIND = 1. If only the constant amplitude phase was observed KIND was set equal to 2. A few instances where the ionization at the Salisbury reflection point was entirely or almost absent, so that no echo or one too small for point-by-point measurement was returned, were assigned KIND = 4. All other echoes, in which the envelope of the Doppler beats did not match one of the above definitions, were given the value 3 for KIND. In Figure 6.6, the St. Kilda echo (which shows saturation of Doppler 2 receiver on beat maxima) was

judged to be of KIND 1, mainly because the early maxima did not appear to indicate an exponential decrease in the sky wave during the early part of the echo. However, the final results indicate that the section of trail involved had less than the nominal 2×10^{14} electrons per metre. At the other stations the echo was definitely of decay type (KIND = 0).

Next the scanned echoes were measured. For the 35 mm. films from St. Kilda a filmreader of the rear-projection type was already in existence for reading wind information. For this purpose both film and measuring cursor moved in the horizontal (time) direction. The original intention to have electrical readout of time intervals had not been carried out, and readings were taken by eye using a scale fastened to the screen.

The author carried out the additions to this film reader which were necessary for electrical readout of the cursor's position. A fixed, straight potentiometer card had a regulated 10V supply connected to it and was traversed by a wiper attached directly to the cursor assembly. The potential at the wiper was measured and indicated, upon command, by a Hewlett- Packard 405CR digital voltmeter. Calibration could be adjusted so that the readout agreed with the reading on the scale fixed to the screen.

In addition, the film reader was equiped to read vertical distances (echo amplitudes) in a novel manner. Horizontal lines were marked on a sheet of Melinex (or Mylar) plastic, stretched vertically just behind the screen and fastened at its top end to an ordinary spring blind roller. Below the screen the Melinex passed around a roller which diverted it into a horizontal path, and its end was clamped in a carriage which ran on horizontal rails within the desk attached at the foot of the screen. A second potentiometer card furnished a reading of the position of this carriage, and thus of the cursor lines drawn on the Melinex. Because both potentiometer wipers moved with their cursors, instead of being indirectly driven by (say) the handwheel shafts, there were no problems of backlash. No stretching of the plastic blind was noticed, and in any case readings in both directions were always made relative to some datum point of the film record, so that stability of zero readings was not a necessity.

The author has subsequently arranged the control system* necessary for automatic punching of each D.V.M. reading onto cards by an IBM 026 punch. With this arrangement errors of manual transcription and manual punching of numerical readings are eliminated. Unfortunately the punch was not available in time for use in reading the 1961 data.

Using this film reader the echo waveforms for the St. Kilda, Sheedys and Direk receivers were measured. For each echo trace a card was eventually punched containing the X (time) and Y (signal amplitude) coordinates of up to 8 Doppler maxima or minima. The computer programme employed for processing these data cards (Section 7.6) was so written that it allowed some freedom in the choice of these points, and at the same time imposed certain requirements. Essentially the points used had to be the best 8 or less for defining the beat envelope.

Reading the profile records, on paper stock, demanded a different technique. A film reader of the epidiascope type was constructed. To achieve sufficient image brightness without overheating the paper in the reading gate the magnification was kept down to 4 diameters. Even so, it was necessary to use two 150 watt enlarger bulbs (admittedly with a rather inefficient system for concentrating light on the film). For simplicity the full width of the paper was visible on the screen. This arrangement was preferred also because the cam in the rocking-mirror camera did not give the image a constant rate of travel across the paper. Using a record made in the camera with a constant frequency signal applied to the display, a matching time scale was made up for the film-reader screen so that the correct scale factor was always applied at each point of the triangular trace. With this scale it was possible to read to a limiting accuracy of about ± 0.01 second over a 1 second interval, provided the echo was not within approximately 1 second of the points where the mirror travel reversed. Because of excessive non-linearity in these parts of the cam, echoes so located were either not read or classified as being of poor quality, depending on their ease of reading. In view of these added complications and because the full potential accuracy of this

* (Stone, 1966a).

reader was needed, the author personally read all the profile records.

In Appendix 1 the details of how echo extrema were chosen at the film-reading stage, and of the logic used in processing the coordinates of the extrema, are explained by reference to two hypothetical echo waveforms. This logic takes account of whether the echo appears to be from underdense (KIND =0,1) ionization, of possible receiver overload on Doppler maxima, of sky wave levels which initially were either greater or less than the ground wave, and of various reasons why the echo quality must be classified as poor. The way in which ground wave levels at the Sheedy's Farm and Direk stations were inferred from echo waveforms is also explained.

7.2 Delay in starting the cameras

For comparison of St. Kilda and Salisbury echo amplitudes, it was at first thought that the time of specular passage t_o for the St. Kilda echo could with sufficient accuracy be taken to precede the start of the film record by a fixed time interval (the mean time needed to start the camera). This was not so in practice, and steps were taken to improve the accuracy of timing.

Since the decay of an underdense echo is extrapolated back to t_o, uncertainty in fixing this instant results in corresponding uncertainty in the initial echo amplitude and the line density estimate. If only the main station and the most distant (Salisbury) outstation had been used for amplitude measuring and the latter had been moved to greater distances, as at first intended, occasional measurement of the triggering delay might have provided sufficient accuracy in t_o. However, the smaller ratios in echo amplitude introduced by the records from the less distant stations 2 and 3 were subject to larger relative errors for a given uncertainty in t_o.

Only a quarter or less of the meteors which were actually reduced contained sufficient information in their echo waveforms for unambiguous fixing of t_o. Instead, it was necessary to scan the wind and the radiant films simultaneously for records (several per wind film, or about one for every 10 meteors used in the survey) from which the delay between t_o and the start of the wind record could be measured. (From the orbit work, fig-

ures were available giving the position of t_o in the radiant record). Similar measurements were later carried out, if possible, on the turbulence film. The measured time delays were then assumed correct also for the wanted echoes near them.

This process was long and tedious. Some further details are given in Appendix 2, with some relevant statistics. It is estimated there that, by adjusting the assumed time delay as described above, the r.m.s. error in the adopted position of t_o was kept down to $\pm$ 0.03 sec. If a constant delay had been assumed, on the other hand, certain echoes would have suffered errors up to 0.25 sec.

7.3 The transmitting and receiving polar diagrams

Details of the method by which the radiation and sensitivity patterns of the transmitting and receiving antennas were measured have been given by Nilsson (1963), who devised the method. Here the results, as applied in the present investigation, are presented and discussed with emphasis on differences among the receiving stations.

Briefly, the method used was one of substitution. At St. Kilda a standard receiving antenna was constructed. It was a replica of the other receiving antennas both there and at Salisbury, but instead of relying on the ground as a perfect conductor it used a square wire mesh ground plane of side 50' (i.e. nearly twice the wavelength), laid on the ground, as a reflector. An aircraft carrying a 5 watt transmitter was flown over St. Kilda and over the transmitter at Adelaide. Although a crossed ferrite dipole antenna was used in the aircraft, with suitably phased feed arrangements, its radiation pattern was not uniform in azimuth relative to the aircraft because of the effect of the metal fuselage longerons. Therefore in both flights the flight patterns were of ascending spiral form, arranged to be nearly identical in each flight, so that the aircraft should present as far as possible the same aspect to the ground antenna throughout the flights. The aircraft was tracked from the ground with theodolites, and its altimeter readings were transmitted to the ground

via its VHF radio. A standard narrow-band Doppler receiver was connected to each antenna of interest, viz. the standard and Doppler 2 at St. Kilda and the transmitting array at Adelaide. A chart recorder kept continuous records of receiver output with time, and tape recorders and time markers were arranged so that altimeter and theodolite readings could be later correlated with the charts.

The necessary ranges and directions were calculated with the aid of the 7090 computer so that the graphs of receiver output vs. time could be converted to tables which indicate the variation of the product, $G_R G_A$, of the gains of the ground and aircraft antennas, as a function of aircraft position. On the assumption that G_A was the same on both flights for a given elevation and azimuth of the aircraft, the gains of the antennas on the ground could be directly compared. These relative G_R values for the Doppler 2 and transmitting aerials were converted to absolute power gain by assuming that the standard antenna had its theoretical polar diagram.

In this way it was shown that, despite the proximity of Doppler 2 antenna to others in the direction-finding array, its polar diagram was not significantly different from that of the standard. Therefore it has been assigned the theoretical pattern in this investigation; this pattern is illustrated in Figure 7.1, expressed as power gain normalized to a maximum of 10. The maximum power gain relative to an isotropic radiator is 5.16.

The same polar diagram has been assumed for all the outstation receiving aerials, with considerable confidence in the case of Salisbury, where the aerial was several wavelengths from all metallic objects, but less confidently in the case of the Sheedy's Farm and Direk outstations. The latter both had a metal tube rather than a wooden support pole for the 27 Mc/s dipole, and the VHF transmitting Yagi was mounted above the dipole on an extension of the tubular support. However the largest dimension of the Yagi was less than 1/8 wavelength at 27 Mc/s, and the use of coaxial feed cables and a balance-to-unbalance transformer for the dipole minimized 27 Mc/s current in the support pipe below the dipole. Therefore the accuracy of the theoretical polar diagram for these aerials

is probably quite adequate, taking into account the various other uncertainties associated with their use. As a precaution, however, the part of the analysis dealing with trail electron density profiles and hence with echo amplitudes was arranged to treat results for Salisbury and St. Kilda separately from, as well as in combination with, results for the other stations. (V. Chapter 8).

Figure 7.1 also shows the polar diagram finally adopted for the CW transmitting antenna. Here the peak power gain, once more normalized to 10 for drawing convenience, is actually 11.3 . Neglecting fine structure near the zenith, the general pattern is that of a broad-beam antenna directed vertically upward, with perhaps a slight bias towards the south, and no minor lobes. It has been modified slightly from the original results of the aircraft flights, to reduce the peak at 137° azimuth (rel. true north) to a level compatible with the echo rate data.

To illustrate this comparison with the echo rates, Figure 7.2 shows the combined sensitivity of the Adelaide - St. Kilda system as a function of azimuth and zenith angle (relative to true north, and with origin at St. Kilda), for echoes occurring at the mean height of 93 Km. Allowance is made for the separation of the stations, the orientation of each antenna, and the range of the reflection point. Resonance is assumed not to occur. The sensitivity is expressed in terms of the line density (electrons/metre) which would give a 1 microvolt skywave signal at the receiver terminals if the transmitted power were exactly 300 watts. (This signal is assumed to give roughly the smallest readable echo amplitude, but is probably rather smaller than the threshold level for actually triggering the recording sequence. A signal generator set for 2 microvolts e.m.f. and matching the 75 ohm input impedance would produce the same terminal voltage when connected to the receiver). At stations 2 and 3 the 27 Mc/s. aerials had the same azimuth setting (12°W) as those at station 1 (St. Kilda). Hence the St. Kilda sensitivity map is also valid for Sheedy's Farm and Direk.

Figure 7.2 includes also a sensitivity map for the Adelaide - Salisbury system. The Salisbury aerial was directed to azimuth 12°E. In this map, for convenience, the angular coordinates again have St. Kilda

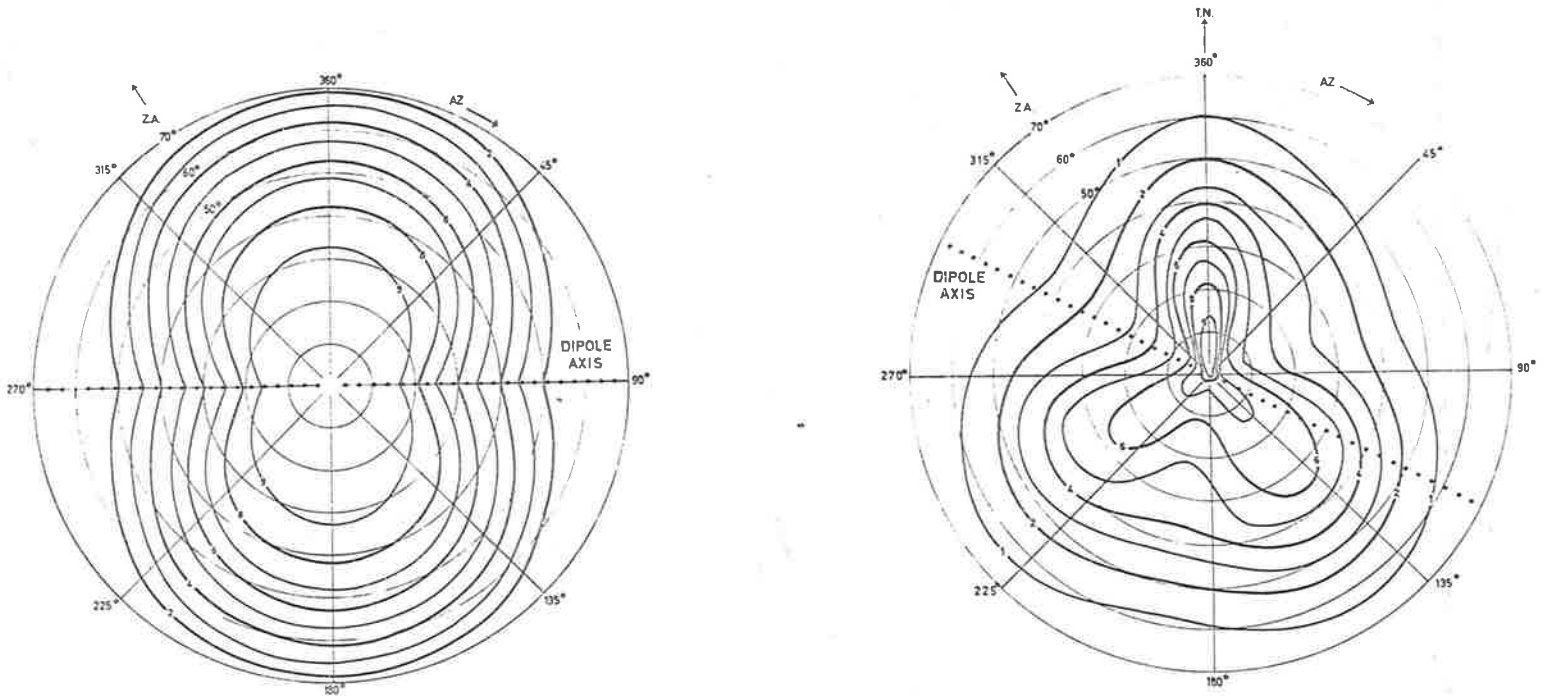

Figure 7.1. Antenna gain polar diagrams (normalized to 10 max.). Left: receiving dipoles. Right: CW transmitting array.

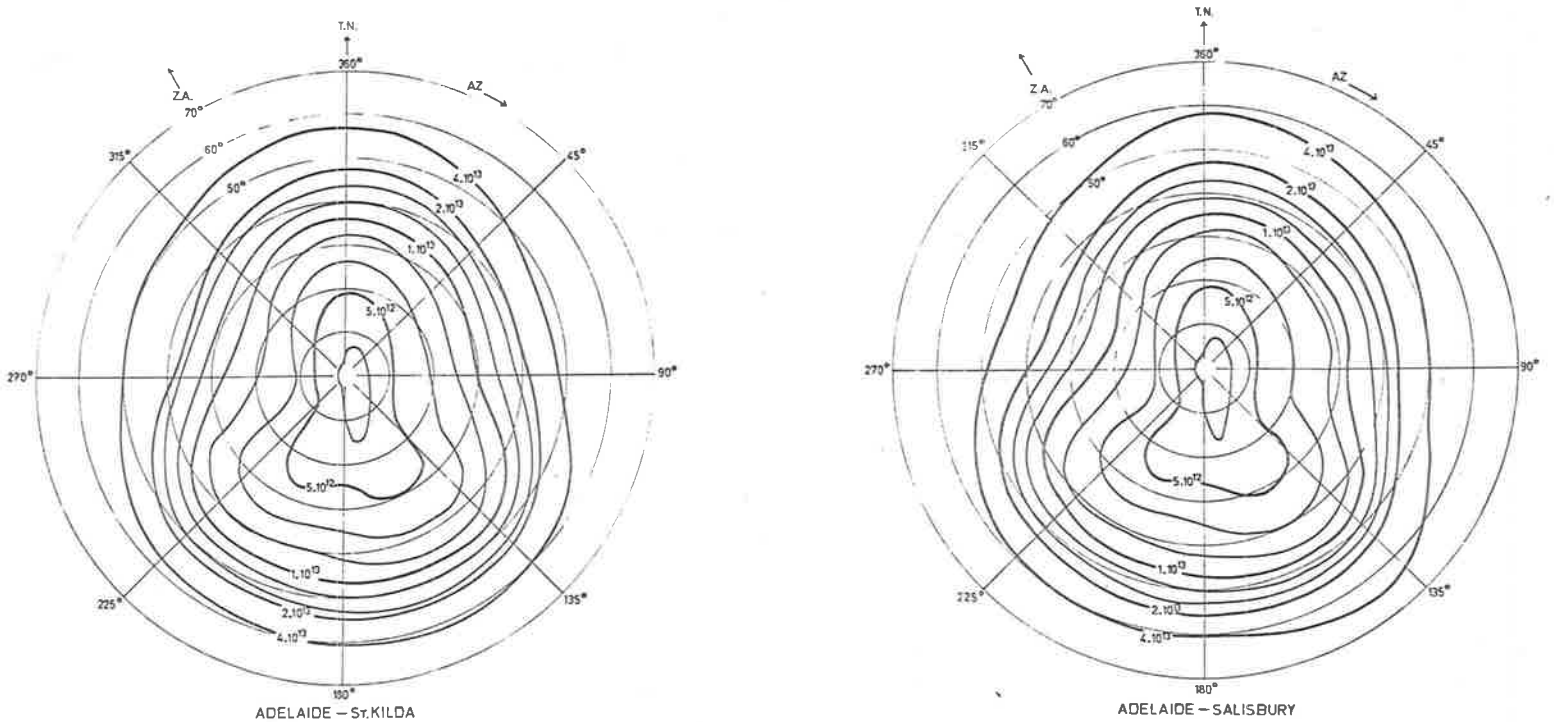

Figure 7.2. Overall system sensitivity for two receiving stations as a function of azimuth and zenith angle. The electron line densities marked on the contours are those which would produce a 1 microvolt skywave signal at the receiver terminals for a transmitted power of 300 watts. Reflection point heights are taken as 93 Km.

as origin. It can be seen that the influence of the receiving dipole polar diagrams on the overall system sensitivity is small, and the pattern of sensitivity is essentially controlled by the transmitting antenna.

For all the echoes used in the survey, Fig. 7.3 shows the distribution of numbers detected in each sector of the sky measuring $2\frac{1}{2}^{\circ}$ in zenith angle by 5° in azimuth (again as seen from St. Kilda). To compare this distribution with the sensitivity maps in Fig. 7.2 we must recall that the probability of detecting a trail by radio depends in a complicated way on the zenith distance of the reflection point. The probability is zero at the zenith and the horizon, with a peak at intermediate zenith angles determined to some extent by the polar diagram(s). This behaviour is evident in Fig. 7.3; no meteors were detected closer to the zenith than 15° or further from it than $67\frac{1}{2}^{\circ}$. The distribution in azimuth is in fair agreement with Fig. 7.2 . The southward bias is more marked in Fig. 7.3 (rate) than 7.2 (sensitivity), but this need not signify an error in the polar diagram. Weiss (1957) showed that the earlier Adelaide equipment also detected a majority of echoing points southward of the system, or more explicitly to south-east and south-west, and that this was a consequence of the apparent concentration of radiants near the Sun and the anti-solar point, and the apex of the Earth's way, due to the ellipticity of meteor orbits and the Earth's motion respectively.

7.4 The prior reduction of radiant data

Certain points connected with the calculation of the radiants and orbits of the meteors used in this survey (Nilsson 1963, 1964) can usefully be discussed at this stage.

Firstly consider the station map in Fig. 6.2, and the rectangular axes with origin at St. Kilda fixed by the Sheedy's Farm and Direk outstations. Define the coordinates of Sheedy's Farm to be (b,0,0), those of Direk (0,c,0), and those of the transmitter (d,0,0). Then if a meteor trail is detected at a distance R_o from St. Kilda under the condition of specular reflection, the parametric equation of the trail is

$$\begin{aligned} x &= lR_o + \lambda\epsilon \\ y &= mR_o + \mu\epsilon \\ z &= nR_o + \nu\epsilon \end{aligned} \qquad \ldots 7.4.1$$

where l, m, n are the direction cosines of the range vector R_o,

λ, μ, ν " " " " " " trail, and

ϵ is a position coordinate measured along the trail from the reflection point. If ϵ is defined to be positive below the reflection point, i.e. in the direction of meteoroid travel, then ν is negative.

In particular, let ϵ_2 and ϵ_3 be the positions of the specular reflection points for Sheedy's Farm and Direk (stations 2, 3 respectively). Then on the mid-point approximation, (v. Section 6.1), it is easily shown that

$$\lambda = \frac{\epsilon_2}{b/2}$$

$$\mu = \frac{\epsilon_3}{a/2} \qquad \ldots 7.4.2$$

However, this approximation is too inexact for use with the Adelaide station layout. Instead a solution in powers of $1/R_o$ is used, and sufficient accuracy is obtained by using terms to the second order in $1/R_o$. In this solution two expressions become available for the direction cosine ν, one from $\nu = -(1 - \lambda^2 - \mu^2)^{\frac{1}{2}}$ and one from the specularity condition involving the six direction cosines together with R_o and d. The two values for ν agree only if the measured values of l, m, n, R_o, ϵ_1, and ϵ_2 are such as to imply exactly specular reflection. Now such an over-determined system can be transformed so that any chosen variable becomes the one with the redundant value. Nilsson chose the quantity n, the vertical direction cosine of the line of sight, since the uncertainty in its measured value could be estimated from the magnitude of that value. Note that the reflection point height as measured is nR_o. We shall speak of the "redundant height" $n'R_o$, where n' is the re-calculated value of n.

With redundant information thus available, it was logical to try to bring the data into better all-round consistency with the assumption of specular reflection, by adjusting some measured quantity within the limits of its experimental error. Therefore Nilsson applied a so-called "optimization" procedure to the meteor velocity, i.e. the variable whose measurement was the most complicated and whose value was least certain as a consequence. The velocity was adjusted subject to a limit set by

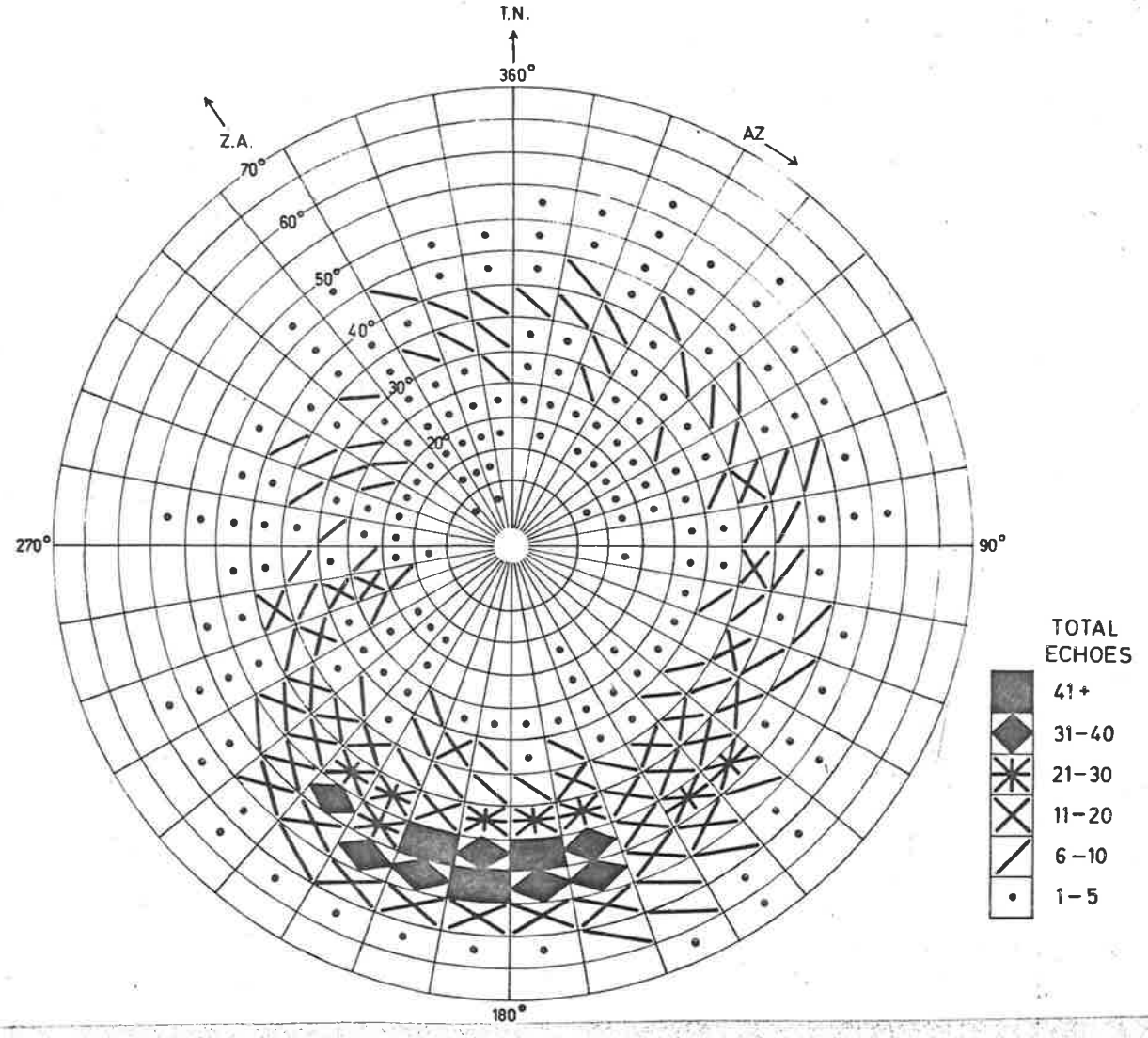

Figure 7.3. Distribution of meteors in azimuth and zenith angle in the 1961 survey.

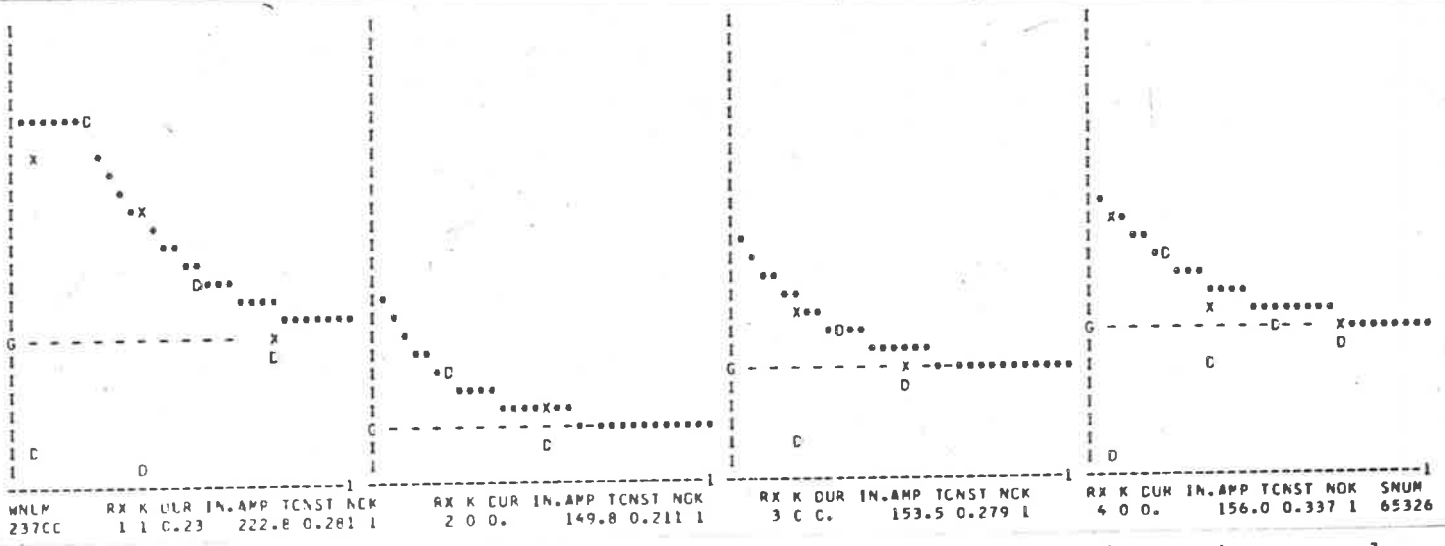

Figure 7.4. Typical results printed in programme ENVLO, for meteor number 23700. (Film records for 23700 are in Figs. 6.6 and 6.7). Each graph of echo amplitude against time represents one film record as interpreted in the computer. Note that two traces are inverted in the film record but not in the printed graphs.

Legend: G - - , receiver output on ground wave alone;

D, data points (Doppler extrema) as read;

X, translation of Doppler minima into skywave amplitude, plotted relative to G - - as zero

(Doppler maxima transform into themselves, i.e. into existing "D"'s);

***, fitted amplitude-time curve.

Time in seconds is marked on the horizontal axis. The total range of amplitude is 500 film-reader units.

the quality of the diffraction patterns. For a typical echo the limit was about ±6%. This adjustment had the effect of altering each of ε_1, ε_2, λ and μ in the same ratio. The aim of the procedure was to bring the redundant height within (16 - 12n) Km. of the observed height nR_o. The expression (16 - 12n) was not an estimate of the uncertainty in nR_o alone, but of the sum of the uncertainties in nR_o and $n'R_o$, the latter usually being expected to be the worse. If the desired height agreement was achieved without reaching the limit on velocity adjustment, a quality indicator variable NQ was set equal to 1, and the adjusted values of v, λ, μ, and ν (the main results of the radiant analysis) were adopted. Failing such agreement of the heights, the set of v, λ, μ, ν giving the best agreement subject to the limits on v was adopted, but NQ was set to zero as an indicator of poor quality.

In either case, the measured value of n was left untouched in the optimization routine. Thus the procedure did not set out to bring the data into exact specular form, but only into its neighbourhood, as defined by the probable reading errors.

7.5 General note on computer programmes

None of the aspects of the 1961 survey carried out at Adelaide - routine wind measurements, turbulence, orbits, trail profiles, or diffusion coefficients - was planned with the possibility in mind of using a digital computer to help analyze the results. It is also true that none of the analyses could have been carried to its present degree of completeness without the availability of one of these machines.

In both of the projects of this thesis, it was correctly anticipated that the data would be very numerous, would contain much scatter in values, and would be difficult to represent and summarize by the usual statistical techniques. Hence the author has made considerable use of both the machines alluded to above, and has adopted an attitude to their use which is at present unusual, but whose advantages are being increasingly realized. Where a computer is used as an aid to organizing and understanding a large volume of data, the greatest efficiency in its use is attained when the data are organized and presented in

the form of visual patterns readily acceptable to the eye. Thus it is inefficient to have the machine print a table of numbers when it can with almost equal ease and negligible extra computation time be made to print them as a graph. Similarly, a diagram showing the distribution of many values of a variable is a valuable (and easily obtained) adjunct, and is sometimes preferable, to the statistical measures with which we customarily try to summarize such distributions. Finally, a point brought out in the next section is that when a computer is used to make large numbers of decisions, as in fitting a model to data, it can frequently be made to give a better visual indication of the correctness of these decisions than a numerical index of "goodness of fit", for example, can provide.

The reader will therefore find that in the present work at least as much emphasis has been placed on using the computer to collate information and present it in readily absorbed form as on mechanizing tedious calculations with its aid. It is felt that this approach is especially applicable to geophysics, with its large volumes of often "noisy" data.

All programmes used have been checked, either by manual calculation of results for comparison with those from the programme, or by causing the machine to produce graphical indication that the programme has functioned correctly.

The following sections describe briefly the roles of a number of programmes in the reduction and analysis of the data. In Appendix 3 most of these programmes are summarized by flow diagrams, together with remarks on the computational details where appropriate.

7.6 Echo waveform reduction

The reduction of raw echo-amplitude-time data was performed using the 7090 computer. The logic of the reduction process is given in Appendix 1, and some details of the computer programme appear in Appendix 3.

Using the machine for this first part of the analysis had several advantages. It made the numerical results available in a convenient form (magnetic tape) for subsequent analysis. It ensured that proper weighting was applied to amplitude data in the fitting of exponential decays. (In finding by eye a best-fit exponential to varying numbers of points covering a wide dynamic range, improper weighting is quite probable).

Most important, it enabled the printing of graphical information (see Figure 7.4) in identical format for every echo, and from these graphs overall quality and goodness-of-fit were much more easily assessed than from any numerical quantities. (The necessity for subjective decisions about some echoes was unavoidable. However, through having all the graphs available simultaneously for review, the author was able to be more consistent in these decisions than if the reduction had been done graphically by hand and over a necessarily long period). Finally, it provided experience in the manipulation of Doppler information which will be valuable if, later, the step is taken of recording echo waveforms on magnetic tape for playback and subsequent analysis by a computer without intermediate use of film.

The raw data from the film reading took the form of some 9000 punched cards (either 4 or 5 per meteor). Firstly all of these cards were processed in a single computer run, at the completion of which every graph was examined by the author. On the basis of this examination the films for some echoes were re-read to correct obvious errors, or to include data points, not originally read, which were needed for proper definition of the envelope of the Doppler waveform. It was found that a considerable proportion of the underdense (KIND 0) echoes had been read with too few data points, due to a misunderstanding in the film-reading. Without this graphical review of the results, the fault would quite possibly not have been detected. The corrections were processed again in the computer, and the sequence of review and correction was repeated twice more. So few meteors then required further amendment that to process them would have been uneconomical.

7.7 Data-display subroutines

The graphs used in evaluating each echo as described in Section 7.6 were generated using the author's PLOT subroutine. In subsequent work this subroutine has been continually revised and expanded so that it is now a very versatile aid for the analysis of any data capable of graphical display. The most important addition has been the facility for plotting a scatter diagram of an unlimited number of points, and finding statistical measures of the distribution.

This subroutine is now available for general use at W.R.E. Salisbury (Stone 1966b) and some details appear in Appendix 3. It is unusual in using the computer's line printer as a plotting device and in setting no limits to the number of points to be plotted or the number of graphs (either superimposed or in separate blocks) per page. The scatter diagram facility is also uncommon, and has the added advantage that the means and standard deviations of both coordinate variables, and the correlation coefficient, are always found.

Automatic scaling in both horizontal and vertical directions is available to the user at will. If the scales are instead preset by the user, points lying outside the plot are indicated by printing a special character at the nearest point on the edge of the plot. Such points do not affect the statistical measures found in the scattergram mode. Thus, by a suitable choice of scale factors, unrealistically large values of either coordinate can be conveniently ignored, but are still visible in the plot.

The scattergram can be thought of as a two-dimensional frequency table. For one-dimensional frequency tables a different display method is needed. The author has adapted for the 7090 at W.R.E. an existing subroutine HIST* and incorporated certain refinements. This subroutine prints a histogram of the numbers of events recorded in up to 106 successive classifications. Subroutine HIST has been used extensively (as has the plotting one) in the trail profile analysis (Chapter 8).

These display subroutines are simple and convenient to use. For example, using PLOT, it would be possible with three Fortran calling instructions to produce a scattergram of as many (x,y) coordinate pairs as can be stored in the remainder of computer memory, i.e. some 11000 pairs in the machine at W.R.E. The execution time for this unusually large assignment would be of order two seconds; smaller tasks are very much more quickly performed. Using HIST, a histogram of 106 columns with column frequencies of any practically likely size is generated, by means of just one Fortran instruction calling the subroutine, in less than 0.1 second.

---

* I.B.M. SHARE program no. 1561 .

7.8 Finding the fourth reflection point

Let us now return to the data reduction. The next step logically following the reduction of the echo amplitude data was to calculate the Salisbury reflection point's position on each trail. In fact this work was carried on concurrently with testing the methods of amplitude data treatment, and was found to contain some unforeseen difficulty.

The surfaces of constant total range, for a radar system whose transmitter and receiver are separate, are the set of confocal spheroids with foci at the transmitter and receiver. Specular reflection from a meteor trail at a certain total radar range implies that the trail is tangent to the spheroid whose parameter is the given range. Therefore, assuming that the direction cosines of the trail and the position in space of the main station reflection point are accurately known, the problem is to find the spheroid with foci at Adelaide and Salisbury to which the trail is tangent. The difficulty is that these assumptions do not hold.

In Section 7.4 we indicated that the more directly measured height nR_o of the main station reflection point did not in general agree with the height $n'R_o$ calculated on the assumption that all of l, m, λ, μ, ν and R_o were accurate. (For definitions see the Section mentioned). That is, the data available for the present problem were inconsistent. As a result, both analytic and iterative (approximate) solutions were tried for some time without success, because they contained the implicit assumption that the data represented specular reflection.

A method of solution which is given in Appendix 3 was finally adopted. In it the trail is assumed to have been correctly located in space, but both the main station and Salisbury reflection points are moved along the trail in an iterative process until specular geometry is attained with suitable precision for each. The result of interest, viz. the distance separating these two reflection points, is then readily found. In addition, the new height found for the main station reflection point is the height used in subsequent analysis. For meteors with NQ = 1, i.e. those for which Nilsson's optimization of the trail direction cosines λ, μ, ν was successful within the range of experimental error (Section

7.4), this new height is almost identical with the "redundant height" $n'R_o$. Thus it differs from the originally measured value by an amount which, for NQ = 1, is justifiable on the basis of experimental uncertainty.

Appendix 3 also describes a programme for the IBM 1620 which was written to find the fourth reflection point for each meteor. Most of the programme was devoted to the calculation, the input taking the form of cards (one per meteor) bearing direction cosines and the other necessary data abstracted from the results of the orbit reduction. Two cards of results were punched by the computer for each meteor. For the purpose stated in the next paragraph, it was convenient to process every meteor, and not merely those for which an actual echo had been recorded at Salisbury. This calculation was very accurate; in Appendix 3 evidence is given to show that the r.m.s. error in the calculated distance from a known reflection point to one for station 4 was of order 20 metres. The r.m.s. percentage error in the distance was less than 2%.

A very necessary added feature of the programme was a test of the degree of inconsistency in the input data. This was carried out by comparing the original and the computed values of the total radar range and of the line-of-sight direction cosines l, m and n . The total range has a reading uncertainty of approximately ± 2 Km., and in the coordinate system with an axis along the Adelaide - St.Kilda line each of l, m and n has a reading error of order ± 0.05 . For meteors with which one or more of these tolerances was exceeded in attaining specular geometry, an indication of poor quality was stored as a special code in an output card. Subsequent programmes translated this into a zero value for a quality-indicator variable NGEOM. In the case of a meteor whose data were within tolerance of specularity, NGEOM = 1 . It will be seen that NGEOM should be fairly well correlated with NQ, the variable indicating whether the optimization of λ, μ, ν was successful in the orbit reduction (Sect. 7.4). In Appendix 3 this statement is substantiated by a table.

A point of some importance which is also made in the same part of Appendix 3 is that the absolute accuracy of height measurement with the

Adelaide equipment is ±2 Km. or ±3 Km., depending on the selection of meteors.

7.9 Antenna gain product for each echo

The next step in reducing the data was to combine the cards containing geometrical information (last Section) with the magnetic tape of echo amplitude results (Section 7.6). This task and the calculation of the product of transmitting and receiving antenna gains for each echo were carried out simultaneously. From the assembled information, the minimum detectable underdense line density (defined as in Section 7.3) was found for the position in space of each of the four reflection points on every meteor trail. In making this minimum line density estimate a nominal value was assumed for the radiated power from the transmitter, and the following Section details how the nominal power value was subsequently improved.

In Appendix 3, a 7090 computer programme with which the above work was done is described. Its results for each echo were written on another magnetic tape. In addition, it printed tables of minimum line density as a function of position in the 93 Km. plane, which were used in constructing the maps of this quantity's variation in Section 7.3. For this programme there were about 8000 input data cards altogether, and (as with the echo amplitude cards) a good deal of care was required in checking their contents and their order.

7.10 Fluctuations in power and sensitivity

The fundamental measurements made on an underdense echo were V, the receiver output voltage, extrapolated back from the recorded section of the echo to t_o, and V_G, the receiver output voltage on groundwave alone, measured about a second after t_o or as soon as possible afterwards. The conversion of V and V_G into the electron line density α involved several equipment parameters, some of which (viz. radar range and the gain of the transmitting and receiving aerials) have already been discussed. The remaining parameters are

(a) the power P_T radiated by the transmitter,

(b) the receiver sensitivity S, defined as the ratio of rectified voltage output V to r.m.s. voltage v at the input terminals, and

(c) the voltage attenuation factor A along the groundwave path.
Their determination, for each echo, is described below.

Consider first a system employing only one receiver. Its output on groundwave alone is

$$V_G = (P_T^{\frac{1}{2}} S)/A \qquad \ldots 7.10.1$$

From the radar equation (3.1.5), for a uniform trail of zero radius, and if the receiver matches the aerial impedance , we have

$$\alpha = \frac{V}{P_T^{\frac{1}{2}}} \left(\frac{128\pi^3 R_o^3}{G_T G_R \sigma_e} \right)^{\frac{1}{2}}$$

$$\text{i.e.,} \qquad \alpha = V/(P_T^{\frac{1}{2}} S) \quad F \qquad \ldots 7.10.2a$$

$$\text{or, using 7.10.1,} \qquad \alpha = \frac{V}{V_G} \frac{1}{A} F \qquad \ldots 7.10.2b$$

where F is the square root of the bracketed expression, whose symbols are those of Section 3.1 . In the case of interest, F can be found for each echo because the position of the reflection point is known.

The use which can be made of Eq. 7.10.2 depends on what other measurements have been carried out. If there have been none, the assumption that A is constant allows the values of V/V_G for individual echoes to be interpreted as directly proportional to α . If there has been made one set of simultaneous absolute measurements of V_G, S, and P_T (at a time t_1), then A can be found from 7.10.1. Hence α becomes known absolutely, rather than relatively, provided A is still taken as constant.

If, at a later time t_2, V_G and S (but not P_T) are measured again, the complication arises that the groundwave input voltage calculated from $V_G = V_G/S$ may have changed since time t_1. The line density α can be found for an echo occurring at or near time t_2 by deciding on the current value of either A or P_T, in one or both of which a change has evidently taken place. To solve for α in the case of an echo occurring between t_1 and t_2, taking into account the new measurements at t_2, either A or both P_T and S must be estimated in some way which is based on the states of the system at times t_1 and t_2 . (If A is chosen, V_G for each echo will also be used, in Eq. 7.10.2b . However, A is subject to such weather conditions as rain showers, and so may vary with time in a more complicated way than

P_T and S . If P_T and S are chosen for estimation, then V_G is not explicitly required in the relevant equation, 7.10.2a).

Actually, as has been described in Chapter 6, pairs of absolute measurements of V_G and S were made at both of stations 1 and 4 (St. Kilda and Salisbury) , at intervals of a day or less. Although P_T was not measured often or precisely, its value at the start of each recording period could be estimated within a factor of 2 . In any case, the measured ratios of line density α among reflection points were considered more important than absolute values of α . The latter were dependent on the initial value chosen for P_T , but the former were not.

Hence, as in the simplified example above, a choice had to be made of either estimating P_T , S_1, and S_4 (number subscripts denote stations), or estimating A_1 and A_4 and using V_G , for each echo. The choice was influenced by the wish to use echoes detected at stations 2 and 3, where the receiver sensitivities S_2 and S_3 were unknown and variable due to the use of slowly-acting automatic gain control. It was decided to estimate P_T, S_1 and S_4 in a way which used not only the semi-regular absolute measurements of V_G and S at stations 1 & 4 but also the echo-by-echo changes in V_G recorded at both of them. Because no further information was available from the almost constant values of V_G at stations 2 and 3, S_2 and S_3 could not be directly estimated. Instead, the groundwave attenuation factors A_2 and A_3 were found at the start of each recording period from A_1 and A_4 by applying the known fine-weather ratios $A_1:A_2:A_3:A_4$, and were assumed constant through the recording period. (This appeared at least as probable as the alternative assumption, viz. that A_2 and A_3 were unchanging functions of A_1 and A_4 only). Thus the radar equation was used in the form 7.10.2a for stations 1 and 4, and in the form 7.10.2b for stations 2 and 3.

A few trials showed that it would be impractical to extract by hand from the data a compatible set of models of the time variations in P_T, S_1 and S_4 . Hence the 7090 computer was used for this task. In the process, it was made to graph all the relevant data and results as functions of time. Thus violently discordant items of data could be detected and removed, and the efficiency of various models compared, visually.

To obtain the set of models which was eventually used, it was assumed that changes in the radiated power P_T were either serious enough to constitute sudden failure or smooth and gradual. The former were irrelevant; the latter were to be determined. In a prediction-correction routine, a model of the time variation of P_T was first constructed in agreement with the gain standardization results (absolute V_{G1} and S_1, or V_{G4} and S_4), and was then used to predict the groundwave outputs V_{G1} and V_{G4} for subsequent echoes. If both predictions differed in the same sense from the actual output voltages (averaged over all echoes in a 12-minute period), the radiated power model P_T was corrected to remove part of the deviations. Otherwise any fluctuations in V_{G1} and V_{G4} were ascribed to receiver gain changes. The power model P_T (incorporating any correction) was then used to make predictions for later echoes, and so on. A chart in Appendix 3 gives a little more detail of the computation.

The practical details of the above procedure were settled upon by graphical comparison of the results of various methods. These differed chiefly in ways of constructing an initial (predictor) model of the variations in power P_T, and in smoothing and integrating provisions. In the comparison process it was found that voltage gain S could be defined as a function of time to within $\pm 10\%$ for all receivers.

The final model of the transmitter power P_T showed fluctuations of order $\pm 20\%$, superimposed on a gradual upward trend throughout most recording periods. The total upward drift did not exceed 10% in any period. The question of whether this trend was really in P_T, or in both receiver gains S_1 and S_4, can only affect the ratio of line densities measured at those stations to the second order in S_1/S_4.

Because the methods of solving the radar equation for echoes at stations 2 and 3, and at stations 1 and 4, differed considerably, it is difficult a priori to state the accuracy of ratios of line densities found at the former to line densities found at the latter. Due consideration was given to this fact in analyzing the line density information. Some results which indicate that no major errors arose through including stations 2 and 3 in the analysis appear in Section 8.2.

To summarize the above discussion: in solving the radar equation for each echo which was used in the later analysis, a method was evolved which was designed to combine all the available data relating to transmitter power and receiver sensitivity as consistently as possible. All the tests which were applied to the method indicated that this aim had been achieved.

7.11 Trail profile and diffusion coefficient analysis

Almost all of the steps involved in reading and reducing the data to a form suitable for analysis have now been described. Chapters 8 and 9 contain the methods and results relating to ionization profiles and to diffusion coefficients respectively. Here it is only necessary to make a few remarks about the practical aspects of data handling in the analysis.

Three programmes, all for the 7090 computer, were used to carry out most of the analysis. Their manner of operation is described briefly in Appendix 3; their functions were as follows.

The first programme completed the data reduction process, and collated and displayed the results which pertained to ionization profiles. About half of the programme was concerned in each of these two tasks.

To complete the data reduction it was necessary

(a) to read the magnetic tape of interim results mentioned in Section 7.9,

(b) to solve the radar equation for underdense echoes, according to the method discussed in Section 7.10, and form line density estimates by other means for echoes which were not of the decay type,

(c) to apply corrections for the effects of reflection point movements along the trail upon measurements of line density and diffusion coefficient, as set out in Section 3.7,

(d) to find which echoes should be suspected of resonance, occurring with transverse polarization of the incident radio wave (see Section 3.6),

(e) to classify the data as to quality, using previously recorded "indicator variables" which gave the results of tests in the orbit reduction, in finding the fourth reflection point, and in reducing the amplitude-time information, together with (c) and (d) above, and

(f) to write a magnetic tape containing the final results for each meteor.

To display the results, the graph- and histogram-plotting subrout-

ines described in Section 7.7 were employed in the programme. For economy in computing time it was desirable, in one pass, to accumulate all the pages of graphical output which were required, and also to write the output tape of final results. As a consequence, the programme was quite large, using almost all of the machine's core memory plus its full resources for supplementary memory on magnetic tape.

The second programme was concerned with presenting the diffusion coefficient versus height distributions for chosen periods, again in graphical form. Given the initial and final dates of the period, the programme found (from the output tape written by the first programme) the diffusion coefficients D measured on each meteor trail which had been recorded on or between those dates. The values of log D and its height derivative were plotted against height, for the whole period, and in subsets for each four hours of the day. Separate distributions were plotted for the various quality classes alluded to in (e) above.

There were several large-scale similarities between this programme and the ionization profile programme which preceded it. The likenesses lay in reading input data from magnetic tape, in collating it with the help of other tapes to give extra memory capacity, in presenting graphical results by means of the plotting subroutine, and in overall large size. Of course there was no magnetic tape output from the diffusion coefficient programme, because no data reduction took place in it.

The third programme used in analyzing the results was an extensively modified version of an IBM library programme, written for a 709 machine, for performing multiple regression analysis. This programme was used to investigate which parameters of the meteor and the atmosphere were most strongly correlated with the height of maximum ionization and the diffusion coefficient. The author's modifications firstly made the programme suitable for the 7090 machine, but were chiefly a set of non-trivial changes which allowed up to 2500 sets of observations (instead of the original 200) to be examined at a time. Hence the tape of meteor results could be read as input data. In using this programme care was taken not to attribute physical significance to apparent relationships which might actually have sprung from mutual dependence on a third variable. A special feature of the programme, described in Appendix 3, facilitated avoiding this trap.

CHAPTER 8

IONIZATION PROFILE RESULTS AND DISCUSSION

8.1 Some parameters of the meteors used in the investigation

On the magnetic tape of results from the orbit analysis there were entries representing 2204 meteors, observed from December 1960 to December 1961 inclusive. This tape, and the echo amplitude measurements, provided the basic data for the present investigation. The removal of duplicated records, and records with errors in either the echo number or the time of observation, from the tape left 2173 meteors altogether. Of these, 1658 were observed in or after May, i.e. while the receiver sensitivities were being monitored, and therefore could potentially be assigned values for the electron line density α at the reflection points.

Much of the discussion in this chapter involves the two classification schemes which were applied to the data for all echoes. These schemes have been set out previously but it is helpful to summarize them here. This is done in Tables 8.1 and 8.2. Table 8.3 shows how many meteors were assigned to each classification group.

Table 8.1

Definition of quality index INDEXQ

INDEXQ	Tests passed, or attributes
1	All echoes yielding an estimate of line density
2	Reflection point motion correction applied to data
3	As 1; decay-type (KIND=0) only; specular within tolerance; orbit optimization successful; good amplitude-time record
4	As 1; incident polarization known to be within 45° of trail axis if echo of decay or transitional type (KIND=0 or 1); any polarization for persistent echo.

Note: an echo might qualify for any number of INDEXQ values (or for none).

Table 8.2 Definition of KIND

KIND	Echo characteristics
0	Underdense. Exponential decay.
1	Slightly overdense. Both constant-amplitude and exponential decay phases discernible.
2	Overdense, with duration exceeding 1 second. Reasonably constant amplitude. Line density taken as 2×10^{15} electrons/metre.
3	Either confused echo, not obviously KIND 0, 1 or 2, or of KIND 1 with too few Doppler extrema to define shape properly.
4	(Salisbury station only) Amplitude too small to be read, and taken as 1 microvolt.

Note: an echo might qualify for one value only of KIND.

Table 8.3. 1658 meteors classified by echo type and quality index

		Quality index . . 1	2	3	4
Trails yielding 4 values of α		546	505	116	230
3		395	423	259	149
2		130	107	134	54
1		133	100	150	123
0		454	523	999	1102
Reflection points where KIND =	0	2613	2526	1659	1152
(and α was available).	1	1009	937	—	455
	2	125	125	—	125
	3	—	—	—	—
	4	15	15	—	15
Total reflection points where KIND =	0	3324			
(as assigned before processing).	1	1358			
	2	125			
	3	1810			
	4	15			

The echoes of chief interest were those with KIND equal to 0 or 1. Approximately three-quarters of these could be reduced to yield line density estimates. In most cases there were two or more usable reflection points per meteor trail, so that the wind shear information needed for the calculation of reflection point motion (INDEXQ = 2) was generally available. Only decay-type echoes could be classified as having INDEXQ = 3. The other requirements for this classification eliminated about one-third of the decay-type echoes for which α was measurable (INDEXQ = 1). It is to be expected that echoes for which INDEXQ = 3 represent high quality measurements of both the geometry of the trajectory and

the echo amplitude-time relation. The group INDEXQ = 4, for which the incident polarization was known to be more nearly parallel than perpendicular to the trail axis, contained approximately 40% of all echoes. This is roughly the proportion expected from consideration of the details of the classification method (Appendix 3).

So that the diffusion coefficients might be examined for each of the 13 months of the survey, it was necessary that echoes in the period Dec. 1960 - April 1961 be accepted although the electron density could not be measured. This prevented the making of corrections to their D values for the distortion of the decay waveform by reflection point motion, i.e. these meteors did not have D values calculated for INDEXQ = 2. However, during and after May 1961, only the reflection points where α was known were included in any analysis of D values. This allowed a clearer comparison of diffusion coefficients in the classes INDEXQ = 1 and = 2.

In connection with the remainder of this chapter it is stressed that (1) no meteor trail with more than one persistent-type echo (KIND 2) was analysed for its electron density profile, because of the impossibility of comparing in two such echoes. However, this rule was not allowed to prevent the application of the correction for reflection point motion to diffusion coefficients measured elsewhere on such trails.
(2) trails for which the measured reflection geometry was not specular, within reasonable limits, were similarly not used in this analysis.

We now consider briefly the distributions of values of those parameters which define the sample of meteors analyzed.

Figure 8.1 is a histogram showing the meteor velocity associated with every pair of reflection points, both on the same trail and having INDEXQ = 1. There is no significant difference from similar results for the other quality index classes. Neither is there any apparent correlation between the number of reflection points giving usable amplitude data per meteor trail and the meteor velocity. Therefore this figure, with one entry per reflection point pair, is little different from that given by Nilsson (1963) with one entry per meteor. The letter M below the figure indicates the mean velocity, approximately 34 Km/sec. The two peaks arise from astronomical causes.

In Figure 8.2 is shown the frequency distribution of height differences between reflection points for pairs of points with INDEXQ = 1. Both the arithmetic mean and modal separations were of order 0.8 Km., and there was an upper cutoff at 3 Km. Not all of these pairs of points were used in the trail profile analysis, or in measurements of $\frac{d}{dh}(\log D)$. It was felt that although the orbit reduction was able to measure the distances along the meteor trajectory between t_o points to within 100m., rather larger height differences should be rejected in the profile work because the heights to which the α measurements pertained would not be those of the t_o points if reflection point motion due to wind shear was important. Therefore a lower limit of 400 m. was arbitrarily set, and separations leading to height differences smaller than this figure were simply not used. The effective mean difference in height thus became 1.1 Km.

In Chapter 3 the effective heights where α was measured were denoted by $h - Vt_5 \cos\chi$, where h is the height of the t_o point, $V \cos\chi$ is the vertical component of reflection point motion, and t_5 is the elapsed time from t_o to the centre of the time interval in which the decay time-constant was measured. For INDEXQ = 2 the height differences between the values found for $h - Vt_5 \cos\chi$ were used, and the only overall difference was that approximately 80 height differences out of nearly 4400 now fell in the previously empty range from 3 to 5 Km., obviously arising from echoes of transitional type (large t_5) in the presence of strong wind shear. Echoes passing the tests for quality indices 3 and 4 were given the same reflection point heights as for index 1. The height differences in these two classes were distributed as for INDEXQ 1.

The distribution of measured values of wind shear appears in Figure 8.3, and the reflection point speeds derived from them according to Equation 3.7.3 are shown in Figure 8.4. In constructing these histograms trails with only one value of α available are excluded. These frequency distributions are notable for their long "tails" of large values of both quantities, allied with very prominent central peaks in the regions of zero shear and zero reflection point speed. Because of this complete departure from Gaussian or normal frequency distribution there is little

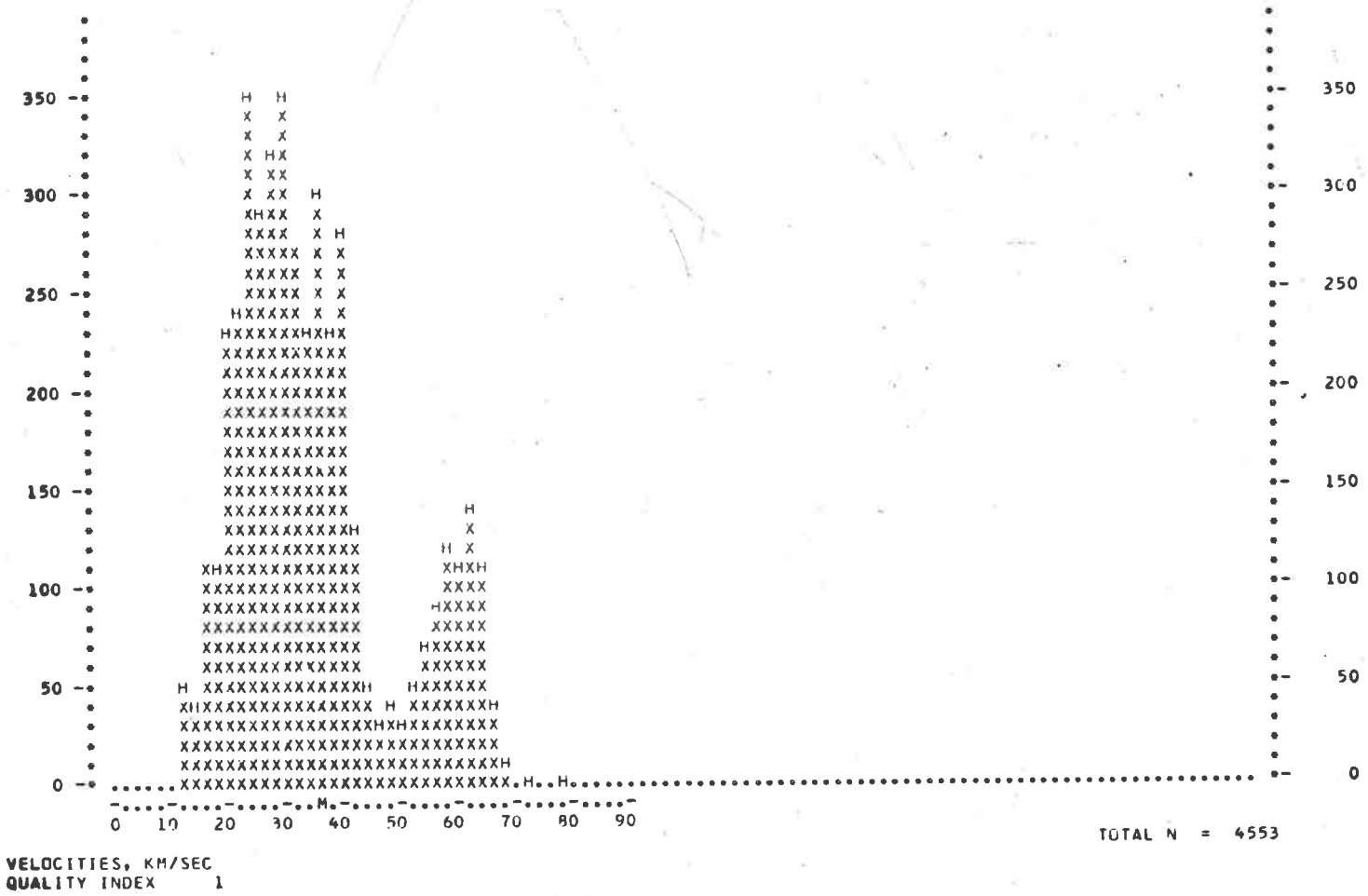

Figure 8.1. Velocity Distribution

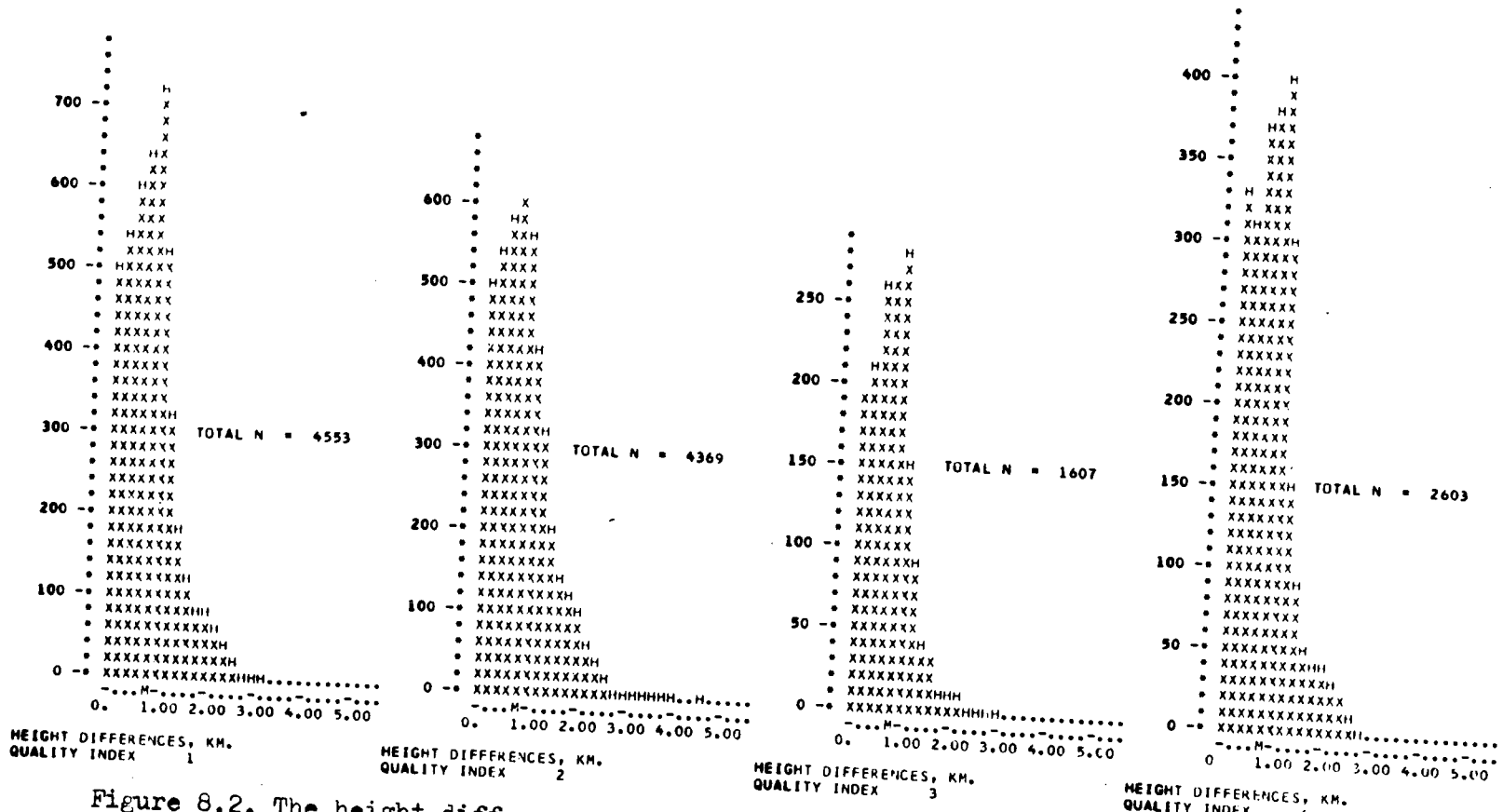

Figure 8.2. The height differences among the reflection points used in the trail profile analysis.

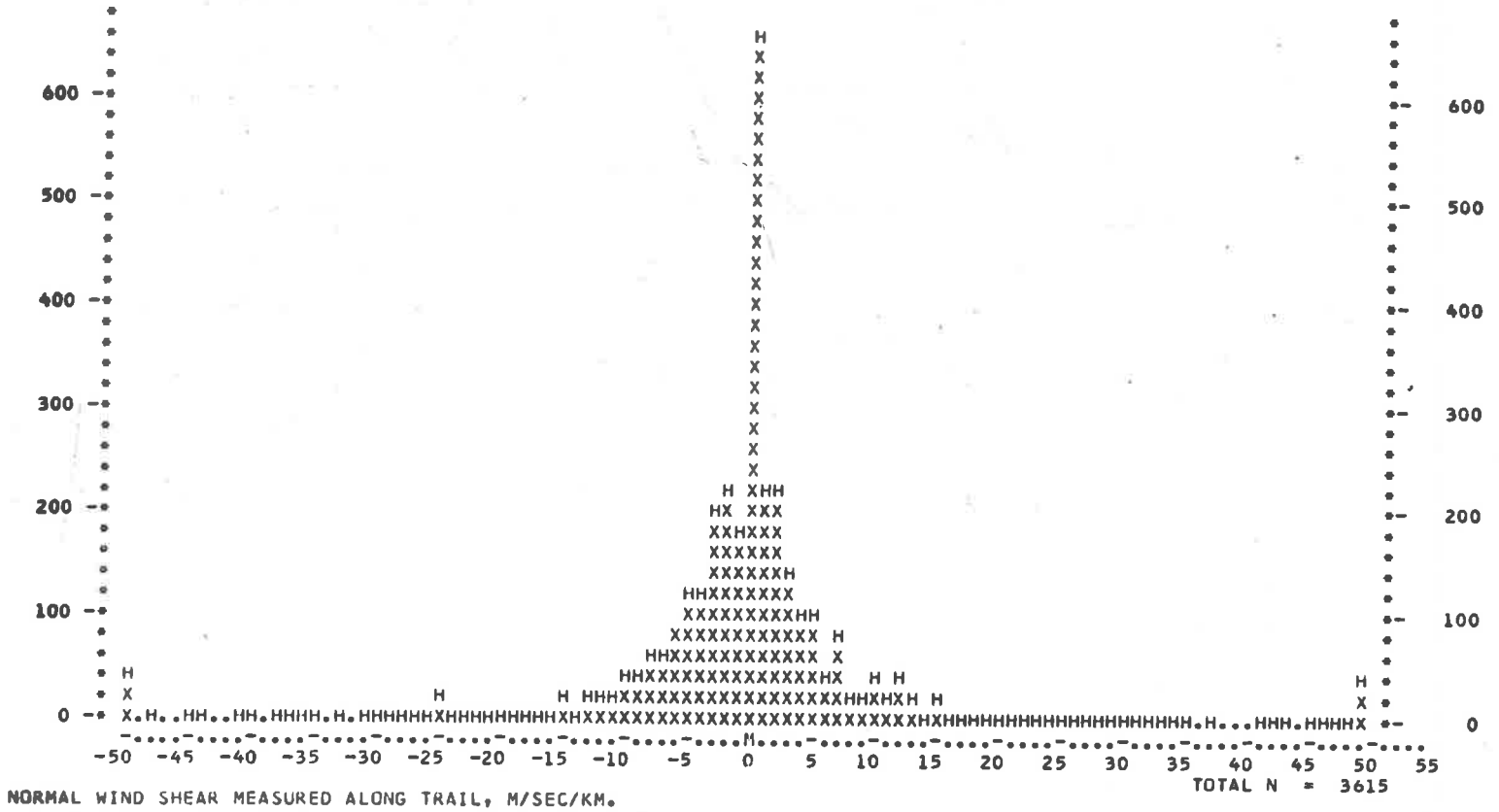

Figure 8.3. Measured shear in the line-of-sight component of the trail drift speed.

point in calculating r.m.s. shears or speeds. Instead we may note that 50% of the shears were between ± 5m/sec per kilometer of trail length, but individual shear values extended more or less continuously to magnitudes beyond 50 m/sec/Km. The reflection point speed had a 50% probability of being smaller than 0.5 Km/sec., but individual values were as large as 8 Km/sec. Roper (1962) examined the rate of change of the Doppler beat frequency in 70 echoes recorded in December 1960. He found that the r.m.s. rate of change in the line-of-sight drift was 9.1 m/sec^2, so that if the wind speed measurement was made 0.2 sec. after t_o the error made was only of order 2 m/sec., comparable with the film reading errors. Assuming a linear wind gradient, he calculated the speeds of reflection point motion along the trail, and found an r.m.s. value ~ 1 Km/sec. with some cases of speeds up to 6 Km/sec. In both his and the present results the arithmetic mean speed was zero. The central peak in Figure 8.4 is slightly narrower than that in Roper's distribution. Thus the two methods gave results agreeing in most respects.

8.2 Accuracy of determination of profile shapes

In this section we establish the accuracy with which the ratio of the electron line densities at two reflection points could be measured. Questions of absolute accuracy in line density are discussed in following sections.

To find the shape of a profile of line density versus height, the distances between reflection points were required as well as the relative line densities at the points. It has already been stated (Section 7.8) that the Salisbury reflection point's position could be found relative to that for St. Kilda with an accuracy of about ± 25 metres, or ± 2%. The other spacings were known with similar accuracy from timing measurements on the film records. This precision was more than adequate.

Only one method could be used to check the reliability of ratios in line density. This was to extract from the data all pairs of points within a suitably short distance of each other, and examine the deviations of their line density ratios from unity. The distance limit chosen was 200 m., less than one-half the length of a central Fresnel zone. Hence,

if the trail was nearly uniformly ionized over the central zone and a few zones to either side, the two line density measurements should have agreed closely. Figures 8.5 and 8.6 show the results of this analysis. The former relates to all available pairs of points with the required small spacing; the latter to St. Kilda - Salisbury pairs only.

Firstly, comparing the figures as a whole, we see that the distributions for all reflection points (Figure 8.5) are not wider than those for the better calibrated St. Kilda and Salisbury receivers only (Figure 8.6). This is a welcome confirmation of the accuracy of the receiver gain analysis (Section 7.10). Secondly, the distributions for INDEXQ = 1 are of quite surprising width. The standard deviation of the binary logarithm of the ratio is approximately 1.0, i.e. a factor of 2 in the ratio itself, and about 5% of ratios show extreme discrepancies between 2^3 and 2^8.

Restriction of the set of echoes to good-quality decay-type examples only (INDEXQ = 3) immediately removes all ratios outside the range ($2^{-2.5}$, $2^{3.5}$) and leaves only 3% outside ($2^{-2.0}$, $2^{2.0}$). However, this is still a much wider range than one would expect from consideration of the measuring process. The time-constant of a smoothly decaying underdense echo could be read within 10%. Since the centre of the interval over which the measurement was made was generally less than one time-constant after the beginning of such an echo, it follows that the uncertainty in line density due to reading errors was also only of order 10%. Even the occasional waveforms for which this uncertainty was as large as 30% can clearly not have been responsible for ratios of $\frac{1}{4}$ or 4. ....

The 5% of INDEXQ 1 data leading to ratios from 2^{-8} to 2^{-3}, or from 2^3 to 2^8, are assumed in following discussion to be incorrect, and are therefore ignored. If in some cases this assumption is over-conservative, the number of meteors involved is clearly negligible.

Smaller errors, making up the broad peak of the INDEXQ = 1 histogram in Figure 8.5, have <u>not</u> been visibly reduced in the histogram for quality index 3. (Clearly another influence was responsible for these smaller and more numerous discrepancies.) Since, also, a 60% reduction

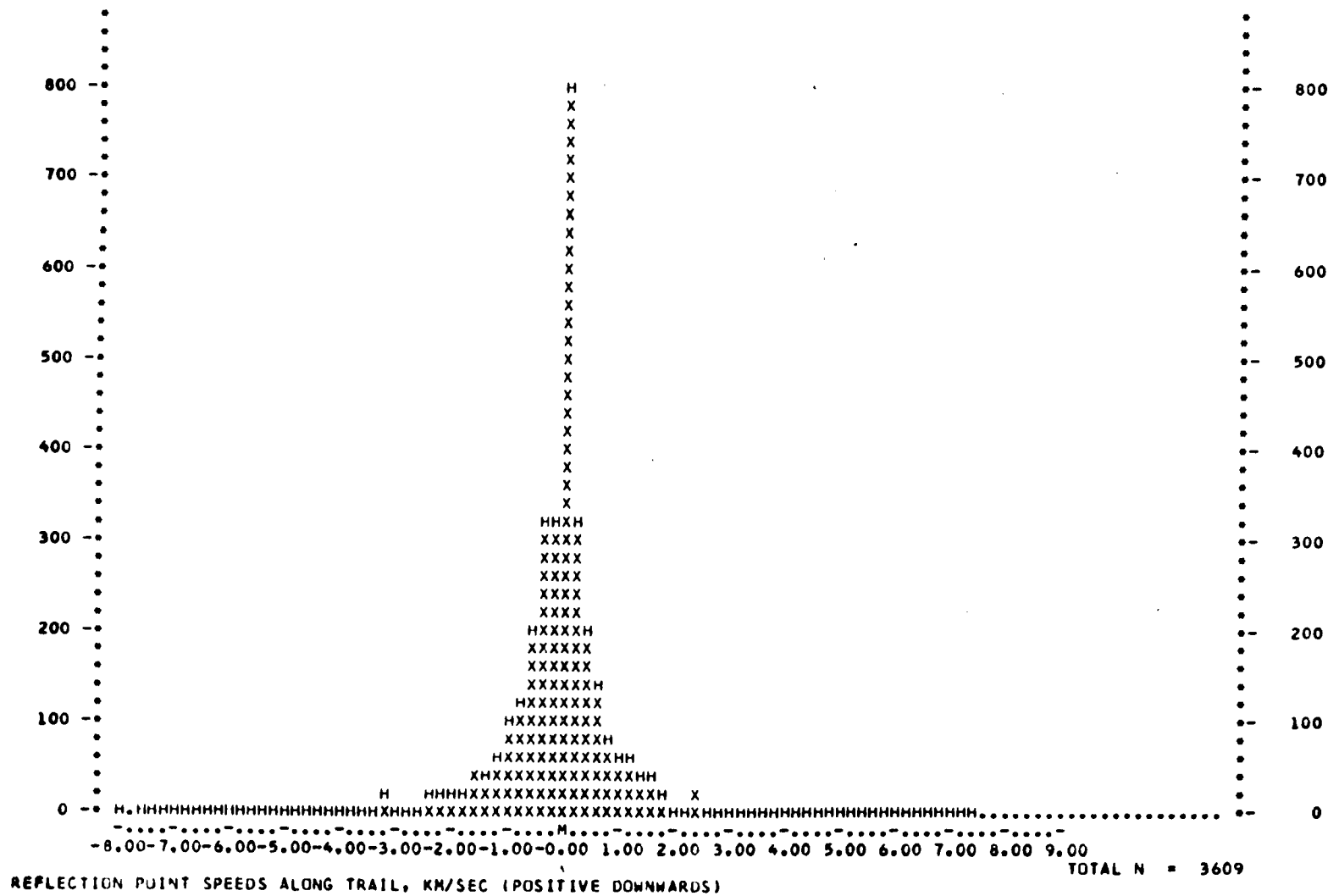
800
700
600
500
400
300
200
100
0
-8.00 -7.00 -6.00 -5.00 -4.00 -3.00 -2.00 -1.00 -0.00 1.00 2.00 3.00 4.00 5.00 6.00 7.00 8.00 9.00
TOTAL N = 3609
REFLECTION POINT SPEEDS ALONG TRAIL, KM/SEC (POSITIVE DOWNWARDS)

Figure 8.4.

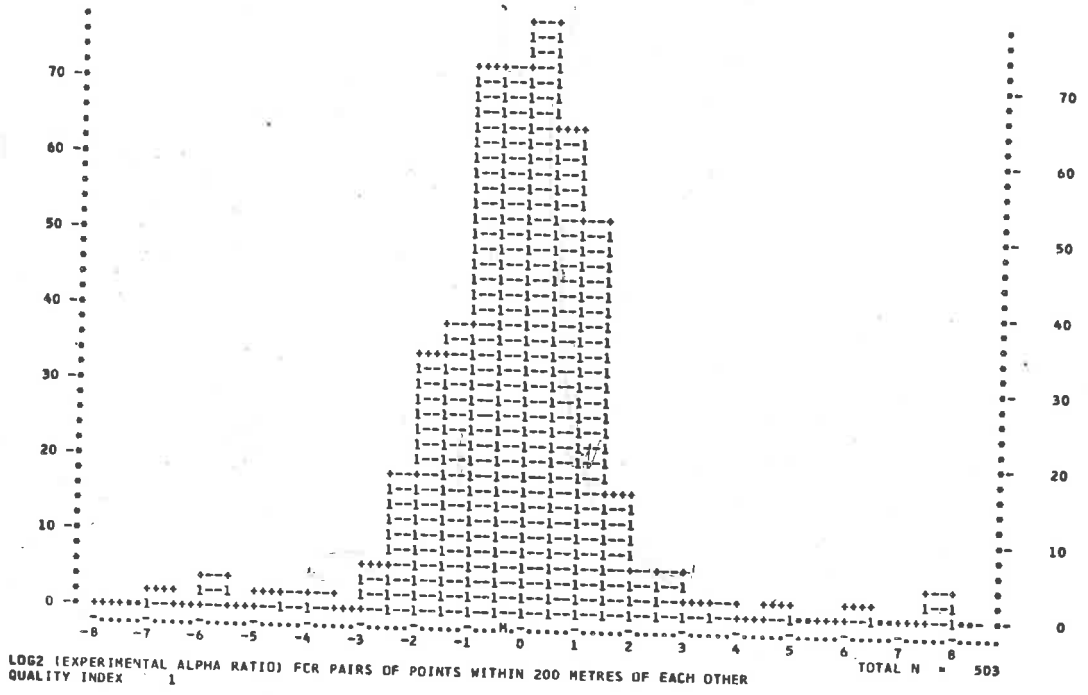
LOG2 (EXPERIMENTAL ALPHA RATIO) FOR PAIRS OF POINTS WITHIN 200 METRES OF EACH OTHER
QUALITY INDEX 1
TOTAL N = 503

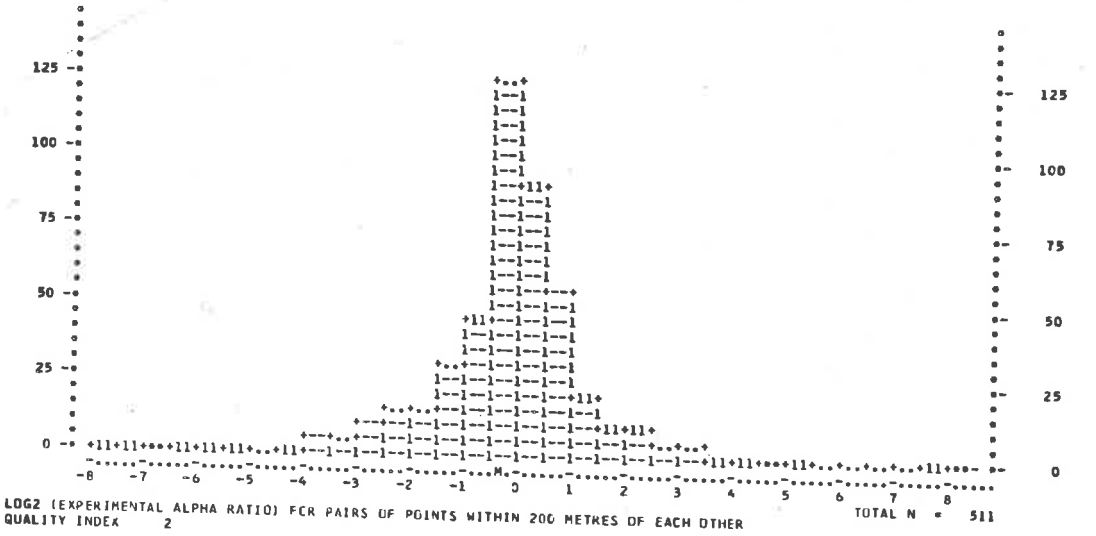
LOG2 (EXPERIMENTAL ALPHA RATIO) FOR PAIRS OF POINTS WITHIN 200 METRES OF EACH OTHER
QUALITY INDEX 2
TOTAL N = 511

Figure 8.5.

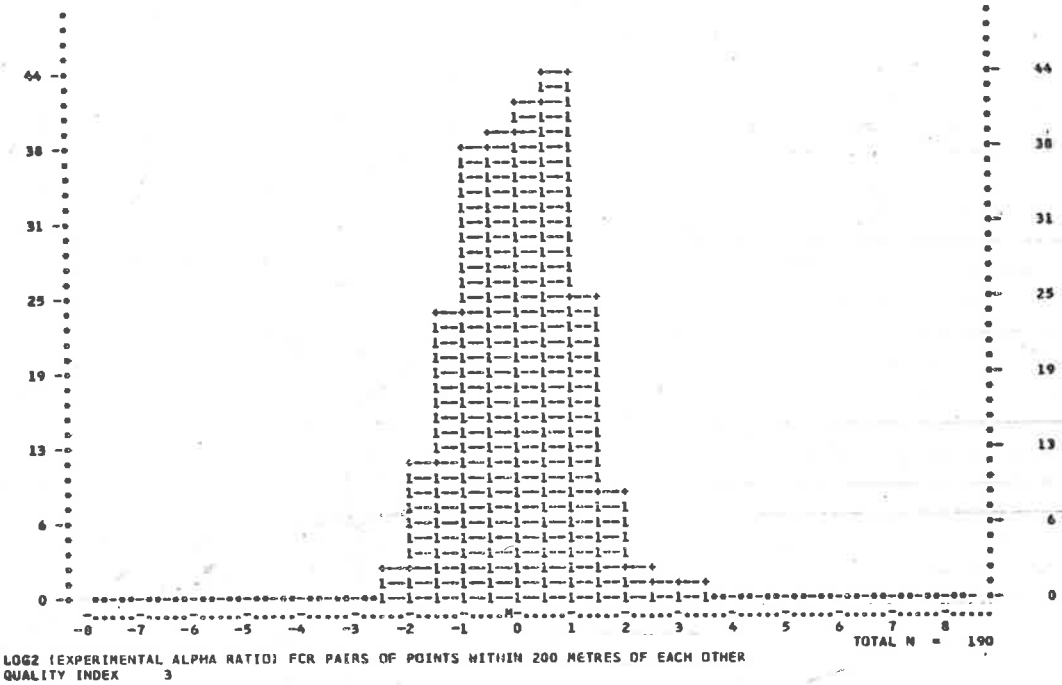

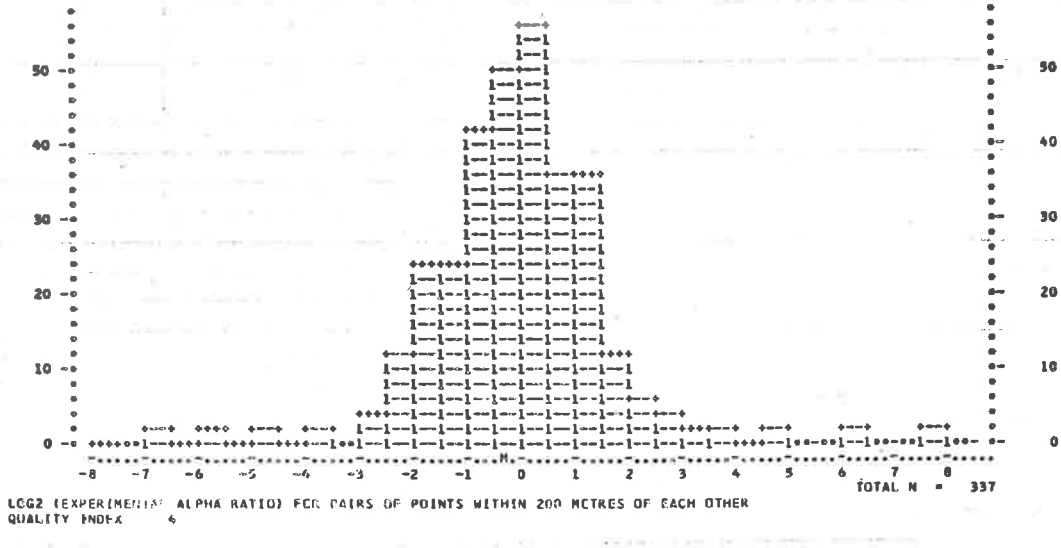

Figure 8.5. (continued).

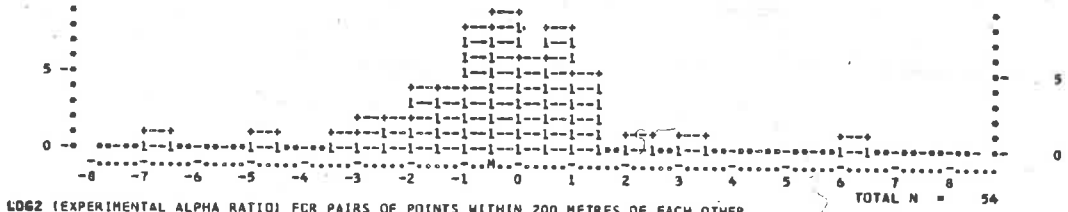

LOG2 (EXPERIMENTAL ALPHA RATIO) FOR PAIRS OF POINTS WITHIN 200 METRES OF EACH OTHER
QUALITY INDEX 1
ST. KILDA AND SALISBURY REFLECTION POINTS ONLY

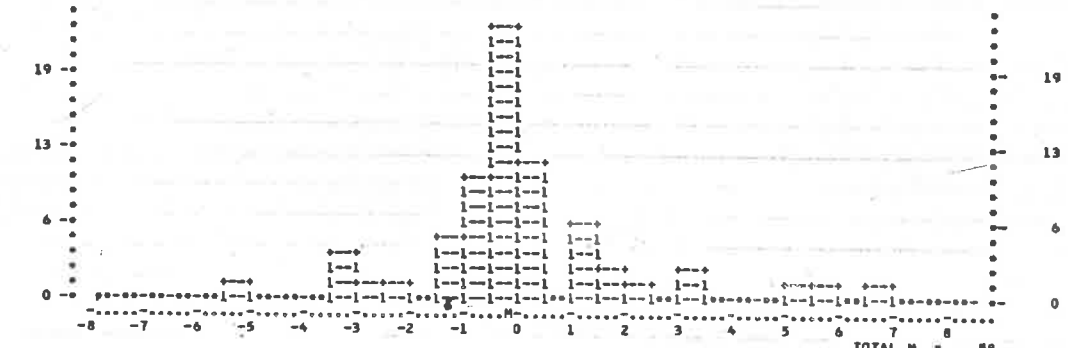

LOG2 (EXPERIMENTAL ALPHA RATIO) FOR PAIRS OF POINTS WITHIN 200 METRES OF EACH OTHER
QUALITY INDEX 2
ST. KILDA AND SALISBURY REFLECTION POINTS ONLY

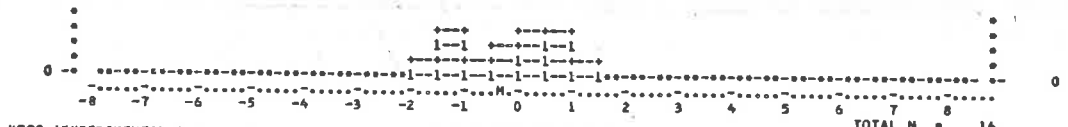

LOG2 (EXPERIMENTAL ALPHA RATIO) FOR PAIRS OF POINTS WITHIN 200 METRES OF EACH OTHER
QUALITY INDEX 3
ST. KILDA AND SALISBURY REFLECTION POINTS ONLY

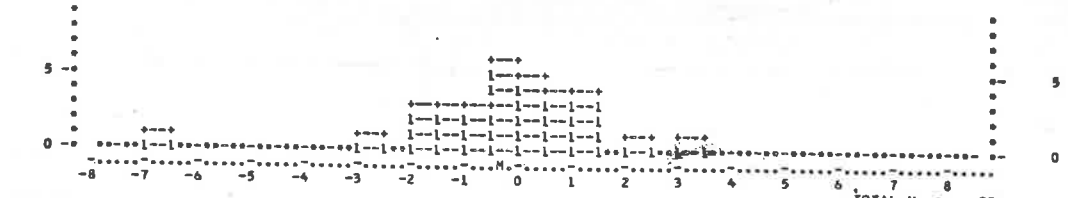

LOG2 (EXPERIMENTAL ALPHA RATIO) FOR PAIRS OF POINTS WITHIN 200 METRES OF EACH OTHER
QUALITY INDEX 4
ST. KILDA AND SALISBURY REFLECTION POINTS ONLY

Figure 8.6.

in the volume of data was imposed by the INDEXQ 3 tests, it was occasionally preferable to use the INDEXQ 1 data in subsequent analysis.

Progressing to INDEXQ = 4, we find that the ratio distributions are of identical shape with those of the set INDEXQ = 1. Thus resonance had negligible effect on the determination of α. We hence expect that, as is shown later, its effect on the diffusion coefficients was also small. This is no proof that resonance enhancement at the start of echoes was never large. Perhaps the effect of resonance usually vanished during the triggering delay period. Southworth (1962) has suggested that in the reduction of multi-station Fresnel patterns, the phase changes at resonance may give rise to apparent meteoroid accelerations. With this idea in mind, the author has examined the decelerations found in this survey by Nilsson (unpublished), i.e. the differences among the three velocity measurements for each meteor, but has found no correlation, either positive or negative, with incident polarization. This supports the view that resonance was unimportant in most of the echoes dealt with, even in their early stages. Hence little further consideration is given to the non-resonant set of echoes (INDEXQ = 4).

The ratios of line densities at closely spaced reflection points are brought considerably closer to unity by the correction for reflection point motion. In Fig's. 8.5 and 8.6, the distributions of this ratio having INDEXQ = 2 are much more sharply peaked than any others. If the few large values of the ratio are disregarded for the moment, we can say that the standard deviation of the ratio from unity is better than halved.

In Figure 8.7 is shown the distribution of the reflection-point-motion correction factor which was applied to α. The restriction on reflection point spacing does not apply to this distribution, which is for all reflection points where α was measured from a decay-type or transitional echo. The narrow central peak indicates that the correction to the α estimate seldom exceeded a factor of $\sqrt{2}$. (However, the distribution has long shallow "tails"; the only empty columns are those printed as +**+). The effectiveness of these generally small corrections in improving the agreement of α values for closely spaced reflection points (Figure 8.5) is striking.

Clearly the few line densities which were greatly modified by the correction routine arose from the similar "tails" of Figures 8.3 (wind shear) and 8.4 (reflection point speed along trail). So far it has not been convenient to check in detail whether these large "corrections" to the α estimates made a net improvement in the smoothness of the ionization profiles concerned, or not. Some evidence that at least any influence for the worse was negligible comes from Fig. 8.5. Among the pairs of points with close spacing, the ratios of line density lying outside the range $(2^{-4}, 2^{4})$ numbered approximately 30 out of 503 for INDEXQ = 1 (uncorrected), and 36 out of 511 for INDEXQ = 2 (corrected), an insignificant difference.

The distribution of the correction factor applied to the measured echo decay time-constant for reflection point motion appears in Figure 8.8. The same remarks on format and long "tails" apply to this histogram as to Figure 8.7 . Once again the vast majority of the correction factors (here, ~80%) were between $\frac{1}{\sqrt{2}}$ and $\sqrt{2}$; the mean of their logarithms (shown by M below the axis) was not significantly different from zero.

Still further use can be made of Figures 8.5 and 8.6, in assessing how nearly equal the sensitivities of the receiving stations were. Since reflection points appeared at all azimuths, taking an incorrect value for the sensitivity of one station would result in two equally off-centre peaks in each distribution in Figures 8.5 and 8.6. No such behaviour is evident. The sole example of a histogram with a central minimum (Figure 8.6, INDEXQ = 3) contains too few points to be significant. All others clearly have only one maximum, centred upon unity ratio of the line densities. From the narrowest of these distributions (Figure 8.5, INDEXQ = 2) it is evident that there are no off-centre peaks further from unity than $\frac{1}{\sqrt{2}}$ or $\sqrt{2}$, at most; thus no station's sensitivity was in error to this extent for any significant time.

Greenhow and Neufeld (1957), in their two-station ionization profile experiment, were able to make two checks that their stations had operated at equal sensitivity. One method was identical in principle with that just outlined, viz. examination of the ratio of line density estimates for reflection points which were close together on a single

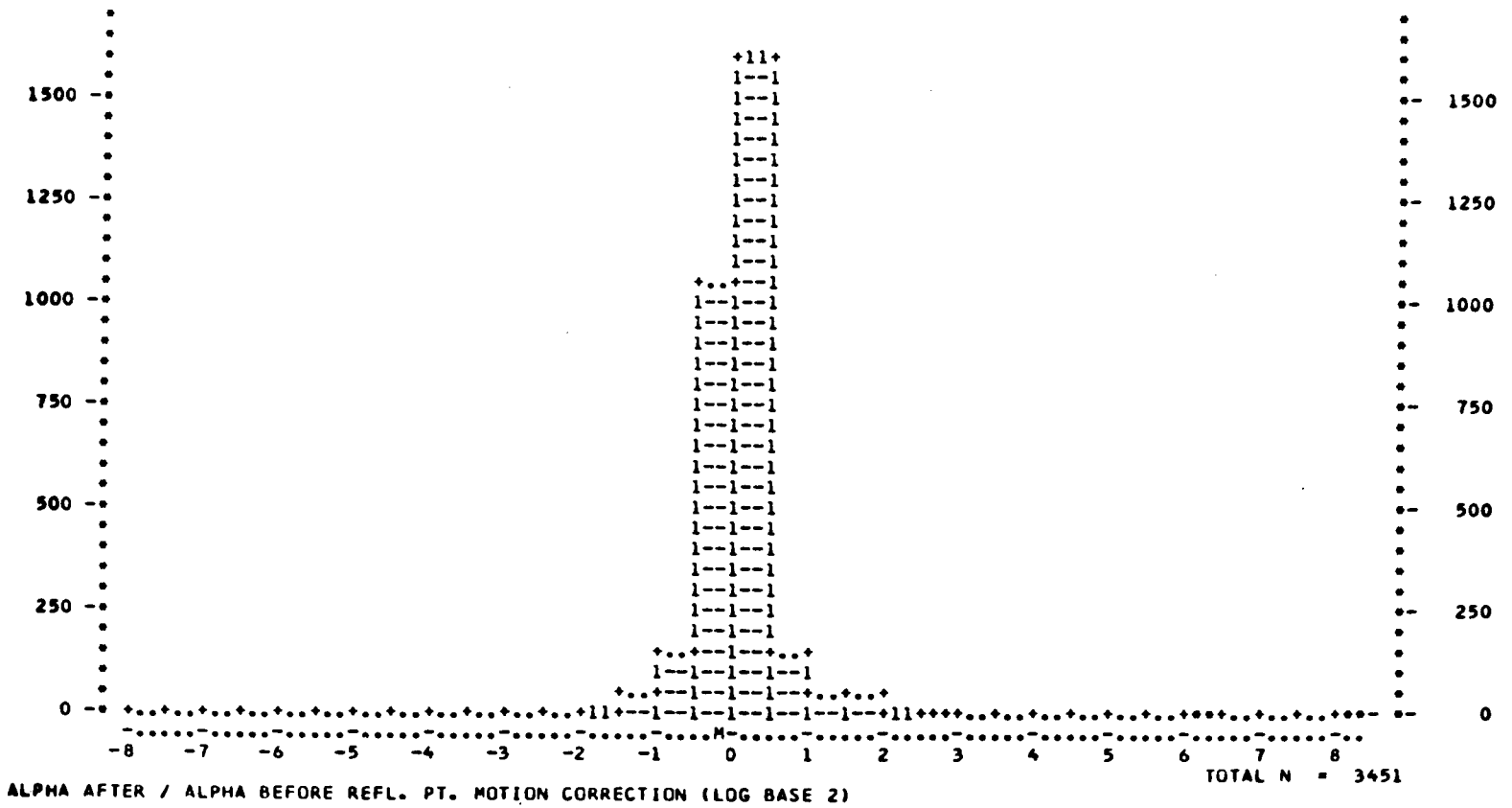
1500
1250
1000
750
500
250
0
-8 -7 -6 -5 -4 -3 -2 -1 0 1 2 3 4 5 6 7 8
TOTAL N = 3451
ALPHA AFTER / ALPHA BEFORE REFL. PT. MOTION CORRECTION (LOG BASE 2)

Figure 8.7.

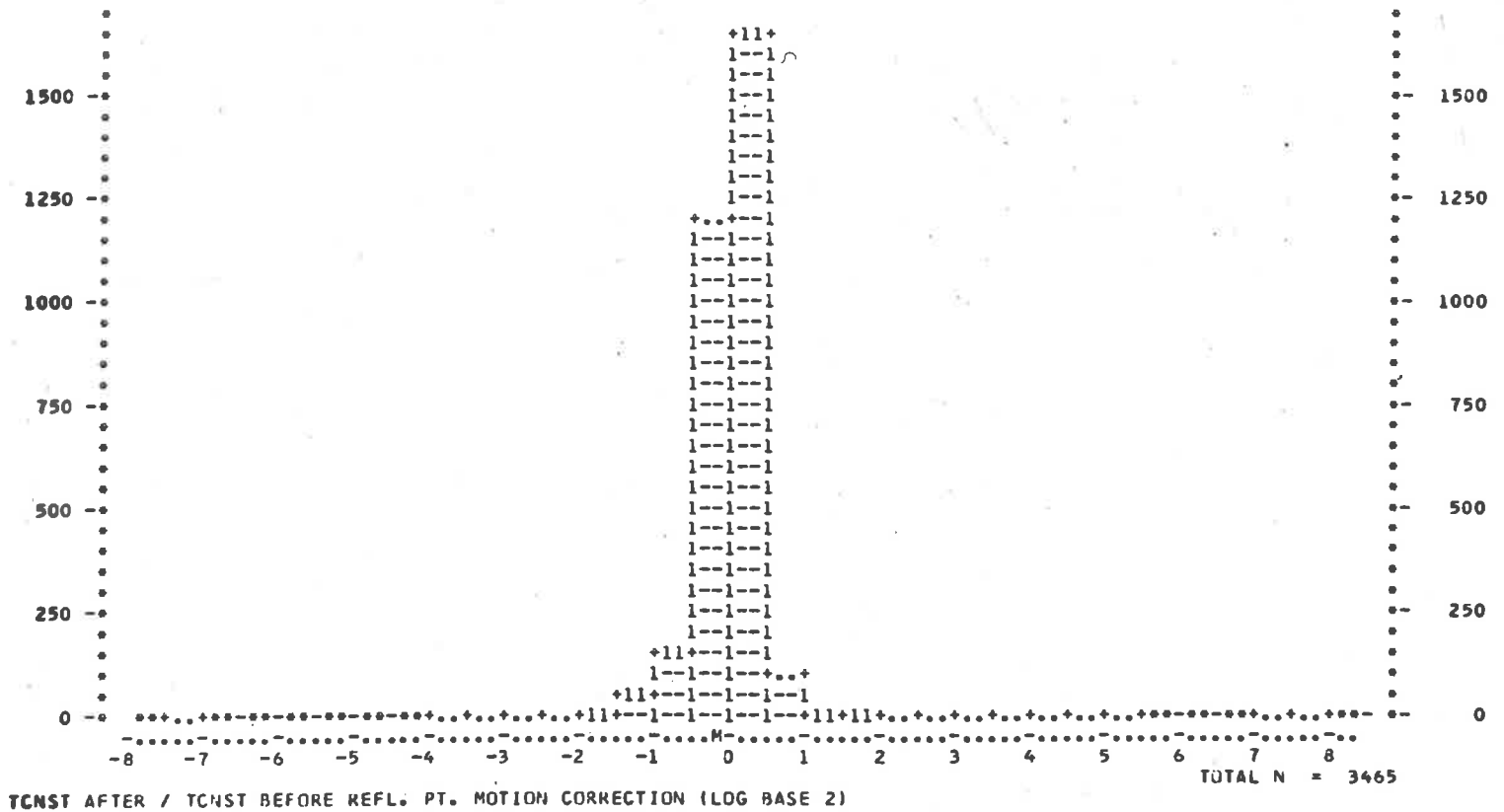
1500
1250
1000
750
500
250
0
-8 -7 -6 -5 -4 -3 -2 -1 0 1 2 3 4 5 6 7 8
TOTAL N = 3465
TCNST AFTER / TCNST BEFORE REFL. PT. MOTION CORRECTION (LOG BASE 2)

Figure 8.8.

trail. In the other method the rates of detection at the two stations, each of which was able to trigger the recording system, were simply compared. In practice, observed ratios of line density at all separations were modified in accordance with the detection rates, and the ratios at small separations were then used as a check on the results.

Because only the main station in the Adelaide system could trigger the equipment, and at least the Sheedy's Farm and Direk outstations also had to return usable echoes, rate comparisons were meaningless. However, the sensitivities of the stations were further examined as follows. Histograms were prepared showing the distribution of log $(\frac{\alpha i}{\alpha j})$, where i,j are all possible pairs of station numbers, for each month's meteors. Only decay-type echoes were used, for greater accuracy in α, and the magnitude of reflection point separation was not taken into account.

These histograms were carefully examined, and certain minor corrections to the data were made using them. For certain pairs of stations, notably 1 and 4, there was a marked skew tendency; for other pairs this tendency was absent. The skewness can be satisfactorily explained as the result of differences in triggering and recording among the stations, which led to differences in effective detection threshold levels for equal receiver voltage gains. In general the skew tendencies displaced the mean logarithm of the ratio of line densities from zero, but the peak or modal value remained at or very near zero. However the peak too was displaced from zero in a minority of the histgrams, and it hence appears that α values measured at stations 2 and 4 may have differed systematically from the others, by factors of order 0.9 and 1.2 respectively. At station 2 a slight mismatch between antenna and receiver may have been responsible; no explanation has been found in the case of station 4. However, these possible errors were so small, relative to the range of observed ratios of line density, that no large-scale correction to the data has seemed to be justified.

Summing up: the separations between reflection points were measured to better than 2% accuracy. For decay-type echoes, systematic differences between stations in line density measurements were 20% or less, and random uncertainty from the film-reading was generally of order 10%

with occasional excursions to 50%. By contrast the ratio of line densities at points ≤ 200 m. apart typically deviated from unity by a factor of 2. Exclusion of transitional echoes removed some large deviations but left the typical factor of 2 nearly unchanged. The correction for reflection point motion roughly halved the r.m.s. disagreement between values of line density measured at closely spaced reflection points.

8.3 Absolute values of line density in underdense trails

Throughout this project, echo amplitudes have been interpreted directly in terms of electron line density. As has been pointed out, the chosen method of analysis of the ionization profile shapes needed only the ratios of line density measurements from all available reflection points on each trail. However, considering the completeness with which other parameters of the 1961 survey meteors are now known, it is fitting to seek all possible accuracy for the individual line densities, since by combining these to estimate the integrated electron content of the trail an idea of the mass of the meteoroid may be gained. It is also of interest to find how small a line density could be detected by the system.

The following factors, which have already been individually discussed, could affect the determination of line density α in an underdense trail:

(1) the range R (uncertainty $\delta_R / R \lesssim 2\%$);

(2) the aerial power-gains G_T and G_R, receiver voltage sensitivity S_R, and transmitter power P_T, expressible as an overall voltage sensitivity $V = (P_T G_T G_R)^{\frac{1}{2}} S_R$ (uncertainty $\delta_V / V \sim 20\%$);

(3) the ratio r_0/λ of initial trail radius to radio wavelength;

(4) enhancement of the reflection coefficient of the trail by plasma resonance (relative uncertainty $p \lesssim 20\%$ in α);

(5) any significant dependence of the reflection coefficient on the angles between the trail, the line of sight, and the earth's magnetic field (relative uncertainty m in α);

(6) errors due to motion of the reflection point along the trail in conditions of wind shear (relative uncertainty s in α, largely corrected in the underdense echoes of quality class 2);

(7) random errors arising in film reading (relative uncertainty d in α, generally of order 10% or less, occasionally 30%).

The combined influence of factors (1) to (7) on the formation of an estimate α_e of the line density can be summarized in the expression

$$\alpha_e \simeq \alpha(1+\delta_R/R)^4 (1+\delta_V/V)^{-1} (1+p)(1+m)(1+s)(1+d)\exp(-Cr_c^2/\lambda^2)$$

where C is a positive constant.

From this expression and the known uncertainties listed above it is clear that the absolute line density should have been correctly estimated to within a factor of 2 if the initial radius and magnetic effects were not large.

An approximate check on the accuracy of absolute values of underdense line density was made by observing how sharply their distribution terminated at its upper end, and how close the termination was to the theoretical transition point between underdense and overdense scattering. The distribution was computed and plotted for each combination of receiving station number (1 to 4) and quality index (1 to 4). The resulting histograms are reproduced in Appendix 4. In all 16 of them the upper cutoff is quite sharp and occurs between 10^{14} and 2×10^{14} electrons/metre, somewhat below the transition point of 2.4×10^{14} electrons/metre given by Kaiser and Closs (1953). At stations 1, 2 and 3, some 5% of the line density values exceeded 2×10^{14} electrons/metre. Some of these high values arose from the sources of uncertainty listed above. Others were from transitional echoes which were not recognised as such because their duration at near-constant amplitude was only as long as the triggering delay, or less; this is evident from the sharper cutoff at station 4, where no delay was involved. Since underdense and overdense scattering behaviour are expected to merge smoothly near $\alpha = 2.4 \times 10^{14}$ m^{-1}, it is surprising to find so few apparently underdense echoes having α in excess of this value.

The initial radius attenuation (Chapter 3), of which no account was taken in the data reduction, must be considered in assessing the reliability of the absolute line density measurements. It would have been difficult to apply a correction for this effect to individual echoes, because of the uncertainty (and the presumed diurnal variability) in initial trail radius at any height. However, the cutoff of the uncorrected α

values is so near to its theoretical position as to suggest that typical meteors in this survey suffered attenuation by no more than a factor of 2. In the following Section the initial radius question is considered further.

The distributions of log α for underdense echoes of the other quality classes are little different from those for quality 1. In all of them the upper cutoff in log α is approximately at the theoretical point of transition to overdense scattering. The smallest values of log α are also approximately equal in all the distributions. Making allowance for experimental error, we may state that the survey had a practical lower limit of $\alpha \sim 1 \times 10^{13}$ m^{-1} (radio magnitude +7).

The mean and modal values of $\log_{10} \alpha$ in the results for stations 1, 2 and 3 both lie at 13.8 or 13.9 approximately (radio magnitude $\sim$ +5.6). At station 4 the corresponding values are about 13.7, confirming the existence of a small systematic error (an underestimate of α by about 20%) in the measurements from that station.

Because the experimental results fall somewhat below the expectation according to theory, it is deduced that line density as measured from underdense-type echoes at stations 1, 2 and 3 is systematically low by a factor of up to 2. Both this fact and a slight additional bias in the values from station 4 are negligible in comparing the line densities on an individual trail with each other. Attenuation of the echoes due to non-zero initial trail radii is one possible cause of the under-estimation of line density.

8.4 Absolute values of line density for transitional echoes

We have defined a transitional (KIND 1) echo to be one exhibiting first the nearly constant amplitude characteristic of overdense reflection and then an exponential decay, both within the 1.2 sec. recording interval of the equipment.

There are two methods of determining line density α from transitional echoes. One makes use of the exponential decay, as with underdense echoes, and the other makes use of both parts of the echo. Here the results of the two methods are compared with each other and with the underdense results from §8.3.

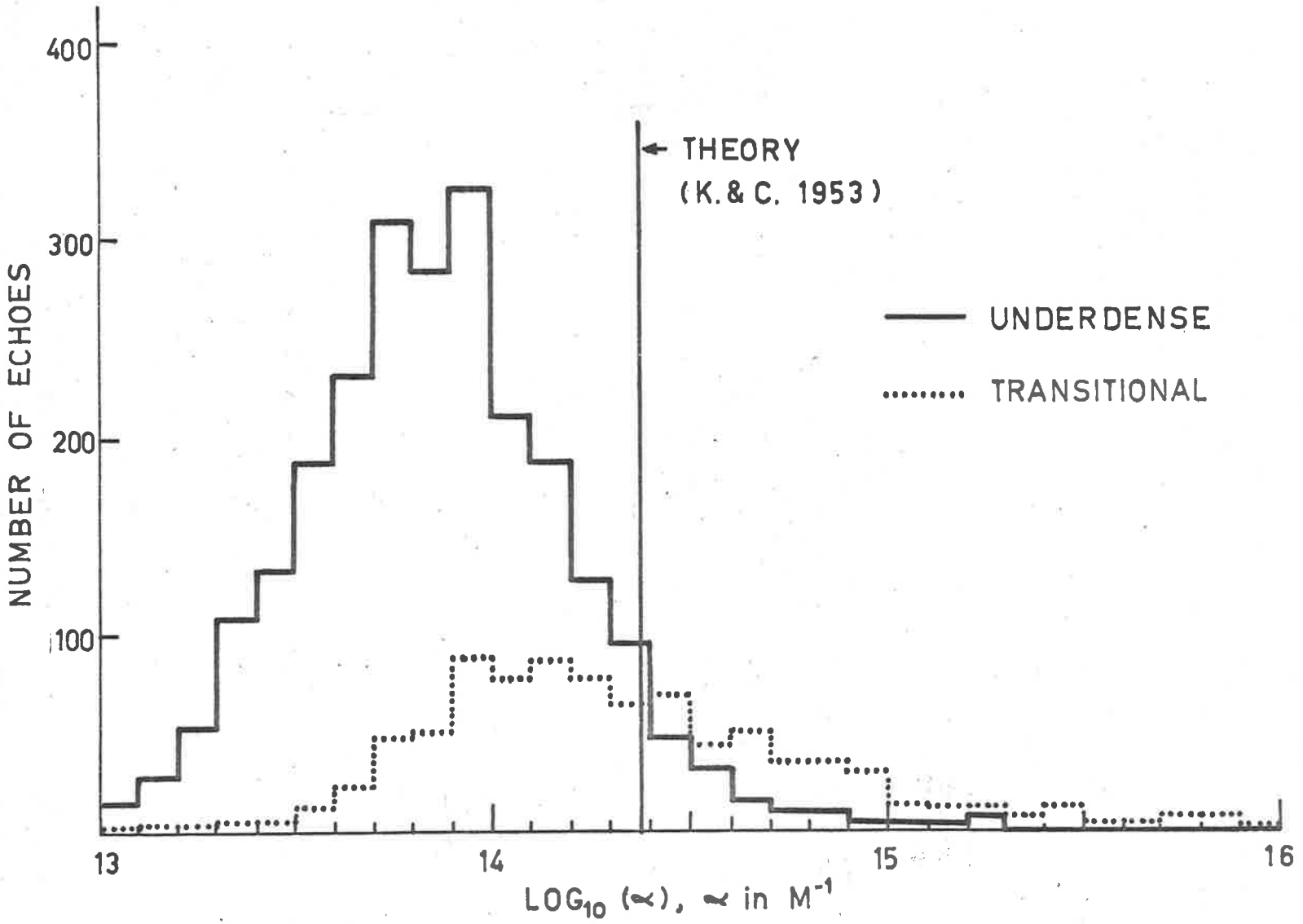

Figure 8.9 Distributions of $\log_{10}\alpha$ for underdense and transitional echoes (INDEXQ = 1), showing departure from theoretical cross-over line.

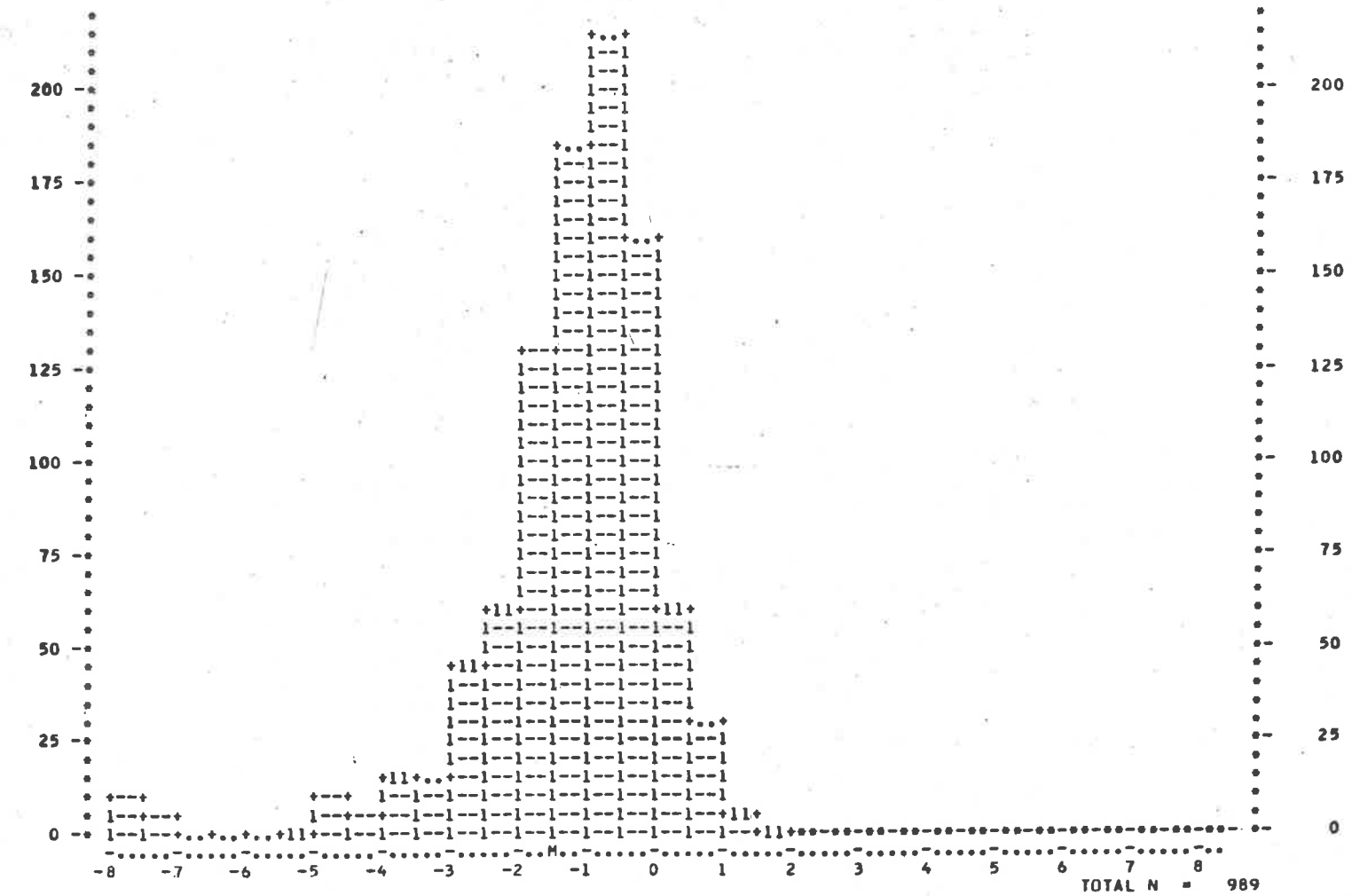
200
175
150
125
100
75
50
25
0
-8 -7 -6 -5 -4 -3 -2 -1 0 1 2 3 4 5 6 7 8
TOTAL N = 989
RATIOS OF OVER- TO UNDER-DENSE ALPHA (LOG BASE 2)
QUALITY INDEX 1

Figure 8.10.

In the first method, α is found from the amplitude of the exponential decay extrapolated to time t_o at the beginning of the echo. The resulting α distributions are shown with their underdense counterparts in Appendix 4, where separate graphs appear for each station. The underdense total and transitional total from all stations for INDEXQ 1 are shown in Fig. 8.9, together with the theoretical line density at which the two forms of scattering should merge (Kaiser and Closs 1953). In this diagram the change from one scattering mode to the other is smooth, but both distributions are considerably to the left of the positions they should occupy if the change occurred at the theoretical line density. Thus the suggestion (§ 8.3) that underdense line densities were underestimated by a factor of order 2 is strengthened, and applies to transitional echoes also.

It has already been stated that no instrumental factor is known which might explain such a discrepancy. A hint of the true cause lies in the results of the second method of finding line density for transitional echoes. From Eq. 3.3.3, the critical density radius vanishes at the time

$$t_{ov} = 7.1 \times 10^{-17} \lambda^2 \alpha / D \qquad \ldots 8.4.1$$

Then substituting for D and re-arranging,

$$\alpha = 8.9 \times 10^{13} t_{ov} / \tau \qquad \ldots 8.4.2$$

For brevity, designate values of α measured according to the extrapolation method as α_A; according to Eq. 8.4.2, as α_B. Distributions of $\log_2(\alpha_B/\alpha_A)$ were printed for all transitional echoes, and also for transitional echoes at the St. Kilda and Salisbury reflection points only, in each relevant INDEXQ class, viz. 1,2 and 4. All six distributions were identical in shape. Fig. 8.10 shows the one for all reflection points and INDEXQ = 1. It is neither central nor symmetrical. The outlying ratios from 2^{-4} to 2^{-8} are explained as cases where a large rapid decrease in signal level at the collapse of the over-critically dense region of the trail was mistaken for the subsequent slower, low-amplitude exponential decay. Otherwise the ratio α_B/α_A is seen to have varied from approximately $2^{-4} = \frac{1}{16}$ to only 2^{+1}. The modal value of the ratio is about $2^{-5/6} = 0.6$.

The effect upon α_A and α_B/α_A of a given ratio r_o/λ (where r_o is the initial trail radius and λ the radio wavelength) is readily calculated

from Eq's. 3.5.1, 8.4.1 and 8.4.2. It is found that α_B/α_A is a complicated function of r_o/λ and the true line density α, and that it is less than unity only for $\alpha \leq 10^{14}$ m^{-1}. and $0.05 \lesssim r_o/\lambda \lesssim 0.1$. For example, if $r_o/\lambda = 0.08$ and $\alpha = 5 \times 10^{13} m^{-1}$., one obtains $\alpha_B/\alpha_A \simeq 0.7$, $\alpha_A \simeq 0.8\alpha$. The range of α_A between $5 \times 10^{13} m^{-1}$. and $2 \times 10^{14} m^{-1}$. is densely populated in the present results, and the condition $0.05 \lesssim r_o/\lambda \lesssim 0.1$ implies $0.5m. \lesssim r_o \lesssim 1m.$ at 93Km. altitude when the parameters of the Adelaide equipment are substituted.

Evidently much (though not all) of the anomalous behaviour of α_B and α_A/α_B can be explained if trails with just less than 10^{14} electrons/m. have initial radii of 0.5 to 1m. at heights near 93Km. These radii are similar to results cited in §3.5. One other factor is capable of providing a similar explanation, viz. the mathematically equivalent possibility of the equipment's triggering delay having been underestimated. For the most common values of echo decay time-constant a systematic error of 0.15 to 0.3 sec. in the triggering delay would have been necessary; this is considered highly unlikely. All the remaining possible causes of error listed in §8.3 would tend to make α_A exceed α if $\alpha_B/\alpha_A < 1$, or vice versa.

Thus the major points noted in connection with transitional echoes are as follows. Determination of line density by extrapolation of the final decay back to t_o gives results which join smoothly with those found similarly for underdense echoes. Both are up to 50% low in absolute value. Determination of line density from the length of the nearly-constant-amplitude part of the echo gives smaller answers still. At least a partial explanation of these facts is possible if trails at 93Km. have initial radii between 0.5m. and 1m.

8.5 Evaluation of the reflection point motion theory

The point has now been reached where the effect of the correction for reflection point motion on line density determinations can be evaluated, i.e. we can compare the log α distributions for INDEXQ = 2, found in Fig's. A-4-2 and -6, with those for other quality index values. The reader will recall that in this correction process the estimation of line density at the t_o point was abandoned, in favour of making the most reliable determination of α possible from a given waveform. This determination

was taken to apply, not necessarily to the point of minimum meteoroid range (the t_o point), but to the location on the trail of the moving reflection point at the time when the decay time-constant was being measured. Therefore it was quite possible that the best determination of α available from a transitional waveform might apply to an underdense point on the trail, or vice versa.

The only discernible new feature of the distributions in Figures A-4-2 and -6 is a tendency for them to be a little broader than those for other quality index values. KIND 1 echoes (A-4-6) contain an increased but still small proportion of excessively large or excessively small α values, but this is not the case for KIND 0 echoes. With the latter (Figure A-4-2) the peaks of the distributions are wider, but the bases are practically unchanged. Thus it seems that the correction routine is prone to error when used on certain transitional echoes, and that its effect is negligible for underdense echoes and the remainder of those in the transitional group.

It is interesting to relate this finding to §8.2. There it was shown that considerable improvement in the consistency of line density measurements, at points spaced 200m. or less along a given trail, was obtained by correcting for reflection point movement. Here, with a mean spacing of 1Km., no such improvement occurs. Therefore one or both of the basic assumptions of the correction method is wrong. Either
(a) the wind gradient over distances of order 1Km. is far from linear, whereas that over 200m. or less is nearly linear, or
(b) the electron density gradient of a trail over distances of order 1Km. is much less well represented by an arc of an exponential curve, or by a straight line, than is the gradient over 200m. or less. From the work of Roper (1963), possibility (a) is a considerable exaggeration of the wind shear situation. The work of Rice and Forsyth (1963,1964) indicates that (b) deserves serious attention; trails which are "rough", with irregularities of ionization having a scale length of tens, or one or two hundreds, of metres, can distort the "Cornu spiral" for a radio echo sufficiently to make a measurement of line density relate to a point some distance from the point of minimum range (t_o point). Such displacements of the point of measurement would tend to be nearly equal for closely-spaced t_o points, but not

for t_o points spaced 7Km. If so, the calculated wind and line density gradients, used in allowing for reflection point motion due to wind shear, would be fairly reliable for small reflection point spacings, but not for large ones.

These conclusions apply to the measurement of electron line density. In the following chapter, it is shown that, although some minor points of interest are brought to light, there is similarly no major improvement in diffusion coefficient measurements when the correction for reflection point motion is applied.

The negative character of these conclusions does not reduce their importance. On the contrary, it has been shown that one of the few mechanisms which might have accounted for anomalies in diffusion coefficient and line density measurements does not, in fact, account for them. It should be noted that this result has been obtained even though the expected magnitude of errors due to reflection point motion was calculated to be a considerable fraction of the observed scatter. Hence an even stronger perturbing mechanism clearly operates to cause this scatter. Indirect evidence of the nature of this perturbation is brought forward in the next chapter.

8.6 Comparison of line density ratios with predictions

The process by which the sets of line density measurements were combined statistically was simple but unusual. It was designed to make efficient use of all the available data, and to be as little affected as possible by occasional severe errors in a single α value among several on a trail. Essentially the method was to estimate $\frac{1}{\alpha}\frac{d\alpha}{dh}$ for each available pair of points, and also the positions of the two points relative to the height of maximum ionization h_{max}. The same function was then evaluated assuming the trail to have, in turn, each of a set of four model profiles. For each model profile the observed and predicted values of $\frac{1}{\alpha}\frac{d\alpha}{dh}$ were plotted as a point on a scatter diagram. Comparison of the scatter diagrams indicated the relative goodness of fit of each model profile to the data.

For convenience in what follows, we write

$$Q = \frac{1}{\alpha}\frac{d\alpha}{dh} \quad \left(= \frac{d}{dh}(\ln \alpha) \right) \qquad \ldots 8.6.1$$

The model profiles are shown at the bottom of Fig. 8.11 . They were taken from the following sources.

Profile (a) was based on the evaporation theory. Above h_{max} it followed the shape given by Eq. 2.4.3, which is an approximation to the complete solution of the theory. It was felt (see Chapter 2) that this shape, without modification, did not adequately represent the prediction of the full theory for the part of the trail below h_{max}. Therefore the relevant abscissae $h_{max}-h$ were multiplied by 1.5, so lengthening the lower part of the trail in that ratio, and the extreme terminal of the trail was rounded so that it met the line $\alpha = 0$ gently rather than abruptly. These measures improved the adherence of the model to the exact solution for average meteor velocities.

Profile (b) was the profile suggested by Greenhow and Neufeld (1957) as a possible (but not unique) conclusion from their two-station radar experiment. With the relatively minor exception of some necessary smoothing, this and the next two profiles were not modified from their original published form.

Profile (c) was the profile given by Hawkins and Southworth (1958) for a selection of meteors observed simultaneously at two stations with Super-Schmidt cameras.

Profile (d) was little different in essentials from (c). It was the profile given by Jacchia, Kopal and Millman (1950) for the notably fragile (and therefore short-trail) meteors of the Draconid stream, also observed photographically. The "tail" above h_{max} was ignored by the method of analysis finally chosen, and only the narrower peak distinguished (d) from (c).

The annotation of Fig. 8.11 indicates the ranges of visual magnitude to which (b), (c) and (d) apply.

The upper curves of Fig. 8.11 show the profile derivative Q as a function of $(h - h_{max})$ for profiles (a) to (d). It can be seen that, for (b), (c) and (d), Q is not as well-behaved as one might wish. The magnitude of Q remains well-bounded only if the profile does not approach the axis $\alpha = 0$ too abruptly at either end. However, after some experimentation with the computer programme involved, it was found that not many items

of data were wasted if, for points above h_{max} having $\alpha < 0.3\alpha_{max}$ according to the model, Q was given a large negative value so that the point went outside the limits of the scatter diagram. (Any such points were then indicated identifiably at the edges of the scattergram, but ignored in finding a correlation coefficient). From Fig. 8.11 it can be verified that this provision took care of ill-behaved values of Q for all the model profiles.

To estimate Q from a pair of reflection points α_1, α_2 $(h_1 > h_2)$ observed on a single trail, the points were simply assumed to be connected by a trail segment whose electron density vs. height profile was linear. Then at $h = (h_1 + h_2)/2$,

$$Q \quad (= \frac{1}{\alpha}\frac{d\alpha}{dh}) \simeq \frac{2(\alpha_1-\alpha_2)}{(h_1-h_2)(\alpha_1+\alpha_2)} \qquad \ldots 8.6.2$$

However, in predicting Q from the model profiles, a standard central-difference differentiation formula was used for the $\frac{d\alpha}{dh}$ factor so that only one parameter, $(h-h_{max})$, had to be specified. The use of different formulae for measuring and for predicting Q was justified in that the largest experimental height differences h_1-h_2 were much shorter than the shortest model profiles.

The prediction of Q required an estimate to be made of the position of h_{max} relative to the reflection points, for every meteor. This was a difficult requirement to satisfy with the set of reflection points covering only 4 Km. of the height range occupied by the trail. To make the estimate of h_{max} for each meteor it was assumed, basically, that the trail profile was convex, i.e. did not contain a minimum. Then if the reflection point with the largest value of α was not at the upper or lower end of the set of reflection points, its height was taken as h_{max}. If, on the other hand, this point was the highest or lowest of the set, some height increment dh, preferably a constant for simplicity, had to be respectively added to or subtracted from the reflection point height to give the h_{max} estimate.

The value to be used for dh was fixed in the following empirical but quite sensitive manner. Using two months' data, values of dh from 0 to 3 Km. were tested in turn by printing scatter diagrams of the observed values of Q against $(h - h_{max})$. Here, as before, h is the mean height of the pair of reflection points used to find Q. For a valid choice of dh , it was reasonable to expect that the distribution of the values of $(h-h_{max})$ should be smooth, showing neither an undue concentration at $(h-h_{max}) = 0$ nor a thinly occupied region on each side of h_{max}. On comparison of the plots for the different choices of dh , it was immediately obvious that dh = 1 Km. was appropriate.

In the above way h_{max} was estimated, for all useful meteors, from the data for quality classes 1 and 2 . For values 3 and 4 of the quality index, h_{max} was set to the value found for quality index 1. For later use, an estimate of the peak line density α_{max} was made too. When h_{max} was located at a reflection point, α_{max} took the value of α at that point. If however h_{max} was offset from a reflection point by the distance dh, then α_{max} was made 1.5 times as large as the nearest α value.

Examples of the eventual results of the above procedures, scatter diagrams of predicted versus observed values of Q, are reproduced in Fig's . 8.12 to 8.17 inclusive. Originally 16 pages of these diagrams were printed by the computer, with a separate page for each combination of model profile, (a) to (d), and quality index INDEXQ (1 to 4). The plots for INDEXQ 2 and 4 are not shown here, since they give very little further information, either on ionization profiles, or on reflection point motion effects and plasma resonance. On each page reproduced, the left-hand plot contains data from all stations, and the right-hand plot contains the subset of data from stations 1 and 4 only. The latter subset has the advantages of possibly more reliable calibration of the receivers and of a mean height difference exceeding the mean for all pairs of reflection points. The disadvantage is the smaller number of data points available.

Finally it should be pointed out that Q is positive below h_{max}, for a trail with a single maximum of α , and negative above h_{max}. Hence if the profiles contain no minima of α, points in the upper right quadrant

should represent reflection points below h_{max}, and those plotted in the lower left quadrant should represent reflection points above h_{max}.

By reference to the indicated diagrams, the following facts can be verified.

Fig. 8.12, INDEXQ=1, profile (a); the experimental values of Q lie entirely within the range (-4.8, +4.8). If the right-hand plot be taken as of superior quality, the reliable values of Q lie in (-3.0, +3.0). The most frequently occurring value is zero (approximately), and the arithmetic mean does not differ significantly from zero. Therefore trails were most commonly detected near h_{max}. However, the distribution of Q_{obs} is not symmetrical about the peak. Instead, the frequencies of values from -1 to -0.2 fall away more rapidly than those of values from 0.2 to 1. (There is no significant asymmetry outside the range from -1 to 1).

Near maximum ionization the frequency of detection of a given value of Q must depend on the length of trail over which Q ($= \frac{1}{\alpha}\frac{d\alpha}{dh}$) has that approximate value, rather than on the $\frac{1}{\alpha}$ factor which is important near the ends of the trail. Therefore the average profile is deficient in small negative gradients of α near α_{max}, i.e. line density tends to increase sharply to a maximum with decreasing height, and then fall away less sharply below the maximum point.

Not one reflection point out of 3501 was sufficiently far distant from h_{max} to raise the magnitude of Q_{pred} above 0.1 using the evaporation profile (a). Allowance must be made for the likelihood that large values of $(h - h_{max})$ occurring in the data would have been underestimated, because of the rather small upper limit of observable reflection point separations. Nevertheless it is clear from Fig. 8.11 that the observed distribution of Q could only result from profiles like (a) if the probability of detecting the ends of the trail greatly exceeded that for its central region.

Thus the evaporation theory completely fails to describe the observed profiles.

Fig. 8.16 , INDEXQ=3, profile (a); it will be remembered that the indicator of specular geometry, NGEOM, was required throughout this analysis to have the "good" value 1 . Therefore the effects of selecting echoes such that INDEXQ=3 were to require additionally that NQ (accuracy in the orbit programme) and NOK (amplitude-time waveform) both indicated good quality, and to remove all transitional and persistent-type echoes. As a result, the observed values of $\frac{1}{\alpha}\frac{d\alpha}{dh}$ cover a narrower range, given as (-3.0, 3.2) by the plot for all stations and as (-1.4, 2.0) by the plot of St. Kilda - Salisbury pairs if we neglect (respectively) 4 and 1 isolated larger values. The peak of the distribution still has the same asymmetry as before, and because the tails are attenuated the mean of Q_{obs} is now displaced (to approx. 0.09) by the stronger influence of the asymmetric peak.

Fig's. 8.15 and .17, INDEXQ=1 and 3, profile (d); comparison of these pages with Fig. 8.11 illustrates the fact that even model profile (d), the narrowest of the set, has $|Q| \gtrsim 1.5$ only over very restricted regions at the extreme ends of the profile. The scattergrams bear out the implication of this fact, viz. that observations with reflection points in these regions should be uncommon. Below h_{max} no value in excess of +1.1 has been predicted. Above h_{max} few cases have occurred where $(h-h_{max})$ has been large enough to place the reflection point in the forbidden region $\alpha < 0.3\alpha_{max}$ on the model profile. (The $ signs, at the bottom of the left-hand plot in Fig. 8.15 for example, result from the latter eventuality, and in that plot they represent 22 out of 3501 points). Yet even the good-quality underdense reflection points, in the plot of St. Kilda - Salisbury data with INDEXQ 3 (Fig. 8.17 , right), have given numerous values of Q_{obs} as large as 1.5 in absolute value.

In seeking the reason for such anomalously large values of Q_{obs}, let us for the moment take a pessimistic view of the accuracy of α when its quantitative measurement from a KIND 1 or KIND 2 waveform was attempted. The qualitative fact remains that distinctly underdense and distinctly overdense modes of reflection frequently occurred simultaneously in the

data, at reflection points whose height difference was only of order 1 Km. Therefore, regardless of whatever uncertainty arose from measuring α at the conclusion of the persistent phase in KIND 1 echoes, the INDEXQ 3 (underdense only) data must necessarily understate the true total range of $\frac{1}{\alpha}\frac{d\alpha}{dh}$ values. Hence we conclude that an undetermined, but certainly non-zero, proportion of the observed large values of Q_{obs} arose from profiles which were either shorter than (d) or at any rate contained sections where α changed with height more rapidly than the steepest parts of (d), but closer to h_{max}.

Fig's. 8.12 to 8.15, INDEXQ=1, profiles (a), (b), (c), (d); if we now try to ignore observed values of Q exceeding, say, 1.5 in magnitude, then the model profile whose peak best resembles the true profiles can be determined from the remaining smaller values of Q_{obs}. Unfortunately, the correlation coefficients calculated for each plot are more sensitive to the large experimental and predicted Q values than to these smaller ones. Therefore we cannot make use of the correlation coefficients at this stage, and must examine the detailed frequency-of-occurrence codes in individual scattergram cells in order to evaluate the goodness of correlation between experiment and prediction near the origin of axes (i.e. near h_{max}). It is immediately obvious from the diagrams that neither the modified evaporation profile (a) nor the one suggested by Greenhow and Neufeld (b) comes within reach of the observations. On the other hand, both (c) and (d) predict gradients Q of the right order of magnitude, provided only the region near h_{max} is considered. Now these two profiles are generally similar in shape. After careful examination of the relevant scattergrams, Fig's 8.14 and 8.15, the author feels that (d) fits the observations somewhat better over the range where (c) and (d) differ significantly, viz. $h-h_{max} \gtrsim 1$ Km., while below h_{max} both profiles appear to be rather too long. To improve (d) in this respect it would probably suffice to use a symmetrical model profile, having the form of the present upper half of (d) both below and above h_{max}.

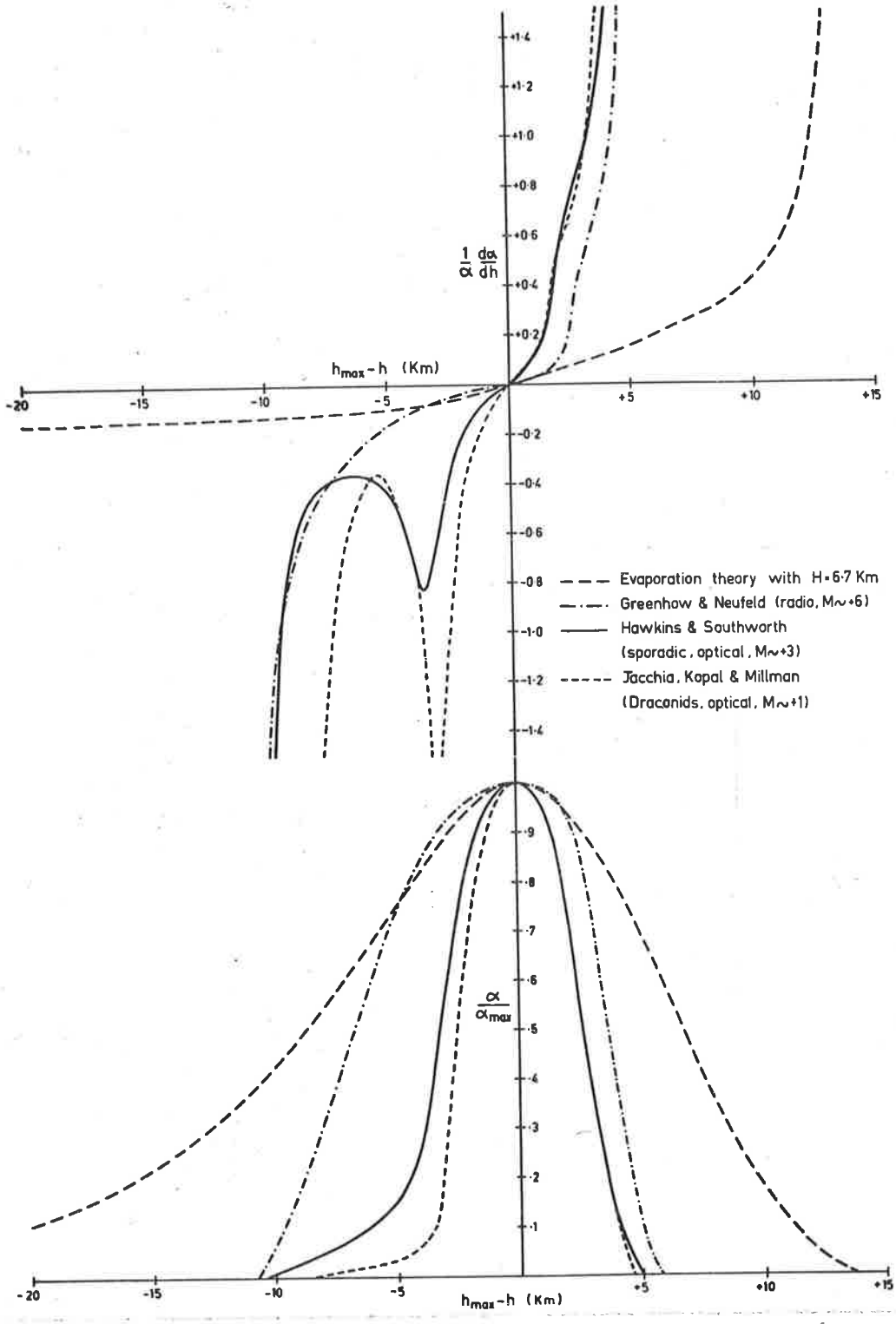

Figure 8.11. Model electron line density profiles (below) and modified derivative $Q=\frac{1}{\alpha}\frac{d\alpha}{dh}$ (above) versus height.

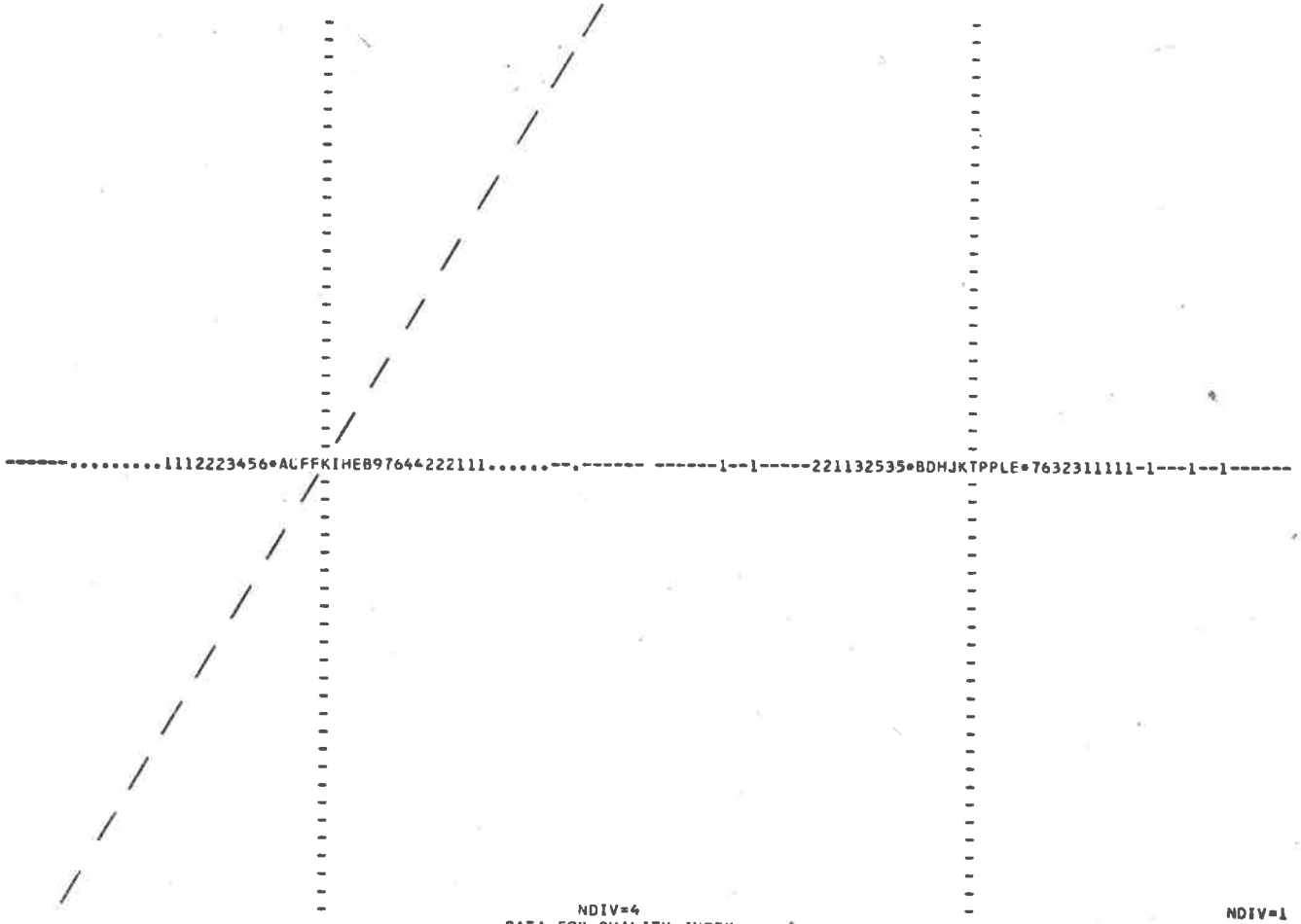
NDIV=4
DATA FOR QUALITY INDEX 1
NDIV=1
ALL REFLECTION POINTS
3501.000 0.037 -0. 1.116 0. -0.
ST. KILDA AND SALISBURY REFLECTION POINTS ONLY
534.000 -0.021 -0. 1.020 0. -0.
PREDICTED VS. EXPERIMENTAL VALUES OF (1/ALPHA) D(ALPHA)/D(H)
INCREMENT PER CELL IS 0.2 IN BOTH X AND Y DIRECTIONS
EVAP. PROFILE, H = 6.7 KM., EXTENDED BELOW HMAX FOR BETTER 'EXACT' FORM

Figure 8.12

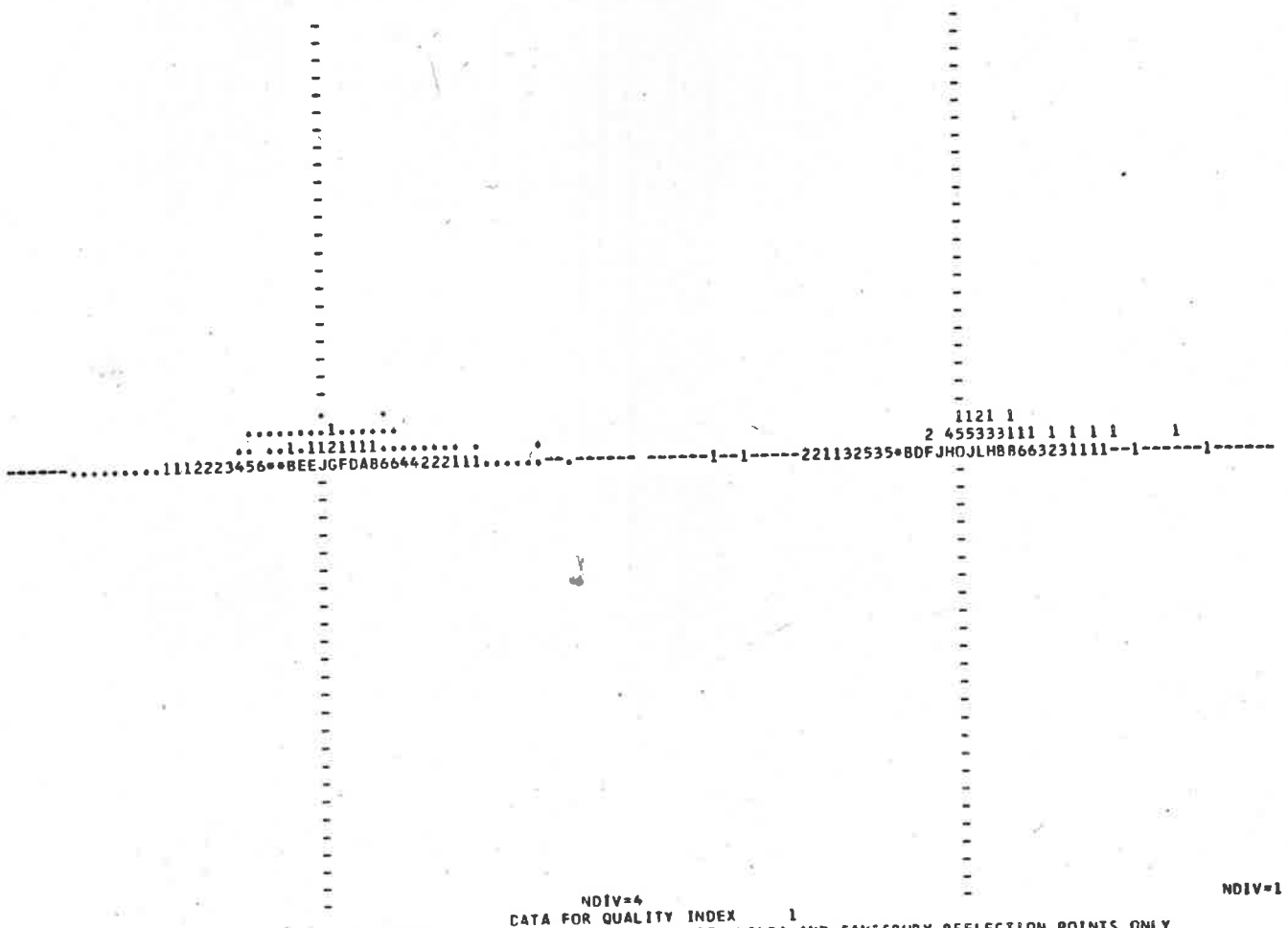

DATA FOR QUALITY INDEX 1

ALL REFLECTION POINTS

3501.000 0.037 0.016 1.116 0.064 0.071

ST. KILDA AND SALISBURY REFLECTION POINTS ONLY

534.000 -0.021 0.027 1.020 0.078 0.177

PREDICTED VS. EXPERIMENTAL VALUES OF (1/ALPHA) D(ALPHA)/D(H)

INCREMENT PER CELL IS 0.2 IN BOTH X AND Y DIRECTIONS
GREENHOW AND NEUFELD IONIZN. MV +6 - +8

Figure 8.13

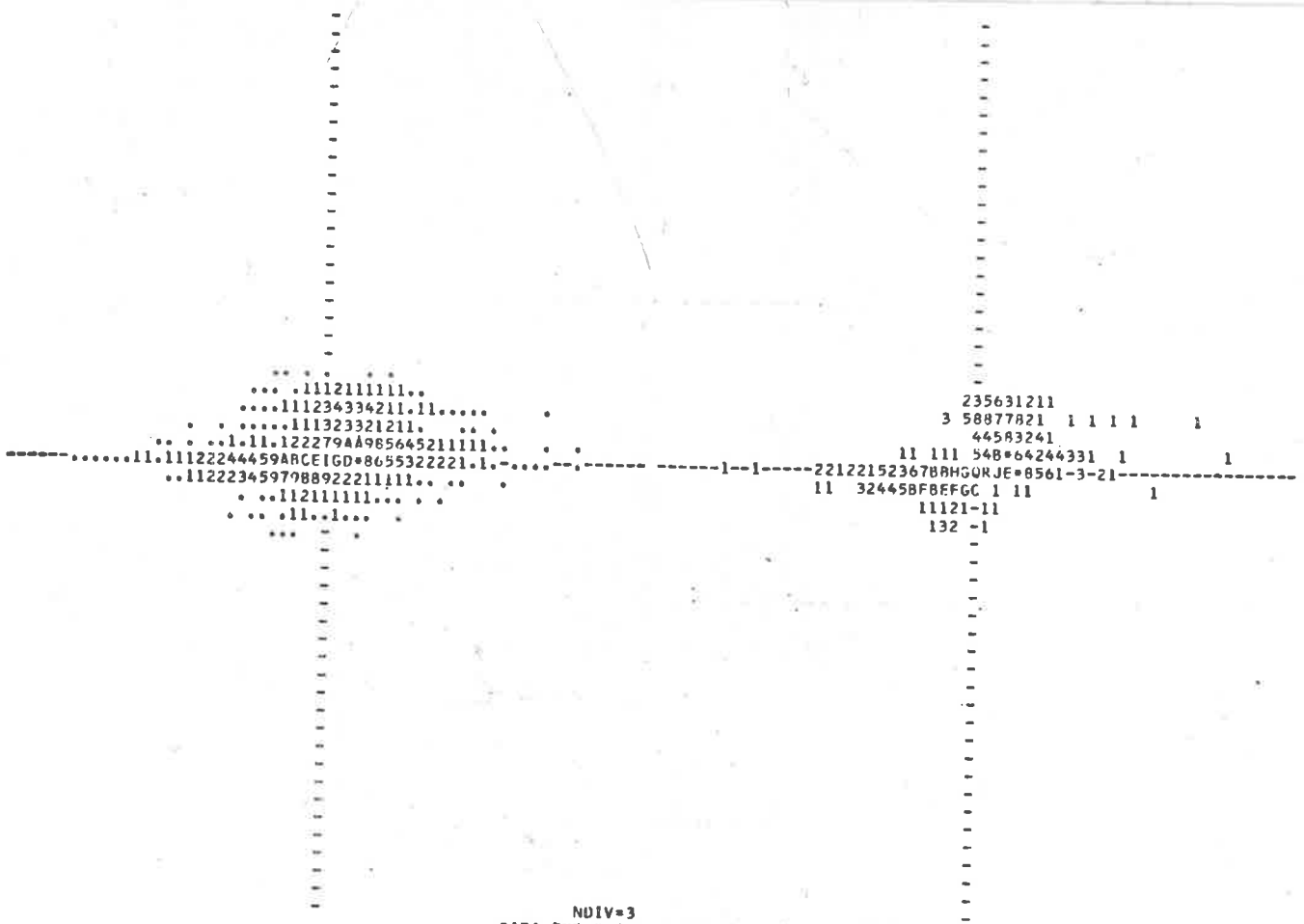

NDIV=3
DATA FOR QUALITY INDEX 1

ALL REFLECTION POINTS
3501.000 0.037 0.064 1.116 0.258 0.291

ST. KILDA AND SALISBURY REFLECTION POINTS ONLY
534.000 -0.021 0.084 1.020 0.298 0.402

PREDICTED VS. EXPERIMENTAL VALUES OF (1/ALPHA) D(ALPHA)/D(H)

INCREMENT PER CELL IS 0.2 IN BOTH X AND Y DIRECTIONS
HAWKINS, SOUTHWORTH SPORADIC OPTICAL MV +4

Figure 8.14

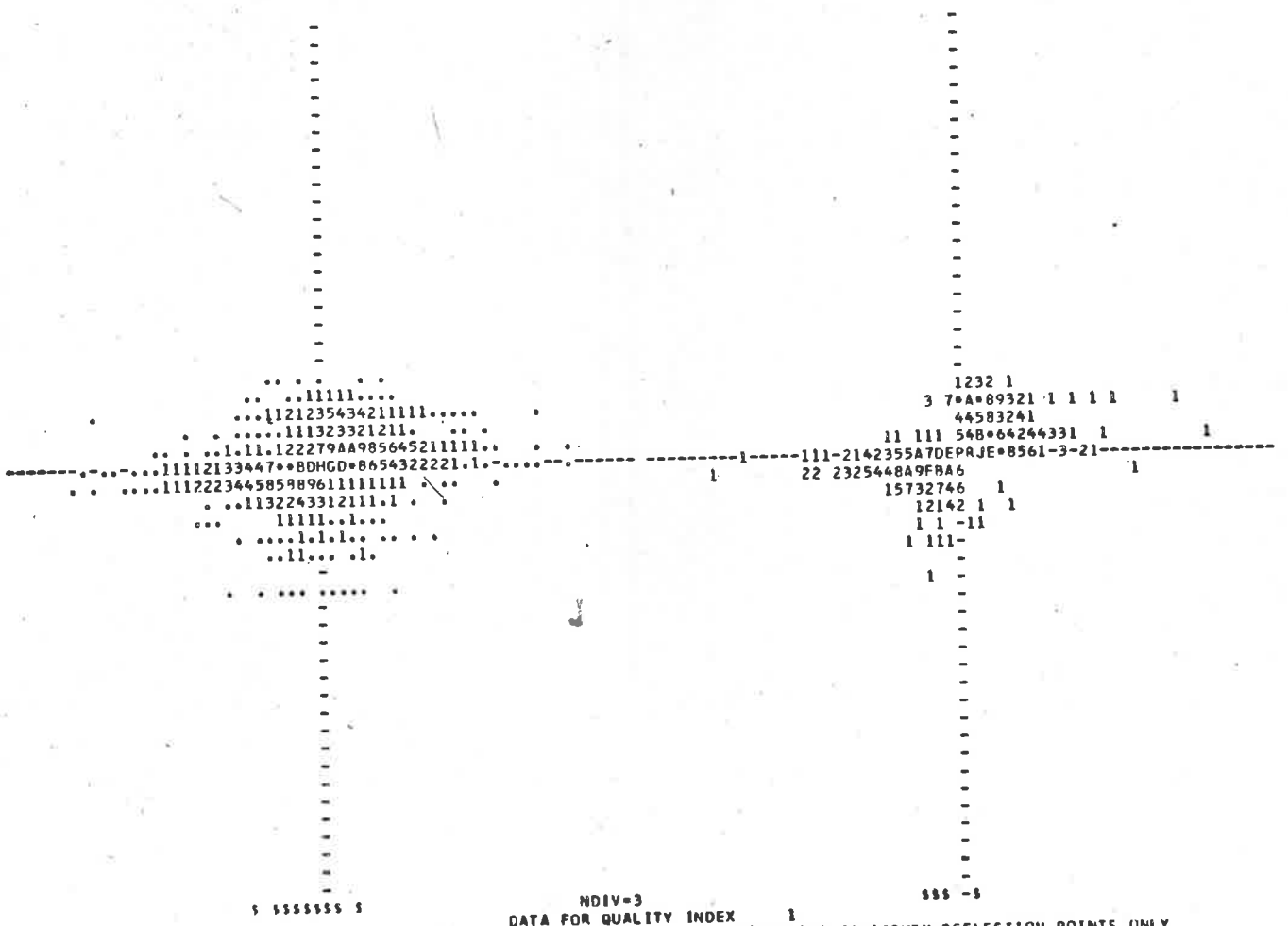
NDIV=3
DATA FOR QUALITY INDEX 1
ALL REFLECTION POINTS
3479.000 0.041 0.030 1.119 0.309 0.283
ST. KILDA AND SALISBURY REFLECTION POINTS ONLY
528.000 -0.017 0.045 1.025 0.336 0.407
PREDICTED VS. EXPERIMENTAL VALUES OF (1/ALPHA) D(ALPHA)/D(H)
INCREMENT PER CELL IS 0.2 IN BOTH X AND Y DIRECTIONS
JACCHIA ET AL. DRACONIDS VISUAL MV +1

Figure 8.15

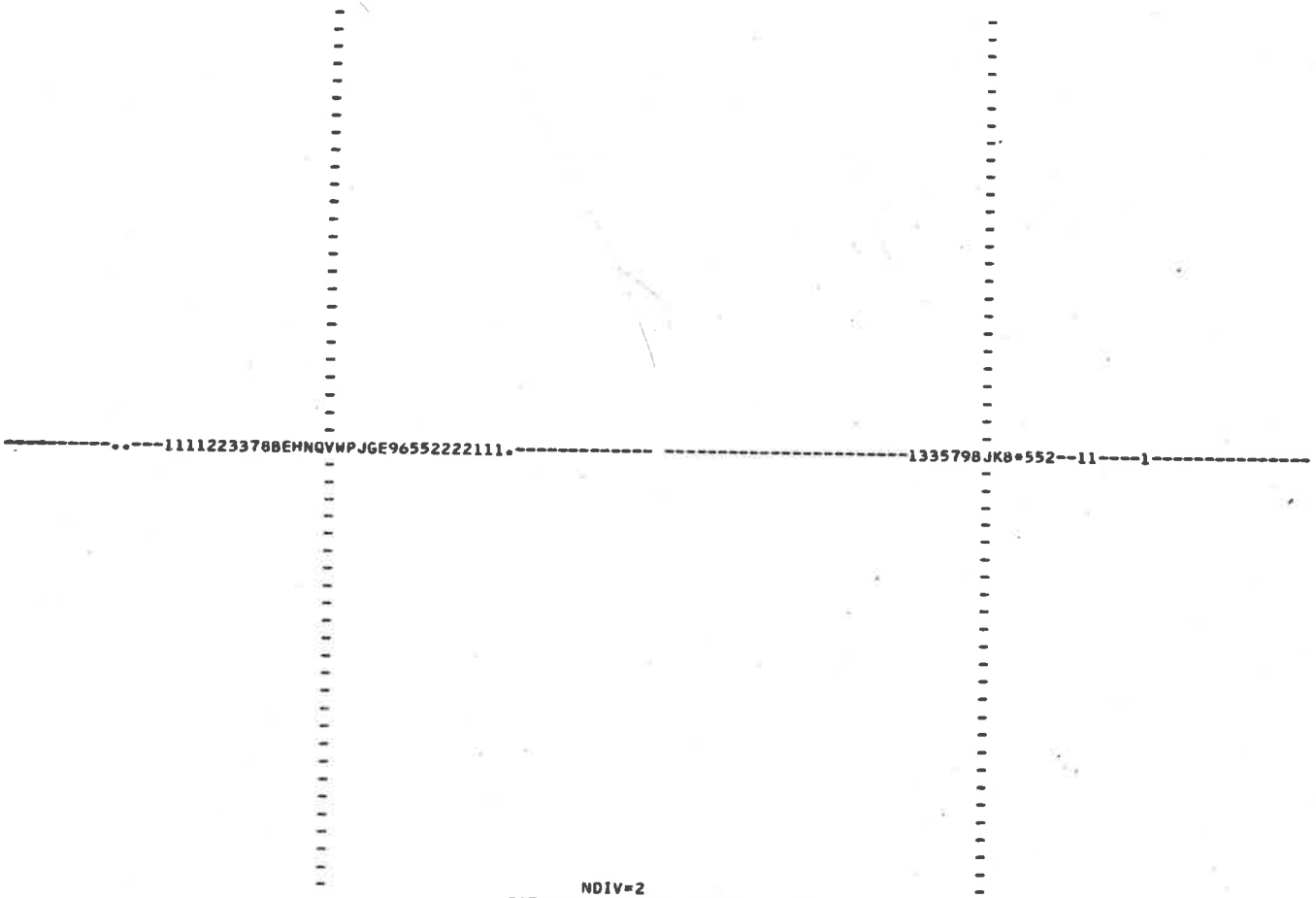
----------..---1111223378BEHNQVWPJGE96552222111.---------- ----------1335798JKB*552--11----1----------
NDIV=2
DATA FOR QUALITY INDEX 3
ALL REFLECTION PCINTS
1198.000 0.079 -0. 0.939 0. -0.
ST. KILDA AND SALISBURY REFLECTION POINTS ONLY
118.000 0.093 -0. 0.648 0. -0.
PREDICTED VS. EXPERIMENTAL VALUES OF (1/ALPHA) D(ALPHA)/D(H)
INCREMENT PER CELL IS 0.2 IN BOTH X AND Y DIRECTIONS
EVAP. PROFILE, H = 6.7 KM., EXTENDED BELOW HMAX FOR BETTER 'EXACT' FORM

Figure 8.16

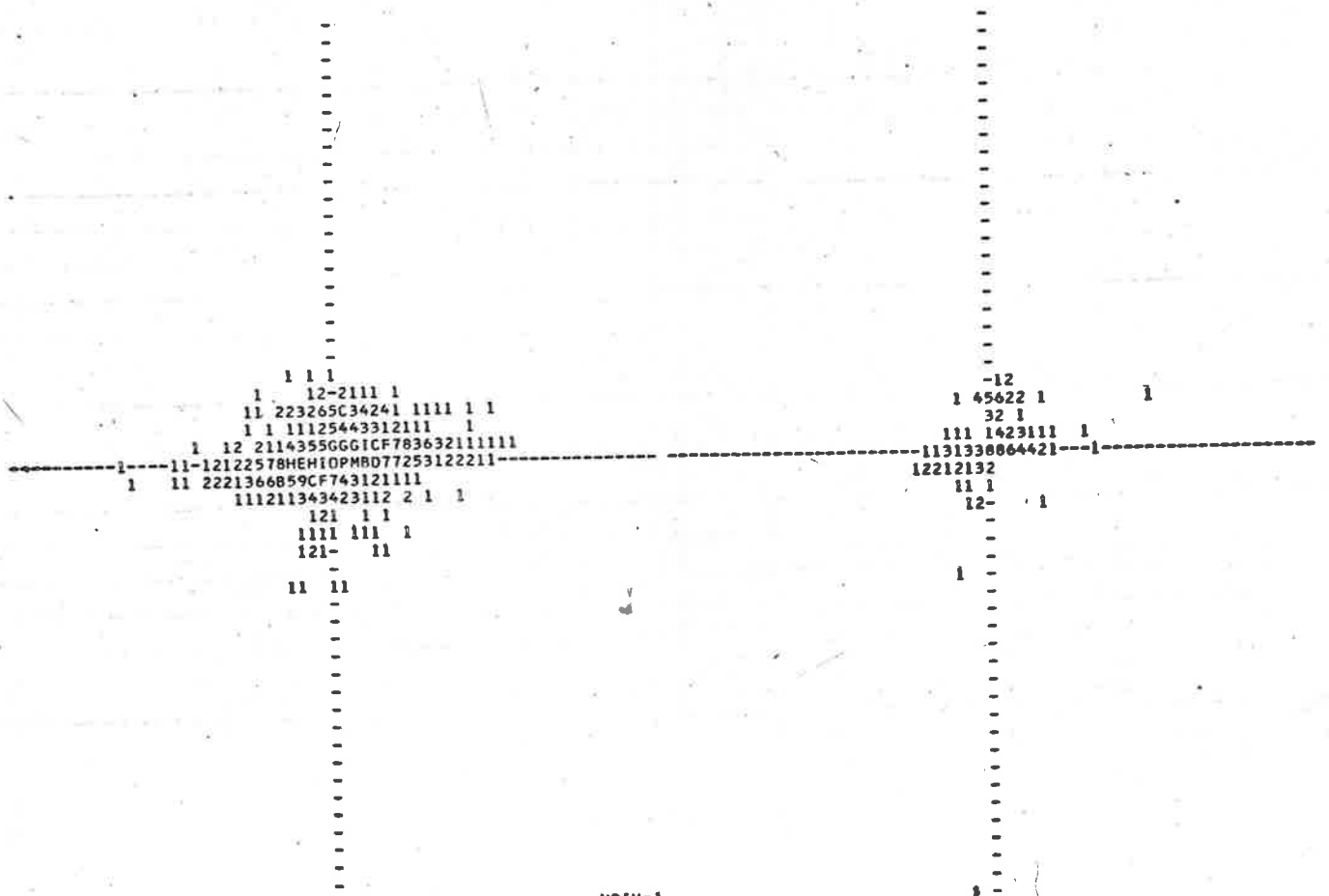
NDIV=1
DATA FOR QUALITY INDEX 3
ALL REFLECTION POINTS
1191.000 0.082 0.057 0.941 0.296 0.233
ST. KILDA AND SALISBURY REFLECTION POINTS ONLY
116.000 0.102 0.117 0.650 0.351 0.281
PREDICTED VS. EXPERIMENTAL VALUES OF (1/ALPHA) D(ALPHA)/D(M)
INCREMENT PER CELL IS 0.2 IN BOTH X AND Y DIRECTIONS
JACCHIA ET AL. DRACONIDS VISUAL MV +1

Figure 8.17

PROFILES CLASSIFIED BY SHAPE

SKETCHES SHOW ELECTRON LINE DENSITY TO RIGHT AND REFLECTION POINT HEIGHT UPWARD
ONLY THE * ORDER * OF VALUES OF THESE VARIABLES IS REPRESENTED
(METEORS RETURNING MORE THAN 1 PERSISTENT - TYPE ECHO OR A HEIGHT DIFFERENCE OF 200 METRES OR LESS ARE EXCLUDED)

'LINEAR' AND 'CONVEX' PROFILES

CODE	1234	1230	1200	4321	3210	2100	2134	2130	4312	3124	3120	4213	3214	4123
SKETCH														
INDEXQ 1	22	46	57	15	37	57	11	44	17	10	38	14	9	9
INDEXQ 2	22	58	52	26	53	43	9	41	10	7	35	9	6	13

'IRREGULAR' PROFILES

CODE	1324	4231	2314	4132	1423	3241	2143	3412	2413	3142
SKETCH										
INDEXQ 1	14	13	11	8	7	5	18	12	5	11
INDEXQ 2	8	7	4	9	6	4	14	10	6	11

'CONCAVE' PROFILES

CODE	1243	3421	1342	2431	1432	2341	1320	2310
SKETCH								
INDEXQ 1	16	9	14	9	5	12	59	40
INDEXQ 2	17	5	19	9	6	10	57	29

SINGLE REFLECTION POINT USABLE

CODE	1000
INDEXQ 1	132
INDEXQ 2	100

Table 8.4. Qualitative classification of trail profile shapes.

To summarize this Section; it has been shown that none of the model profiles suggested by previous workers explain the very rapid increases and decreases in line density with increasing height which were sometimes observed. There is some indication of a tendency for line density to increase suddenly (with decreasing height) immediately above h_{max}. However, the majority of trails detected had the reflection points within a short distance of a comparatively smooth maximum of ionization. The width of this peak has been shown to be best fitted by the profile given by Jacchia, Kopal and Millman for photographed Draconid meteors, and in particular by modifying the latter to a symmetrical form so that its extent below h_{max} is slightly reduced.

These conclusions from the model profile method are compared with the results of other methods, and made more explicit numerically, in the following Section.

8.7 Discussion of model profile results

Firstly an alternative method of analyzing the line density data is pointed out. It leads to similar conclusions to those in the preceding Section. Then an experiment which has given results in conflict with the present ones is examined, and shown to have had a possible tendency to biased errors. By allowing for this bias the conflict is eliminated. The present results agree well with those from several past experiments, using widely differing equipments.

The alternative analysis is detailed in Appendix 5; its main feature is the choice of a model ionization profile which is a Gaussian function of height. The "standard deviation" L of this profile about h_{max} is simply determined from the data. In Appendix 5 the value of L found from all usable line density measurements (INDEXQ 1) is 4.3 Km. With selection of good-quality underdense echoes only (INDEXQ 3) the value is 6.8 Km. Hence the Gaussian profile which fits the data best extends some 7 Km. in height between points of half maximum line density (i.e. between heights $h_{max} \pm 0.69L$). For the Draconid profile, chosen in §8.6 as the best fit among published profiles, the height extent between half-maximum points is 5Km., in fair agreement. The fit of the Gaussian profile to the data is marginally better than the fit of the Draconid profile.

The failure of the evaporation theory to account for the results just presented is not surprising, in view of the considerable weight of evidence for the common occurrence of fragmentation (Chapter 4). It is more surprising to find that the model profile suggested by Greenhow and Neufeld (1957), although shorter than the evaporation profile, is still far too long to match the new data. This profile ((b) in §8.6) was derived from radar observations of a similar sample of meteors, and so might be expected to agree with the present findings.

The geometry of Greenhow and Neufeld's experiment has therefore been examined, as set out in Appendix 6, by simple mathematical simulation. The conclusion reached is that the measured height differences Δh between the two reflection points on each trail were systematically over-estimated. While the modal value of the ratio (Δh/true height difference) was fairly close to unity, its distribution was asymmetrical, and the mean ratio varied (with height) between 1.15 : 1 and 1.83 : 1, with an overall mean of 1.62 : 1.

A second reference to Fig. 8.11 will help in re-evaluating the profile suggested by Greenhow and Neufeld. The most unusual feature of this profile in comparison with the other profiles shown there is the extended, flat region of near-maximum ionization. In fact the profile shown is more rounded near the peak than the original, due to the need for smoothing in the analysis of Section 8.5. It now seems highly probable that the numerous line density ratios which lay close to unity and led to this feature arose from pairs of points separated by much less than the assumed 4 Km. in height. If, therefore, the curve is modified to halve the height extent of its truncated peak while retaining at least the original gradient of the steep beginning and ending portions, the result is little different from either of the two narrower profiles, (c) and (d) in the diagram. Profile (d) has been shown to fit the Adelaide results well. Thus, Greenhow and Neufeld's results have been brought into reasonable agreement with the author's.

The four remaining sources of information on profile lengths are the Schmidt photographic data and radio data of Hawkins and Southworth (1958 and 1963), and the V.H.F. radio experiments of Evans and Brockelman (1963) and of Greenhow and Watkins (1964). These have been compared

in Chapter 4; briefly, the mean height extent of the trails between half-maximum points, and the peak magnitudes, were of order 10 Km. (M∼+ 3), 8 Km. (M∼+ 9), 5Km. (M∼+ 7), and 3 Km. (M∼+ 5) respectively. The height extent found by Greenhow and Neufeld (1957) was 13Km.; corrected, this becomes 8 Km. (M∼+ 6). The author's results are 5 Km. (Draconid profile) or 7 Km. (Gaussian profile), (M∼+ 6).

Taking this evidence on balance, it appears that trails from peak magnitude +3 to +9 have a mean height extent, between the half-maximum points, of 5 to 8 Km., nearly independent of magnitude. In a significant number of trails the profile shows deep irregularities on a height scale of tens of metres. There is a tendency for the profiles to be asymmetric about h_{max}, with abrupt commencements.

8.7 Tentative classification of individual profile shapes

This section presents the results of a somewhat over-simplified attempt to classify the trail profiles in a qualitative fashion as "linear", "convex", "irregular", and "concave". In order to estimate the position of the point of maximum ionization relative to the reflection points, the line densities and reflection point heights were sorted for each trail; the profile shape classification was an extension of the sorting process.

Table 8.4 is a facsimile of a table by which the sorting results were summarized. Every observed profile for INDEXQ values 1 and 2 was given a code of as many digits as there were usable reflection points. Successive digits in the code were for reflection points at successively decreasing heights, and each digit gave the position of that reflection point in a list ordered by decreasing line density. Thus, for example, a first digit of 3 indicated that the highest reflection point had the third largest line density value on that trail. Zeros in the rightmost digit or digits of the code represented profiles on which not every station contributed a line density measurement. The table is otherwise self-explanatory, with the aid of the sketches which illustrate the form of

each coded profile.

There are 24 4-station profiles possible, of which 8 are "linear" or "convex", 10 "irregular", and 6 "concave". For 3-station profiles these numbers are 6, 4, 0, and 2 respectively. Since the proportions differ markedly, and since there were more 3-station than 4-station profiles recorded, it is necessary to analyze each set separately. (There appears to be little point in examining trails with 2 or less reflection points usable). Consider the null hypothesis that in the 4-station case each profile had an equal probability of occurrence, and similarly for the 3-station case. Then the significance of the differences in the frequency of occurrence of (convex + linear), irregular, and concave profiles may be tested, as summarized in Table 8.5 . In this table, O and E signify observed and expected numbers of events, and the final column is the probability that the calculated value of x^2 , with DF degrees of freedom, is not a product of chance alone.

Table 8.5. x^2 test for irregularity in profiles.

Stations	INDEXQ	Trails	Convex, lin. O E	Irreg. O E	Concave O E	x^2	DF	Sign'ce
4	1	276	107 (92)	104 (115)	65 (69)	3.73	2	85%
	2	247	102 (82)	79 (103)	66 (62)	10.5		99.5%
3	1	264	165 (176)	–	99 (88)	2.06	1	95%
	2	273	187 (182)	–	86 (91)	0.41		50%
				Irreg. + concave O E				
4	1	276	107 (92)	169 (184)		3.67	1	95%
	2	247	102 (82)	145 (165)		7.04		99%

From the table we may conclude, for INDEXQ 1 and 4-point profiles, that the tendency to convex rather than irregular trails is real, and that the numbers of concave trails are not significantly different from those expected to arise in a random assortment of profile codes. The attempt to correct the data for reflection point motion brings added weight to the first conclusion. However, for 3-point trails the excess of

convex over concave profiles is barely significant, and disappears if the data for INDEXQ 2 are used.

From the same data we may estimate the significance of the excess of "top-heavy" trails over expectation, for profiles with 4 points, where the attribute of "top-heaviness" is defined as an excess of the sum of the last two profile code digits over the sum of the first two. It is readily seen that this represents a tendency for larger values of α to be observed at the upper reflection points. The alternative categories might be called "balance" (equality replacing excess in the above definition) and "bottom-heaviness"; they are combined in Table 8.6. Each of the three categories can occur in 8 ways, so that equal frequencies should arise by chance.

Table 8.6. x^2 test for tendency to observe large α at top of trails.

Stations	INDEXQ	Trails	"Top-" O	"Top-" E	"Bal."+"Bottom-" O	"Bal."+"Bottom-" E	x^2	DF	Sign'ce.
4	1	276	116	(92)	160	(184)	9.39	1	> 99.5%
4	2	247	107	(82)	140	(165)	11.1	1	~ 99.9%

Even taking the significance tests with the grain of salt recommended in most texts on statistics, the reality of the tendency for the most intense ionization to occur at the upper end of the trail seems quite certain. This simple analysis thus strongly supports the earlier observation (§ 8.6 and § 8.7) that the peaks of some observed profiles tend to be asymmetrical about h_{max}, with the steeper gradient above this height.

The obvious physical interpretation to be given to these results is that in an undetermined but far from negligible fraction of the meteor events observed, the trail was not detectable until sudden fragmentation of the meteoroid occurred. (From Chapter 2, the densities of the individual fragments were therefore nearly equal to those of the parent meteoroids, rather than considerably exceeding them).

8.9 Correlation of height of maximum ionization with other variables

The relationship between h_{max} and several other meteor parameters has been examined statistically.

Because of the number of meteor parameters available for such examination, and because some were expected to be interdependent, the analysis was carried out using a carefully selected computer programme (Appendix 3.8). Its special value lay in the optional facility for automatic removal of "independent" variables which were more significantly correlated with other "independent" variables than with the dependent variable. Thus the final regression equation found, using this feature, was the one for the given data with the least residual effects from dependence among the variables.

From the evaporation theory an appropriate form for the regression equation can be found, and its coefficients can then be estimated from experimental data. Equation 2.4.3c can be re-written in the form

$$p_{max} = K(\alpha_{max} \cos^2 x)^{1/3}/v^2 \qquad \ldots 8.9.1$$

where K depends on meteoroid parameters only, and is very approximately constant over most of the ionized trail. The pressure is p_{max} at the height h_{max} where the largest line density α_{max} occurs. For an isothermal atmosphere with scale height H, it can be shown that

$$h_{max} = h_o - \frac{H}{3}\ln\alpha_{max} - \frac{2H}{3}\ln\cos x + 2H\ln v \qquad \ldots 8.9.2$$

where h_o is a constant related to K. Putting $H \simeq 6.5$ Km., we have

$$h_{max} \simeq \text{constant} - 2.2\ln\alpha_{max} - 4.4\ln\cos X + 13\ln v \quad .$$

$$\ldots 8.9.3$$

Using programme NRMC 3, the regression coefficients a_i were estimated in an equation of the form

$$h_{max} = a_1\ln\cos x + a_2\ln v + a_3\ln\alpha_{max} + a_4\cos\frac{2\pi t}{24} + a_5\sin\frac{2\pi t}{24}$$

where t is time of occurrence, in hours. The result obtained was

$$h_{max} = 80.5 - 2.1\ln\cos x + 1.9\ln v + 0.27\ln\alpha_{max} - 3.0\cos\frac{2\pi t}{24} - .03\sin\frac{2\pi t}{24} \qquad \ldots 8.9.4$$

for INDEXQ 1 data for Nov. and Dec. 1961. The automatic reduction facility rejected as not significant all terms other than

$$h_{max} = 92.1 + 1.69 \ln v - 3.14 \cos \frac{2\pi t}{24} \quad . \qquad \ldots 8.9.5$$

The order of rejection was:- $\sin \frac{2\pi t}{24}$ (dependent on ln v), ln cos χ (dependent on ln v), $\ln \alpha_{max}$ (dependent on ln v). The first two of these interdependences probably result from the earth's diurnal rotation, with its influence on the geocentric velocity of the meteors available for detection at any time. For both of the above regression equations, the residual error of estimate in h_{max} was approximately 5.0 Km. It can be seen that h_{max} showed far less dependence on v and α_{max} than predicted by the evaporation theory, and that the relation with cos χ, while also below the predicted strength, had at least the right order of magnitude. The reason for the small correlation of h_{max} and v is not known. The near-independence of h_{max} and ln α_{max}, however, is excellent confirmation of the work of Hawkins and Southworth (1963), since it relates to meteors of magnitudes +5 to +8 approximately, for which they predicted just such a virtual independence. (The mean height of detection for meteors observed at Adelaide is 93 Km., also in good agreement with their predictions).

If fragmentation acts as a randomizing influence on h_{max} by making trail profiles irregular, it would seem prudent to try to replace the use of α_{max} in the above analysis by something less dependent on the vagaries of fragmentation. Obviously it is impossible to measure directly the mass of the meteoroid prior to fragmentation, for example. However, if the process of ablation and production of ionization is at least reasonably independent of particle size, the integrated electron content of the trail should be directly proportional to the mass of the original meteoroid.

Although in general the length of trail spanned by the reflection points was less than the length deduced earlier for the typical profile, an approximate estimate of the total electron content was made by assuming that α varied linearly between reflection points and vanished beyond the observed section of trail. For simplicity, the conflict between this assumption and the placing of h_{max} 1 Km. beyond the highest or lowest reflection point under some circumstances was ignored. In a more refined

treatment allowance could perhaps be made for this and other features of each profile's shape.

From the evaporation theory, it can be shown that it is appropriate to include the logarithm of the meteoroid mass in the regression equation. Write I for the integrated electron content, found as detailed above. For the period May-Dec. 1961, using all trails with 4 reflection points, selected for good quality as for INDEXQ 3 but including transitional echoes, the following regression was found:-

$$h_{max} = 68.9 - 3.3 \ln \cos\chi + 2.7 \ln v - 0.35 \cos\frac{2\pi t}{24} + 0.35 \ln I \quad \ldots 8.9.6$$

In arriving at this equation a term in $\sin\frac{2\pi t}{24}$ was automatically deleted because of its interdependence with ln v, and a term in $\ln \alpha_{max}$ was removed because of its very strong dependence (partial correlation coefficient 0.90) upon ln I. Note that the dependence of h_{max} on $\cos\chi$ in Equation 8.9.6 is increased, and is nearly as strong as predicted by Equation 8.9.1, while the coefficient of ln v is also larger than in Equation 8.9.5 (although still far below its predicted value).

Because Equation 8.9.6 represents a longer period than Equation 8.9.5, including parts of all four seasons, it might be expected to yield the greater uncertainty in predicting h_{max}. Instead the standard error of estimate of h_{max} is reduced, from 5.0 to 4.7 Km., and from the detailed statistics this is found to result from a partial correlation between h_{max} and ln I which is twice as strong as that between h_{max} and $\ln\alpha_{max}$. This improvement due to using such a simple estimate of the total electron content of the trail is encouraging.

8.10 Summary of trail profile results

Several forms of statistical analysis have been used in studying the profiles of electron line density produced by over 1600 meteors. For the underdense trails in this sample, the most common line density was approximately 3×10^{13} electrons/metre. The lower limit of detectability was just below 10^{13} electrons/metre, equivalent to a magnitude of about +7 . Up to 4 line density measurements could be made per trail, and the analysis has been concentrated upon trail profile shapes in order to use this information efficiently.

It has been shown that the typical profile was of comparable length (5 to 7 Km. between points of half maximum ionization) with that found by Jacchia, Kopal and Millman (1950) for photographed Draconid meteors (magnitude ~+1), and with one inferred for fainter meteors, between magnitudes +6.5 and +9.7, observed by the Harvard radio system. There was a marked tendency for the highest reflection point on a trail to have the greatest line density. This has been interpreted in terms of sudden fragmentation of some meteoroids into numerous smaller particles.

We have suggested that the initial radii of typical trails near 93 Km. height were 0.5 m. to 1 m., leading to systematically low measurements of underdense line density by a factor of 2 (or less).

An attempt to correct the measurements of line density for motion of the reflection points along the trail due to wind shear has succeeded in reducing the scatter in line densities observed at closely spaced reflection points on the same trail. The absence of such improvement at larger spacings has been tentatively ascribed to small-scale irregularity of the ionization profile. The effects of the earth's magnetic field and of plasma resonance on the line density determinations were found to be small.

The consistency of previous work on trail shapes has been improved, by showing that the model profile suggested by Greenhow and Neufeld (1957) should be reduced in length, to an extent which makes it quite compatible with both the present, and other earlier results.

A statistical examination has been made of the relationships between the height of maximum ionization, the value of line density at that height, the meteor velocity, the approximate total electron content in the observed part of the trail, and other variables. The main results are that the height of maximum ionization h_{max} depended only weakly on the total electron content (which was however more strongly correlated with h_{max} than was χ_{max}), and on the meteor velocity. The former result is in accord with other work, but the small velocity dependence is not understood.

CHAPTER 9

DIFFUSION COEFFICIENT RESULTS AND DISCUSSION

9.1 Introductory comments

Measurements of the ambipolar diffusion coefficient of ionized meteor trails have been made from four-station observations of the decay of radio echoes, in each month from December 1960 to December 1961 inclusive.

The experiment differed from others which have been reported (Chapter 5) in its overall duration, in permitting up to four measurements per trail of the diffusion coefficient, and in the completeness with which the parameters of each meteor's trajectory were known.

The analysis of the large volume of data from this experiment followed three basic methods:

(i) Scatter diagrams were propared, showing the distribution of the logarithm of the diffusion coefficient D with height h, in 4-hour intervals and over all 24 hours, for each recording period. From these were derived profiles, to summarize the height variation of D; cross-sections in narrow height intervals, to examine diurnal changes; and values of H_D, the "diffusion scale height", to examine seasonal changes.

(ii) Similar scatter diagrams were prepared showing the height distribution of D', defined as the gradient of $\log_{10} D$ measured from two reflection points on a trail. These diagrams, and derived profiles of D' versus h, were used in further examination of features of the log D scattergrams, and in finding a second value of H_D for each 4-hour or longer period.

(iii) A multiple correlation technique was applied, to find which parameters of the trajectory and the environment were important in determining D. Time, height, meteor and wind speeds, and the orientation of the trail relative to the geomagnetic field and the electric vector of the radio wave were among the parameters tested.

Parts of the above analysis were repeated with attempted corrections for movement of the reflection points along the trail in a wind shear field, and with subsets of the data from which poor-quality and potentially resonant echoes had been removed, to evaluate the influence of these factors on the scatter observed in D at any height and time.

Meteors of the Geminid stream were given special attention, because of previous anomalous diffusion coefficients obtained for members of this stream.

9.2 Two initial comparisons

A typical scattergram of $\log_{10}D$ * versus height is shown in Figure 9.1, together with the profile derived from it. The data are for September 1961, and cover all hours of the day. We can make direct comparisons between this scattergram and those in Figure 5.2, which show results published by Greenhow and Hall (1961) and by Murray (1959). The origins of axes are all at ($\log_{10}(4D) = 0$, h = 60Km.), and the ratio of horizontal and vertical scales is the same, so that shapes are invariant.

Murray's results are also for the month of September, and cover the whole 24 hours of the day. There is much similarity between his log D vs. height distribution and the author's. The only important difference lies in the slightly increased scatter in log D at any height shown by the present results, due to the inclusion in them of transitional echoes and echoes which did not pass some test of quality. (The results shown are for quality index 1). The distributions of Murray's results and the good-quality September 1961 results are found to be practically identical.

The results of Greenhow and Hall in Figure 5.2 are for 03-06 hours in December (Northern Hemisphere). Their agreement with Fig. 9.1, which is for September 1961 and covers all 24 hours, is poor. The agreement with the second scattergram of Fig. 9.2, which covers hours 04-08 for September 1961, is poorer still. The disagreement is further discussed later.

9.3 The quality classification

Details have already been given (Section 8.1) of the classification scheme by means of which the effects of reflection point motion, of including transitional and poor-quality echoes, and of resonance were isolated for study. Briefly, data which had been corrected or edited to remove these effects were denoted by the values 2,3 and 4 respectively of the quality index INDEXQ. The basic, unedited data were denoted by INDEX = 1.

The scattergrams allow us to assess the differences among the

* The quantity actually plotted was $\log_{10}(4D)$, where D is in $m^2/sec.$, for convenience in locating the axes.

INDEXQ classes. To minimize diurnal effects the comparisons are made, as far as possible, among the plots which represent each 4-hour interval separately.

INDEXQ 2: First the correction for reflection point motion is considered. On comparison of Fig's. 9.2 and 9.3, showing uncorrected and corrected log D values respectively for September 1961, it is obvious that the shape of the distribution for each 4 hours is barely changed by the correction process. In fact, such differences as do exist are not entirely attributable to the correction, because 5-6% of the echoes in each 4-hour group could not have the correction applied to them, due to the absence of any other accurate values of line density for the trails concerned, and were not assigned INDEXQ 2. The removal of this small proportion of the echoes must have influenced the shapes of the distributions, although presumably to a minor extent only.

From Fig. 8.8 we have seen that the corrections made to observed decay time-constants were, in general, too small to remove the scatter in D at any height. Over 80% of the correction factors were smaller than $\sqrt{2}$, and despite the long "tails" of the distribution in Fig. 8.8 only 10% or less of the corrections exceeded a factor of 2. By contrast, the standard deviation of log D from the functional relationships estimated later in this Chapter is very nearly as large as its deviation (approximately 0.25) from its mean value in each of the 4-hourly scattergrams of Fig. 9.2. This deviation in the logarithm is equivalent to a factor of 1.8 in D itself. The distribution of log D about its mean appears approximately normal in these figures (and others), and so about one-third of the measured diffusion coefficients differed from the mean (or the fitted line) by more than a factor of 1.8.

Although one would expect to find the scatter reduced by the attempt to allow for reflection point movement, this is not the case. Instead, in the 24-hour plot and all but one of the 4-hourly plots for the May-Dec. period, the standard deviation of log D increases by about 3% and the correlation coefficient falls similarly. Corresponding slight increases in disorder are also apparent on examination of the month-by-month scattergrams of log Dfor INDEXQ 2, such as Fig. 9.3.

Careful comparison of the 24-hour scatter diagrams for INDEXQ = 1

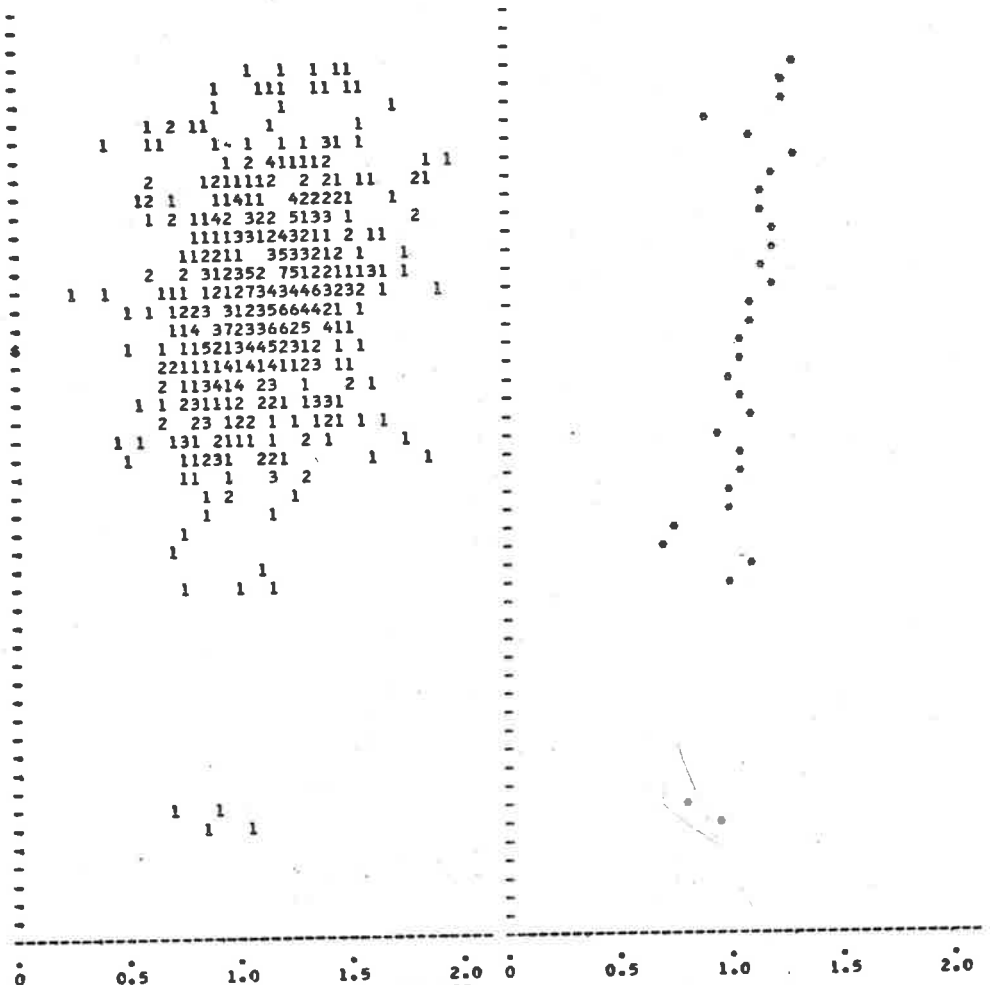

POINTS LOGDM MMEAN SGLOGD SGMITE CORR CFT
579. 1.118 94.3 0.273 5.62 0.22E-00
OVERALL SCATTER IN LOG10(D/DZERO)

MEANS IN HEIGHT GROUPS, FOR ENTIRE PERIOD

••• LOG10(D/DZERO), DZERO =.4 SQ. METRE / SEC. •••
FROM 61 9 22 TO 61 9 29 INCLUSIVE

60 TO 110 KM. INCLUSIVE
QUALITY INDEX 1 PAGE 7

Figure 9.1

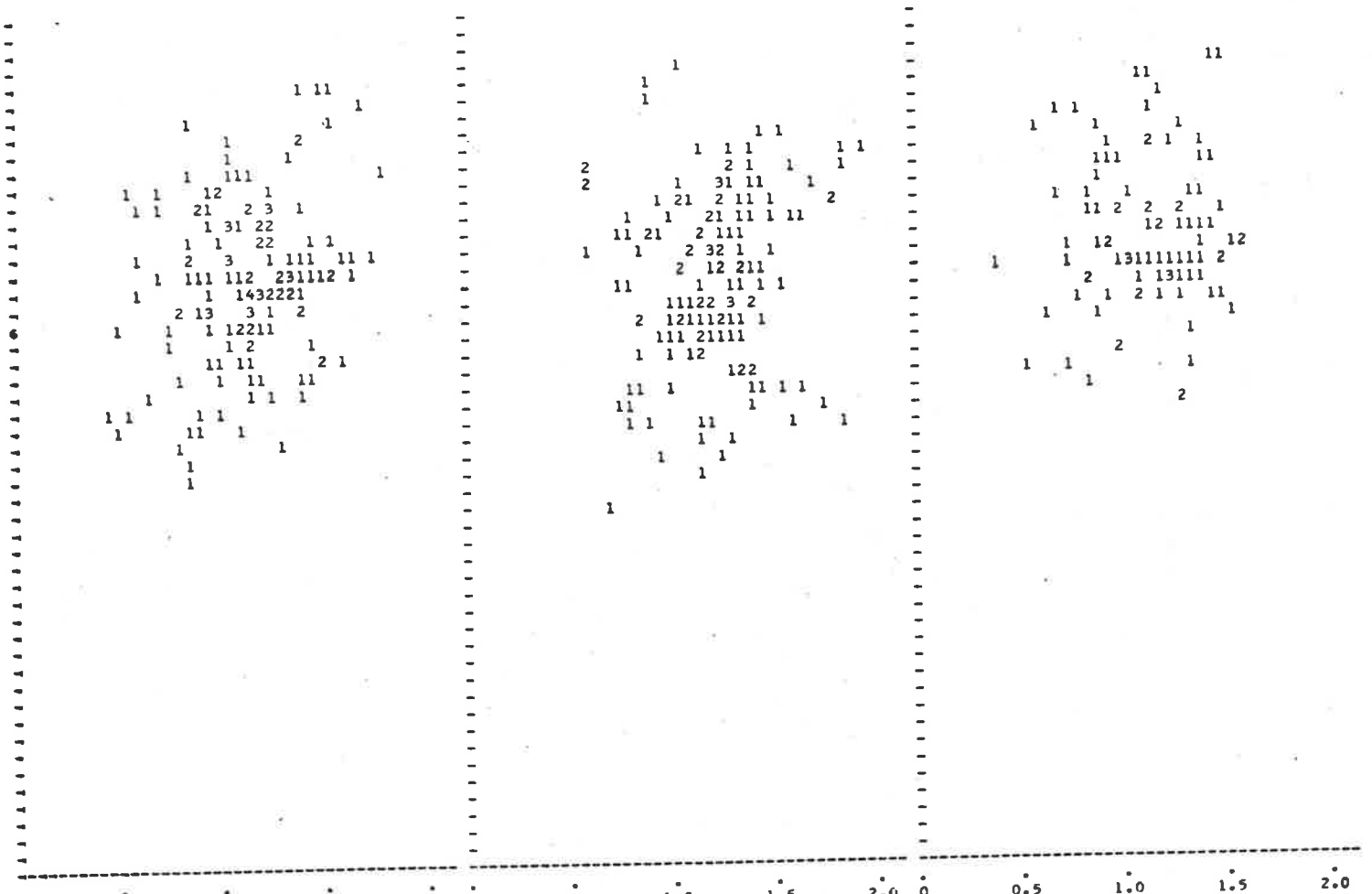
0 0.5 1.0 1.5 2.0
0- 399 HOURS LOCAL TIME
POINTS LOGDM HMEAN SGLOGD SGMITE CORR CFT
155. 1.135 94.7 0.272 4.69 0.24E-00
0 0.5 1.0 1.5 2.0
400- 799 HOURS LOCAL TIME
POINTS LOGDM HMEAN SGLOGD SGMITE CORR CFT
152. 1.207 94.5 0.274 5.13 0.10E-00
0 0.5 1.0 1.5 2.0
800- 1199 HOURS LOCAL TIME
POINTS LOGDM HMEAN SGLOGD SGMITE CORR CFT
96. 1.140 96.6 0.259 4.42 0.21E-01
*** LOG10(D/DZERO), DZERO =.4 SQ. METRE / SEC. *** 60 TO 110 KM. INCLUSIVE
FROM 61 9 22 TO 61 9 29 INCLUSIVE QUALITY INDEX 1 PAGE 1

Figure . 9.2

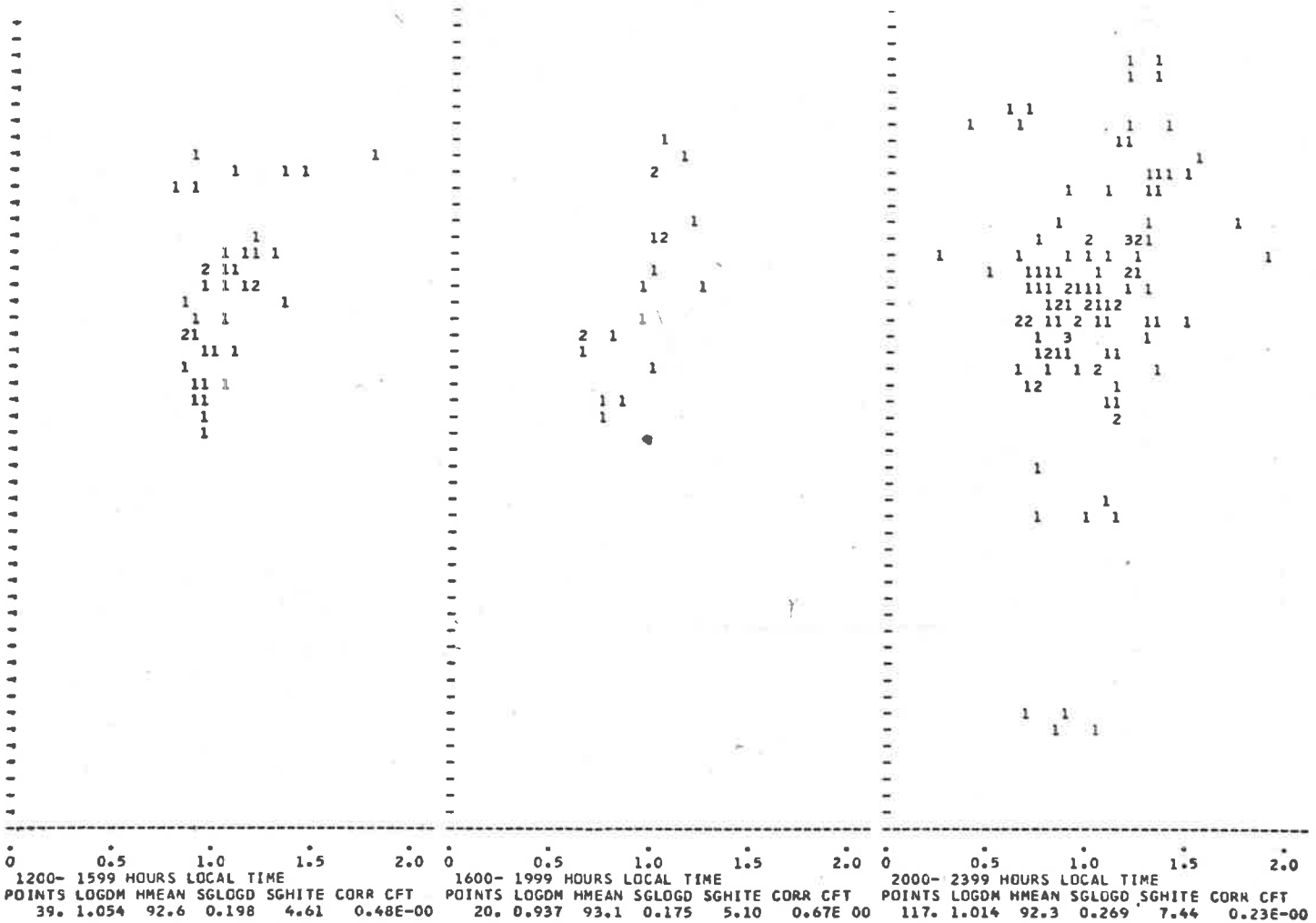
0 0.5 1.0 1.5 2.0
1200- 1599 HOURS LOCAL TIME
POINTS LOGDM HMEAN SGLOGD SGHITE CORR CFT
39. 1.054 92.6 0.198 4.61 0.48E-00
0 0.5 1.0 1.5 2.0
1600- 1999 HOURS LOCAL TIME
POINTS LOGDM HMEAN SGLOGD SGHITE CORR CFT
20. 0.937 93.1 0.175 5.10 0.67E 00
0 0.5 1.0 1.5 2.0
2000- 2399 HOURS LOCAL TIME
POINTS LOGDM HMEAN SGLOGD SGHITE CORR CFT
117. 1.014 92.3 0.269 7.44 0.23E-00
••• LOG10(D/DZERO), DZERO =.4 SQ. METRE / SEC. ••• 60 TO 110 KM. INCLUSIVE
FROM 61 9 22 TO 61 9 29 INCLUSIVE QUALITY INDEX 1 PAGE 2

Figure 9.3

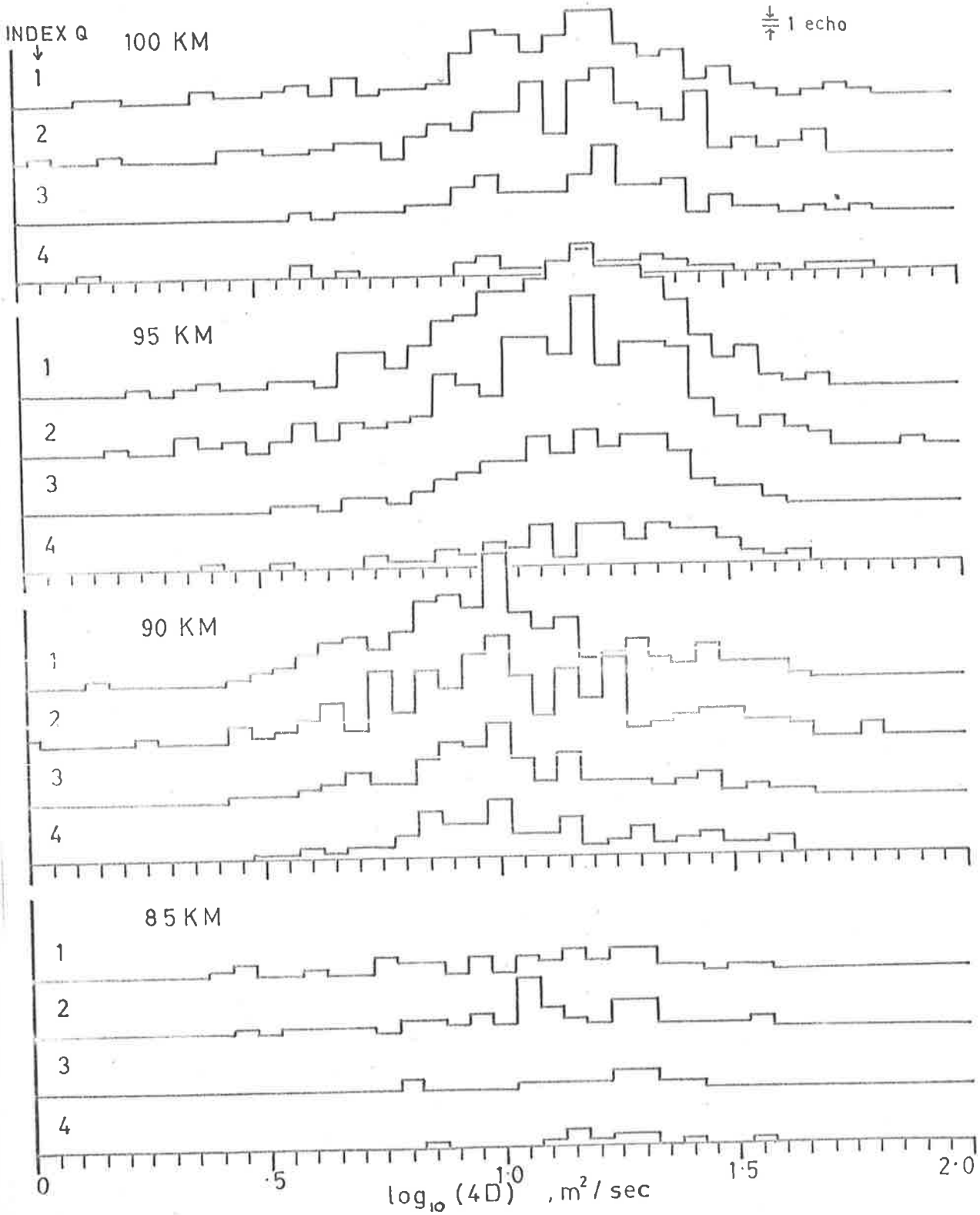

Figure 9.4. Cross-sections of log D scattergrams, May-Dec.

and 2 in the May-Dec. period (not reproduced) shows that points unable to be corrected were fairly evenly distributed in height and in log D. Therefore, as previously implied, their absence from the plots for quality index 2 is not responsible for the decreased correlation,

A check of data for some individual meteors shows that where an ionization profile was reasonably smooth, possibly in spite of some of the echoes being transitional in type, the appropriate corrections to the time-constants were properly made, but were small in magnitude. That is, the corrections for reflection point motion in these cases generally tended to improve the agreement of diffusion coefficients on individual trails, but were seldom greater than 10%, and were thus inadequate to remove all the scatter in D, either on a typical individual trail or, especially, from trail to trail.

On the other hand, where large fluctuations in electron density were found, the correction routine was found to have operated properly from a formal point of view, but the "corrections" to the diffusion coefficients were sometimes excessively large (see Fig. 8.8 again), and showed no general tendency to improve the consistency of the data. This result was by no means unexpected. However, it is disappointing to find irregular profiles so widespread in occurrence that the correction as it stands is of little or no practical use). For, if the irregularities as measured were largely real, the basic assumption that each reflection point traverses a segment of profile which is nearly an arc of an exponential is invalid. Also, as Rice and Forsyth have suggested, the diffusion coefficient controlling the echo decay is not necessarily that for the specular reflection point if the ionization is irregular. Where the irregularities were only apparent, arising from the greater error attendant upon the use of transitional echoes, obviously no useful corrections were to be expected. In brief: checks of individual echoes show that the correction for reflection point motion was useful on fairly smooth trails only.

A general idea of the relationship of the quality index classes is gained from Figures 9.4 and 9.5. The first of these is a series of "cross-sections", in histogram form, taken at various altitudes in the 24-hourly log D vs. h scattergrams for all four quality classes, while Fig. 9.5 shows cross-sections through the D' plots instead of log D itself. In each

case the results for May-Dec. 1961 are used, so that each cross-section, though representing a height range of only 1 Km., contains enough data points to be statistically meaningful. (The lowest height, 85 Km., is possibly an exception to this rule). Inevitably seasonal effects are included in data taken over such a long period, although there are no features in the cross-sections which obviously arise from this particular cause.

Above 105 Km., and below 84 Km., even the 24-hour data become too sparse for the mean values taken in every 1 Km. height interval to define smooth profiles. Hence these levels have been taken as the upper and lower height limits of statistically reliable data for this survey. Continuing the comparison of INDEXQ 1 and 2 in Fig. 9.4, it is seen that the reflection point motion corrections have made the distributions less smooth. Although the overall shapes are similar, on a large scale, at each height, a tendency has been introduced for the points to cluster in minor groups within the overall broad peak. If this tendency is interpreted in terms of increased small-scale order, then clearly such improved order must result from improved agreement among the diffusion coefficients on single trails, and possibly among small groups of trails. This small improvement does not manifest itself as a decrease in the standard deviation of log D from its overall mean, partly because there are slightly more outlying values in the distributions for INDEXQ = 2, and partly because the broad central peaks of the distributions have not been narrowed. In Fig. 9.5, at 90 and 95 Km., a slightly more marked improvement due to the reflection point motion correction is noticeable. Again, though, the improvement is only on a small scale relative to the total range of the variable (D').

INDEXQ 3: Turning to comparison of the original data with its high-quality subset, we find a 30 - 40% reduction in scatter. This statement is true for both log D (Fig. 9.4) and D' (Fig. 9.5) at each height shown. Examination of the original scattergrams shows that the same reductions apply at all heights. However, there is a compensating disadvantage, in that the number of points available is less than one-half the original total (e.g. 1644 values of log D, and 1167 of D', as against 3437 and 2992

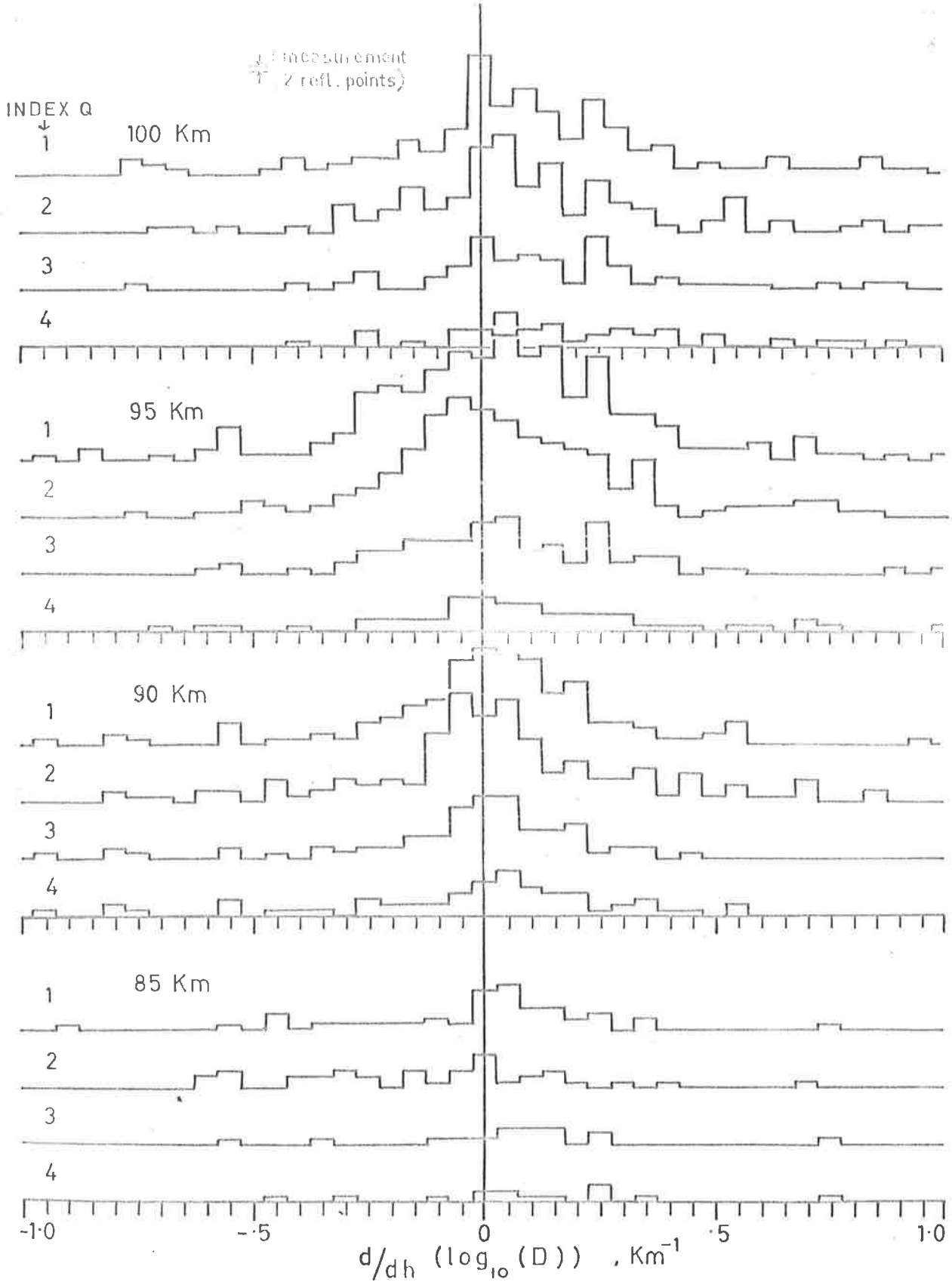

Figure 9.5. Cross-sections of 3' scattergrams, May-Dec. 1961, all INDEXQ.

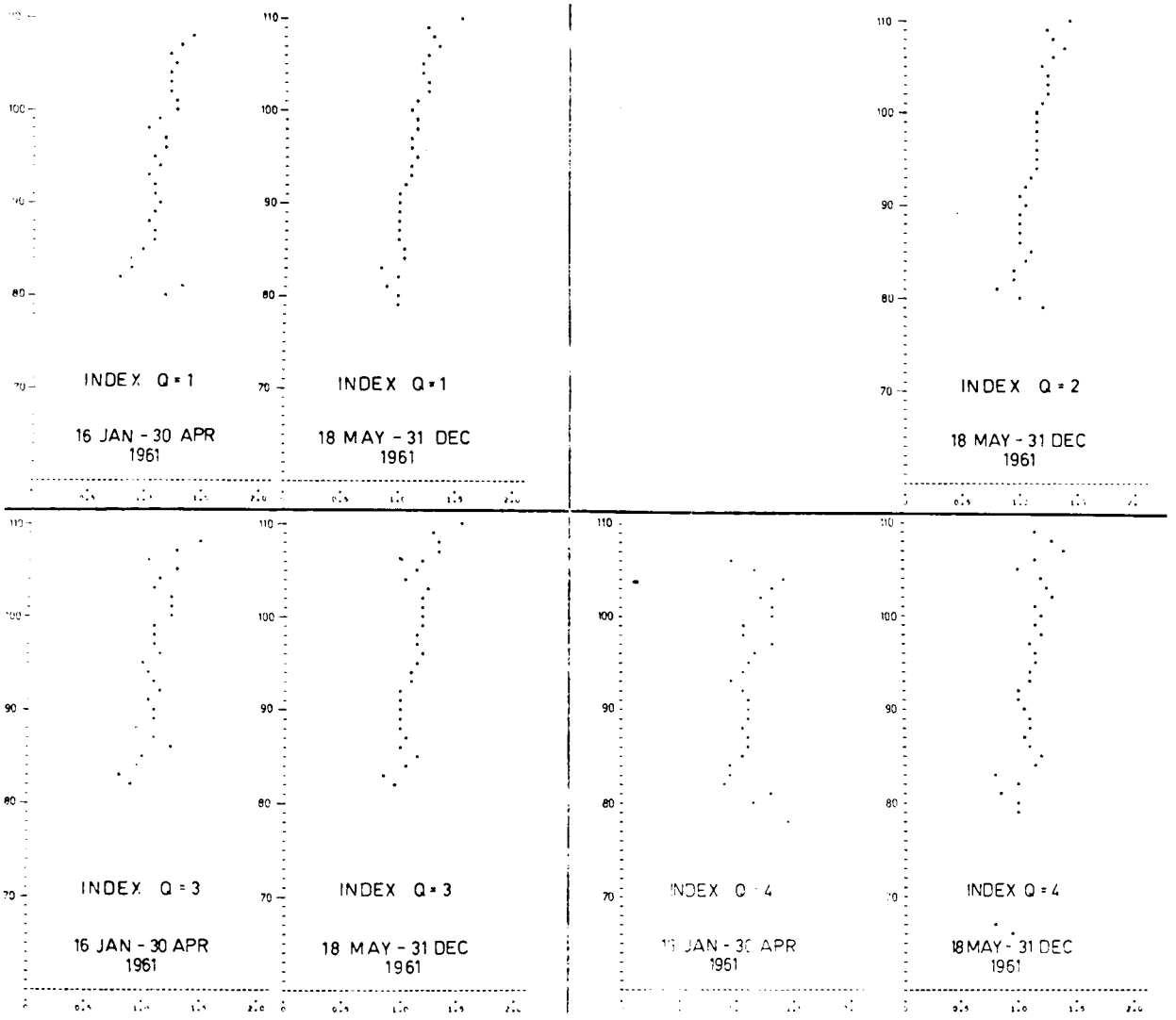

Figure 9.6. Profiles of $\log_{10}(4D)$ for all four stability classes. Each point is the mean of all data in a height interval of extent 1 km.

with INDEXQ=1, for the period May-Dec. 1961). The lessened numbers are of little consequence in the present context, but make it impossible to analyze certain 4-hour intervals for individual months, as seen later. The reduction in scatter is ascribed mainly to the exclusion of transitional echoes and echoes whose waveforms did not adhere very well to an exponential decay.

At the two lower altitudes, 90 and 85 Km., the distributions of log D have not been attenuated to the same degree on both sides of the original central peak. Instead, rather unexpectedly, lower values of the diffusion coefficient have been rejected and the faster decays at these levels have been preferentially retained. A likely partial explanation is that the rejected echoes, whose decay time-constants of over 0.5 sec. were close to the upper limit of the St. Kilda recording system, were removed because their decays could not be reliably distinguished from the slow beats in amplitude caused by two reflecting centres on an overdense trail. Evidently a slightly increased recording time per echo would have been helpful here.

INDEXQ 4: Probably the most notable feature of the echoes with longitudinal polarization is a similar tendency for their decay to be more rapid than the overall mean (INDEXQ=1) below about 90 Km. Figure 9.6 is a reproduction of profiles derived from the 24-hour scattergrams for Jan.-Apr. and for May-Dec. 1961. All four quality index classes are shown, and on close examination the four profiles for each of these periods are seen not to differ systematically between approximately 90 and 105 Km. However, from 84 to 90 Km., the points making up the INDEXQ 4 profiles are displaced to the right relative to those with INDEXQ=1. The displacement represents an addition of approximately 0.1 to $\log_{10} D$. One would expect that resonant echoes from regions of time density roughly 5×10^{13} electrons/m. might readily be assigned KIND 1 instead of 0, and hence that the diffusion coefficient might be overestimated. (See Figure 3.5). The lower the altitude and true diffusion coefficient, the more readily this situation might be thought to arise, since only the resonant peaks of longest duration could be expected to persist until after the beginning of the wind and turbulence records. Removal of res-

onant echoes, then, should on this view reduce the mean diffusion coefficient measured at the lower end of the height range. The opposite effect is observed.

Possibly the cause of this anomaly is over-correction, arising in the following way. Realizing the danger of labelling a resonant underdense echo as transitional, the author tried, where the echo envelope closely resembled the theoretical resonant form of Fig. 3.5, to assign KIND 0 as consistently as possible. In addition, the data for such echoes were labelled as of poor quality (NOK=0), so that they did not later qualify for the class INDEXQ=3. The effect of assigning KIND 0 to these echoes, with the early part of the envelope smoothly convex before the apparently exponential decay, may have been to over-estimate the time-constant of the latter. If so, the displacement of the lower section of the profiles for INDEXQ 4 may imply that the diffusion coefficients of significantly resonant echoes, debarred from this class, were on average not only corrected but over-corrected by the above treatment.

However, the explanation of the apparent distortion of the INDEXQ 4 profiles as due to over-correction of other data not contributing to them (but contributing to the other classes) is not entirely satisfactory. It would be more credible if an anomalously large profile slope had been found with INDEXQ=1, and not with INDEXQ=4, at the heights involved. In fact the behaviour to be explained is the converse, an anomalously small slope with INDEXQ=4. The author can only suggest that perhaps the difficulty in observing slow decays, mentioned in connection with quality class 3, is also involved here.

Our major conclusions in this Section have been that

(1) the correction for reflection point motion (INDEXQ=2) produces a minor improvement in cases of small or moderate wind shear and smooth ionization profiles, but is not very helpful otherwise;

(2) the good-quality data (INDEXQ=3) show 30 -40% reduction of scatter in log D at any height, relative to the INDEXQ=1 data, but only at the expense of a 60% reduction in numbers of echoes, occurring mainly at the extremes of the height range;

(3) the non-resonant echoes (INDEXQ=4) show interesting similarity in

distribution to those having INDEXQ=3, but less reduction in scatter and a possibility of bias in D at the lower heights; and
(4) altitude limits for statistical significance of one month's data in a 1 Km. height interval are approximately 84 and 105 Km. (for INDEXQ=1). The range is slightly extended by analyzing several months at once, or narrowed if the data are subdivided according to hour of observation.

As a result of the above considerations, the following discussion of diurnal and seasonal effects is confined to the original data, viz. the class INDEXQ=1.

9.4 Diurnal variation of the diffusion coefficient

Because of the controversy in the literature over the diffusion scale height and its estimation from radio-echo decay data, this variable has been given priority in the present investigation. A full analysis of the dependence of the diffusion coefficient itself on time and height will not be considered here, but a few brief comments are in order.

Figure 9.7 is similar in form to Fig's. 9.4 and 9.5, but shows the diurnal variation of $\log_{10}(4D)$, instead of the total set of data for all 24 hours. The data in the parent scattergrams are for May-Dec. 1961.

There is not very much apparent diurnal variation in the widths of the cross-sections in each height interval. The left-hand (small D) sides of all cross-sections are largely independent of time, and, indeed, of height also, as regards extent and shape. There are, perhaps, slightly fewer small values of D in the hours 2000-2400 than at other times, in the height intervals centred on 90 and 95 Km. Such variation as is present amounts mainly, however, to a contraction of the right-hand (large D) sides of the cross-sections between 1200 and 2400, and particularly from 1600 to 2000. Thus the distributions of log D are wider in morning than evening at all heights.

The diurnal variation of the mean of log D at each height is similar to that found by Greenhow and Hall for recording periods in Jan.-Feb. 1958 and Jan.-Feb. 1959 (Fig. 5.4), and also to that found by Weiss for June and Dec. 1953 (Fig. 5.3). Weiss found a larger variation for Dec. 1953 (~ 0.35 peak-to-peak in $\log_{10}D$) than Greenhow and Hall found in either year for Jan.-Feb. (~ 0.15 in both years). However, the

variation found by Weiss for June 1953 was smaller still (~0.10). The form of the variation in all sets of observations shows a morning peak, with an afternoon and evening minimum which is slightly broader than the peak. In the present results the peak-to-peak amplitudes of the variation are approximately 0.15 (98-102 Km.), 0.23 (93-97 Km.), and 0.35 (88-92 Km.). Between 83 and 87 Km. there are too few data points for the means to be representative of the distributions. In the 88-92 Km. range, not only is the variation strongest, but the maximum occurs some four hours earlier than at the upper levels.

It is planned to make a detailed month-by-month analysis of the 1961 data, fitting polynomials in height with sinusoidally time-dependent coefficients to the values of log D, after the fashion of the analysis due to Groves which is at present in use here for wind studies. A later section of this chapter describes a simpler multi-variable fitting analysis already carried out.

9.5 The height profiles

We have already seen how a computer programme enabled profiles of log D and of D' to be plotted against height. One profile corresponded to each scatter diagram, and was derived from it by plotting a point at the mean of any data in each 1 Km. height interval. Fig's 9.8 to 9.10 contain several examples of these profiles, and here their non-time-dependent features are discussed.

Firstly a note on the accuracy of each plotted point is in order. In the full results the scattergram corresponding to each profile indicated the reliability of each point. To conserve space the scattergrams are not reproduced, but it has been verified, with their aid, that each of the following comments is substantiated by data from several meteors. Most of the profiles are for INDEXQ = 1; consequently a few data points with large height errors are retained, leading to profile points below the true lower height limit of about 75 Km. Such profile points should be disregarded.

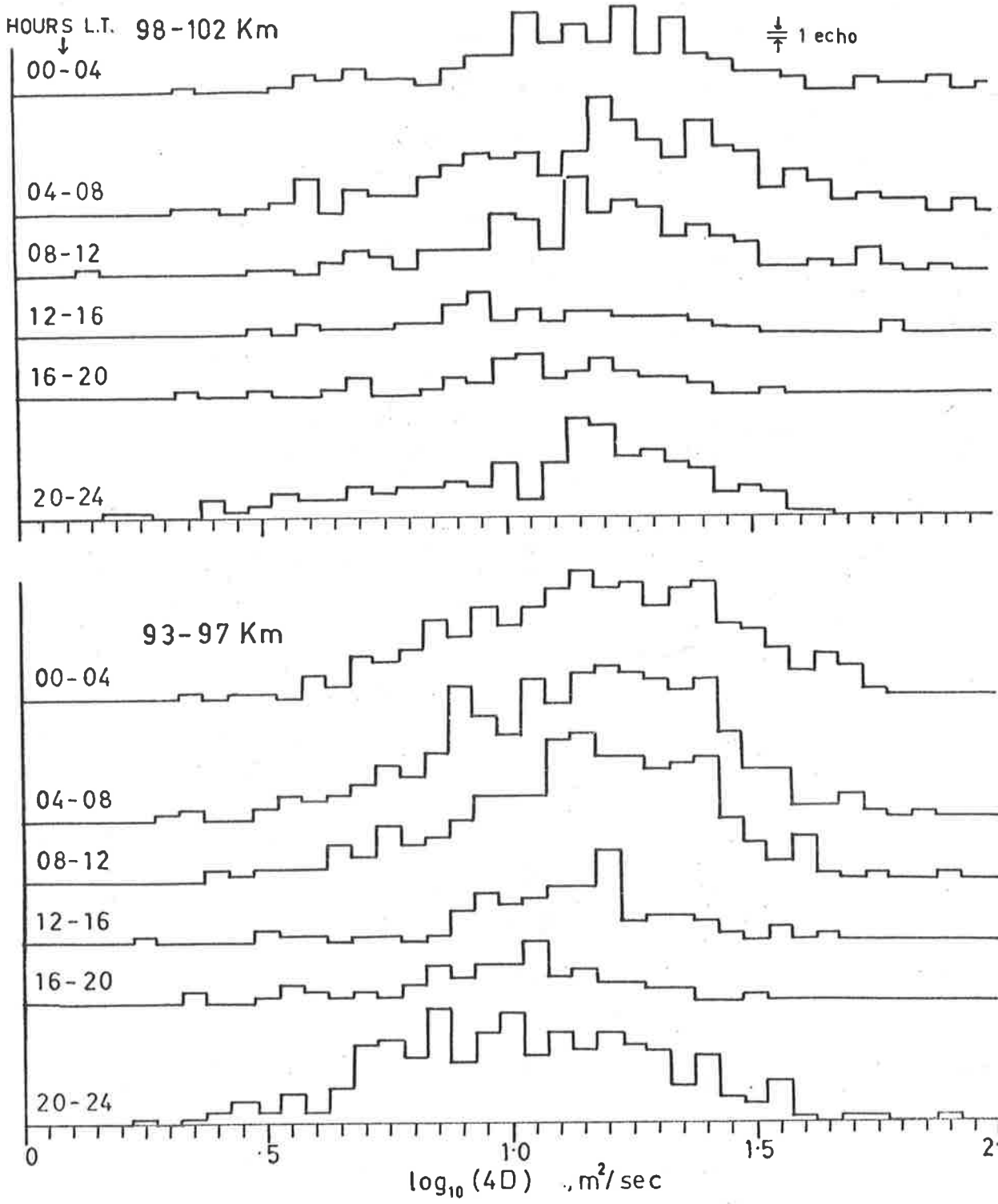

Figure 9.7. Diurnal variation of diffusion coefficient in 5 Km. height intervals, for quality class 1. (Continued overleaf).

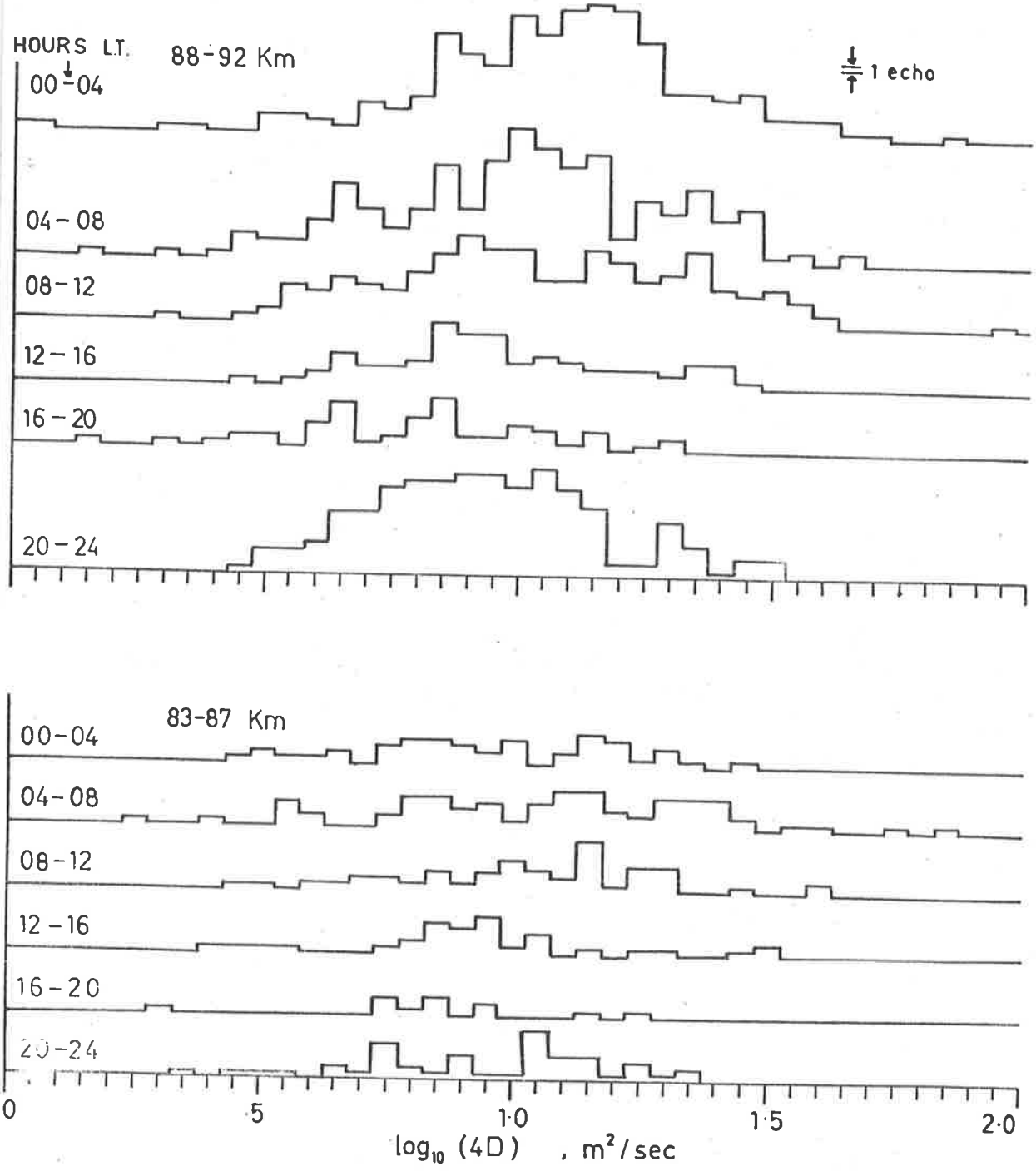

Figure 9.7. (continued). Diurnal variation of diffusion coefficient in 5 Km. height intervals, for quality index 1.

The profiles of all values of $\log_{10}$ (4D) for two periods of several months have been presented in Fig 9.6. The corresponding profiles for each month of the survey are in Fig. 9.8. The quality of all echo data is believed to have been poorest for Dec. 1960 and to have improved until April, when most equipment faults had been cured at St. Kilda. However, the two profiles for April may not be reliable because these two recording periods were very short. Also, few suitable echoes were recorded in the periods 7-15 Dec. 1960 and 11-15 July 1961. The diffusion coefficient profiles show an improvement in smoothness in May, due to the inclusion of Salisbury data from then onwards.

In almost every profile, deviations from smoothness are smallest between 90 and 100 Km., and over this range there is in every case except November an overall increase of log D with height. Usually the increase is of order 0.3 (a factor of 2 in D) or less. It follows that the diffusion scale height measured on a 24-hour basis over the 90-100 Km. height range must exceed 12 Km. This conclusion is only meaningful if the profile slope does not change appreciably with time of day; in fact we shall see that such changes do occur.

At all heights the majority of the profiles show more or less cyclic deviations from a straight line or smooth curve of large radius. The exceptions are those listed above as resulting from scattergrams with too few points. Otherwise the appearance of confused scatter in the profiles, which one would expect if the original scattergrams contained only random deviations from a smooth dependence of log D on height, is conspicuously absent. Between 90 and 100 Km., the profiles generally exhibit from 1 to $1\frac{1}{2}$ cycles of this oscillation, with peak-to-peak amplitude of order 0.2 in $\log_{10}$D, superimposed on the overall increase with height mentioned earlier. Above 100 Km. the original data points are fewer, resulting in increased uncertainty in the profile shape, but it is interesting that two features, a maximum point of the oscillations of log D at 102 or 103 Km. and an adjacent minimum point at 105 or 106 Km., are common to nearly all profiles.

For reasons given earlier, the author is doubtful whether the available data for heights below 85 Km. (perhaps even 90 Km.) are representative of the true diffusion coefficients. In any case the profiles in

Fig. 9.8 generally become confused below 90 Km. However such is not the case in profiles representing each 4 hours of the day separately. In Fig. 9.9a, 4-hourly profiles integrated over the May-Dec. period are shown. INDEXQ 1 data are used. These profiles are well-behaved down to 85 and, excepting the period 1600-1959 hours when echoes were scarce, to 80 Km. The striking changes from positive to negative slope just above 80 Km. in the profiles for the hours 0800-1159 and 2000-2359 will be noted.

Fig. 9.9b, which contains profiles for INDEXQ 3, can be directly compared with Fig. 9.9a. From this comparison, the lowest cycle of oscillation in the 0800-1159 and 2000-2359 profiles seems to be defined by data from echoes of the transitional kind, since it is absent in Fig. 9.9b. The second lowest cycle remains practically unaltered in both profiles, however. The slight relative displacement, discussed previously, of the 80-85 Km. sections of the profiles in the two quality classes is still evident, but the negative gradients near the lower end of the basic (INDEXQ=1) profiles are a more prominent feature. Clearly these negative-gradient sections do not represent the true mean diffusion coefficient, since from Equation 2.7.8 they would mean that the ratio T^2/p decreased with height.

In regard, then, to the implied possibility that Adelaide results tend to favour large diffusion coefficients at low altitudes, we proceed to examine the values given by Murray for Sep. 1953. Fig. 9.10 contains profiles of $\log_{10}D$, found by hand calculation from the scattergrams of Murray and of Greenhow and Hall which were reproduced in Fig. 5.2. There is no negative gradient of log D with height near 80 Km. in Murray's results, which agree very well with the Sep. 1961 profile of Fig. 9.8. Hence it cannot be determined to what extent, if any, his scale height figures were influenced by large values of D in the 80 Km. region, but such influence cannot have been very strong. It remains a possibility, however, in connection with the other months treated by Murray, in each of which the scale height exceeded that found for September 1953.

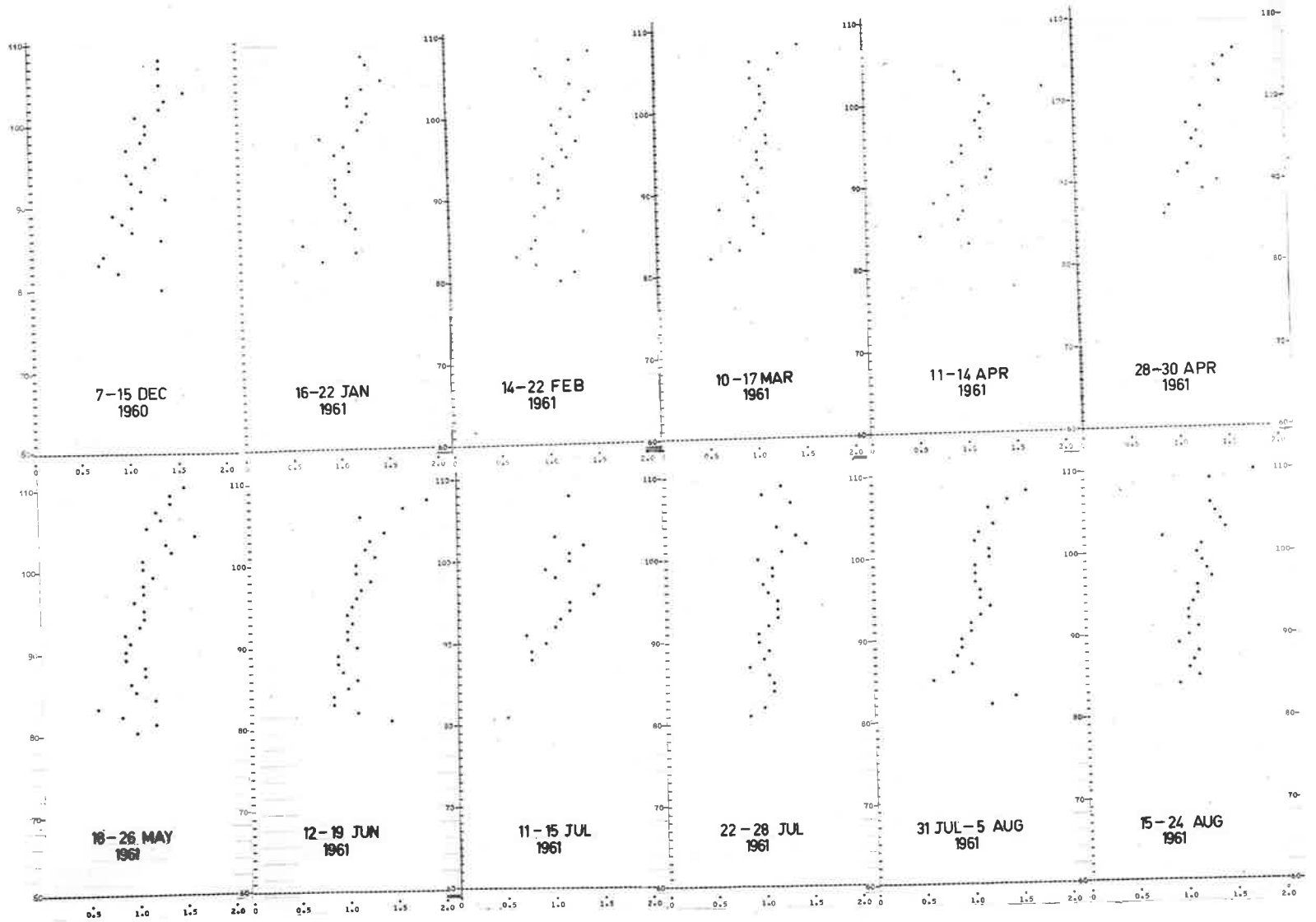

Figure 9.8. . Profiles of log D for all hours combined, in each recording period.

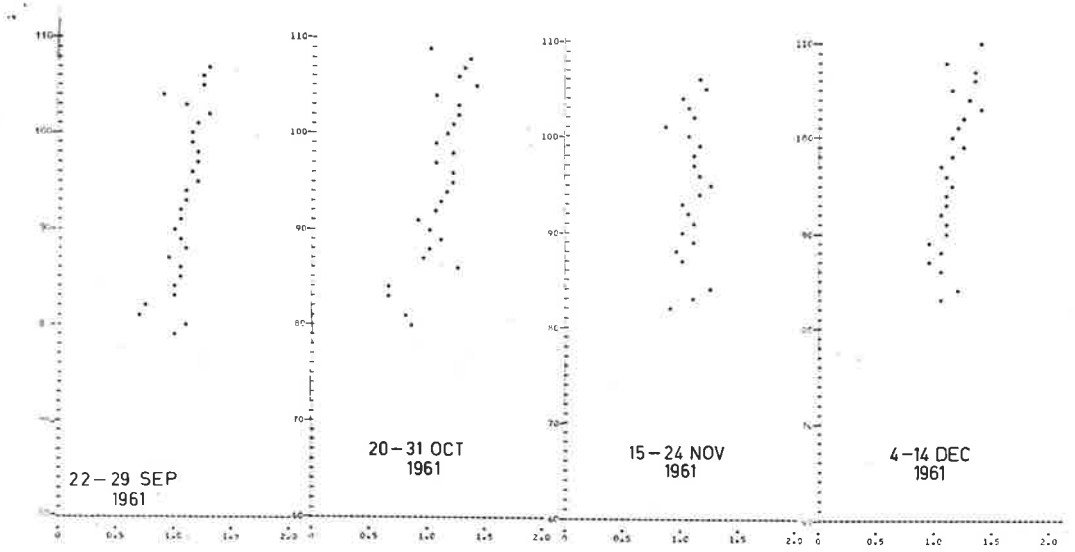

Figure 9.8 continued.

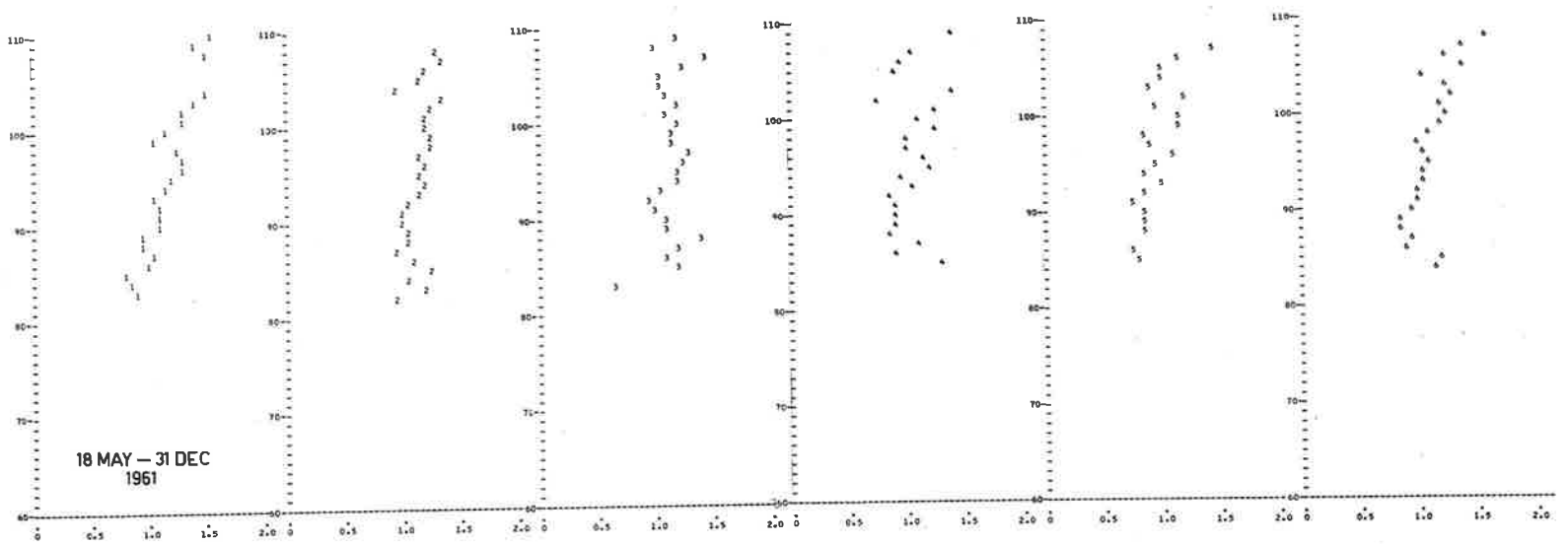

Figure 9.9b. 4-hourly profiles of log D as in lower half of Fig. 9.9a, but INDEXQ = 3.

It is also clear that either poor quality or transitional echo waveforms are responsible for distorting the INDEXQ 1 results below 80 Km., since the incorrect sections of the profiles vanish when such echoes are extracted (INDEXQ=3; Fig.9.9b). We recall from Chapter 8 that in certain transitional echoes the rapid collapse of echo amplitude as the critical density contour vanished was mistaken for the subsequent slower exponential decay. The tendency towards this error was greatest with the slowest exponential decays, viz. those at 75-85 Km., and it is believed to explain the incorrect profile slopes near 80 Km. Since the offending points can be removed by taking INDEXQ 3 data instead of INDEXQ 1, the error is not serious.

Note the important fact that the profile given in Fig. 9.10 for the results of Greenhow and Hall is very similar to Murray's (same figure) over the 90-100 Km. region, but has far fewer points in the doubtful range of heights near 80 Km. Thus the two sets of data differ, not at great heights because of the need for at least one Doppler cycle as Greenhow and Hall claimed, but at the bottom of the height range, in some way connected with transitional echoes.

Those 4-hourly profiles which extend to 110 Km. show interesting progression from large positive to small negative height gradients of log D over the highest 5-6 Km. In Fig. 9.9a (Jan.-Apr. and May-Dec.) the progression is similar for both parts of the year, and appears to follow a 24-hour cycle. Where sufficient data points at these heights are available in the 4-hourly profiles for individual recording periods (not shown), there is a generally similar time variation of the profile slope.

So far the profiles of D', the height gradient of log D measured on individual trails, have not been alluded to. These are not reproduced, since in general they give little information that is not already obvious in the log D vs. h profiles. The extremely large deviations of individual D' values in the parent scattergrams from the mean at any height will already be clear from Fig. 9.5. To show the orders of magnitude involved, a typical mean value of D' taken over all heights is approximately 0.05 Km^{-1}. (i.e. $H_D \simeq 8.6$ Km.). Typically the standard deviation of the data about this mean is $\pm$ 0.3.

A majority of the D' profiles exhibit a slight tendency for D' to increase with height. This tendency is particularly marked at heights of over 100 Km. When the D' profiles are numerically integrated with respect to height, yielding alternative height profiles of logD (e.g. Fig. 9.12), the change in slope of the latter profiles at 105 $\pm$ 5 Km. is often quite striking. Too few readable echoes occurred above 100 Km. to permit detailed study of this feature, but the presence of the turbopause in the same height interval should not be ignored as a possible cause.

9.6 Diurnal and seasonal variation of the diffusion scale height

Questions have been raised in the preceding section as to the accuracy of relating a measured decay time-constant to the diffusion coefficient. Nevertheless, any diurnal or seasonal changes in the former almost certainly result, at least in part, from corresponding changes in the atmosphere, and therefore merit study.

It is easiest to begin by examining the two estimates of the diffusion scale height as functions of time. These estimates we shall call H_{D1} and H_{D2}; the first has been found according to App. 3.7, as the slope of an assumed linear functional relation between $\log_{10}D$ and height, taking due account of the difference between ln D (in the formula) and $\log_{10}D$ (in the scattergrams). H_{D2} is simply the mean value of D' (defined as $\frac{d}{dh}(\log_{10}D)$) from each scattergram of this quantity, again with the appropriate conversion factor.

In Appendix 7 the values of H_{D1} and H_{D2} for each recording period and also for the combined intervals Jan.-Apr. and May-Dec. 1961 are listed, together with certain associated quantities. The uncertainty δh in height determination, required in finding H_{D1}, has been taken as 3.0 Km. From earlier discussion this can be seen to be reasonable for INDEXQ = 1, 2 and 4, and a trifle pessimistic for INDEXQ = 3.

In Fig's 9.11 to 9.14 some values of H_{D1} and H_{D2} from Appendix 7 are plotted. Error bars are drawn for H_{D1} but not for H_{D2}, since errors in the latter are not normally distributed. The graphs are for quality index 1 only. Large differences among the INDEXQ classes arise only where H_D is itself large, due to a low correlation coefficient (implying low significance) or a small number of points in the original scattergram.

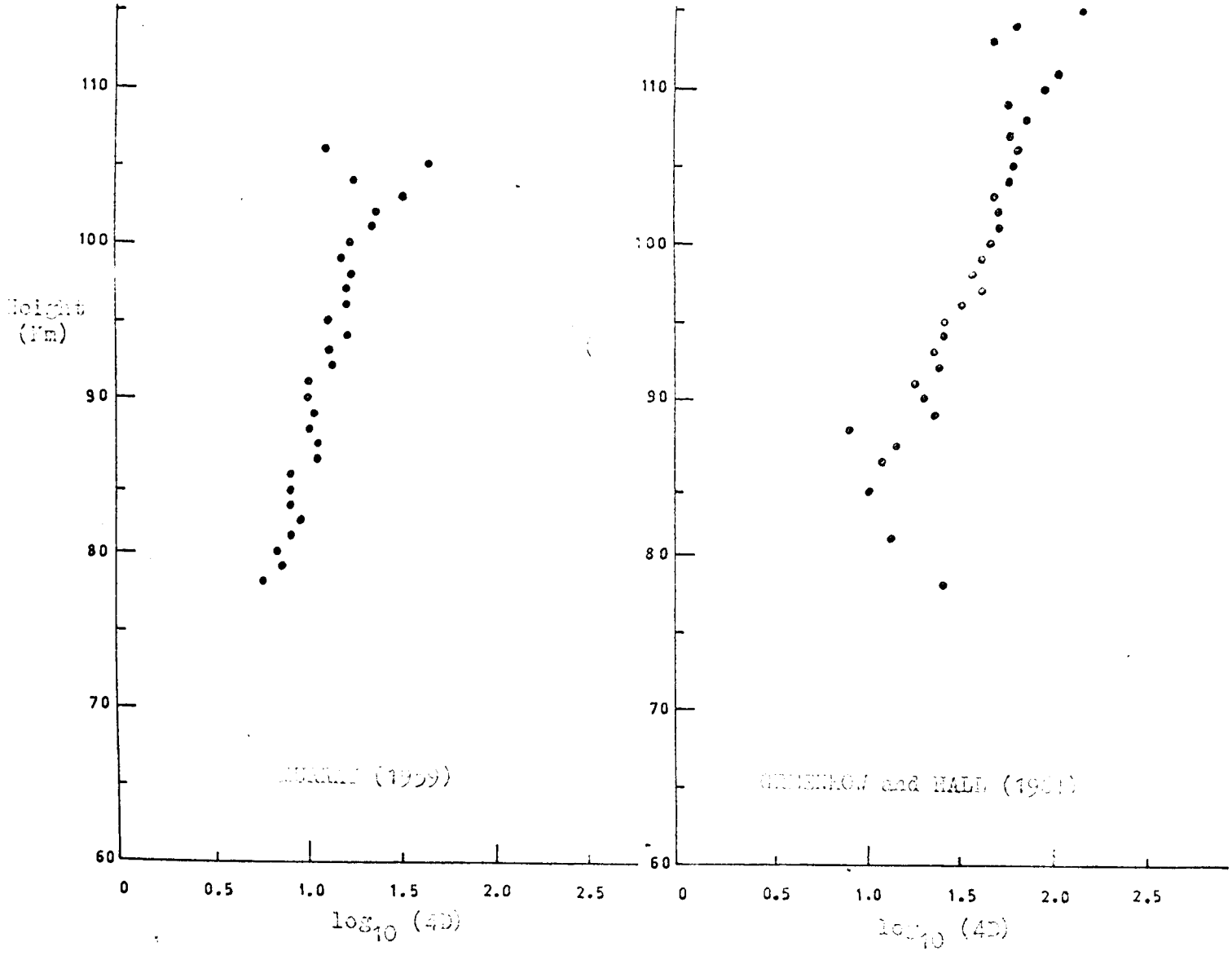

Figure 9.10. Profile ; D from Fig. 9.2 .

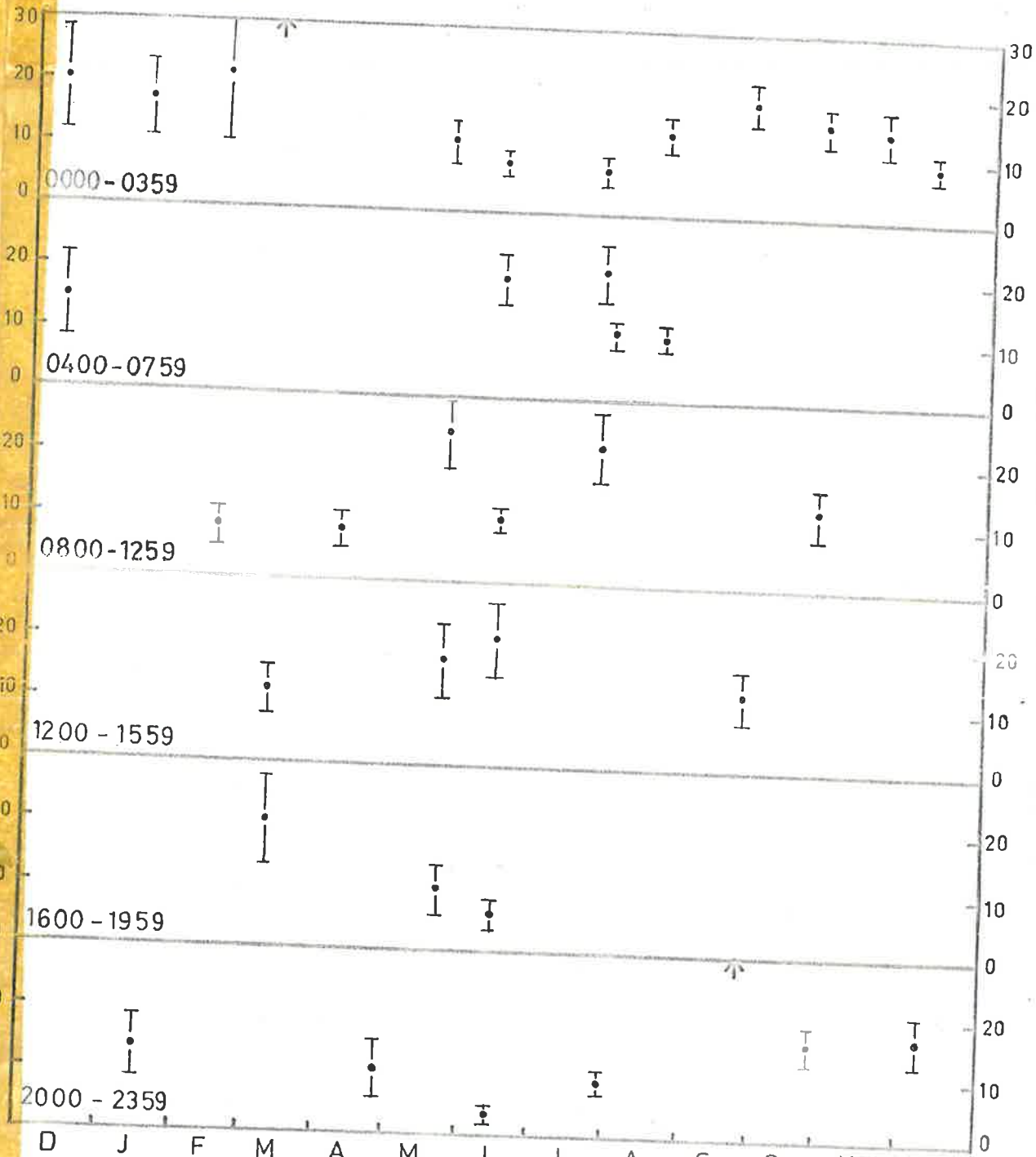

Figure 9.11. Seasonal variation of diffusion scale height H_{eq} in each four hour interval, for 1960-61.

Missing points in the graphs are points of poor significance which were automatically removed from Appendix 7 by the computer programme which printed the table.

Consider the seasonal variation of H_{D1}, as found for the 4-hourly intervals (Fig. 9.11), and likewise H_{D2} (Fig. 9.12). Detailed agreement is not found between H_{D1} and H_{D2}. A more surprising aspect is that apparent seasonal trends in one quality are not reproduced in the other. Thus, for example, H_{D1} for the hours 0000-1359 appears to have a semi-annual variation with maxima at the equinoxes (although the Dec. 1960 and Dec. 1961 points disagree). In contrast, there is a minimum of H_{D2} for the same hours at the spring equinox. In the other 4-hour intervals missing points cause trouble in attempting to discern annual or semi-annual trends in the variation, but the disagreement does not seem as violent. The lack of data is most serious in the afternoon hours, when the detection rate is lowest.

The reduction in accuracy in H_{D1} (and H_{D2}) prior to May 1961, due to the availability of only three instead of four reflection points per trail, is clear from the error bars in Figure 9.11. The disagreement of the two years' values of H_{D1} for hours 0000-0359 in December may be associated with this reduced accuracy in the earlier results. If not, then perhaps the variation of H_{D1} for these hours should be tentatively described as annual (minimum in winter), rather than semi-annual.

Because the detection rate is always a maximum over the hours 0200-1000 approximately, the seasonal variation of H_{D1} determined for the whole 24 hours (Fig. 9.13) resembles that found for the morning 4-hour intervals, in particular 0000-0359 hours. The July minimum is again noticeable, but if a minimum occurs in December it is a subsidiary one only. That is, a smooth curve through the 24-hour H_{D1} results would be a combination of annual and semi-annual trends, both having minima in winter. No such variation is evident in the corresponding H_{D2} values, also plotted in Fig. 9.13, and in fact these values are remarkably constant, with three exceptions. Hence it would seem that either the H_{D2} variations for 4-hour intervals arise only from random errors incurred in taking mean values of D', whose effect is largely removed in the larger samples for

all 24 hours, or two different mechanisms control H_{D1} and H_{D2} on a seasonal time-scale. The first possibility is not favoured because random errors as envisaged would lead to approximately equal numbers of positive and negative H_{D2} estimates, whereas negative values are no more numerous for H_{D2} than for H_{D1}; in fact the two usually take negative values together.

Two possible explanations of the difference between H_{D1} and H_{D2} are as follows; no detailed check has been possible. Firstly, Roper, whose work (1962) on turbulence, using the same meteors as the present investigation, has already been mentioned, has shown that the rate of turbulent dissipation per unit mass varies semi-annually, with minima of order .018 watt/Kg. in winter and summer, and maxima of order .04 watt/Kg. at the equinoxes. This is similar to the seasonal variation in H_{D1}. The small features of the profiles of log D are also reminiscent of the stratification of winds and wind shear (hence of turbulent dissipation rate) reported by various workers (v. Ch.2). However, turbulence should involve a longer minimum time scale above about 80 Km. than is involved in echo decays. Secondly, the randomizing influence of small-scale irregular ionization (Rice and Forsyth 1963, 1964) may be involved; no seasonal variation is likely here. The difference in selection of data for the log D and D' plots is such that log D information is more likely to include data from trails along which the effects of turbulence, or other perturbing influences, vary rapidly with height. There are, of course, at least three recorded echoes for every trail used. The existence of a value of D' guarantees that both echoes from which it is derived are of either underdense or transitional type, and of sufficient quality for an attempted estimate of the decay time-constants. This guarantee does not necessarily hold for pairs of echoes of which one echo contributes to the log D plots. Where it does not hold, either the reflection points are less than 400 m. apart (the smallest spacing used in calculating D'), or the reflection point that yields a log D value must be adjacent to reflection points which are overdense or from which the echoes are badly disturbed. In all three cases the log D value actually obtained is suspect: in the first case, at small spacings, reflection point motion due to turbulent wind shear is the reason. It is

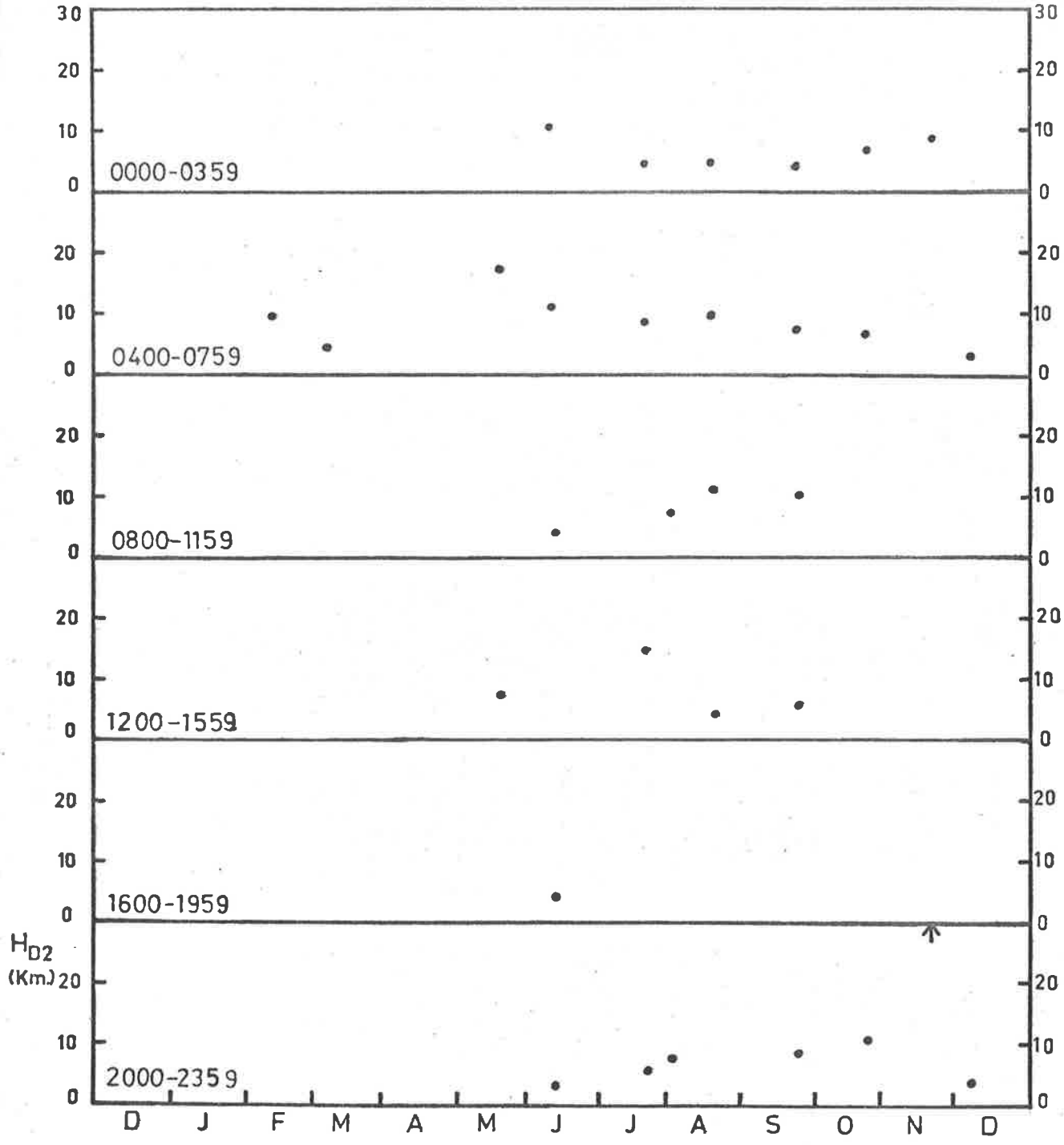

Figure 9.12. Seasonal variation of diffusion scale height H_{D2} in each four hour interval, for 1960-61.

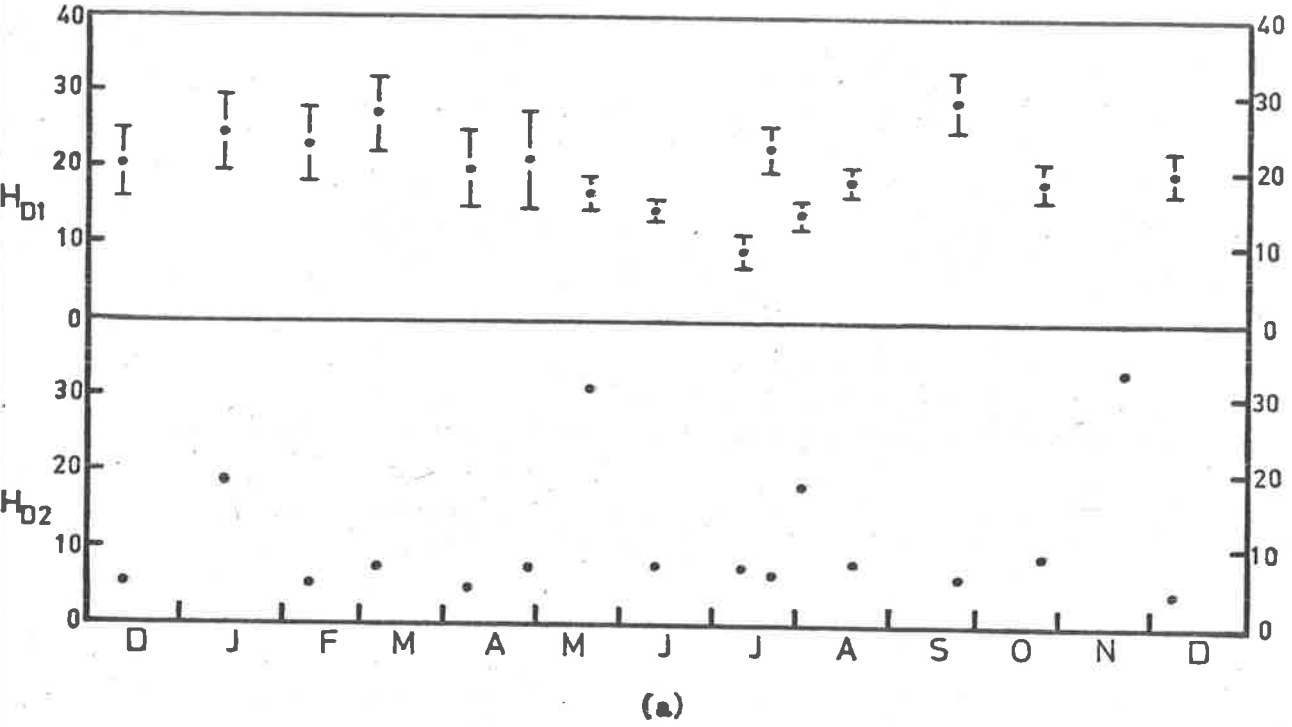

(a)

Figure 9.13 Seasonal variation during 1960-61 of the diffusion scale heights H_{D1} and H_{D2} as determined over all 24 hours.

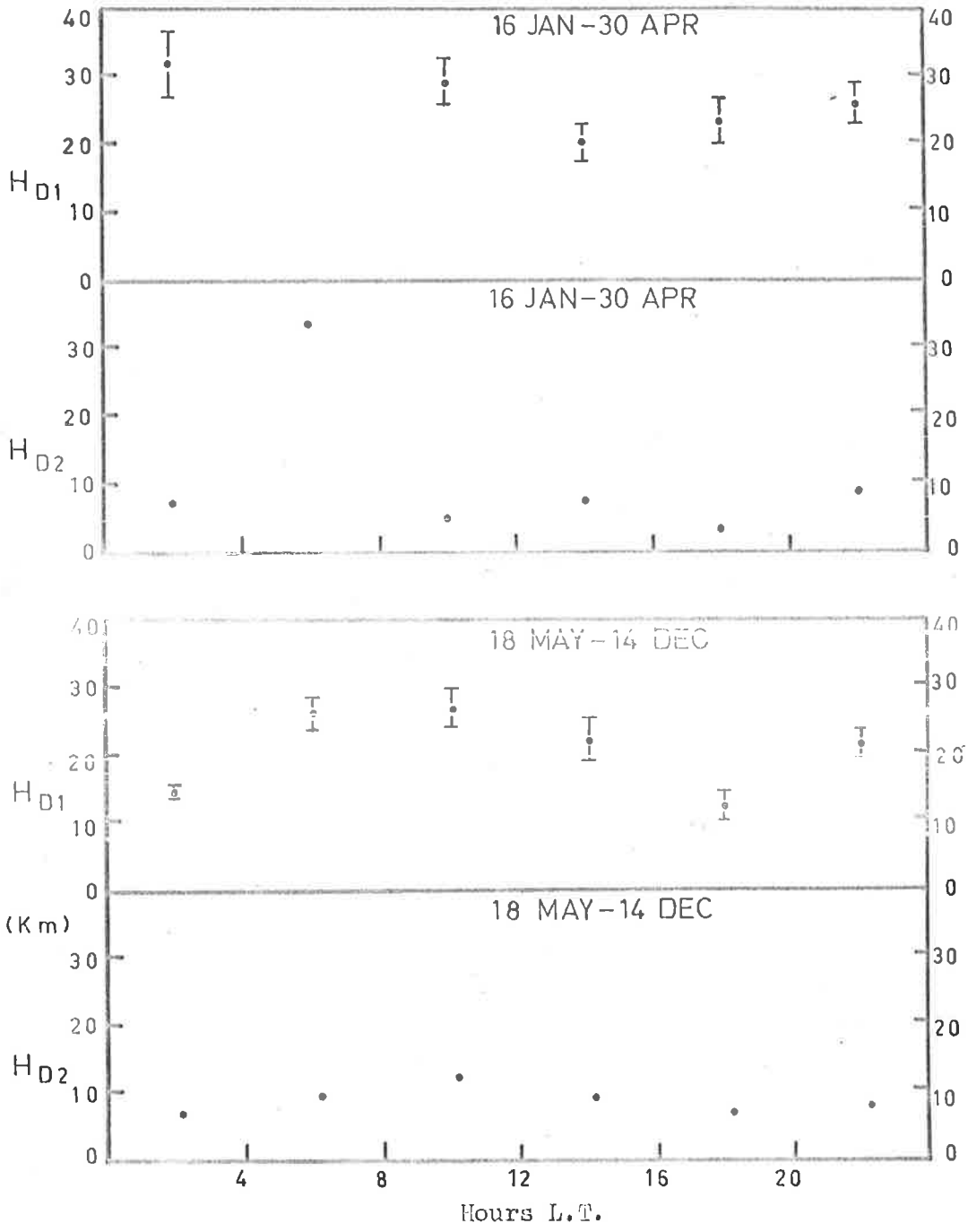

Figure 9.14 . Diurnal variation of the diffusion scale heights H_{D1} and H_{D2} for two low periods in 1961.

just such suspect values which contribute to H_{D1} but not to H_{D2}. Hence any small-scale phenomenon capable of randomizing log D values on an individual trail is more likely to affect H_{D1} than H_{D2}. Such an effect may appear as the anomalously large values found for H_{D1}, or (on the turbulence theory) as a distortion of the true seasonal variation of H_D.

Turning to diurnal variation of H_D, we find the 4-hourly values of H_{D1} and H_{D2} plotted against time of day in Fig. 9.14, which shows both these scale height estimates for the long periods Jan.-Apr. and May-Dec. 1961. In both periods, the two estimates exhibit the same diurnal behaviour: H_D is a maximum (i.e. log D changes least rapidly with height) near sunrise, and has its minimum value near sunset. The consistent excess of H_{D1} over H_{D2} is still present. While H_{D2} values are generally of the order of the pressure scale height (6-10 Km.), H_{D1} is usually between 10 and 30 Km. Such diurnal variation of H_{D1} and H_{D2} as can be measured from the data for individual months shows no significant departures from the trend to maximum H_D in the morning and minimum in the evening.

It is particularly interesting to compare this behaviour of the diffusion scale height with that shown in Fig. 5.5 . There the 1961 results of Greenhow and Hall show a maximum of H_D (found in the same way as our H_{D1}) near midnight, and perhaps a second maximum about 0900, but their 1960(c) figures, found by a different analysis of the same data, show instead a minimum at 0700 hours local time and a maximum at 1900. Thus there is vague similarity between the present results and those in their 1961 paper, but none at all with the findings of their 1960(c) paper. The author doubts that the quality of the present diffusion coefficient data justifies an analysis in terms of atmospheric pressure, density and temperature, and suggests that the analysis along these lines carried out by Greenhow and Hall (1961) should be treated with similar reserve.

9.7 Multiple regression analysis applied to diffusion coefficient results

As a preliminary step towards analyzing diffusion coefficient results without the handicap of a quantized time variable, the multiple regression programme described earlier has been used. The results are

empirical in nature. Because a pair of variables may show association due to experimental limitations or chance, caution is needed in deducing the existence of a causal relationship between them.

The values of log D for each of the four receiving stations were analyzed separately, and it was pleasing to find no significant differences among the stations, with the exception that the dependence of log D on the magnitude of the wind velocity was much smaller at Salisbury than at the other stations. This latter confirms earlier remarks stating that the triggering delays at St. Kilda, combined with the finite Doppler frequency, set an upper limit to diffusion coefficients measured at stations 1, 2 and 3. Slight differences in time dependence of log D are thought to arise from the geographical layout of the system.

Only quality index 1 was used in the analysis.

Let t be time of occurrence of an echo (in hours), h the reflection point height in Km., P the angle between the incident polarization vector and the trail axis (neglecting possible Faraday rotation), v the meteor velocity in Km/sec. and u the line-of-sight wind speed in m/sec. Let D_i be a diffusion coefficient measured at station i . Then the final relations obtained from the analysis were:-

$$\log_{10}D_1 = \text{constant} + .011h + (.023-.00027h)\cos\frac{2\pi t}{24} + (.78-.0080h)\sin\frac{2\pi t}{24} + .096\cos|P| + .0028v + .0063|u|$$

$$\log_{10}D_2 = \text{constant} + .012h + (.039-.00027h)\cos\frac{2\pi t}{24} + (.52-.0050h)\sin\frac{2\pi t}{24} + .15\cos|P| + .0036v + .0072|u|$$

$$\log_{10}D_3 = \text{constant} + .012h + (-.27+.0031h)\cos\frac{2\pi t}{24} + (.63-.0064h)\sin\frac{2\pi t}{24} + .14\cos|P| + .0036v + .0072|u|$$

$$\log_{10}D_4 = \text{constant} + .0078h + (-.045+.00053h)\cos\frac{2\pi t}{24} + (.50-.0047h)\sin\frac{2\pi t}{24} + .15\cos|P| + .0032v + .0024|u|$$

In each case the multiple error of estimation of log D is only slightly less than the observed r.m.s. deviation of this variable from its mean (e.g. .246 and .277 respectively for station 4).

The points worth noting are (1)the coefficient of h corresponds to a diffusion scale height of order 30 Km.; (2)the regression accounts for only a small part of the observed scatter in log D; (3)log D is a maximum in the morning hours near sunrise; (4)the time-variation terms are quite strongly height dependent; and (5)log D is larger for transverse than axial polarization.

9.8 Diffusion coefficients for the Geminid shower

The known properties of meteors from the Geminid stream make them valuable in the investigation of the diffusion coefficient - height relationship.

Photographic work discussed in Chapter 2 has shown that Geminid meteoroids are unusually robust in structure. Their resistance to fragmentation is high, and on average they form longer, more uniform optical trails than other shower or sporadic meteors. Therefore it is almost certain that their ionization profiles are also unusually smooth.

So far this chapter has shown that the atmospheric or meteor parameters usually associated with the ambipolar diffusion of the trail do not exhibit as strong an influence on the measured diffusion coefficients as theory predicts. A theory of the scatter in D at any height and time has been proposed (the reflection point motion mechanism) and found, in many respects, wanting. Its failure has been tentatively ascribed to a phenomenon suggested by Rice and Forsyth (1964), viz., distortion of the "Cornu spiral" associated with an echo because of small-scale irregularity of the ionization profile.

If the Rice-Forsyth theory is correct, i.e. if such small-scale irregularity of ionization is responsible for either the scatter in D or the departure of D from its theoretical height dependence, then Geminid meteors should exhibit reduced scatter or closer adherence to the theoretical D - h profile. A hint that this prediction may be correct lies in Weiss' finding (1955) that the diffusion scale height H_D was three times smaller for 1952 Geminid meteors than for other meteors observed at the same time.

The author has been fortunate in being able to assemble diffusion coefficient information for Geminid meteors observed at Adelaide in four separate years, as follows.

1952: The original data used by Weiss (1955) were available. The Geminid meteors had been selected using a graphical transformation of the reflection point coordinates developed by Elford (1952) and also published by Weiss (1954).

1953: The data for Dec. 1953 used by Murray (1959) were available. A small percentage of erroneous D values was corrected by re-reading the original film records. A computer programme, combining Elford's coordinate transformation and the rapid plotting technique described in §7-7, was used to select the Geminid meteors.

1960, 1961: The Geminids observed in the present survey had already been identified on the basis of their orbital elements. Unfortunately only 10 to 20 Geminids were found in each year, and half of these produced over-dense trails. For those that were suitable, however, the multi-station system had yielded 2 to 4 values of D per trail.

These sets of data are plotted in the format already used ($\log_{10}(4D)$ vs. height) in Fig's. 9.15 to 9.17 inclusive. Control data are included also, in the form of

(a) sporadic meteor results for Dec. 1952 and June 1953,

(b) Sextanid, ζ-Perseid and Arietid shower meteor results for 1953, and

(c) Sextanid shower meteor results for 1961.

It is clear from these plots that the height gradient of D is larger, and the scatter in D smaller, for all sets of Geminid meteors than for controls (a) to (c), or for any of the log D vs. h plots* discussed earlier.

---

* The difference in mean height of occurrence of Geminid meteors between 1952-53 and 1960-61 has been traced (Nov. 1966) to an error in the calibration of the radar range marker generator during 1960-61. Since the emphasis throughout this work has been on height differences between reflection points rather than absolute heights, only second-order corrections are necessary.

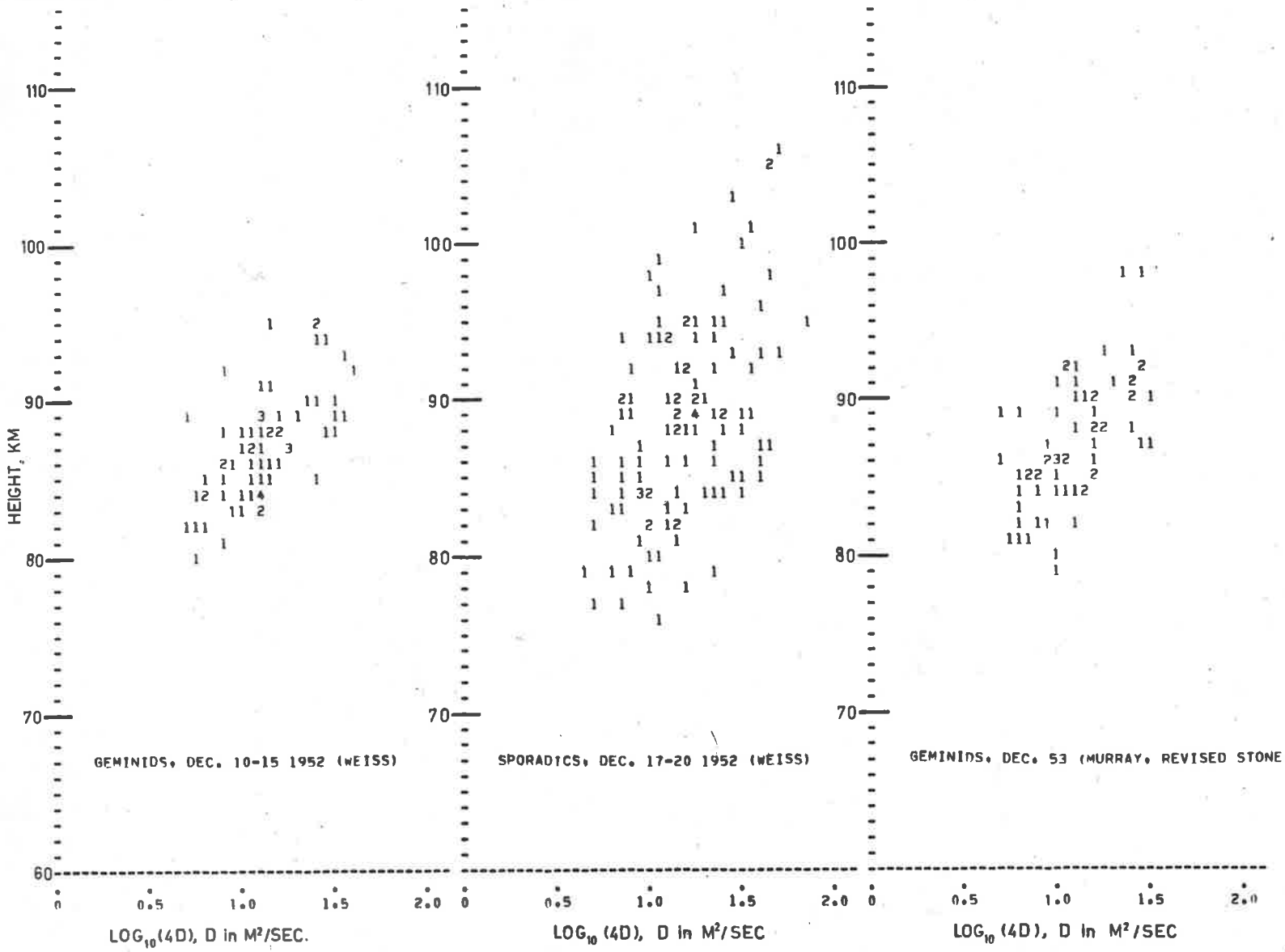

Figure 9.15. Diffusion coefficient versus height for Geminid shower meteors (1952 and 1953), and for sporadic meteors also detected in Dec. 1952.

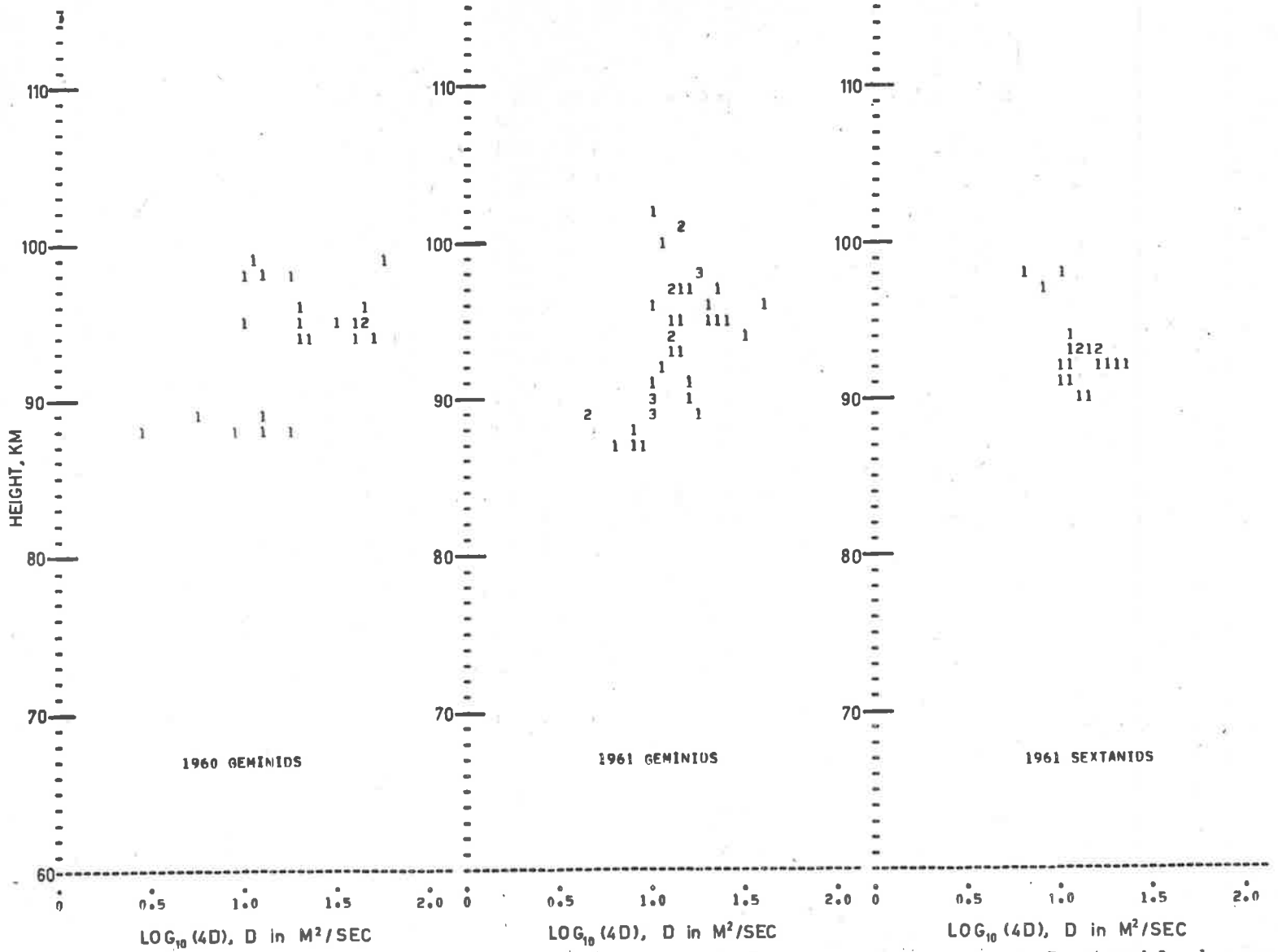

Figure 9.16. Diffusion coefficient versus height for Geminid and Sextanid shower meteors from the 1960-61 survey. (The Geminid and Sextanid streams have similar orbits but differ in meteoroid structure).

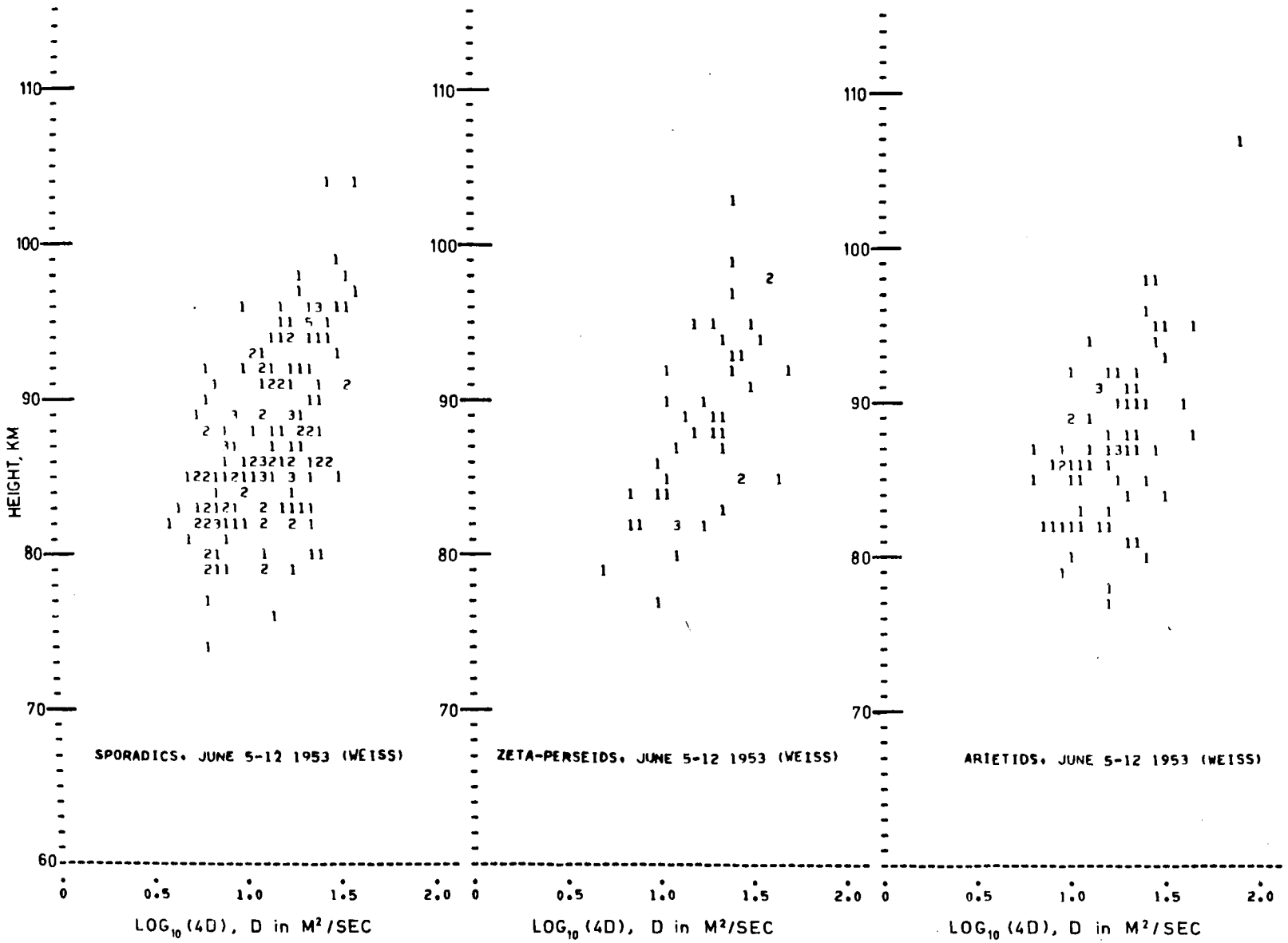

Figure 9.17. Diffusion coefficient versus height for sporadic meteors and meteors of two showers (not Geminids), all from the same period in 1953.

Table 9.1 summarizes the statistical parameters, chiefly H_D, of the scattergrams in Fig's. 9.15 to 9.17. As before, H_D has been found by fitting a linear functional relationship of log D and height to the data. Note that H_D for the Geminids is much closer to the pressure scale height than any other values derived from such scattergrams have been.

It seems highly probable that the unique freedom of Geminid ionization profiles from small-scale irregularities is responsible for this striking improvement of diffusion coefficient measurements. Thus the theory of Rice and Forsyth appears to be the logical starting-point for any future work on the ambipolar diffusion of meteor ionization.

Table 9.1 . Statistics leading to the diffusion scale height H_D, for shower and sporadic meteors.

Sample of meteors	N°. of points	$\overline{\log_{10}(4D)}$	$\bar{h}$ (Km.)	$\sigma_{\log D}$	σ_h (Km.)	Corr. cft. r	H_D (Km.)
Geminids 10-15 Dec 52	70	1.11	87.1	0.22	3.4	0.63	6.9
Sporadics 17-20 Dec 52	119	1.18	88.6	0.23	6.3	0.48	22.6
Geminids Dec 53	69	1.10	87.2	0.21	3.9	0.60	9.8
Geminids Dec 60	23	1.28	93.9	0.33	3.7	0.47	7.3
Geminids Dec 61	42	1.11	93.6	0.19	4.1	0.50	14.7
Sextanids Sep 61	20	1.10	92.9	0.13	2.2	-0.57	-2.5
Sporadics 5-12 June 53	172	1.12	87.4	0.23	5.5	0.56	15.9
ζ-Perseids 5-12 June 53	44	1.25	88.5	0.23	5.9	0.63	17.5
Arietids 5-12 June 53	71	1.21	87.6	0.22	5.2	0.53	19.1

APPENDIX 1

READING AND PROCESSING OF AMPLITUDE-TIME DATA

This appendix sets out the way in which specific extrema of a Doppler waveform are chosen for reading from film or chart records, and the logic used in fitting their coordinates to one of a small set of amplitude-time curves. See also Appendix 3 where the computer programme in which this logic has been mechanized is discussed.

Figure A1.1 shows two hypothetical KIND 1 Doppler waveforms to illustrate some special cases. Consider first Figure A1.1(a), in which the level of the steady output due to the ground wave alone in the absence of an echo is marked GW.

As in the example of 3.4, the skywave initially exceeds the groundwave in amplitude, so that the lower branch of the beat envelope is "reflected" in the zero output line, appearing at A instead of A'. Also overload of the deflection amplifier has occurred at BB' and CC'. Evidently the coordinates of points E,F and G will suffice for determining the time-constant of the exponential decay , but a better determination is possible using D', the reflection of D, as well. The programme determines that the best fit exponential through C'EG is above the level 2(GW) at the time corresponding to D, and accordingly performs the reflection of D to D'. A second reflection is made in the line GW so that D" and F' are located, as shown.

In cases of significant overload it is possible for the person reading the film to detect the condition from the squaring of the waveform. Therefore C is specially coded (as 999) and is represented in the computer by C", at the arbitrarily fixed level 2.5(GW). (This level is chosen as a normally good lower limit for the "true" value C'). A is not read and punched because the person reading is instructed to code only the last-occurring overloaded Doppler maximum; in the programme it is assumed that the skywave is always at least 1.5(GW) prior to C, and therefore H (if punched) is correctly recognized as a minimum. H will then be properly reflected to the other branch of the envelope at H' by the addition of 2(GW).

Since KIND = 1, the computer must be made to determine whether C' and the preceding points are also part of the exponential phase of the

echo. To do this it combines the results of two tests. The first, working from left to right, locates the first point falling significantly below the mean of those before it, provided that the next point is not once more close to or above the mean. The second test, working from right to left, fits exponentials to the last two, three, four, etc. points and at each stage decides whether the point immediately to the left is significantly below the current exponential. If the tests disagree, the result giving the fewer points in the decay phase is chosen, so that no bias toward underestimation of the time constant is introduced. In Figure A1.1(a), C' is the last point before the decay. The echo envelope is henceforth represented by a constant amplitude phase, at a level half-way between the mean and maximum amplitudes of the appropriate points, succeeded by the exponential decay phase already determined. In the "constant-amplitude" phase the actual envelope is frequently not smooth, and the amplitude level representing this part of the waveform has been found empirically to lead to a good approximation to the time when the decay phase begins, as determined by eye for a number of test echoes.

Thus in Figure A1.1(a) points H,C,D,E,F,G and the ground-wave and zero levels are those which would be recorded. Figure A1.1(b) has the same beat envelope but $1\frac{1}{2}$ times the Doppler frequency, and gives more freedom of choice. Points A to H might typically be read for an echo like this. If KIND = 2, usually only two or three points need be punched, since there is little useful information in the amplitude behaviour of a strongly overdense echo.

If KIND = 0^{no}/ attempt is made to fit an initial overdense phase, and less points are necessary. In particular no overloaded maxima need be included except in the extreme case of an echo with large initial amplitude and rapid decay, such that only two turning-points are readable. In fitting an exponential to the amplitude, i.e. in practice a straight line to the logarithm of the amplitude, it is proper to use weights proportional to the squares of the amplitude values. Where an overloaded peak has to be used it is assigned a reduced weight, and the computer records the fact that the echo is probably of poor quality.

(The same indication of poor quality is recorded in a case where the echo data are re-read, and processed a second time, on account of a poor fit to the waveform at the first attempt).

As previously stated, the ground wave at Sheedy's Farm and Direk outstations was not monitored. Now the electron line density at any reflection point can only be estimated by comparison of sky-wave and ground wave amplitudes, assuming an absolute value for the ground wave amplitude and using it as a "secondary standard". Further, the above discussion shows that if the sky-wave exceeds the ground wave in amplitude it is difficult to reduce the echo even to the extent of fitting a decay time-constant unless the ground wave amplitude is known. Fortunately, provided the Doppler period is not too long compared with the echo duration, point X of Figure A1.1(a) can be located by eye at the film-reading stage. X is on the required zero voltage line. It is necessary to measure the ground wave in this way as early as possible, before the long-time-constant gain control system reduces the receiver gain appreciably. If the sky-wave of an echo being read never exceeded the ground wave, the distance from X to the quiescent ground wave level was read from a nearby echo on the turbulence film. The author estimates that X could be located to an accuracy usually better than ± 0.1 GW. The freedom of this approach from major errors is confirmed by results presented in Sections 8.2 and 8.3.

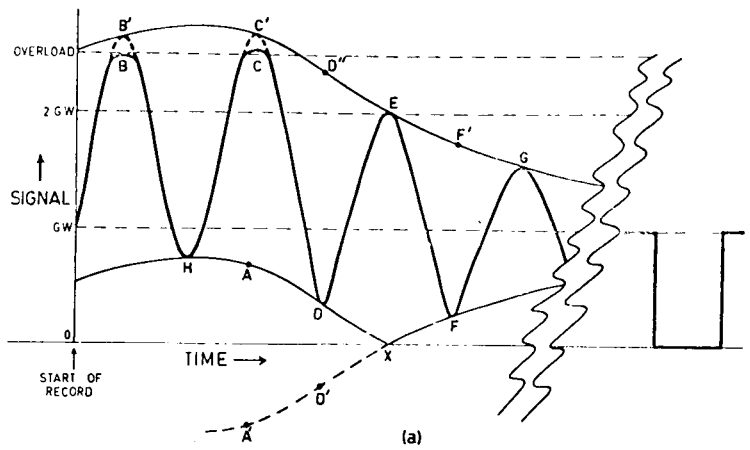

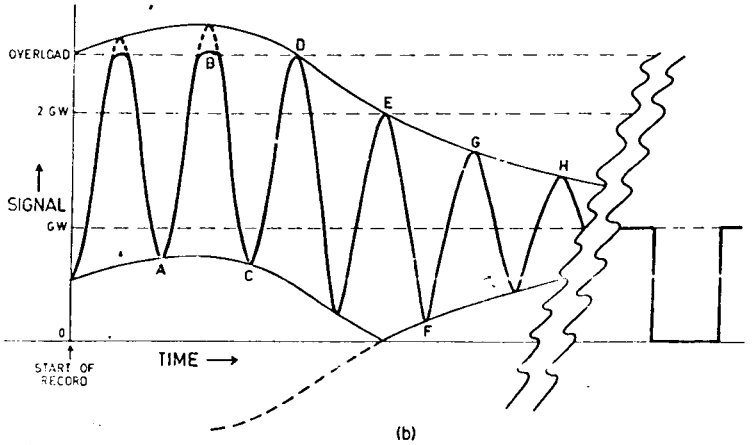

Figure A1.1. (a) Hypothetical KIND 1 Doppler beat waveform to illustrate data reduction (b) Identical waveform but for increased Doppler frequency.

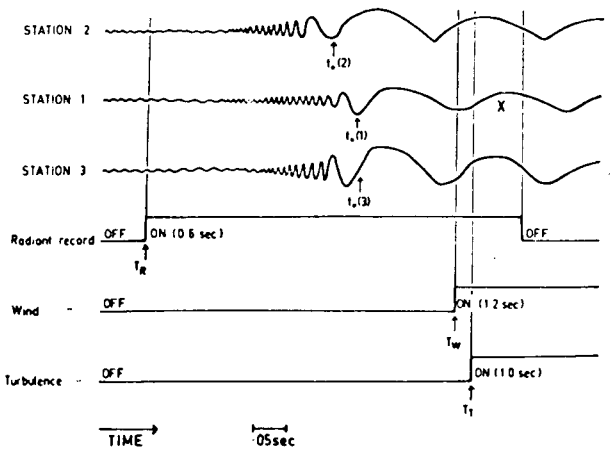

Figure A2.1. Timing diagram for main station recording equipment.

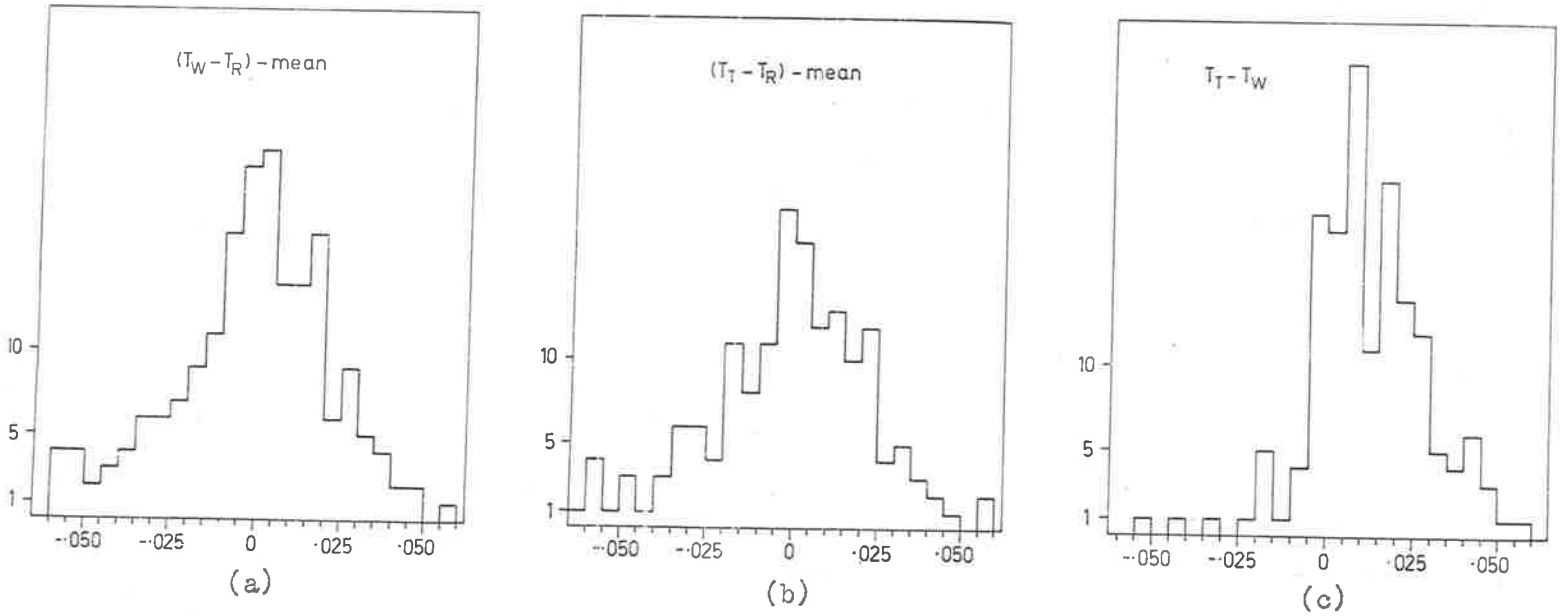

Figure A2.2 (a) and (b): deviations of measured time intervals involved in starting the cameras, from the mean values adopted to represent them. (c): delay between beginnings of wind and turbulence records.

APPENDIX 2

ALLOWANCE FOR DELAY IN STARTING ST. KILDA CAMERAS

In Section 7.2 the need for frequent measurement of the time delay between the instant t_o and the start of the wind (or turbulence) film record was explained. To follow how this information was obtained, consider the sequence of events at the beginning of a recorded echo, as in Figure A2.1. The line for the radiant equipment is displaced in time by an interval equal and opposite to the 1.3 second tape delay. It therefore depicts events at the playback head and display as though they preceded and overlapped the triggering of the wind equipment, i.e. in correct time relationship with the signals being read back from the tape.

The radiant film showed the t_o points and their ensuing Dopplers, although the latter were attenuated and distorted. Sometimes it was possible, using two film readers, to recognize on the radiant film some feature, e.g. a certain phase spike, which was also recognizable at the start of the winds or turbulence record for the same station. The film speeds being known, it was then possible to establish the triggering delay for that meteor and the particular display involved. However, this process could not be applied to every meteor, since finding the necessary records and deciding on a positively identifiable marker (if one existed) often took 5 - 10 minutes. Frequently it was impossible even to say which Doppler cycle on the radiant film was the first recorded on one of the other films.

The following procedure was therefore adopted. The author and a helper, using two adjacent film readers, sought to choose a wind record with a unique feature, approximately once in every 1000 triggers, i.e. on average once per 10 echoes used in the survey. The radiant record of that meteor was found. In Figure A2.1, let X represent such a feature. Then the distances T_WX and T_RX were measured. Later the corresponding measurement T_TX was made, if possible, on the turbulence film for the same meteor.

The values of $(T_W - T_R)$ and $(T_T - T_R)$, in seconds, derived from the above measurements, were plotted against time and date of occurrence. Relative to the signal, these were the delays between the start of the radiant record and the others. For most recording periods it was possible to represent these quantities by a single mean value, but in a few instances there were two or three distinct groups of values in a recording period. The means for both quantities increased more or less stead-

ily from 0.3 to 0.5 second during the year, due to adjustment of the radiant display. Figure A2.2(a) indicates the deviations of all the values of $(T_W - T_R)$ from the adopted mean values, and (b) shows these deviations for $(T_T - T_R)$. From these two histograms, in which the standard deviation is of order .02 second, it can be inferred that the standard deviation of all values of these delay intervals, whether measured or not, was .03 second or less about the adopted mean values. Figure A2.2(c) shows that the extra delay $(T_T - T_W)$ in the start of the turbulence record was $.015 \pm .015$ second approximately.

The output data of the radiant calculations for each echo (Section 7.4) included the positions on the radiant film of all three t_o points relative to one of the simultaneous time marker pulses. Using this information, the t_o point in the echo waveform for station 1 was located on the radiant film for each echo, with much better precision than would have been achieved by inspection alone, and the value of $(t_o(1) - T_R)$ was measured. In subsequent computations this measured interval for each echo, and the current mean value adopted for $(T_W - T_R)$, were combined to fix $t_o(1)$ relative to the start of the wind record, according to the relation

$$t_o(1) \simeq T_W - (T_W - T_R) + (t_o(1) - T_R) .$$

It was then most convenient to find $(T_T - t_o(2))$ and $(T_T - t_o(3))$ by recalculating the intervals between $t_o(1)$, $t_o(2)$ and $t_o(3)$ from the meteor velocity and the reflection point separations.

No statistics were kept of the range of values taken by the individual triggering delays, $(T_W - t_o(1))$ and its counterparts. However, some idea of the gain in accuracy due to the long operation just described is given by the observation that occasional pre-t_o whistles had sufficient amplitude to trigger the equipment up to $\frac{1}{4}$ sec. before $t_o(1)$. In these cases the t_o point appeared on the wind record as much as 0.1 sec. after its commencement, so that assuming constant delay after t_o would in these cases have led to errors up to .25 sec. Using the above method instead for establishing the delay in starting the cameras, there is no reason why these echoes should have been subject to any greater errors than the others. Thus the standard deviation of 0.03 sec. probably applies to all echoes recorded at St. Kilda, and assuming normal distribution only 5% of errors should therefore have exceeded 0.06 sec.

APPENDIX 3

COMPUTER PROGRAMMES

3.1 Echo waveform reduction: programme ENVLO (Figure A3.1)

This programme mechanized the logic of Appendix 1, produced graphical output to show the form and quality of the raw data and of its interpretation, and stored numerical results on magnetic tape. For meteors whose output graphs showed inadequacies in the data or errors in interpretation, manual corrections were able to be made, and added in a later pass of the programme to a copy of the original tape of results.

The fundamental task was to fit an exponential decay to underdense (KIND 0) echoes, a representative constant sky-wave amplitude to overdense (KIND 2) echoes, and both of these with a properly chosen intersection to transitional (KIND 1) echoes.

The flow diagram of Fig. A3.1 shows how the programme was organized. A main programme named ENVLO performed minor duties concerned with magnetic tape handling and printing appropriate instructions to the computer operators, but served chiefly to call a subroutine named GEN approximately once per meteor. For a meteor with echoes from four stations, GEN read data from five punched cards, identified by an index number denoting the particular kind of data contained by the card. Certain other data, not applying to specific meteors, were read in the same way. The first page of the flow diagram shows the kinds of data and corresponding index numbers. In particular card 9 (the first for each meteor) and cards 5 to 8 (usually at the head of each new month's data) supplied the necessary information for locating t_o relative to the beginning of the record for each echo, as explained in Appendix 2. Cards 1 to 4 for each meteor contained the echo amplitude readings.

The second page of the flow diagram shows chiefly the way in which the logic of Appendix 1, for reducing the waveforms, was mechanized in the programme. Note that the magnitude of the line-of-sight wind at station 4 (Salisbury) was also found from the data at this stage.

The correction procedures included

(1) a facility for over-ruling the tests (Appendix 1) defining the starting time of the exponential decay for certain KIND 1 echoes. This was done where the graph indicated that this time had not been properly found,

as occasionally happened. The correct time as estimated by the author was then substituted.

(2) special variables for use as an indicator of overall quality in each of the 4 echoes for a meteor. Uncertainty as to the value of KIND that should have been assigned to an echo, or barely enough data points, or certain conditions detected by the programme itself, all led to an echo's quality being classed as poor.

(3) provision for bypassing all future processing of echoes which were not amenable to correction. To this end, KIND, the variable indicating the type of echo waveform, was set to 3 on the appropriate data card, and the latter was included among the cards containing corrections. Since the other echo waveforms for meteors thus affected might have been satisfactory, the meteors were not deleted from the results. However, no further processing or analysis was performed at any later stage for KIND 3 echoes.

3.2 Graph and scattergram plotting: subroutine PLOT (Figure A3.2)

Points about this subroutine which are not made in Section 7.7 are:-

(a) A complete image of a printed page (132 characters by 60 lines) is stored in computer memory to permit several graphs to be superimposed before printing occurs.

(b) The variable NCHAR (see Figure A3.2) specifies which character is to be used in plotting a graph, or sets certain options if scattergram mode is required instead.

(c) Subsidiary routines ERASER and WRITER are used respectively to clear a block of the page to blanks before plotting, and to cause printing of a completed page image.

(d) The scale factors generated in automatic scaling are constrained to be "simple" numbers $10^n a_i$, where n is an integer, and

$$\{a_i\} = \{1.0,\ 1.5,\ 2.0,\ 2.5,\ 3.0,\ 4.0,\ 5.0,\ 7.5\} \quad ,$$

unless shrinking the plot in one direction by a factor less than 2 will lead to equal spatial (not numerical) scales. If possible, the latter is given priority.

A W.R.E. publication describing this subroutine is available (Stone 1966b).

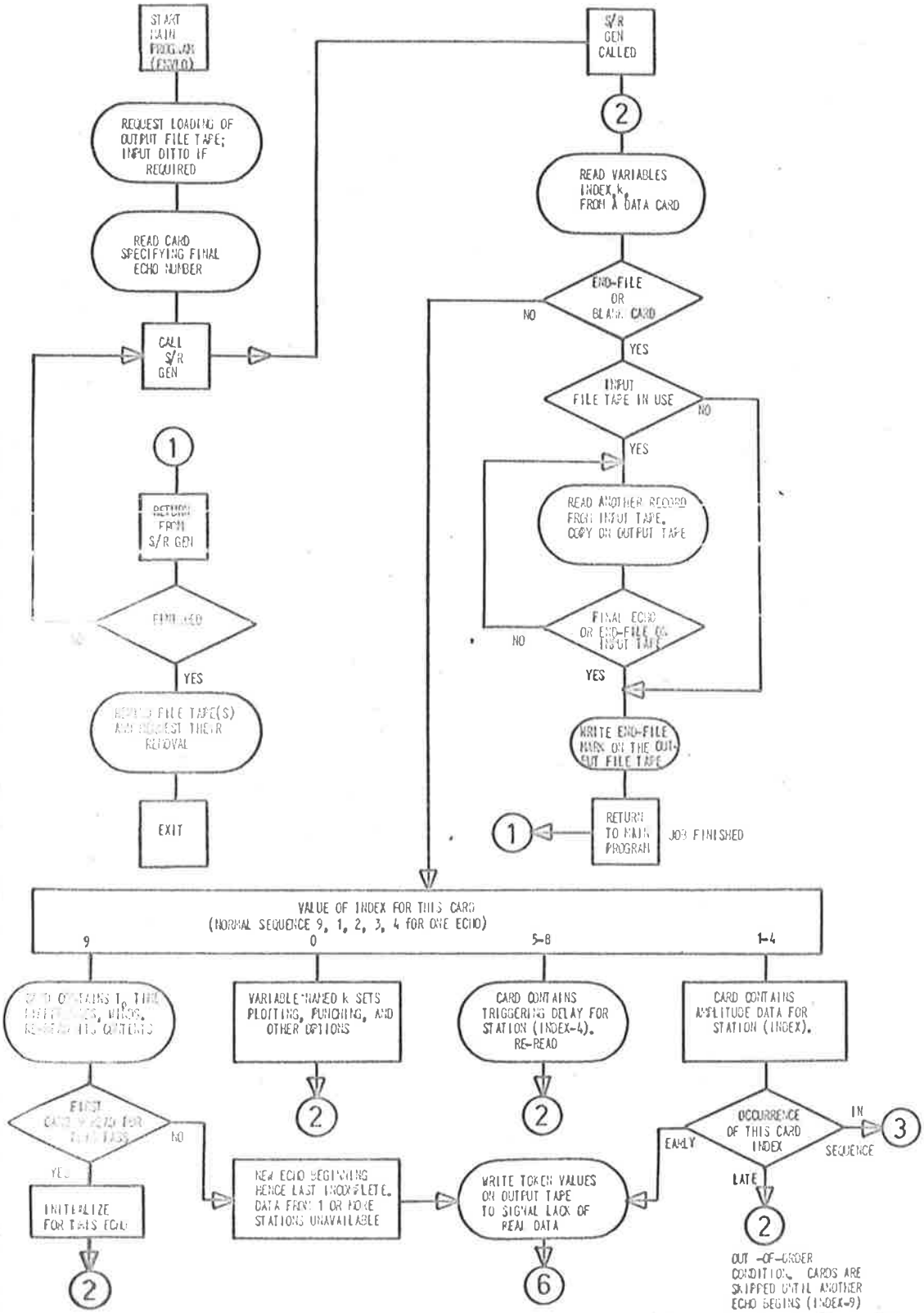

Figure A3.1 Flow diagram of programme ENVLO.

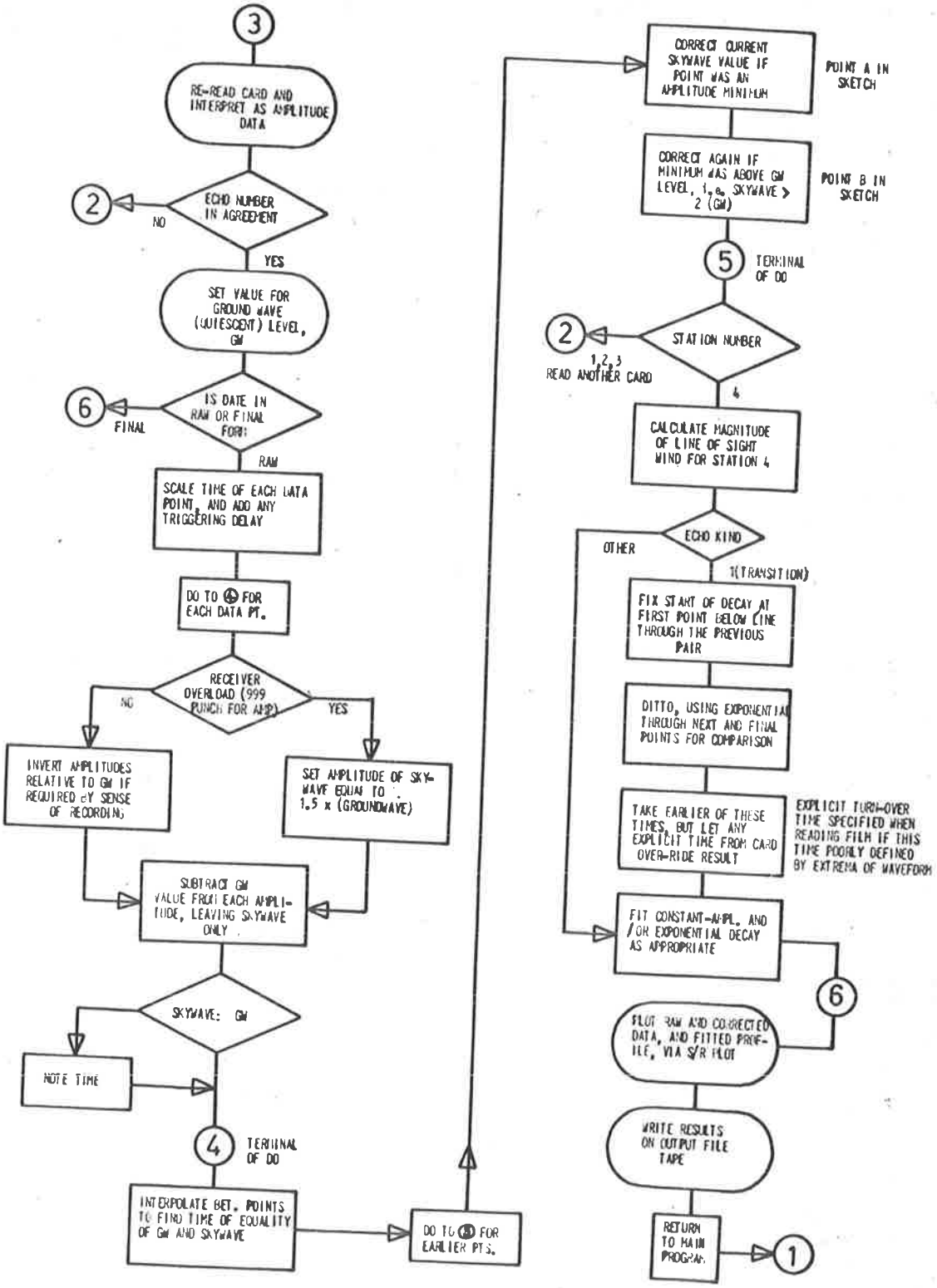

Figure A3.1 (continued).

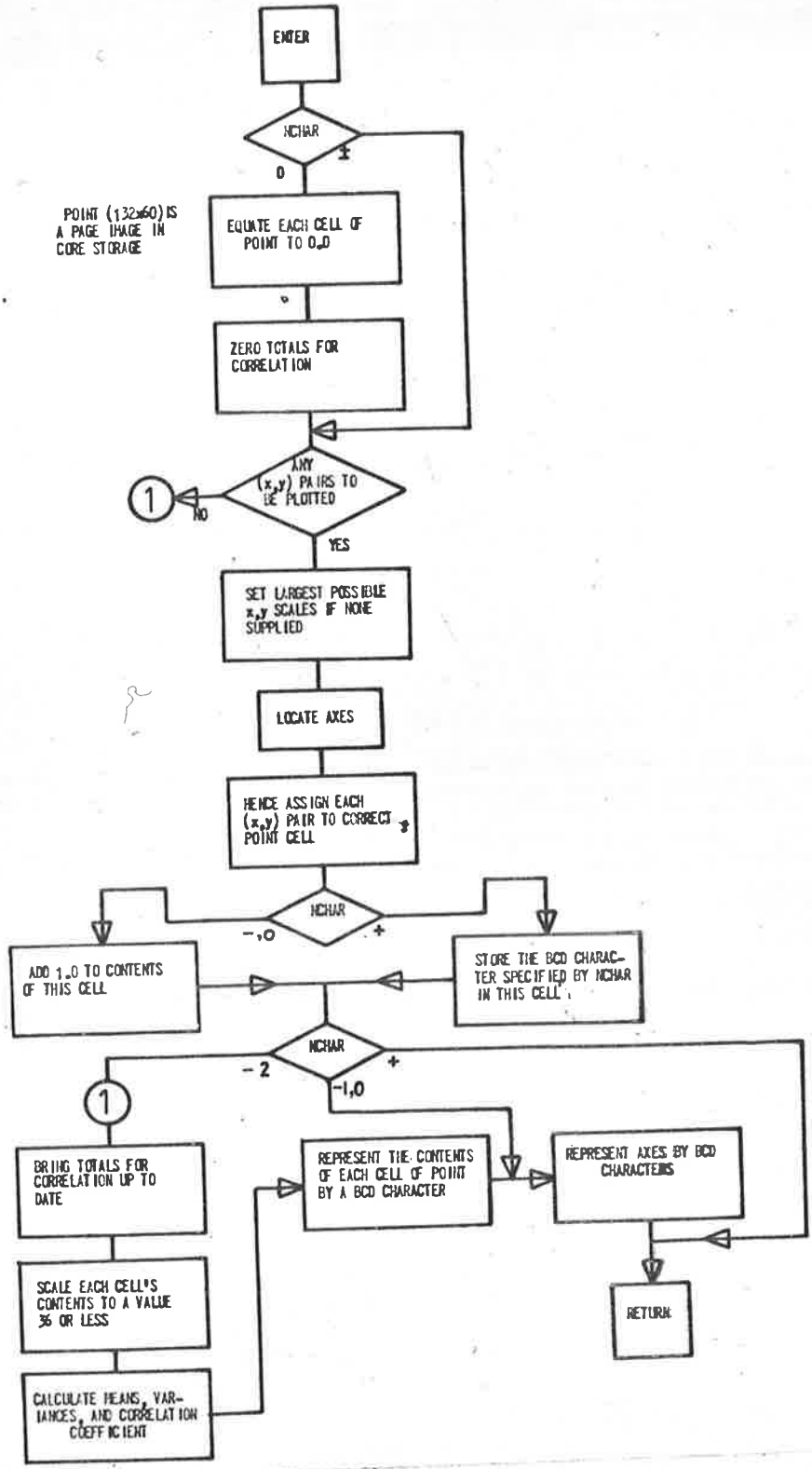

Figure A3.2 Flow diagram of subroutine PLOT.

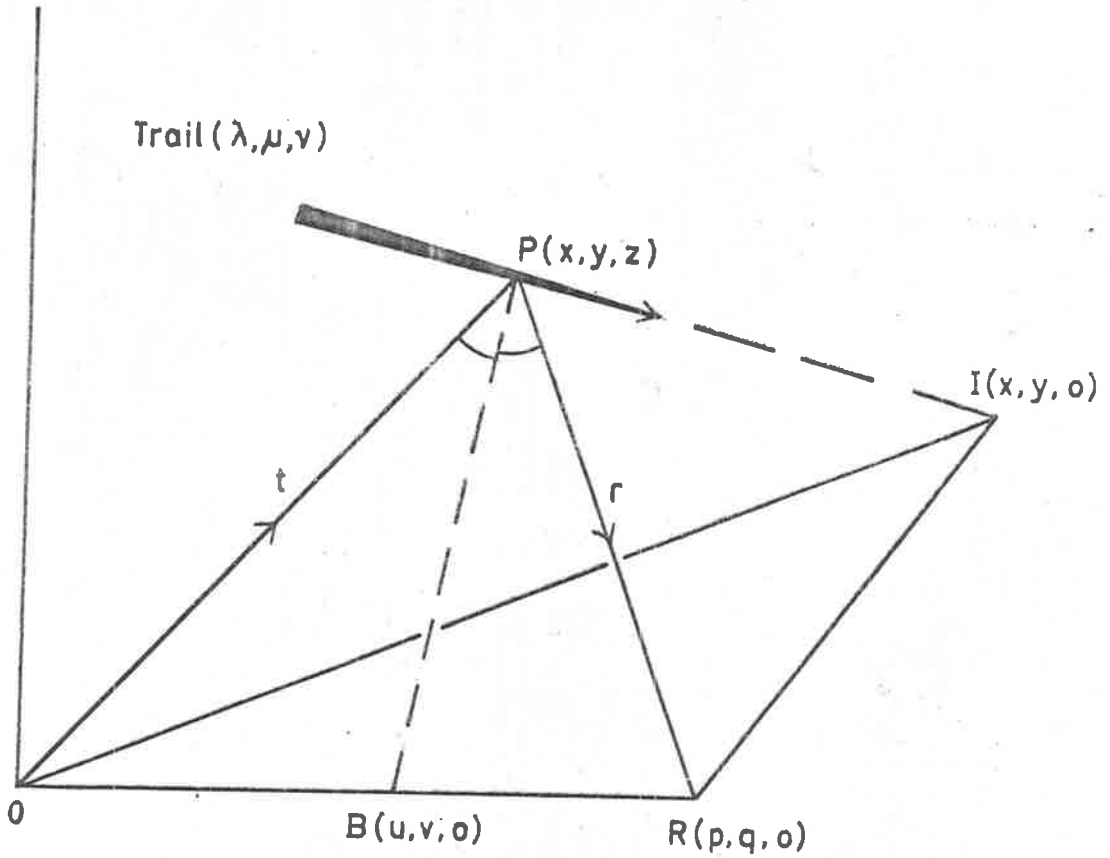

Figure A3.3 Geometry of specular reflection, to illustrate method of locating fourth reflection point (programme 1211E.4) .

3.3 Finding the fourth reflection point: 1211E.4 (Figures A3.3 and A3.4)

Consider Fig. A3.3 , in which the origin of coordinates is taken at the transmitter O. Let specular reflection at the point P(x,y,z) on a trail with direction cosines (λ,μ,ν) produce an echo at receiver R(p,q,0) . Write t = length OP, r = length PR, F = r/t. Let the bisector of angle OPR meet OR in B(u,v,0), and let the projected trail intersect the ground at $I(x_1,y_1,0)$. Then from the properties of the bisector of an angle of a triangle, we have

$$u = pt/(t + r)$$
$$v = qt/(t + r) \qquad \ldots \text{ A3.1}$$

Now the direction cosines of PB are in the ratio

$$x - u : y - v : z \ ,$$

and the condition that PB and the trail are normal is therefore

$$\lambda(x - u) + \mu(y - v) + \nu z = 0 \qquad \ldots \text{ A3.2}$$

Substituting for u and v from A3.1, and for z from the equation of the trail, viz. $(x - x_1)/\lambda = (y - y_1)/\mu = z/\nu$,

we obtain $\lambda x_1 + \mu y_1 + z/\nu = (\lambda p + \mu q)/(1 + f)$ ... A3.3

Values of z, the height of specular reflection, are found as follows for St. Kilda and Salisbury in turn from the data available.

(1)Determine x_1 and y_1 from

$$(lR_o - x_1)/\lambda = (mR_o - y_1)/\mu = nR_o/\nu$$

where the numerators are the coordinates of P, as given by the measurements.

(2)Solve A3.3 for an approximate value of z by putting f = 1 .

(3)Using this value of z find r, t, and hence f. These quantities are simply calculated in terms of λ, μ, ν, z and the ground coordinates p, q, x_1, and y_1 .

(4)Using the new f, solve A3.3 again for an improved value of z.

(5)Repeat from (3) to the desired accuracy.

Figure A3.4 is a flow diagram of programme 1211E.4 (for the 1620 computer) which was used to do this calculation for each meteor.

Several tests have been made of the accuracy with which programme 1211E.4 calculated the reflection point spacings, and of the uncertainty in the estimates of absolute reflection point heights which it provided. First it was necessary to be sure that the primary job of locating the

Salisbury reflection point height had been properly done. For this purpose the data for 45 echoes from January 1961 were used. By supplying to it the ground coordinates (p,q,0) of Direk outstation in place of those of Salisbury, the programme was made to re-calculate the distance along each trail between the main station reflection point heights, a known quantity. Table A3.1 compares the original and re-calculated values of this distance, showing that the accuracy of the calculation was above reproach, particularly since six echoes with NGEOM = 0 were included.

Table A3.1

Re-calculation of separation of St. Kilda and Direk reflection points.

	Original separation	New
Arithmetic mean (Km.), 45 meteors.	-0.135	-0.130
Mean absolute value (Km.)	1.375	1.375
R.m.s. difference (Km.)	0.0233	
R.m.s. percentage difference	1.76%	

A subsidiary programme (1211E.4.2) was written to obtain statistics indicating the discrepancies between the original values of l, m, n, total radar range, and height of main station reflection point, and the values satisfying specular conditions found by programme 1211E.4 . The results (Table A3.2), by an oversight, did not distinguish between NGEOM = 1 and NGEOM = 0. (In Table A3.2 the direction cosines l and m refer respectively to the Adelaide - St. Kilda direction and the approximately eastward direction at right angles. That is, they are in the system of axes in which they were originally measured).

The sensitivity of the height measurement nR_o to small inaccuracies in the other data will be noted from Table A3.2. Evidently an accuracy better than ± 2 Km. cannot be claimed for absolute height measurements. The poor quality of the December 1960 data will also be noted.

The author has since re-examined the change in height of the main station reflection point brought about by programme 1211E.4, for the four combinations of NQ and NGEOM. Table A3.3 contains the details of this check. Here a restricted sample of meteors is involved, those with KIND equal to 3 (unsuitable for echo amplitude processing) at the main station

Table A3.2. Results from programme 1211E.4.2 .

Sample	Dec. 1960	Jan.-Dec. 1961	Re-reads≠
Total meteors*	81	1573	326
Total with NGEOM = 0	34	184	70
Mean abs. dev'n. from specularity in:			
Total radar range	.48 Km.	.12 Km.	.33 Km.
Direction cosine l	.023	.012	.017
" " m	.018	.011	.016
" " n	.026	.014	.022
Height nR_o	3.77 Km.	1.79 Km.	3.18 Km.

≠These echoes were re-read in the orbit work after initial failure in the orbit reduction programme. Most of them have NQ = 0 .

*The data for approximately 200 meteors were not available at the time of this analysis.

Table A3.3

R.m.s. difference in main station reflection point heights nR_o before and after use of programme 1211E.4, for combinations of echo type and quality.

Echo KIND	NQ	NGEOM	Meteors	R.m.s. ht. diff., Km.
0	1	1	717	2.20
	1	0	24	~8
	0	1	322	3.33
	0	0	49	~8
1	1	1	273	2.93
	1	0	10	~8
	0	1	136	4.26
	0	0	31	~8
2	1	1	266	2.59
	1	0	10	~8
	0	1	131	4.20
	0	0	30	~7

having been removed. Two points can be made. Firstly, a strong correlation evidently exists between the attributes KIND = 3 and NGEOM = 0, since by comparison with Table A3.2 most of the latter class are seen to have been removed. This correlation of echo waveform quality with quality of geometrical measurements may be worthy of further study. Secondly, allowing for the fact that the r.m.s. height difference (Table A3.3) is more sensitive than the mean absolute height difference (Table A3.2) to outlying values, the two tables are consistent with the best data (NQ = 1 and NGEOM = 1) being accurate to about $\pm$2 Km. in height. NGEOM = 1 alone appears to provide accuracy within $\pm$ 3 Km.

3.4 Antenna gain product for each echo: ALPHA (Figure A3.5)

In this programme, the minimum detectable underdense line density was found for each reflection point's position in space, and was added to a magnetic tape on which were also copied the results from programme ENVLO.

Figure A3.5 is a flow diagram of programme ALPHA. Two sections of this programme were adapted from a programme used by Nilsson(1963), viz. sections dealing with production of the maps of sensitivity in the 93 Km. plane given in Sect. 7.3, and with finding the azimuth and zenith angle of a given reflection point as seen from various points on the ground. However, Nilsson's programme was concerned only with the production of maps of gain product, sensitivity and similar functions. Programme ALPHA was rendered more complicated by (1) the processing of data for each individual echo, necessitating the reading of cards (4 per meteor) and the reading and writing of magnetic tape; (2) the need to interpolate to the nearest degree in tables of the polar diagrams of the antennas, the intervals of tabulation being 10° (azimuth) and 5° (zenith angle); (3) the introduction by the actual meteor data of reflection point heights different from the 93 Km. mean value used in the maps; and (4) the necessity to make calculations for all four receiving sites rather than one. Requirement (2) above arose, not because it was warranted by the accuracy of the polar diagrams, but because two reflection points on a trail might lie in adjacent cells of the transmitting polar diagram table, rather than in the same cell. In the case of adjacent cells, and

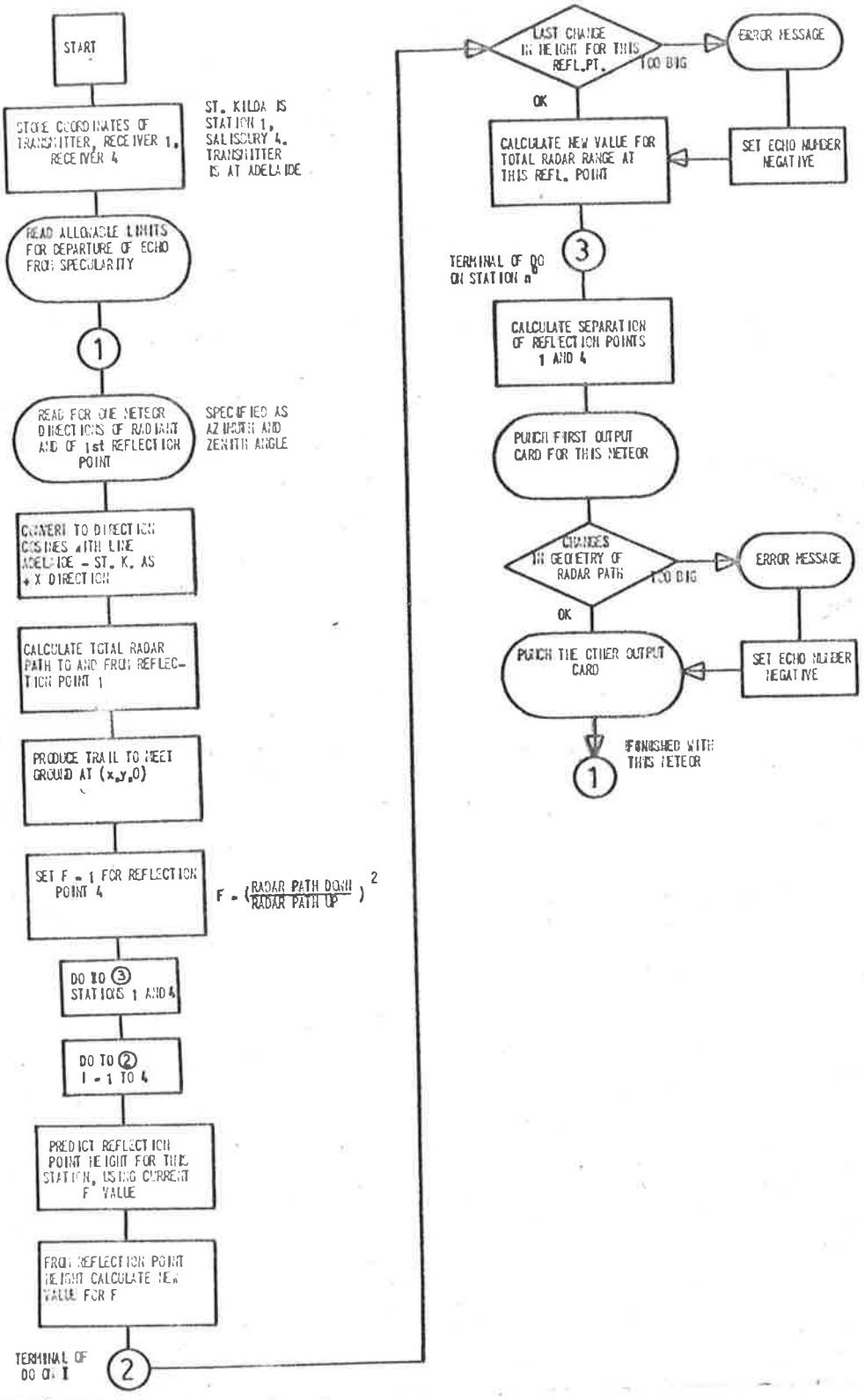

Figure A3.4. Flow diagram of programme 1211E.4 .

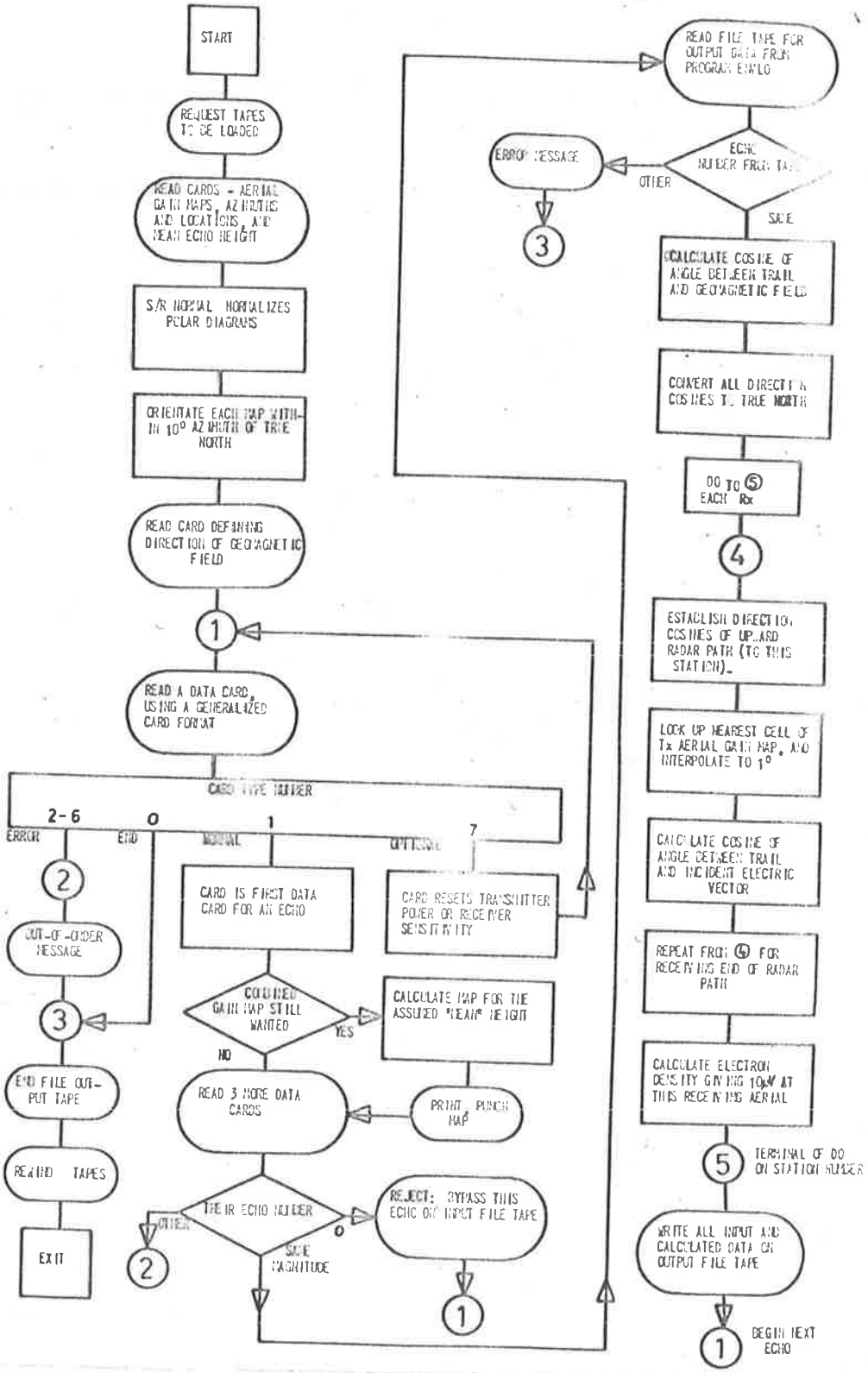

Figure A3.5 . Flow diagram of programme ALPHA.

without interpolation, a much greater difference in transmitter aerial gain would be attributed to these reflection points than their actual separation could justify. For each meteor two input cards were those punched by programme 1211E.4, and one contained any remarks which it was felt should be included with the data. The fourth contained astronomical data from the file tape of the orbit programme, the intention being to make the present file tape a more useful entity for future analysis.

The flow diagram in Fig. A3.5 is otherwise self-explanatory. Although it indicates that the angles between the trail axis and the incident (and reflected) electric vectors of the radio wave were calculated, the calculation made in this programme was in error. A correct calculation was made in the programme which analyzed the trail profile data (Sect. 7.11 and Appendix 3.6).

3.5 Fluctuations in power and sensitivity: STDGW (Figure A3.6)

This programme was written to test methods of handling data, and to display data and results graphically. There was no provision for output of results on magnetic tape for later use in the computer, since this would have been wasted in testing all but the finally-adopted method. The logic of the final method was instead incorporated as part of programme OMEGA 1 (below), which did produce an output tape.

Plotting was done on the WREDOC output converter at W.R.E., up to 16 variables being simultaneously graphed as functions of time. Unfortunately the graphs are unsuitable for small-scale reproduction.

Figure A3.6 is a chart showing an outline of the predictor-corrector method finally used for estimating the transmitter power and receiver sensitivities as functions of time. Details of the graph-plotting have not been included.

3.6 Trail profile analysis: OMEGA 1 (Figure A3.7)

As originally planned, this programme was to perform the functions of collating, analysis and graphical display for both the ionization profile and the diffusion coefficient data. However, it turned out that the length of programme involved was roughly twice that which the 7090 could conveniently accomodate. This and other considerations led to the reconstituting of the ionization profile and diffusion parts as separate

programmes, of which the second (OMEGA 2) is described in Appendix 3.7. The first (OMEGA 1) then dealt with the profile work only.

The logic of the finally-accepted method for estimating transmitter power and receiver sensitivities (Appendix 3.5) was incorporated into the first programme, so that in testing the various methods, no time was wasted in writing possibly unwanted output tapes. Its incorporation increased the execution time of OMEGA 1 by some 10% only. The mode of tape reading which it necessitated was the following. The tape (from programme ALPHA, Appendix 3.4) was read, and estimates of power and sensitivity were found, for each 12 minute interval containing one or more meteors. The tape was then moved backwards to the first meteor in the 12 minutes, and each meteor was further processed individually; information to be collated was stored, and an output tape record was written of all data for the meteor.

The calculation of electron line density for underdense echoes (KIND 0; c.f. Section 7.1) has been described. For overdense echoes whose terminal decay was recorded (KIND 1) a similar calculation was made, using the commencing amplitude and time-constant of the decay, and an alternative value of the density was also calculated from the duration of the persistent phase of the echo and the decay time-constant. For overdense echoes of KIND 2, the nominal value $\alpha = 5 \times 10^{15}$ electrons/metre was adopted; for below-threshold echoes (KIND 4) the minimum detectable line density calculated in programme ALPHA; and for KIND 3 the line density and most other parameters of interest to this analysis were undefined.

A system of classifying the echo amplitude and diffusion coefficient data for each echo was instituted in this programme. Four quality classes were used, denoted by values 1 to 4 of a variable INDEXQ in the programme; "INDEXQ = ..." has been used as a convenient way to indicate quality attributes. We have seen that various quality-indicating variables of an on-off kind were generated at various points in the previous analysis. A different technique was used with final results which were subsequently to be displayed, such as line density. Four replicas of each such result were preserved on tape for every echo, with one

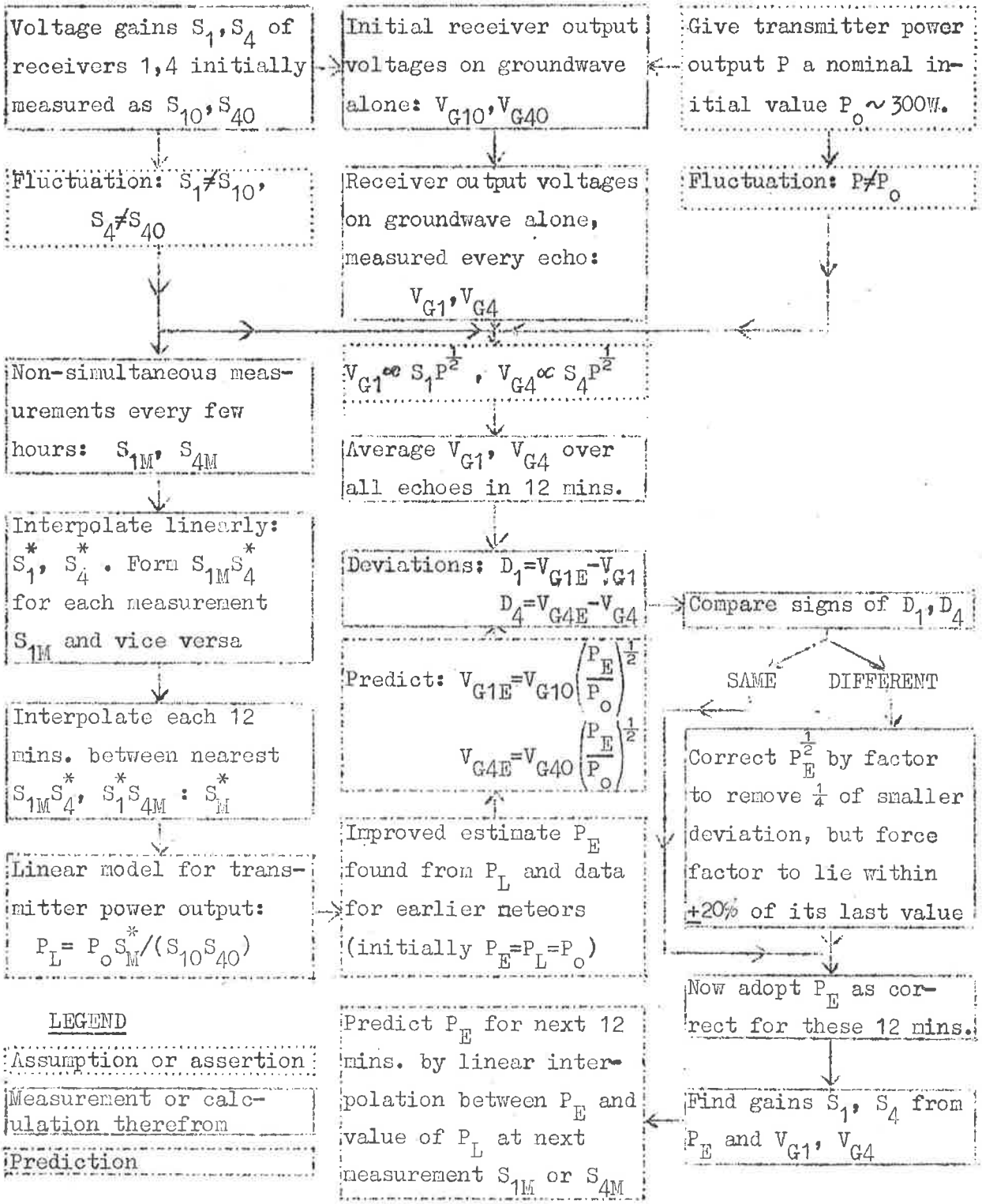

Figure A3.6 . Logical structure of programme STDGW .

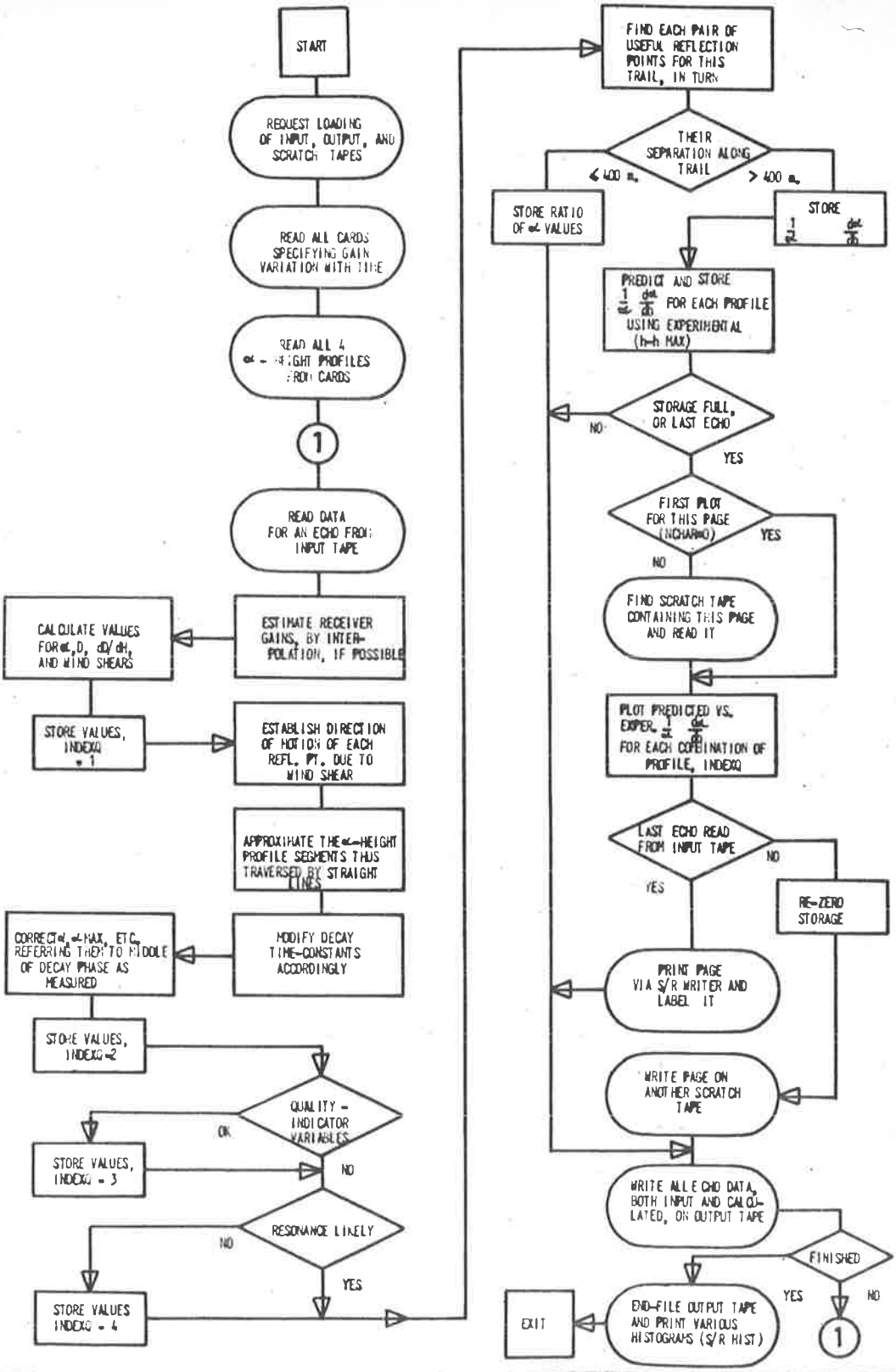

Figure A3.7. Flow diagram of programme OMEGA1.

replica per quality class. When the echo did not pass the requirements for a given classification, recognizable dummy values, usually (but not always) zero, replaced the measured or calculated values of the variables treated in this way.

The values of INDEXQ represented the following classes of data.
(1) all echoes for which KIND $\neq 3$;
(2) as (1), provided that a correction for the effects of reflection point motion could be made in the case of KIND 0 or 1 ;
(3) underdense echoes (KIND 0) only, of good quality as judged from the quality indicators NQ ("optimization" in orbit reduction), NGEDM (tests of specularity in programme 1211E.4) and NOK (quality of amplitude-time data) ;
(4) as (1), provided that the incident polarization could be stated with reasonable certainty to be more nearly longitudinal than transverse.

In making allowance for the effects of reflection point motion on measured line densities and diffusion coefficients (INDEXQ = 2) the first step was to predict the sense of the line-of-sight wind at reflection point 4, whose magnitude had been calculated in programme ENVLO. Although reversals of sense were practically never observed among stations 1,2 and 3, provision was made for this eventuality at greater separation of reflection points. This was done by finding the regression of wind speed on height for stations 1,2 and 3, and giving the wind at point 4 the sign which gave the better agreement with the regression. At each reflection point the local wind shear was then estimated by considering the wind speed at the point in question together with the speed at the reflection points on either side. Where a reflection point was the highest or lowest on a trail only one speed value was of course involved in estimating the wind shear. So that wind speed information was not discarded, u was accepted regardless of KIND at each observed reflection point; this was the only use made of KIND 3 echoes. In a similar manner the quantity $\frac{1}{\alpha}\frac{d\alpha}{dh}$ was estimated at every reflection point with KIND < 2. Note that a value of $\frac{1}{\alpha}\frac{d\alpha}{dh}$ defined <u>at</u> a reflection point differs from a

value defined midway between two points, as used in the trail profile analysis (Section 8.6). Now all the necessary information had been found for calculating revised values of line density, diffusion coefficient and associated variables from Equations 3.7.7 and 3.7.9. This was done, and the new values were stored in the class INDEXQ = 2. Values of line density for KIND 2 or 4 echoes were of course stored unchanged.

In Section 3.6 it was shown that the polarization of a 27Mc/s signal reaching a trail above 90 Km. altitude in the daytime may be significantly rotated (Faraday effect) if the signal travels nearly parallel to the earth's magnetic field. In calculating which echoes (KIND 0 or 1) should be suspected of resonance with transverse polarization, this condition was first examined. Write $\underset{\sim}{r}$ for the unit vector along the path from the transmitter to a reflection point, $\underset{\sim}{a}$ for the direction of the aerial axis, $\underset{\sim}{t}$ for the trail axis, and $\underset{\sim}{g}$ for the direction of the geomagnetic field. Then echoes above 90 Km. between 0600 and 1800 hours local time were not admitted to the class INDEXQ = 4 if the condition

$$\underset{\sim}{r} \cdot \underset{\sim}{g} > \cos 45^{\circ} \qquad \text{held.}$$

If, instead, an echo passed this test, Faraday rotation was assumed to be unimportant. The condition of rejection was then

$$(\underset{\sim}{r} \times (\underset{\sim}{r} \times \underset{\sim}{a})) \cdot \underset{\sim}{t} > \cos 45^{\circ}$$

The vector preceding the scalar product operator is the polarization vector of the signal incident upon the trail.

In the programme the option was incorporated of storing results either corrected or uncorrected for reflection point motion, in INDEXQ classes 3 and 4. The results in these classes presented in Chapter 8 were not corrected. This choice allowed the importance of the quality tests (INDEXQ 4) to be evaluated more easily.

Figure A3.7 is a flow diagram showing in very abbreviated form the manner in which programme OMEGA 1 operated. The only point not made either above or in Chapter 8 is that although many page "images" formed by subroutine PLOT were simultaneously being added to as echo data were read from the input tape, there was room for only one such image in the internal memory of the computer. Therefore use was made of five "scratch" magnetic tapes to hold the remainder of the 160,000 numerical items

needed to represent 20 such pages. Close attention was paid to efficiency in the use of these tapes so that the internal calculations of the computer were not delayed while a tape, having been written with page images, was rewound for additions to be made to the plots.

3.7 Diffusion coefficient analysis: OMEGA 2 (Figure A3.8)

Analysis of the ambipolar diffusion coefficients D calculated from the decay of underdense and transitional echoes was performed by the use of programme OMEGA 2.

The function of this programme can be stated as follows :- Given the magnetic tape of results from OMEGA 1, print scatter diagrams of $\log_{10}D$ vs. height for meteors observed between two chosen dates, showing not only all the results together but also any diurnal effects. Print similar diagrams for the height gradient of D, $\frac{d(\log_{10}D)}{dh}$, as measured for trails yielding two or more suitable echoes. For each such diagram calculate mean values of $\log_{10}D$ or $\frac{d(\log_{10}D)}{dh}$ in 1 Km. height intervals, and display the mean values in similar fashion. Provide mean values, r.m.s. deviations, and correlation coefficients of $\log_{10}D$ or $\frac{d(\log_{10}D)}{dh}$, and height, for each scatter plot. Perform these tasks for each desired value of the quality index INDEXQ. Repeat for as many further pairs of dates as required.

To display the data as outlined above required 10 pages of graphs and/or scattergrams, usually 3 per page, for each value of INDEXQ. Thus complete display of the data recorded between two dates occupied 40 pages. As in OMEGA 1, simultaneous storage of the data and the page images (or either) was completely beyond the capability of the core storage of the 7090, and magnetic tapes were again used to extend the memory size. Therefore the two programmes had an overall similarity. In each case the sequence of operations was (1) To read as much data from an input tape as could be processed at once, making any necessary calculations, meteor by meteor. (2) To collate and plot the data, storing each page image on a scratch tape. (3) To repeat until the plots contained all the data to be processed and displayed. (4) To retrieve the plots from the scratch tapes in the required order and cause them to be printed.

The flow diagram in Figure A3.8 gives an idea of how the above steps were performed in programme OMEGA 2. Some emphasis is placed in the diagram on the way in which the control variable NCHAR, which in normal usage indicates to subroutine PLOT (Section 7.7) whether more data are to follow a present set, was used in the main programme for similar control functions. Figure A3.8 was prepared while the programme was still being tested, and is incorrect in one respect. It indicates that the electron line density and height at the point of maximum ionization were plotted in programme OMEGA 2. In fact it was found expedient to treat these quantities in OMEGA 1; the relevant results are discussed in Section 8.7 and Appendix 5.

There was no magnetic tape output from programme OMEGA 2.

It is now in order to indicate how the methods outlined in 5.4, for estimating a linear functional relation, were applied to the mean values, standard deviations, and correlation coefficients which were computed for every scattergram of log D versus h in the above programme.

In the analysis of the 1961 data, the statistical results obtained for each group of n points are n, $\bar{h}$, $\overline{\ln D}$, σ_h, $\sigma_{\ln D}$, and the correlation coefficient r, where

$$\sigma_h^2 = \frac{1}{n}\Sigma(h-\bar{h})^2 \equiv s_{xx}$$

$$\sigma_{\ln D}^2 = \frac{1}{n}\Sigma(\ln D - \overline{\ln D})^2 \equiv s_{yy}$$

and

$$r = \frac{\Sigma(h-\bar{h})(\ln D - \overline{\ln D})}{n\,\sigma_h\,\sigma_{\ln D}} \equiv s_{xy}/(s_{xx}s_{yy})^{\frac{1}{2}}$$

(In practice the quantity which represents the diffusion coefficient is, for convenience, $\log_{10} D + 0{\cdot}6021$, i.e. $\log_{10}(D/0{\cdot}25)$, but the explanation is simpler in terms of $\ln D$). It can readily be shown that the substitution of these quantities in Eq.5.4.6 gives

$$H_D = \frac{\sigma_h^2 - \delta_h^2}{r\,\sigma_{\ln D}\,\sigma_h} \qquad \ldots \text{ A3.7.1}$$

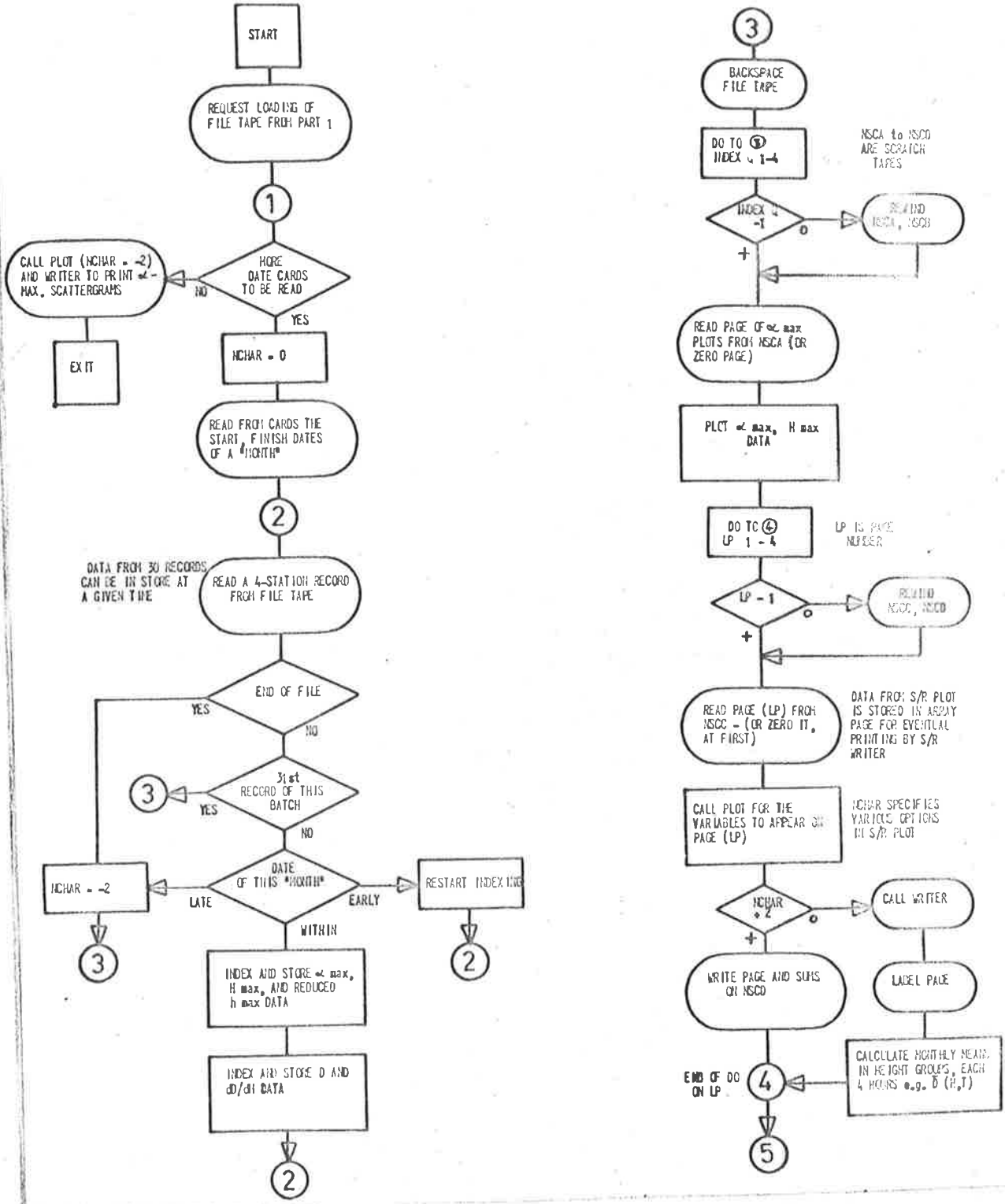

Figure A3.8. Flow diagram of programme OMEGA2 .

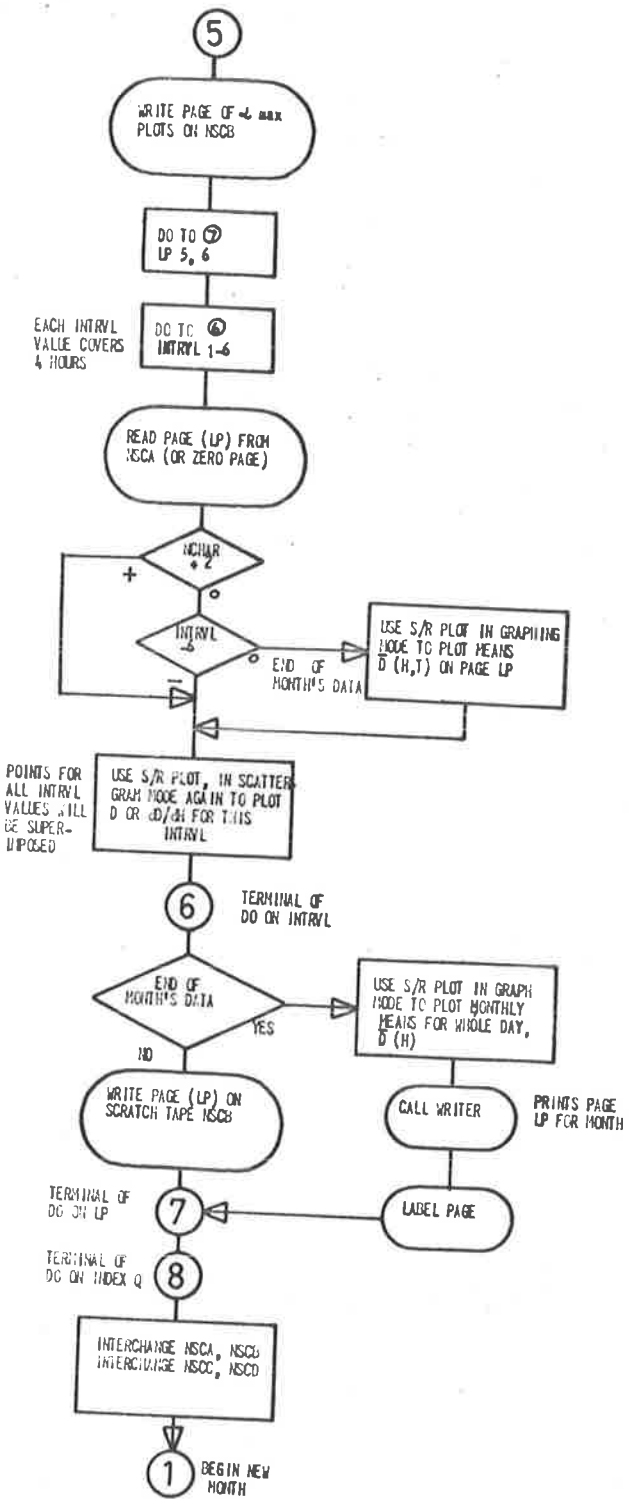

Figure A3.8. (continued).

while the experimental error variance of ln D is, from 5.4.7,

$$\delta^2_{\ln D} = \frac{n}{n-2}(\sigma^2_{\ln D} - r\sigma_{\ln D}\sigma_h/H_D) \quad . \quad \ldots \text{A3.7.2}$$

In Chapter 9 of the text we refer to H_D values found using A 3.7.1 as H_{D1} to distinguish them from values H_{D2} deduced from the measurement of $\frac{d}{dh}(\ln D)$ on individual meteor trails.

There is a danger in the practical use of Eq's. A3.7.1 and A3.7.2 (or, in general, 5.4.6 and 5.4.7) which does not arise with Eq's. 5.4.2 and 5.4.4 in which only the ratio λ of the error variances is required. It may happen that in a small sample the full range of (true height $\pm$ δ_h) is not covered by the data, or that δ_h is over-estimated. If so we have $\sigma^2_h \leq \delta^2_h$ for the set of data in question, and H_D becomes negative and $\delta_{\ln D}$ is undefined. The author has taken the attitude that very occasional occurrence of this condition is to be expected, in groups of points for which n is too small to define properly the shape of the distribution in the scatter diagram, and probably indicates that the value taken for δ_h is correct.

Davies (1958) gives a formula for the variance of the estimated coefficient $\hat{\alpha}$ in Lindley's method. Applying it to finding the standard error of the estimated diffusion scale height in Eq. A3.7.1 , we have

$$\sigma(H_{D1}) = \left[\frac{(\lambda + H^2_{D1})\delta^2_h}{\lambda(\lambda\sigma^2_{\ln D} + \sigma^2_h - \delta^2_h)}\right]^{\frac{1}{2}} \quad \ldots \text{A3.7.3}$$

where, as before,

$$\lambda = \delta^2_h/\delta^2_{\ln D}$$

and $\delta^2_{\ln D}$ is found from Eq. A3.7.2 .

3.8 Multiple correlation and regression: NRMC 3

The following notes on the statistical methods used in this programme may be helpful in judging the significance of results in sections of Chapters 8 and 9. The notes are abstracted from the original description (NRMC: Multiple Correlation Analysis, number 1121 in IBM SHARE programme library).

The programme is for the statistical analysis of a set of points

$$\{P_1 , P_2 , \ldots P_i , \ldots P_M\}$$

where $P_i = (X_1, X_2, \ldots X_j, \ldots X_N)$; $M \leq 200$, $N \leq 40$.

It will perform multiple correlations of the form

$$X_1 = B_1 + B_2X_2 + \ldots + B_NX_N ,$$

where X_1 is the dependent variable and the coefficients B_j are to be statistically evaluated from the data. The points P_i are actually supplied in the form $P_i' = (Z_1, Z_2, \ldots Z_{NO})$, $NO \leq N$, where the Z_k are observational values. The X_l, l=2, ...N, are independent variable "functions" constructed within the programme according to the user's instructions from the actual data Z_k . They may involve the product of two of the Z_k or take the form of a fractional power, exponential, logarithm, or polynomial of degree less than five. In a linear model NO=N and each $X_j \equiv Z_j$.

The entire analysis is based on the NxN symmetric correlation matrix (r_{mn}) , where r_{mn} is the correlation coefficient of X_m and X_n . From the variances of the variables X_j and the elements of the inverse to (r_{mn}) , the regression coefficients B_j and the multiple error of estimate of X_1 are computed, together with the partial correlation coefficients for each X_l with X_1 . All estimates are statistically evaluated and their standard deviations and significance computed. The programme performs a x^2 test of the validity of the assumption that deviations of X_1 from the value given by the regression for each point P_i are normally distributed.

If it is desired to obtain a final multiple correlation with a minimum number of truly independent functions X_l, the following optional procedure is available. The null hypothesis $r_{mn}=0$ is tested for all m>1,

$n>1$ to determine whether X_m and X_n are independent. The largest r_{mn} for which this hypothesis is rejected is then determined and the partial correlation coefficients for X_m and X_n with X_1 are used to find which of X_m and X_n contributes less to the total correlation. The less important one is then removed from the analysis temporarily. If the new estimate of the variance of X_1 about the remaining correlation form is not significantly greater than the original estimate, the removal is made permanent. Almost the entire analysis is repeated with the remaining N-1 terms. If the variance significantly increases, however, the removed variable is reinstated and the next higher r_{mn} investigated. The final result of this procedure is a statistically valid estimate of the correlation of X_1 with a minimum number of truly independent functions.

The author has made several changes in NRMC with the object of matching its capabilities to the meteor data. The most important are listed as they appear in the author's current version NRMC 3.

(1) The system for internal generation of the X_j from the Z_k has been replaced by a less elegant but more flexible procedure in which a subroutine FUNGEN is called and generates the functions X_j. The manner of their definition and generation is altered as necessary by re-writing the relevant sections of FUNGEN; the much more complicated main programme does not then have to be changed. For meteor data, FUNGEN reads the tape of results from programme OMEGA 1 and generates a set of X_j for each suitable meteor. The X_j are all stored on a scratch magnetic tape; 2500 sets may be processed, as against the original 200.

(2) Various changes have been made to adapt the programme to the particular 7090 installed at W.R.E. Salisbury. In particular the "double-precision" arithmetic involved in inverting matrix (r_{mn}) has been changed to the standard system which is now an integral part of the Fortran programming language for the 7090.

(3) Because of the large numbers of points able to be analysed, the listing of original and re-calculated values of X_1, is replaced by the use of subroutine PLOT to draw a scattergram of predicted versus observed values. PLOT is also used to present a histogram of the frequencies of various deviations of X_1 from the regression. This complements the original χ^2 test for normal distribution of the deviations which is retained.

APPENDIX 4

DISTRIBUTIONS OF ABSOLUTE LINE DENSITY

The histograms on the following seven pages show the distribution of electron line density measured at each station. The separate pages each give this information for a different combination of echo type (KIND 0, underdense, and KIND 1, transitional) and the quality index INDEXQ. The distributions were printed as part of programme OMEGA1 (v. Section 7.11), and are discussed in Chapter 8.

Histogram columns having an X at their head are "full", i.e. contain the number of measurements indicated by the scale . The characters . H ' respectively indicate that the contents of the column exceed the next lower scale graduation by .01 to .49, .50, or .51 to .99 of the smallest scale interval.

The letter M below the horizontal axis denotes the position of the mean of each distribution.

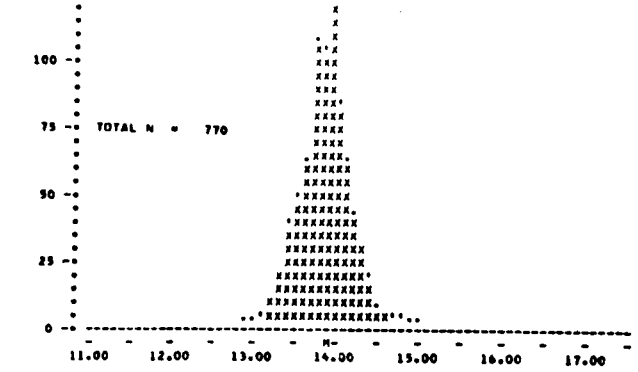

LOG10 (ALPHA) FOR TYPE 0 ECHOES RECORDED AT STATION 1 WITH QUALITY INDEX 1

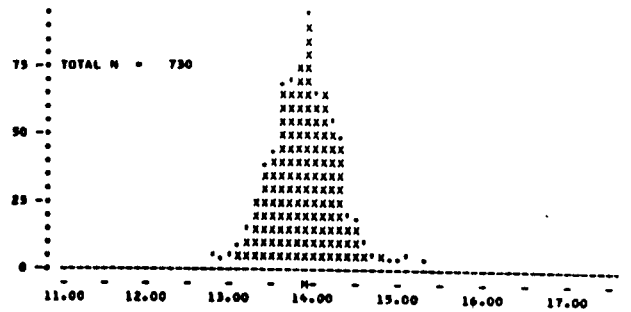

LOG10 (ALPHA) FOR TYPE 0 ECHOES RECORDED AT STATION 2 WITH QUALITY INDEX 1

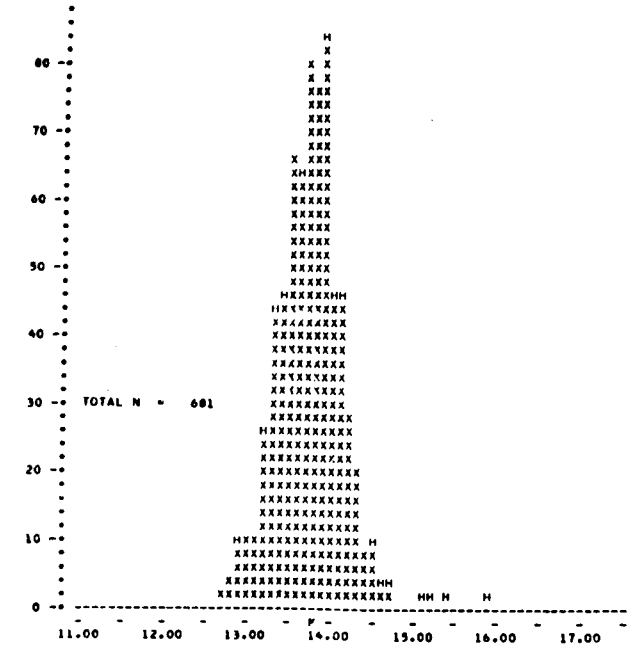

LOG10 (ALPHA) FOR TYPE 0 ECHOES RECORDED AT STATION 3 WITH QUALITY INDEX 1

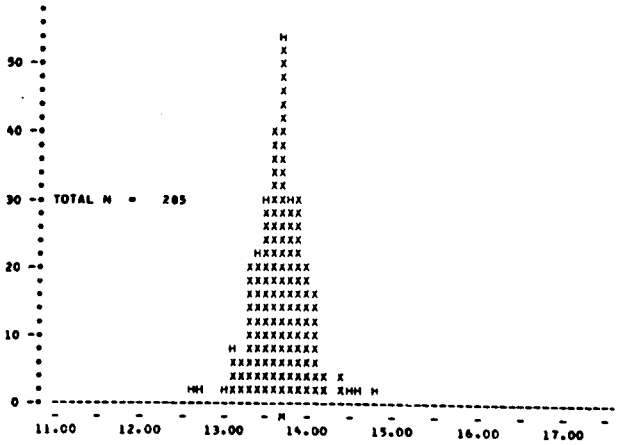

LOG10 (ALPHA) FOR TYPE 0 ECHOES RECORDED AT STATION 4 WITH QUALITY INDEX 1

Figure A-4-1

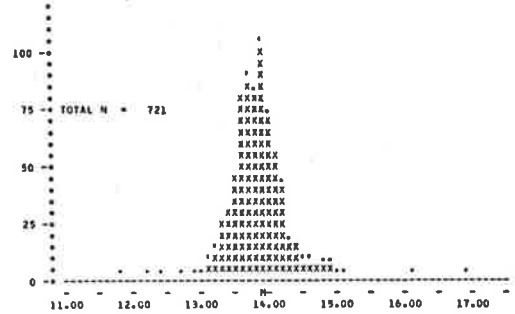

LOG10 (ALPHA) FOR TYPE 0 ECHOES RECORDED AT STATION 1 WITH QUALITY INDEX 2

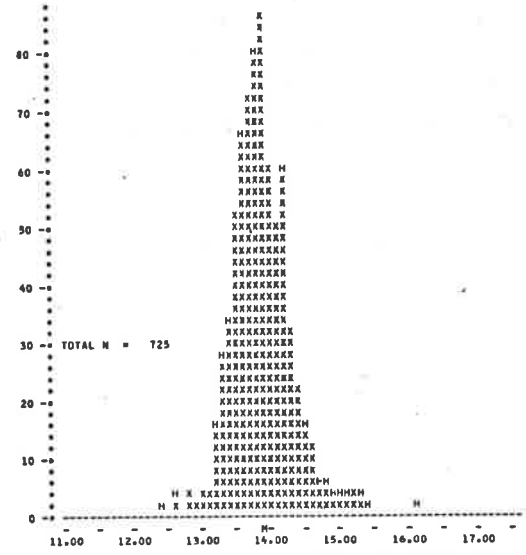

LOG10 (ALPHA) FOR TYPE 0 ECHOES RECORDED AT STATION 2 WITH QUALITY INDEX 2

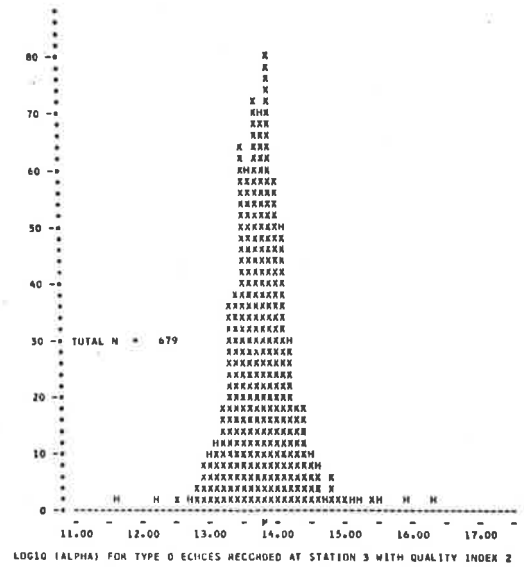

LOG10 (ALPHA) FOR TYPE 0 ECHOES RECORDED AT STATION 3 WITH QUALITY INDEX 2

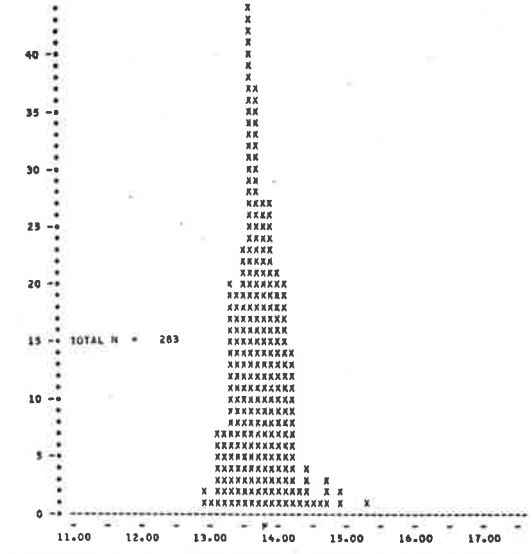

LOG10 (ALPHA) FOR TYPE 0 ECHOES RECORDED AT STATION 4 WITH QUALITY INDEX 2

Figure A-4-2

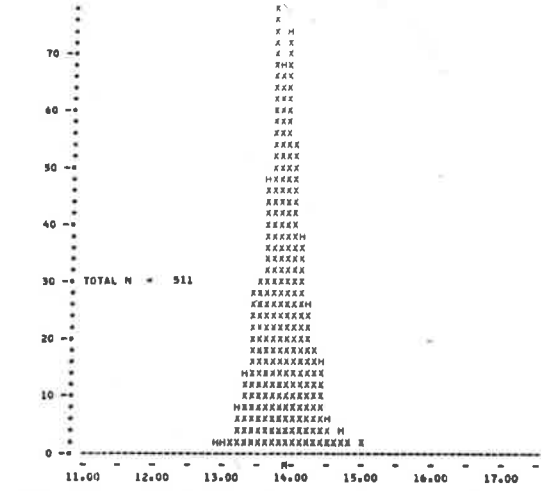

LOG10 (ALPHA) FOR TYPE 0 ECHOES RECORDED AT STATION 1 WITH QUALITY INDEX 3

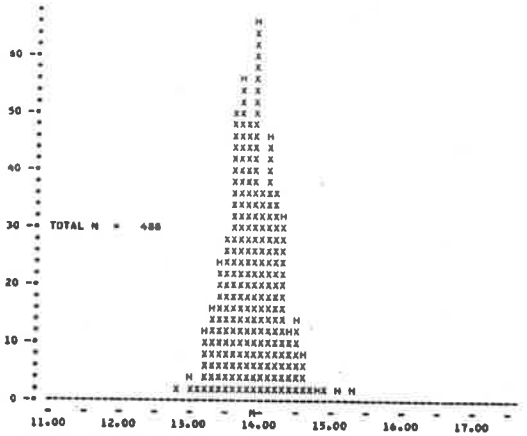

LOG10 (ALPHA) FOR TYPE 0 ECHOES RECORDED AT STATION 2 WITH QUALITY INDEX 3

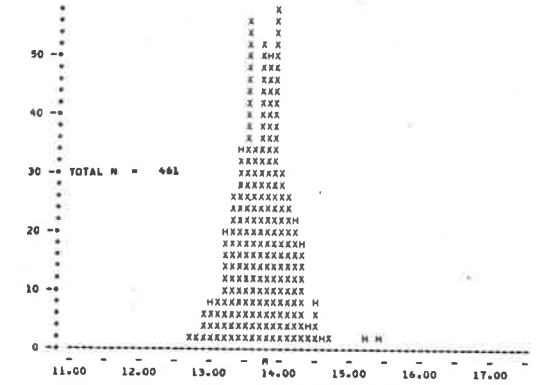

LOG10 (ALPHA) FOR TYPE 0 ECHOES RECORDED AT STATION 3 WITH QUALITY INDEX 3

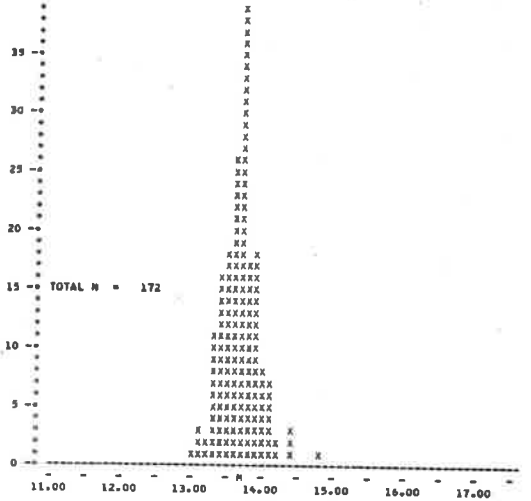

LOG10 (ALPHA) FOR TYPE 0 ECHOES RECORDED AT STATION 4 WITH QUALITY INDEX 3

Figure A-4-3

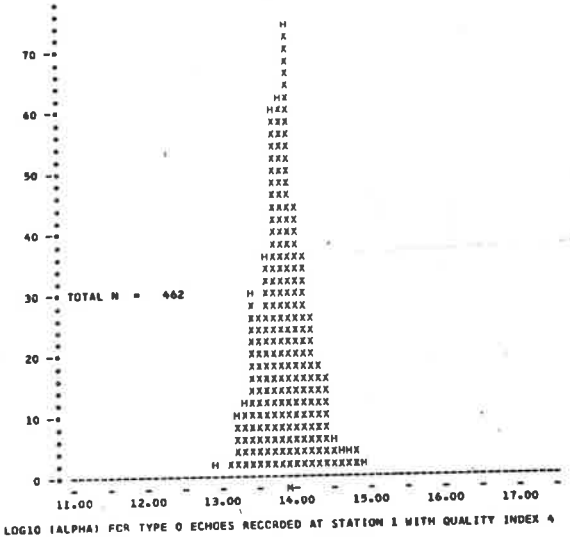

LOG10 (ALPHA) FOR TYPE 0 ECHOES RECORDED AT STATION 1 WITH QUALITY INDEX 4

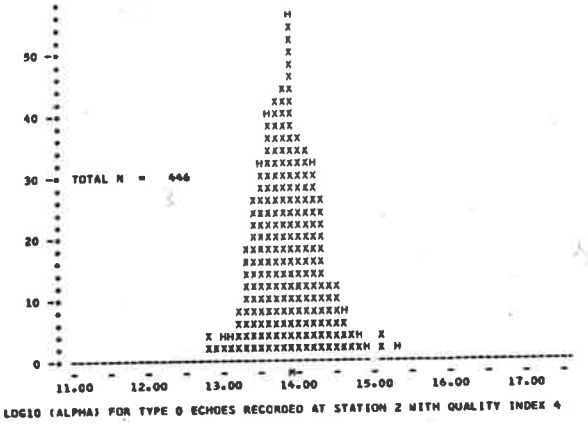

LOG10 (ALPHA) FOR TYPE 0 ECHOES RECORDED AT STATION 2 WITH QUALITY INDEX 4

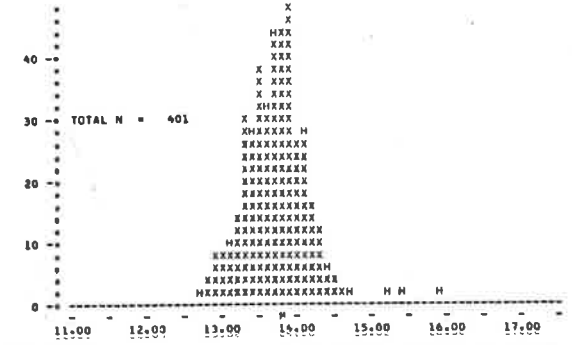

LOG10 (ALPHA) FOR TYPE 0 ECHOES RECORDED AT STATION 3 WITH QUALITY INDEX 4

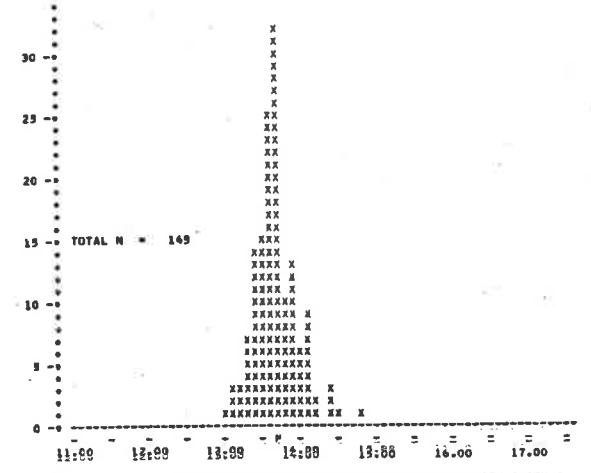

LOG10 (ALPHA) FOR TYPE 0 ECHOES RECORDED AT STATION 4 WITH QUALITY INDEX 4

Figure A-4-4

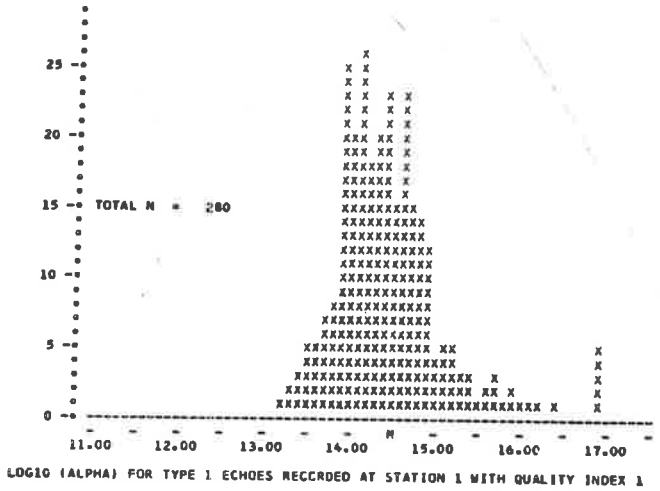

LOG10 (ALPHA) FOR TYPE 1 ECHOES RECORDED AT STATION 1 WITH QUALITY INDEX 1

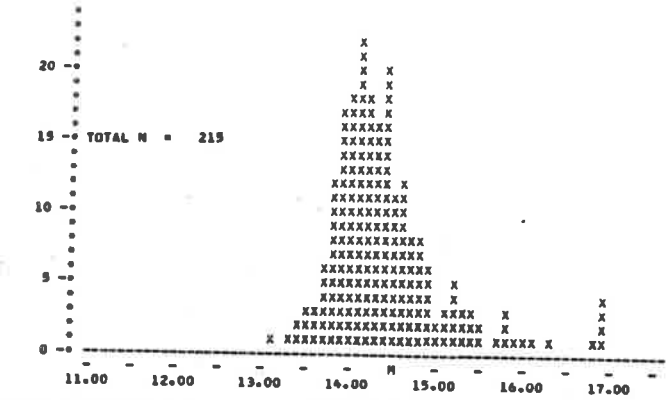

LOG10 (ALPHA) FOR TYPE 1 ECHOES RECORDED AT STATION 2 WITH QUALITY INDEX 1

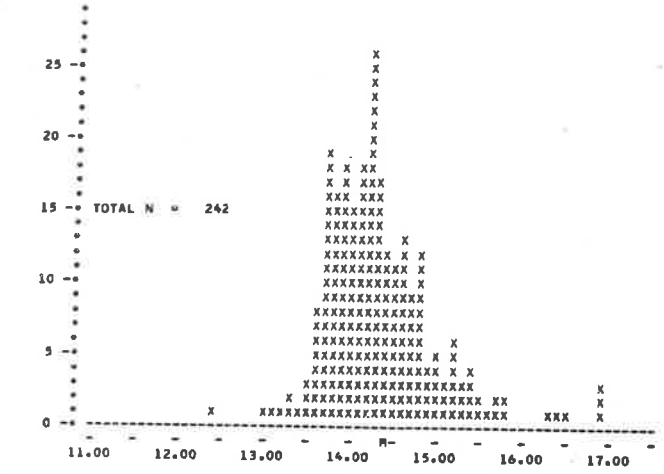

LOG10 (ALPHA) FOR TYPE 1 ECHOES RECORDED AT STATION 3 WITH QUALITY INDEX 1

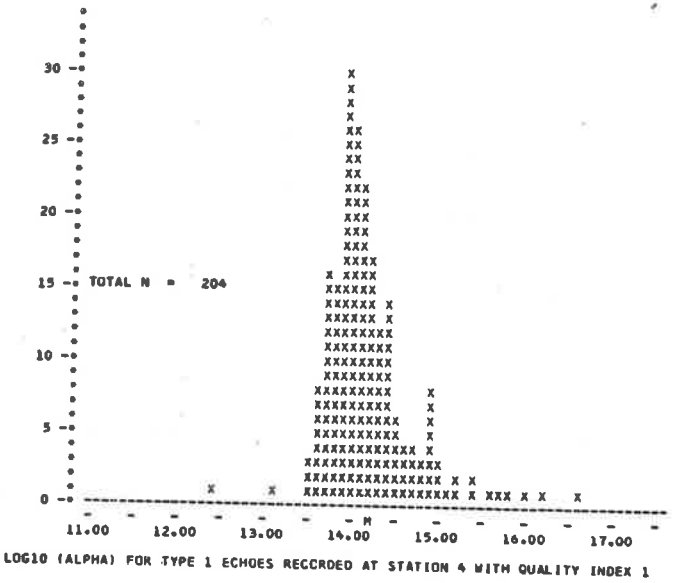

LOG10 (ALPHA) FOR TYPE 1 ECHOES RECORDED AT STATION 4 WITH QUALITY INDEX 1

Figure A-4-5

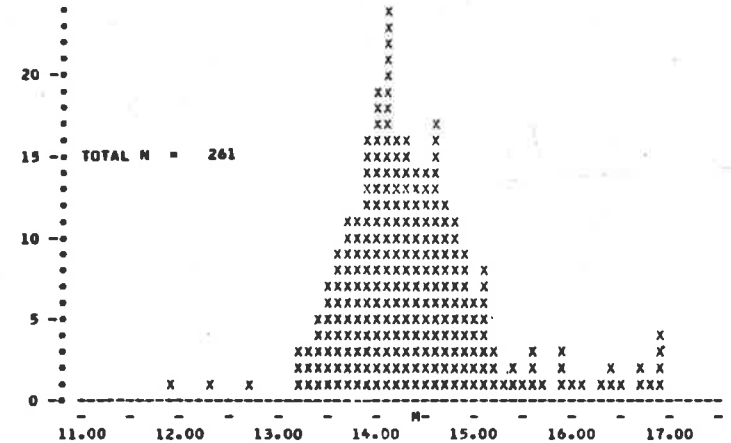

LOG10 (ALPHA) FOR TYPE 1 ECHOES RECORDED AT STATION 1 WITH QUALITY INDEX 2

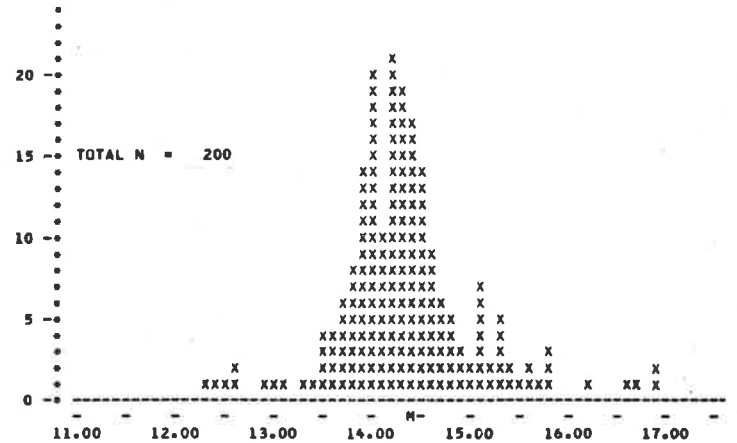

LOG10 (ALPHA) FOR TYPE 1 ECHOES RECORDED AT STATION 2 WITH QUALITY INDEX 2

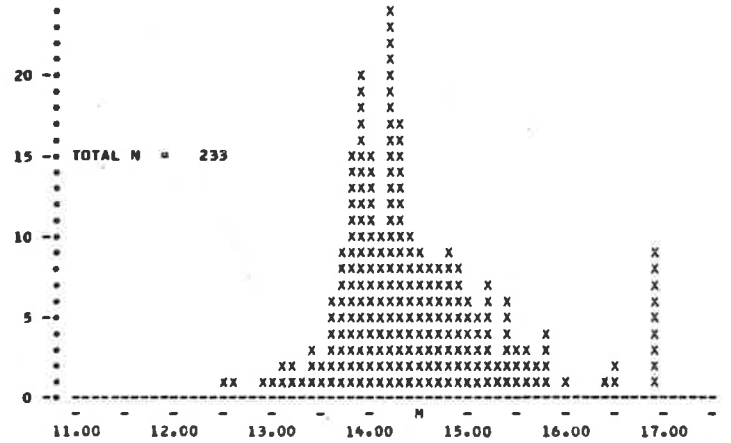

LOG10 (ALPHA) FOR TYPE 1 ECHOES RECORDED AT STATION 3 WITH QUALITY INDEX 2

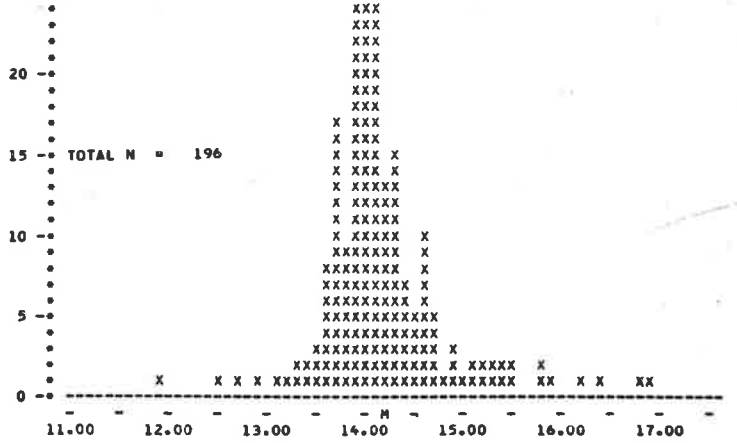

LOG10 (ALPHA) FOR TYPE 1 ECHOES RECORDED AT STATION 4 WITH QUALITY INDEX 2

Figure A-4-6

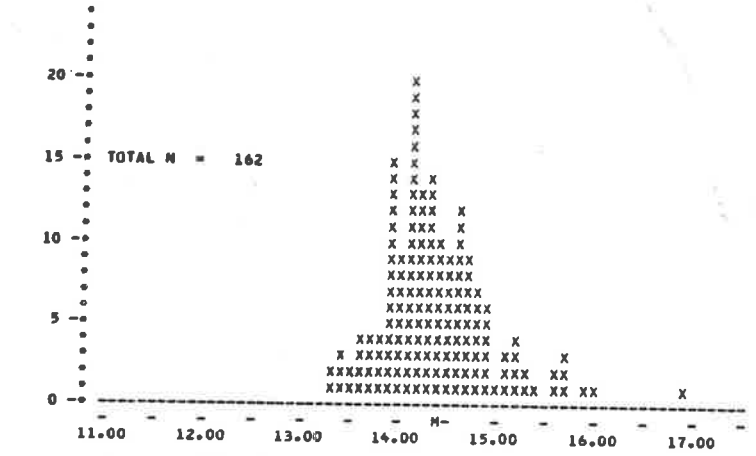

LOG10 (ALPHA) FOR TYPE 1 ECHOES RECORDED AT STATION 1 WITH QUALITY INDEX 4

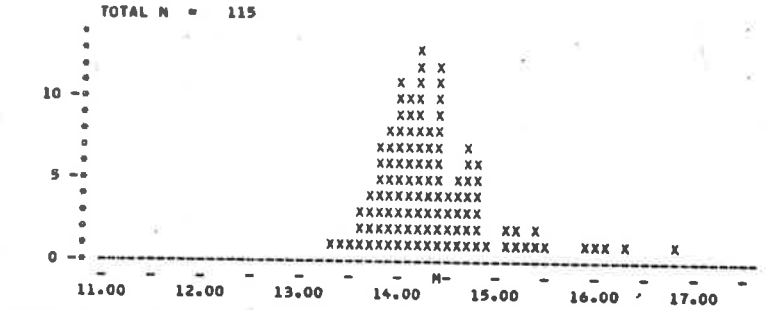

LOG10 (ALPHA) FOR TYPE 1 ECHOES RECORDED AT STATION 2 WITH QUALITY INDEX 4

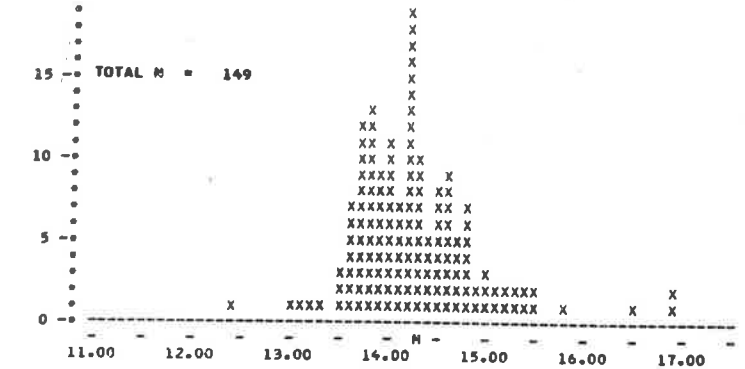

LOG10 (ALPHA) FOR TYPE 1 ECHOES RECORDED AT STATION 3 WITH QUALITY INDEX 4

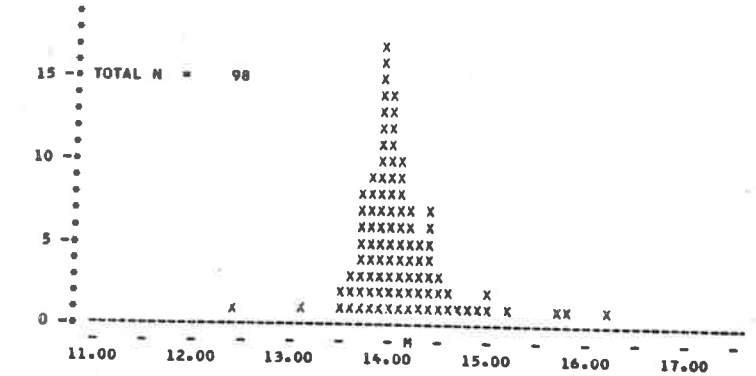

LOG10 (ALPHA) FOR TYPE 1 ECHOES RECORDED AT STATION 4 WITH QUALITY INDEX 4

Figure A-4-7

APPENDIX 5

THE EQUIVALENT GAUSSIAN PROFILE

A bonus is associated with the choice of $\frac{1}{\alpha}\frac{d\alpha}{dh}$ as the variable by which ionization profiles are characterized. For an electron line density profile of Gaussian form, the dependence of $\frac{1}{\alpha}\frac{d\alpha}{dh}$ on height (measured from h_{max}) is very simple.

Consider a trail on which

$$\alpha(h) = \alpha_{max} \exp[-(h-h_{max})^2/L^2] \qquad \ldots A5.1$$

Upon differentiation it follows immediately that

$$Q = \frac{1}{\alpha}\frac{d\alpha}{dh} = -2(h-h_{max})/L \quad . \qquad \ldots A5.2$$

Hence if a linear dependence of Q on $(h-h_{max})$ can be shown to exist, or nearly so, in experimental data, its gradient leads to the scale length L describing what we shall call an equivalent Gaussian profile (Eq. A5.1).

A pair of scatter diagrams, in which observed values of $h-h_{max}$ were plotted as vertical coordinate and their associated values of Q were plotted as horizontal coordinate, was constructed for each value of the quality index INDEXQ. The format was similar to the plots of predicted vs. observed values of Q, and the pair for quality index 1 is reproduced as Fig. A-5-1. There is, of course, no connection with any of the model profiles (a) - (d). The left-hand plot is for all available data, while the right-hand plot uses data from stations 1 and 4 only. As before, the numbers below each plot are statistical parameters of the distribution of plotted points; the values for INDEXQ 1 and 3 are given in Table A5.1.

Table A5.1. Correlation of Q and $y = h-h_{max}$.

INDEXQ	Data	Points	Q	y	σ_Q	σ_y	Corr. cft.
1	All	3501	.037	-.135	1.116	1.408	-.431
	St.K.-Salis.	534	-.021	-.166	1.020	1.494	-.513
3	All	1198	.079	-.277	0.939	1.380	-.376
	St.K.-Salis.	118	.093	-.500	0.648	1.500	-.405*

*Probably too few points for accuracy.

In all eight scatter diagrams the range of $(h-h_{max})$ is approximately from -4 to +4 Km., and the mean reflection point height is a few hundred metres below h_{max}. As judged by eye the correlation between Q and height is better than between the observed and predicted values of Q (v. § 8.5), and the correlation coefficients bear this impression out.

As discussed in Chapter 5, the regression lines of $y = (h-h_{max})$ on Q and of Q on y can be found by purely formal means. However, unless something is known about the experimental error in one variable or both, neither of these lines is necessarily a better estimate of the gradient of any underlying linear functionality than is the other regression line, or any line of intermediate slope. There is no evidence which might indicate either the absolute experimental error in either variable, or the ratio of the two experimental errors. As a guess, one might assume that the standard error in determining y is $\delta_y \sim 0.5$ Km.

Table A5.2 gives three values of the scale length L of the equivalent Gaussian profile for each plot. Two are calculated from the regression slopes of y on Q and of Q on y; these are the limits of the range of possible values of L. The third value is that found using Eq. 5.4.6, assuming $\delta_h = 0.5$ Km.

Table A5.2 . Scale length of equivalent Gaussian profiles.

INDEXQ	Data	L, Km.		
		(reg.^{n} y on Q)	(reg.^{n} Q on y)	(δ_y = 0.5 Km.)
1	All	1.08	5.86	4.26
	St.K.-Salis.	1.50	5.72	5.06
3	All	1.10	7.82	6.80
	St.K.-Salis.	1.88*	11.42*	10.16*

* Unreliable: too few plotted points.

APPENDIX 6

MATHEMATICAL SIMULATION OF AN EXPERIMENT OF GREENHOW AND NEUFELD

In this Appendix the geometry of the two-station experiment of Greenhow and Neufeld (1957) is examined. With reference to the short review of their method given in Section 4.3, it is clear that the height extent of the profile would have been over-estimated if the values found for the height difference Δh between the pair of reflection points on each trail were systematically too large. The expression used in finding Δh was given in Eq. 4.2.1, viz.

$$\Delta h \simeq (v^2 t^2 \cot E)/l \qquad \ldots A6.1$$

The author has therefore checked the accuracy of this expression, using a method of numerical analysis based on the method by which the height of the Salisbury reflection point was found (§7.8). An array of azimuth-zenith angle pairs was set up, covering one vertical half of the region of overlap of the transmitting and receiving aerial patterns. Naturally the true reflection points were scattered about the assumed mean altitude of 92.5 Km. Hence all potential reflection points at a given azimuth and zenith angle and at altitudes 70,80,90,100 and 110 Km. were used in the analysis if they satisfied the range restrictions used by Greenhow and Neufeld to limit the apparent elevation E.

Let the direction cosines of the line of sight to the main-station reflection point, relative to that station as origin and with the other station in the positive x-direction, be (l, m, n), and those of the trail (λ, μ, ν). Then given the radiant zenith angle x, we have $\nu = \cos x$, and it can be shown that

$$\lambda = \frac{ln\nu \pm m\sqrt{1-n^2-\nu^2}}{n^2-1} \qquad \ldots A6.2$$

The other trail direction cosine μ is then given by

$$\mu^2 = 1 - \lambda^2 - \nu^2 \quad ,$$

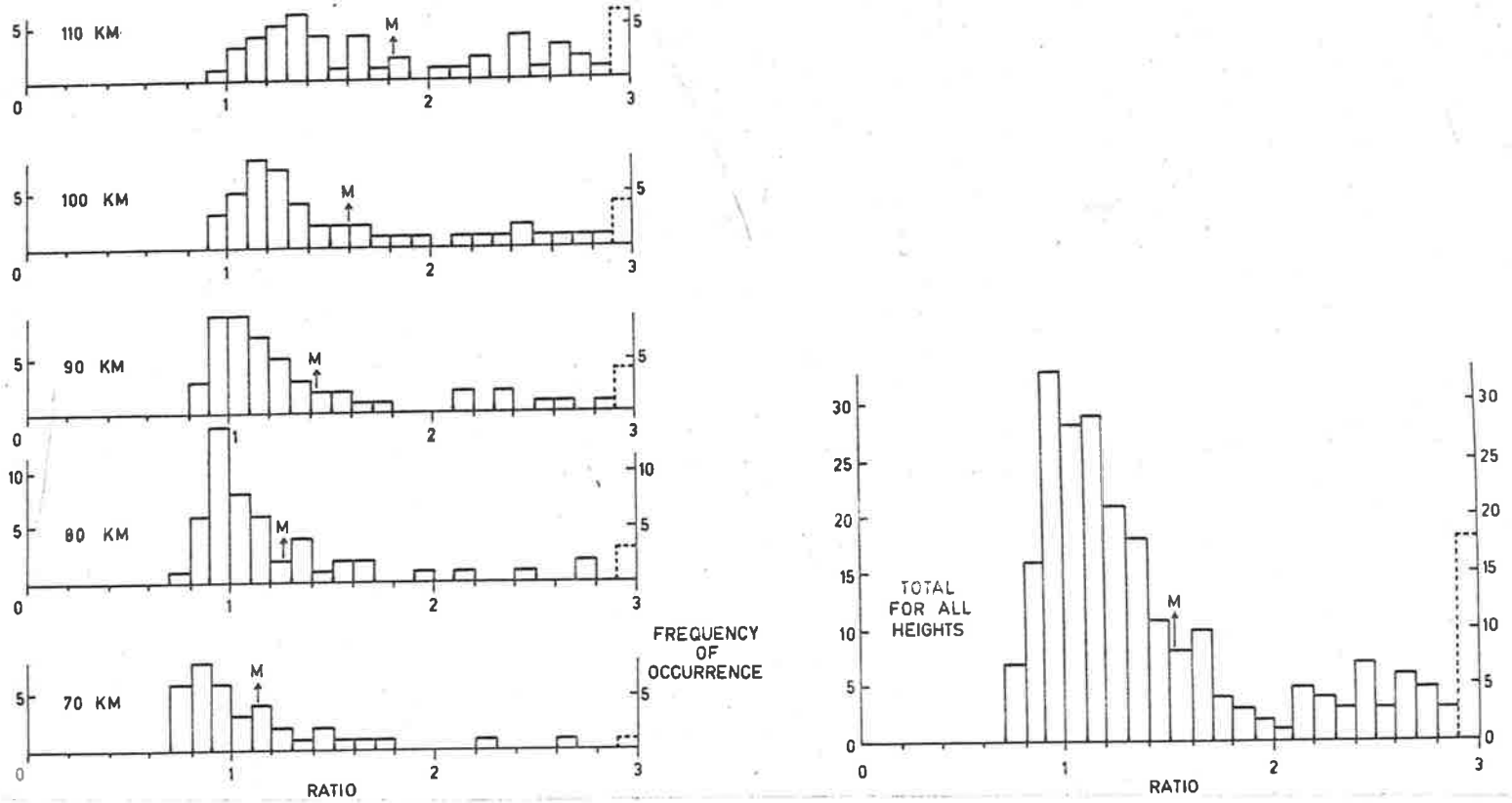

Figure A6.1 Ratios of actual height differences found in simulation of the two-station experiment of Greenhow and Neufeld to height differences given by their formula, for main station reflection points at various heights.

and its sign is determined from the specularity condition

$$l\lambda + m\mu + n\nu = 0 \ .$$

If the quantity under the square root sign in A6.2 is negative specular reflection is impossible, but otherwise there are two pairs (λ, μ), or two trail orientations, which give specular reflection from the chosen reflection point location (l, m, n, height) with a given radiant zenith angle x.

The analysis gave x the successive values 15°, 30°, 45°, 60°, 75° at each potential main-station reflection point in the azimuth-zenith angle array. Where specular reflection was possible the true height difference, and the true distance vt along the trail between this reflection point and that for the distant station, were computed using the iterative method detailed in Section 7.8. From the known range the elevation angle estimate E was found, and then E and vt were used to find the estimate Δh of the height difference yielded by A6.1. Thus the procedure simulated the original experiment closely in that Δh was subject to identical approximations applied in the same order. It was, of course, not possible to simulate the effect of experimental errors in v.

For each of the five reflection point altitudes a "map" of the height differences, and the error in A6.1, was produced, showing these quantities as functions of the zenith angle and azimuth of the upper reflection point. Finally the data from those "trails" in each map which gave rise to estimated height differences between 3.0 and 5.0 Km. were summarized. The summary information is reproduced in Fig. A-6-1. From these results it is apparent first of all that the errors in E and in A6.1 itself combine to produce values for Δh which were very asymmetrically distributed about the true height differences. At no height was the height difference under-estimated by more than 30%, but over-estimation of order 100% was common and the occurrences of over-estimates by 200% or more (the dashed column at the extreme right in each histogram) were too frequent to be disregarded. The histograms show that while the modal value of the ratio Δh/true height difference was fairly close to unity at each reflection height, the mean ratio (denoted by the letter M) varied between 1.15 and 1.83. The overall mean was 1.62 .

REFERENCES

Ananthakrishnan, R. (1960) Nature 187, 675

Ananthakrishnan, R. (1961) Nature 190, 896

Belrose, J.S. (1963) Chapter 1 of "Propagation of radio waves at frequencies less than 300 Kc/s.", AGARDograph 74, Pergamon Press, London.

Billam, E.R., Browne, I.C. (1956) Proc. Phys. Soc. 69, 98

Booker, H.G., Cohen, R. (1956) J.G.R. 61, 707

Brysk, H. (1958) J.G.R. 63, 693

Brysk, H. (1959) I.R.E. Trans. AP-7, S330

Burgess, B. (1963) Page 315 of "Radio astronomical and satellite studies of the atmosphere", ed. Aarons, J., North-Holland, New York.

Cole, A.E., Kantor, A.J. (1963) A.F.C.R.L. Res. Rep. 63-396

Davies, O.L. (ed.) (1958) "Statistical methods in research and production" 3rd Ed., Oliver & Boyd, London.

Elford, W.G. (1954) Ph.D. thesis, University of Adelaide.

Elford, W.G. (1964) Paper presented to A.G.U., Washington (in NASA publ. X-650-65-220, GSFC, June 1965).

Ellyett, C.D. (1950) Phil. Mag. (7)41, 694

Eshleman, Von R. (1955) I.R.E. Trans. AP-3, 32

Eshleman, Von R. (1956) Stanford University Contract AF19(604)-1031, Report No. 5.

Eshleman, Von R. (1957) J.A.T.P. 10, 57

Evans, S. (1954) M.N.R.A.S. 114, 63

Evans, J.V., Brockelman, R.A. (1963) Tech. Rep. 332, M.I.T. Lincoln Labs.

Francey, J.L. (1963) Aust. J. Phys. 16, 500

Francey, J.L. (1964) Aust. J. Phys. 17, 315

Greenhow, J.S. (1954) Phil. Mag. (7)45, 471

Greenhow, J.S., Neufeld, E.L. (1955) J.A.T.P. 6, 133

Greenhow, J.S., Neufeld, E.L. (1956) Proc. Phys. Soc. B69, 1069

Greenhow, J.S., Neufeld, E.L. (1959) Proc. Phys. Soc. 74, 1

Greenhow, J.S., Hall, J.E. (1960a) M.N.R.A.S. 121, 174

Greenhow, J.S., Hall, J.E. (1960b) M.N.R.A.S. 121, 183

Greenhow, J.S., Hall, J.E. (1960c) J.A.T.P. 18, 203

Greenhow, J.S., Hall, J.E. (1961) P.S.S. 5, 109

Greenhow, J.S., Watkins, C.D. (1964) J.A.T.P. 26, 539

Gregory, J.B. (1961) J.G.R. 66, 429

Groves, G.V. (1959) J.A.T.P. 16, 344

Hawkins, G.S. (1956) Proc. I.R.E. 44, 1192

Hawkins, G.S., Southworth, R.B. (1958) Smith. Cont. Astrophys. 2, 349

Hawkins, G.S., Southworth, R.B. (1963) Harvard Radio Meteor Project, NASA Res. Rep. 2.

Hawkins, G.S. (1963) Smith. Cont. Astrophys. 7, 23

Hawkins, G.S., Southworth, R.B., Verniani, F. (1964) Harvard R.M.P. NASA Res. Rep. 10

Hemenway, C.L., Sobermann, R.K., et al. (1961) Smith. Cont. Astrophys. 5, 89

Herlofson, N. (1948) Repts. Prog. Phys. 11, 444

Herlofson, N. (1951) Arkiv för Fysik 3, 247

Hines, C.O., Forsyth, P.A. (1957) Can. J. Phys. 35, 1033

Huxley, L.G.H. (1952) Aust. J. Sci. Res. A5, 10

Jacchia, L.G., Kopal, Z., Millman, P. (1950) Astrophys. J. 111, 104

Jacchia, L.G. (1955) Astrophys. J. 121, 521

Jacchia, L.G. (1963) Ch. 22 of "The moon, meteorites and comets", ed. Middlehurst, B.M. and Kuiper, G.P. (The solar system, Vol. 4) University of Chicago Press.

Kaiser, T.R., Closs, R.L. (1952) Phil. Mag. (7)43, 1

Kaiser, T.R. (1953) Advances in Physics (Phil. Mag. Suppl.) 2, 495

Kaiser, T.R. (1955) "Meteors" (Suppl. to J.A.T.P.), 52

Kashcheyev, B.L., Lebedinets, V.N. (1963) Smith. Cont. Astrophys. 7, 19

Kochanski, S. (1964) J.G.R. 69, 3651

Kolmogoroff, A. (1941) C.R. Acad. Sci. U.R.S.S. 30, 301

Lazarus, D.M., Hawkins, G.S. (1961) Smith. Cont. Astrophys. 5, 291

Leowenthal, M. (1956) TR Tech. Rep. 132, M.I.T. Lincoln Lab.

Levin, B. Yu. (1962) Nature No.4854, 527

Levin, B. Yu. (1963) Soviet Astronomy - AJ 7, 233

Lindley, D.V. (1947) J. Roy. Stat. Soc. B9, 218

Lovell, A.C.B., Clegg, J.A. (1948) Proc. Phys. Soc. 60, 491

McKinley, D.W.R. (1961) "Meteor science and engineering", McGraw-Hill, New York.

Manning, L.A. (1953) J.A.T.P. 4, 219

Manning, L.A., Villard, O.G. Jr., Peterson, A.M. (1953) Trans. A.G.U. 34, 16

Manning, L.A. (1958) J.G.R. 63, 181

Manning, L.A. (1959) J.G.R. 64, 1415

Manning, L.A., Eshleman, Von R. (1959) Proc. I.R.E. 47, 186

Manning, L.A. (1963) J.A.T.P. 25, 183

Manning, L.A. (1964) Radio Sci. 68D, 1067

Murray, E.L. (1959) P.S.S. 1, 125

Nilsson, C.S. (1963) Ph.D. thesis, University of Adelaide.

Nilsson, C.S. (1964) Aust. J. Phys. 17, 205

Öpik, E. (1937) Pub. Ast. Obs. Tartu 29, No. 5

Öpik, E. (1958) "Physics of meteor flight in the atmosphere", Interscience, New York.

Pearson, P.H.O. (1965) (Weapons Res. Est., Salisbury, S.A.) Private communication.

Rao, M.S., Armstrong, R.L. (1958) Can. J. Phys. 36, 1601

Rice, D.W., Forsyth, P.A. (1963) Can. J. Phys. 41, 679

Rice, D.W., Forsyth, P.A. (1964) Can. J. Phys. 42, 2035

Robertson, D.S., Liddy, D.T., Elford, W.G. (1953) J.A.T.P. 4, 255

Robinson, B.B. (1965) J.G.R. 70, 3793

Roper, R.G. (1962) Ph.D. thesis, University of Adelaide.

Roper, R.G., Elford, W.G. (1963) Nature 197, 963

Roper, R.G., Elford, W.G. (1965) NASA Publication X-650-65-86, GSFC

Southworth, R.B. (1962) Harvard R.M.P. Res. Rep. 14

Stone, B.J. (1966a) Laboratory Report, Physics Dept., Uni. of Adelaide.

Stone, B.J. (1966b) Dept. of Supply, W.R.E. Salisbury, IBM 7090 Subprogram Specification IL . .0

Stroud, W.G., Nordberg, W. (1961) NASA Tech. Note TN D-703

Tchen, C.M. (1954) Phys. Rev. 94, 4

U.S. Std. Atmos. 1962 , U.S. Govt. Printing Office, Washington

Verniani. F., Hawkins, G.S. (1964) Harvard R.M.P. NASA Res. Rep. 5

Weiss, A.A. (1954) Aust. J. Phys. 8, 148

Weiss, A.A. (1955) Aust. J. Phys. 8, 279

Weiss, A.A. (1957) Aust. J. Phys. 10, 77

Weiss, A.A. (1958) Aust. J. Phys. 11, 591

Weiss, A.A. (1959) Aust. J. Phys. 12, 54

Weiss, A.A. (1960) Aust. J. Phys. 13, 532

Weiss, A.A., Elford, W.G. (1963) Proc. I.R.E.Aust. 24, 197

Whipple, F.L. (1950) Astrophys. J. 111, 375

Whipple, F.L., et al. (1951-1955) Papers on the physical theory of meteors, in Astrophys. J. 113, 475; 114, 448; 116, 203; 118, 555; 119, 438; 120, 572; 121, 241; 121, 521.

Whipple, F.L. (1963a) J.G.R. 68, 4929

Whipple, F.L. (1963b) Ch. 19 of "The moon, meteorites and comets" (see reference for Jacchia (1963)).

Williams, E.J. (1959) "Regression analysis", Wiley, New York.